

MABS MONOGRAPH AIR BLAST INSTRUMENTATION 1943 - 1993

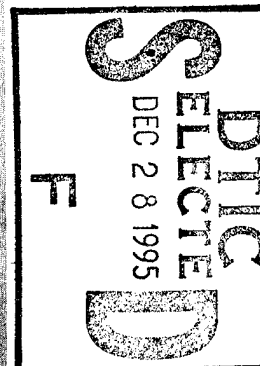
August 1995

MEASUREMENT

TECHNIQUES

AND

INSTRUMENTATION



Volume 2 The High Explosive Era, 1959 - 1993

Published by:
Defense Nuclear Agency
6801 Telegraph Road
Alexandria, VA 22310-3398

Approved for Public Release;
Distribution is Unlimited.

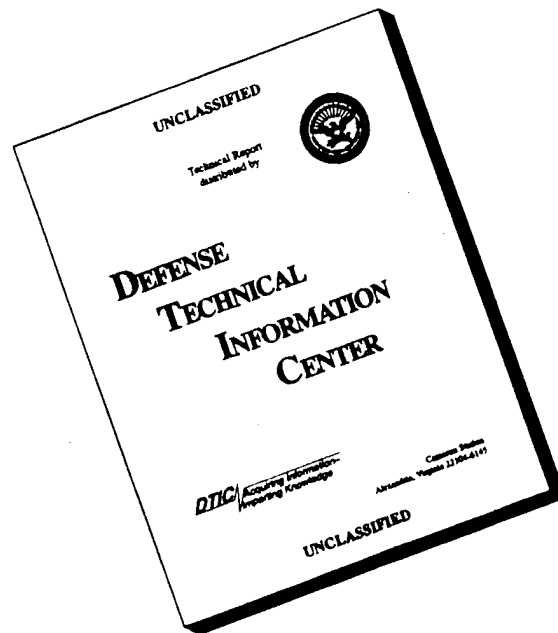
19951228 026

Destroy this report when it is no longer needed. Do not return to sender.

PLEASE NOTIFY THE DEFENSE NUCLEAR AGENCY,
ATTN: CSTI, 6801 TELEGRAPH ROAD, ALEXANDRIA, VA
22310-3398, IF YOUR ADDRESS IS INCORRECT, IF YOU
WISH IT DELETED FROM THE DISTRIBUTION LIST, OR
IF THE ADDRESSEE IS NO LONGER EMPLOYED BY YOUR
ORGANIZATION.



DISCLAIMER NOTICE



THIS DOCUMENT IS BEST QUALITY AVAILABLE. THE COPY FURNISHED TO DTIC CONTAINED A SIGNIFICANT NUMBER OF PAGES WHICH DO NOT REPRODUCE LEGIBLY.

REPORT DOCUMENTATION PAGE			Form Approved OMB No. 0704-0188	
Public reporting burden for this collection of information is estimated to average 1 hour per response including the time for reviewing instructions, searching existing data sources, gathering and maintaining the data needed, and completing and reviewing the collection of information. Send comments regarding this burden estimate or any other aspect of this collection of information, including suggestions for reducing this burden, to Washington Headquarters Services Directorate for Information Operations and Reports, 1215 Jefferson Davis Highway, Suite 1204, Arlington, VA 22202-4302, and to the Office of Management and Budget, Paperwork Reduction Project (0704-0188), Washington, DC 20503				
1. AGENCY USE ONLY (Leave blank)		2. REPORT DATE 950801	3. REPORT TYPE AND DATES COVERED Technical 930917 - 940531	
4. TITLE AND SUBTITLE MABS Monograph, Air Blast Instrumentation, 1943 — 1993 Measurement Techniques and Instrumentation Volume 2—The High Explosive Era, 1959 — 1993			5. FUNDING NUMBERS C - DNA 001-92-C-0144 PE - 62715H PR - AB TA - HB WU- DH327450	
6. AUTHOR(S) Ralph E. Reisler, John H. Keefer, and Noel H. Ethridge				
7. PERFORMING ORGANIZATION NAME(S) AND ADDRESS(ES) Applied Research Associates, Inc. 4300 San Mateo Blvd., NE Suite A220 Albuquerque, NM 87110-1260			8. PERFORMING ORGANIZATION REPORT NUMBER N/A	
9. SPONSORING/MONITORING AGENCY NAME(S) AND ADDRESS(ES) Defense Nuclear Agency 6801 Telegraph Road Alexandria, VA 22310-3398 TDTR/Flohr			10. SPONSORING/MONITORING AGENCY REPORT NUMBER N/A	
11. SUPPLEMENTARY NOTES This work was sponsored by the Defense Nuclear Agency under RDT&E RMC Code B4662D AB HB 00007 5200A AB 25904D.				
12a. DISTRIBUTION/AVAILABILITY STATEMENT Approved for public release; distribution is unlimited.			12b. DISTRIBUTION CODE	
13. ABSTRACT (Maximum 200 words) Blast wave measurement techniques and instrumentation developed by Military Applications of Blast Simulators (MABS) participating countries to study blast phenomena during the high explosive era are summarized. Passive and active gages, both mechanical self-recording and electronic systems, deployed on one-half ton to multi-ton explosive tests during the period 1959 to 1993 are presented. The country and the year the gage was introduced are included with the description. References are also provided.				
14. SUBJECT TERMS Active Devices Mechanical Systems Pressure Gauges High Explosives Free-Field Pressure Sensing Electronic Recording			15. NUMBER OF PAGES 246	
			16. PRICE CODE	
17. SECURITY CLASSIFICATION OF REPORT UNCLASSIFIED	18. SECURITY CLASSIFICATION OF THIS PAGE UNCLASSIFIED	19. SECURITY CLASSIFICATION OF ABSTRACT UNCLASSIFIED	20. LIMITATION OF ABSTRACT SAR	

UNCLASSIFIED

SECURITY CLASSIFICATION OF THIS PAGE

CLASSIFIED BY:

N/A since Unclassified.

DECLASSIFY ON:

N/A since Unclassified..

SECURITY CLASSIFICATION OF THIS PAGE

UNCLASSIFIED

PREFACE

This effort was sponsored jointly by the Defense Nuclear Agency (DNA) under contract DNA001-92-C-0144 and the Norwegian Defence Construction Service.

The work was carried out under the direct management of Mr. Mark Flohr of DNA and Mr. Arnfinn Jenssen of Norway.

The Steering Committee of the International Symposium on the Military Applications of Blast Simulation (MABS) recommended that a series of monographs be prepared dealing with topics of interest to all MABS participating countries. The subject matter proposed was (a) a History of MABS; (b) Blast Wave Measurement Techniques and Instrumentation - Passive and Electronic Devices; and (c) Photogrammetric Blast Wave Measurement Techniques.

Blast wave measurement techniques and instrumentation of the participating countries over the past fifty years was to be covered. Three reports came about as a result of the effort:

- Volume 1 : Air Blast Measurement Techniques and Instrumentation - The Nuclear Era, 1943 to 1963
- Volume 2 : Air Blast Measurement Techniques and Instrumentation - The High Explosive Era, 1959 to 1993
- Volume 3 : Air Blast Structural Target and Gage Calibration - Measurement Techniques and Instrumentation, 1943 to 1993

The photograph on the front cover of this report is the detonation of the 100-ton TNT block-built hemispherical charge at the Defence Research Establishment, Suffield, in 1961.

Accession For	
NTIS	CRA&I <input checked="" type="checkbox"/>
DTIC	TAB <input type="checkbox"/>
Unannounced <input type="checkbox"/>	
Justification	
By	
Distribution /	
Availability Codes	
Dist	Avail and/or Special
A-1	

CONVERSION TABLE

Conversion factors for U.S. Customary to metric (SI) units of measurement.

MULTIPLY _____ BY _____ TO GET
TO GET _____ BY _____ DIVIDE

angstrom	1.000 000 X E -10	meters (m)
atmosphere (normal)	1.013 25 X E +2	kilo pascal (kPa)
bar	1.000 000 X E +2	kilo pascal (kPa)
barn	1.000 000 X E -28	meter ² (m ²)
British thermal unit (thermochemical)	1.054 350 X E +3	joule (J)
calorie (thermochemical)	4.184 000	joule (J)
cal (thermochemical/cm ²)	4.184 000 X E -2	mega joule/m ² (MJ/m ²)
curie	3.700 000 X E +1	*giga becquerel (GBq)
degree (angle)	1.745 329 X E -2	radian (rad)
degree Fahrenheit	$t_k = (t^{\circ}f + 459.67)/1.8$	degree kelvin (K)
electron volt	1.602 19 X E -19	joule (J)
erg	1.000 000 X E -7	joule (J)
erg/second	1.000 000 X E -7	watt (W)
foot	3.048 000 X E -1	meter (m)
foot-pound-force	1.355 818	joule (J)
gallon (U.S. liquid)	3.785 412 X E -3	meter ³ (m ³)
inch	2.540 000 X E -2	meter (m)
jerk	1.000 000 X E +9	joule (J)
joule/kilogram (J/kg) radiation dose absorbed	1.000 000	Gray (Gy)
kilotons	4.183	terajoules
kip (1000 lbf)	4.448 222 X E +3	newton (N)
kip/inch ² (ksi)	6.894 757 X E +3	kilo pascal (kPa)
ktap	1.000 000 X E +2	newton-second/m ² (N-s/m ²)
micron	1.000 000 X E -6	meter (m)
mil	2.540 000 X E -5	meter (m)
mile (international)	1.609 344 X E +3	meter (m)
ounce	2.834 952 X E -2	kilogram (kg)
pound-force (lbs avoirdupois)	4.448 222	newton (N)
pound-force inch	1.129 848 X E -1	newton-meter (N·m)
pound-force/inch	1.751 268 X E +2	newton/meter (N/m)
pound-force/foot ²	4.788 026 X E -2	kilo pascal (kPa)
pound-force/inch ² (psi)	6.894 757	kilo pascal (kPa)
pound-mass (lbm avoirdupois)	4.535 924 X E -1	kilogram (kg)
pound-mass-foot ² (moment of inertia)	4.214 011 X E -2	kilogram-meter ² (kg·m ²)
pound-mass/foot ³	1.601 846 X E +1	kilogram/meter ³ (kg/m ³)
rad (radiation dose absorbed)	1.000 000 X E -2	**Gray (Gy)
roentgen	2.579 760 X E -4	coulomb/kilogram (C/kg)
shake	1.000 000 X E -8	second (s)
slug	1.459 390 X E +1	kilogram (kg)
torr (mm Hg, 0° C)	1.333 22 X E -1	kilo pascal (kPa)

*The becquerel (Bq) is the SI unit of radioactivity; 1 Bq = 1 event/s.

**The Gray (GY) is the SI unit of absorbed radiation.

TABLE OF CONTENTS

Section	Page
PREFACE	iii
CONVERSION TABLE	iv
FIGURES	viii
TABLES	xiii
 1 INTRODUCTION	 1
 2 HISTORY AND SUMMARY OF MEASUREMENTS	 2
 3 FREE-FIELD AIRBLAST - PASSIVE DEVICES	 15
3.1 Displacement Systems	15
3.1.1 Canadian Wire, Cantilever Drag Gages	15
3.1.2 Australian DPI Gage	17
3.1.3 DRES Deformation Gage	21
3.1.4 DRES Fluid Ejection (SQUIRT) Gage	25
3.1.5 Cubes	25
3.1.6 Bursting Diaphragm Gage	33
3.2 Fiber Optic Bier Gage	36
 4 FREE-FIELD ACTIVE DEVICES, PRESSURE SENSING	 42
4.1 Piezo-Resistive	42
4.1.1 Kulite Pressure Gage	42
4.1.2 Endevco Model 8510	42
4.1.3 Subsonic Differential Pressure Gage	44
4.2 Variable Reluctance	49
4.2.1 CCC Gage	49
4.2.2 SRI MAD Gage, Ultradyne S-30	53
4.3 Strain Four Arm Bridge	58
4.3.1 Schaevitz-Bytrex HFG Gage	58
4.3.2 Dynisco Gage	58
4.3.3 SRI Total Drag Probe	58
4.3.4 SRI-BRL Drag Force Gage	61
4.3.5 BRL Bi-Axial Drag Gage	61

TABLE OF CONTENTS (Continued)

Section	Page
4.3.6 H-Tech Snob Gage	65
4.3.7 AFWL High Pressure Gage	68
4.3.8 CRC Snob Gage	73
4.3.9 NMERI Snob Probe	73
4.3.10 BRL Cantilever	77
4.3.11 Internal Strain Gage (ISG) Transducer	77
4.3.12 DRES Drag Cylinders	80
4.4 Piezo-Electric	80
4.4.1 LC33, CL60, BC33CZ, and LZF Gages	80
4.4.2 B2 and MQ10 Gages	83
4.4.3 KKQ Gage	96
4.4.4 BRL Piezo-Electric Gages	96
4.4.5 PCB 113A Gage	103
4.4.6 H-Tech Greg Gage	110
4.4.7 Piezo Zinc Oxide Chip	110
4.4.8 German Pitot Pressure Gage	110
4.5 Mechanical Self-Recording Systems	117
4.5.1 BRL-Self-Recording Gages	117
4.6 Fiber-Optic Sensors	132
4.6.1 Optical Fabry-Perot Resonator Pressure Sensor	132
4.6.2 High Bandwidth Fiber Optic Sensor	137
4.7 Bar Pressure Gages	137
4.7.1 General Atomics Quartz Bar Gage	142
4.7.2 SRI Quartz Bar Gage	142
4.7.3 ST4 Piezoelectric Pressure Bar Gage	142
4.7.4 CERF Piezoresistive Bar Gage	144
4.7.5 WES Bar Gage	144
4.7.6 NMERI Bar Gage	148
4.7.7 S-CUBED Bar	153
4.7.8 Photoelastic Sapphire Bar	161
4.8 Other Systems	163
4.8.1 DRES ABTOAD Gage	163

TABLE OF CONTENTS (Continued)

Section	Page
4.8.2 DRES Blast Gage Station	163
4.8.3 Hot Wire Anemometry	168
4.8.4 Laser Velocimetry	177
4.8.5 Vortex-Shedding Anemometer	177
4.8.6 Free-Flight Cylinders	182
4.8.7 Lovelace Free-Flight Drag Spheres	187
4.9 Electronic Recording	189
4.9.1 Oscilloscope	189
4.9.2 Magnetic Tape	189
4.9.3 Digital Recording Systems	197
5 CONCLUSION	215
6 REFERENCES	216
APPENDIX	
A U.S. BIBLIOGRAPHY	A-1
B CANADIAN BIBLIOGRAPHY	B-1
C U.K. BIBLIOGRAPHY	C-1

FIGURES

Figure	Page
1 Multi-ton (500-ton) explosion	6
2 Multi-burst (two 1000-lb) explosion	7
3 Test bed for multi-ton trial, Operation Direct Course	13
4 Test bed for 1000-lb HE trial	14
5 Standard wire gage on two-foot stand	16
6 Standard wire gage after the blast	16
7 Idealized stress-strain relationship	18
8 Ground-mounted steel and aluminum cantilevers	18
9 Deformed cantilever at a distance of 296 m showing that the majority of the bending occurs at the base	19
10 A set of platform-mounted solder cantilevers	20
11 Schematic of DPI gage	22
12 Pre-shot DPI gage installation	23
13 Post-shot view of DPI gages	24
14 DRES fluid ejection gage	26
15 Squirt gage	27
16 Low pressure fluid-ejection gage	28
17 Field model of mercury surface tension gage (exploded view)	29
18 Cubes in position on west line	32
19 Mechanical drawing (side view) of pressure gage	35
20 Australian bursting diaphragm gage	37
21 Anderson blasgage	38
22 Production spectrometer design	40
23 Drawn quartz rod	41
24 Kulite HK pressure gage	43
25 Configuration of the differential pressure gage	45
26 Differential pressure gage mounted in pylon 5.5 inches (0.14 meters) above the ground surface for the Mighty Mach IV test series	46
27 Configuration of the modified differential pressure probe with added side-on overpressure sensor. The probe is Model XCW-8-WZ-200, made by Kulite Semiconductor Products, Inc	47
28 Differential pressure gage	48
29 Comparison of the data from the differential pressure gage with predictions obtained by the flow-field reconstruction method - 1000-lb HE test	50
30 Differential pressure gage record comparison	51
31 SRI-MAD gage	54
32 SRI-MAD gage: (a) assembled gage and (b) gage components	55
33 Dust sampler (explosive closures not shown)	57
34 Drawing of Bytrex pressure transducer	59

FIGURES (Continued)

Figure		Page
35	Drawing of Dynisco pressure transducer	59
36	Total drag probe assembly	60
37	Drag force gages	62
38	Assembly drawing of BRL bi-axial drag gage	63
39	Exploded view of BRL bi-axial drag gage	64
40	Typical gage mounting system	66
41	Schematic of H-Tech snob gage	69
42	H-Tech snob gage	70
43	AFWL high pressure sensor hardware assembly	71
44	Typical channel for AFWL high pressure gage	72
45	CRC snob probe	74
46	CRC snob/greg probe	75
47	NMERI snob probe schematic	76
48	BRL cantilever gage	78
49	Internal strain pressure gage	79
50	3.5-inch finned drag force transducers	81
51	3.5-inch finned drag force transducer in mount	82
52	Gage stand setup for 20-ton trial	84
53	Cross section of gage in lead block	85
54	MQ10 pressure gage	91
55	FQ11C pressure gage	92
56	MQ18 pressure gage	93
57	MQ20 pressure gage	94
58	Comparison of UK MQ10 piezo-electric gage pressure time curves from SES 1961, 100-ton TNT trial with Brode's "point source" theoretical curves	95
59	Schematic of KKQ dynamic pressure gage	97
60	Type 1 piezo-electric gage	98
61	Type 2 piezo-electric gage	99
62	Type 3 piezo-electric gage	100
63	Type 4 piezo-electric gage	101
64	Diagram of static overpressure transducer housing	104
65	Diagram of total head half-inch probe	105
66	Schematic of piezoelectric gage recording system	106
67	Photograph of ground baffles	107
68	Above the surface mounting of piezoelectric gages	108
69	Piezo-electric field records from an HMX 1000-lb explosion	109
70	Schematic of H-Tech greg gage	111
71	Photograph of H-Tech greg gage	112
72	Proposed zinc oxide-silicon chip high pressure side-on gage	113
73	Proposed zinc oxide-silicon chip high pressure face-on gage, Design A ..	114
74	Proposed zinc oxide-silicon chip high pressure face-on gage, Design B ..	115
75	Federal Republic of Germany pitot pressure station	116

FIGURES (Continued)

Figure		Page
76	Schematic of electrical hookup for German pressure gages	116
77	Single diaphragm self-recording gage pressure sensor	118
78	BRL negator pressure gage	120
79	Standard disc pressure gage	122
80	Self-recording dynamic pressure gage	123
81	Nondirectional system	124
82	A nondirectional self-recording system	125
83	Arrival time system	126
84	Very low pressure gage	128
85	BRL pressure sensors	129
86	New tape recorder, Exline Model 245	130
87	Fluid time marker	131
88	High pressure fluid supply and pressure regulator	131
89	Sample plots of pressure-time records from HE field tests	133
90	HE field records from self-recording gages	134
91	Fabry-Perot resonator sensor head design	135
92	Optical circuit for a Fabry-Perot resonator sensor	136
93	Schematic of a Fabry-Perot optical resonator	136
94	Schematic of the optical configuration of a photoelastic pressure sensor ..	139
95	High bandwidth fiber optic airblast pressure sensor, conceptual design ...	140
96	A high-pressure bar gage	141
97	Generic high-pressure bar gages	141
98	Piezoelectric pressure bar gage, Model ST-4	143
99	Redesigned piezoresistive bar gage modified for extrusion-filling process .	145
100	Original piezoresistive bar gage	146
101	Detailed cross-section of a typical bar gage	147
102	Typical installation techniques for a bar gage	149
103	WES bar gage ready for installation	150
104	WES bar gage installation sequence	151
105	NMERI short bar	152
106	NMERI long bar	152
107	Skinny bar gage	154
108	Air-jacketed bar	154
109	NMERI ceramic bar	155
110	S-Cubed bar gage design	156
111	The S-Cubed armored bar	158
112	The S-Cubed unarmored bar gage on HURRICANE LAMP 3	158
113	The S-Cubed damped bar gage	159
114	Side-on mercury-coupled-bar static overpressure gage	160
115	The photoelastic sapphire bar gage technique	162
116	Schematic of ABTOAD detector development	164
117	Airblast time-of-arrival detector lines	165

FIGURES (Continued)

Figure	Page
118 The original blast gage station; (a) three-view sketch, (b) sensor array, and (c) exploded view of densitometer	166
119 Sketches of (a) the current blast gage head and (b) the beta-source module (500 mCi Pm-147, PHC 80955) which is mounted in the sting	167
120 Stand configurations for mounting gage heads in field trials; (a) single head and (b) vertical array of three heads	169
121 Schematic of density station	170
122 Density gage station in position under the Mylar membrane	171
123 Densitometer records from 1000-lb HE explosion	172
124 Probe/sensor configurations (dimensions: inches)	173
125 Schematic of anemometry systems electronics	174
126 Closeup, side-view photograph of anemometer probe holder assembly, Station 9 (R = 29.5 feet)	175
127 Rear view of anemometer probe holder assembly	176
128 Comparison of dynamic pressure vs. time histories obtained from TRW anemometry measurements with those obtained from BRL differential gage measurements, Shot 10	178
129 Miniature laser doppler velocimeter probe (SDL)	179
130 ISL LDV probe (SDL)	180
131 Flow diagram and photograph of a fluctuating wake	181
132 Vortex-shedding anemometer (top plate removed to expose 16.9 mm obstruction)	183
133 Calibration of the vortex-shedding anemometer (16.9 mm obstruction)	184
134 Geometrical layout of high-speed VSA	184
135 Field installation of three-channel vortex-shedding anemometer	185
136 Pre-shot views of the free-flight cylinder project	186
137 Pre-shot picture looking away from ground zero of steel sphere installation 30SB2	188
138 Trailer equipped with raster oscilloscope and camera system	190
139 WSMR multi-channel magnetic oscillographs mounted in recording trailer	191
140 CEC VR-3300 tape recorder	193
141 Honeywell 7600 tape recorder	194
142 Honeywell 101 tape recording van	195
143 SE-7000 magnetic tape recorder, vertical or horizontal useage, EMI SE Labs Ltd., Feltham, England, 1972	196
144 Leach recorder being placed in the ground prior to test	198
145 Digistar recorders	200
146 UK digital recording facility	201
147 The Pacific Instruments digital data recording system	203
148 Block design of an SDRS channel	204
149 First generation (original) HDAS electronics board (digital/memory side)	207
150 HDAS electronics board (top) and stycast-encapsulated board (bottom)	207

FIGURES (Continued)

Figure		Page
151	WES hardened data acquisition system	208
152	Gage components	209
153	Gage dimensions	209
154	Integrated single-channel, sensor-transient recorder	210
155	Integrated digital records	210
156	DRI DAAS system block diagram	212
157	DRI DAAS configuration	213

TABLES

Table		Page
1	Major high explosive test involvement of the USA	3
2	Passive gages	9
3	Mechanical self-recording time gages	9
4	Active devices: electronic sensors	10
5	Gage systems using sensors noted in Table 3	11
6	Recording systems for blast measurement	12
7	Cube, cube mass, face area, coefficients, and exponents for the power-law functions $D=aV^{**b}$ and $V=cD^{**e}$ derived from experiments over the desert surface at the test site	31
8	Fitted functions for dynamic pressure impulse versus cube displacement on 1000-pound (450-kilogram) charges	31
9	Fitted functions for dynamic pressure impulse versus average cube displacement for 2500-ton charges derived using data from MISERS GOLD, DISTANT IMAGE, and MINOR UNCLE	34
10	Peak overpressure for Anderson blasgage	39
11	Summary of properties of Foulness pattern standard piezo-electric transducers	86
12	Nominal MQ10 gage characteristics	87
13	Nominal FQ11C gage characteristics	88
14	Nominal MQ18 gage characteristics	89
15	Nominal MQ20 gage characteristics	90
16	Characteristics of BRL piezo-electric blast gages	102
17	BRL self-recording sensor characteristics	119
18	Summary of predicted sensor characteristics	138
19	Free flight drag sphere locations	187
20	Digi-Star stand-alone recorder	199

SECTION 1

INTRODUCTION

The high explosive era followed on the heels of the initial ban on the atmospheric testing of nuclear explosives in 1958. (A permanent ban on such tests occurred in 1963.) HE testing efforts were international in flavor from the very beginning. In 1959, researchers at the Suffield Experimental Station (now the Defence Research Establishment, Suffield), Alberta, Canada, were conducting airblast studies using block-built TNT charges of up to five tons. Word of such work reached former nuclear blast researchers at the Ballistic Research Laboratories, Aberdeen, Maryland, through international meetings. It wasn't long before the U.S. and Canada were joining forces to conduct HE tests at Suffield using the block-built TNT charge procedures they had developed. Expansion of the effort soon occurred and the researchers at AWRE, U.K., were involved. The charge configuration was a hemisphere at first and later became a sphere. Charges in sizes of 20 tons, 50 tons, 100 tons, and 500 tons were used and found to provide an effective simulation of nuclear airblast.

SECTION 2

HISTORY AND SUMMARY OF MEASUREMENTS

The first large-scale high explosive event took place at the Suffield Experimental Station, Canada, in 1964. This charge was 500 tons in weight and was configured as a hemisphere of 33-pound brick-size blocks of TNT. In the years to follow, large block-built TNT charges were configured as spheres using styrofoam as supplementary supports. In 1969, researchers who had been working with ammonium nitrate fuel oil (ANFO) saw their efforts bearing fruit when a 20-ton and a 100-ton charge were successfully detonated. ANFO provided a more cost-effective alternative to TNT and besides, TNT was becoming short in supply. Although the ANFO required a container, either bags or one made of fiberglass, it was found to be satisfactory in most respects and has continued to this day to be the explosive of choice for large-scale tests of 100 to 4000 tons.

Smaller 1000-lb castable charges were found to be very useful and cost-effective in studying blast wave phenomena. In 1959, a joint Canadian-US test series was conducted at Suffield using cast TNT spherical charges to examine height-of-burst effects. From this time forward, effective use of 1000-lb HE charges was made in research efforts to understand the complexities of various height-of-burst scenarios.

The high explosive discussed above was found to produce jetting, which of course resulted in disturbances to the desired blast wave. Jetting did not always occur in the direction of experiments, but when it did, major problems were encountered in interpreting the results. Although a great deal of work was carried out to eliminate these jets, nothing devised was able to solve the problem. For 1000-lb research, the TNT was replaced with Pentolite in an effort to overcome jetting and to gain a quality, repeatable explosive for high-fidelity testing. The Pentolite did not provide the quality desired and in the 80's an HMX-based material, TPH-3342 (later Arcadene 317) was tested and found to be an excellent source meeting the quality and repeatability requirement. However, it was noted the material is expensive and on some occasions produced some jetting, which fortunately was in a direction away from test areas. Work continues in the US to produce a cost-effective, quality explosive for 1000-lb to 20-ton sizes in castable form.

Summarized in Table 1 are the major high explosive tests of 1000 lbs or larger where the US has been involved. Information as to such tests conducted by other MABS countries was unavailable. Shown in Figure 1 is a photograph of a multi-ton HE detonation. Figure 2 is a photograph of a multi-burst, two 1000-lb height-of-burst HE detonation.

The instrumentation used successfully on nuclear events was directed toward blast measurements from the high explosive. Gages that measure long-duration blast waves were now to measure durations considerably shorter in time. Some gages did not have the response capability to accurately record the blast wave. Thus, gages and recording systems were developed having higher response times and the capability to adequately record the phenomena.

Many of the questions that were raised during the nuclear era remained not fully answered; the high explosive simulation techniques provided the opportunity to investigate these issues

Table 1. Major high explosive test involvement of the USA.

Item	Operation/Test	Year	Number of Shots	Charge Wt.	Charge Position	Explosive	Location of Test
1	SUFFIELD	1959	1	5T	Surface Hemisphere	TNT-BLK	DRES
2	SUFFIELD	1960	1	20T	Surface Hemisphere	TNT-BLK	DRES
3	SUFFIELD	1961	1	100T	Surface Hemisphere	TNT-BLK	DRES
4	FLATTOP	1963	3	20T	Surface Sphere	TNT-BLK	NTS
5	BLOWDOWN	1963	1	50T	Tower Hemisphere	TNT-BLK	Iron Range, Australia
6	SNOW BALL	1964	1	500T	Surface Hemisphere	TNT-BLK	DRES
7	SAILORHAT	1965	3	500T	Surface Hemisphere	TNT-BLK	Hawaii
8	DISTANT PLAIN	1966-67	8	20-100T	Surface, Tower, Sphere, Hemisphere	TNT-BLK, Propane in Balloon	DRES
9	PRAIRIE FLAT	1968	1	500T	Surface Sphere	TNT, BLK	DRES
10	MINESHAFT	1968	2	100T	Surface Sphere	TNT, BLK	Utah
11	ANFO (1)	1969	2	20T	Surface Hemisphere	ANFO	DRES
			1	100T	Surface Hemisphere	ANFO	DRES
12	HOB - BRL, DRES	1969	10	1000 lb.	HOB	TNT	DRES
13	MINERAL ROCK	1969	1	100T	Surface Sphere	TNT	Utah
14	DIAL PACK	1970	1	500T	Surface Sphere	TNT	DRES
15	ANFO (2)	1971	2	24T	1-Surface Sphere, 1-Sphere	ANFO	DRES
16	MIDDLE GUST	1971	2	1-20T, 1-100T	Surface Sphere	TNT	Colorado
17	MIXED COMPANY	1972	1	500T	Surface Sphere	TNT	Colorado
18	PRE-MINE THROW	1973-74	2	1-7T, 1-100T	Surface Sphere	Nitro-Methane	NTS
19	DIPOLE WEST	1973-75	24	216 & 1000 lb.	HOB Sphere	TNT, Pentolite	DRES
20	PRE-DICE THROW II	1975	2	1-100T, 1-120T	Surface Sphere Cylinder	TNT ANFO	WSMR
21	PRE-DICE THROW	1976	1	600T	Surface Hemisphere	ANFO	WSMR
22	MISERS BLUFF	1977-78	3	1-1000 lb, 2-118T	Surface Hemisphere	ANFO	WSMR, Arizona

Table 1. Major high explosive tests of the USA (Continued).

Item	Operation/Test	Year	Number of Shots	Charge Wt.	Charge Position	Explosive	Location of Test
23	MIGHTY MACH	1978-82	36	64, 216 1000 lb.	HOB Sphere	Pentolite	DRES
24	MILL RACE	1981	1	600T	Surface Hemisphere	ANFO	WSMR
25	DISTANT RUNNER	1981	2	120T	Surface Hemisphere	ANFO	WSMR
26	PRE-DIRECT COURSE	1982	1	24T	Tower Sphere	ANFO	WSMR
27	DIRECT COURSE	1983	1	600T	Tower Sphere	ANFO	WSMR
28	HOB 83	1983	5	216 & 1000 lb.	HOB Sphere	Pentolite	DRES
29	MINISCALE I, II	1984-85	2	22T		ANFO	WSMR
30	HOB 84	1984	5	216 & 1000 lb.	HOB Sphere	Pentolite	DRES
31	MINOR SCALE	1985	1	4740T	Surface Hemisphere	ANFO	WSMR
32	DIAMOND ARC	1985-87	10	1000 lb.	HOB Sphere	8-HMX 2-Ireset	DRES
33	MISTY PICTURE	1987	1	4685T	Surface Hemisphere	ANFO	WSMR
34	MISTY PORT	1988	3	1000 lb.	1-DOB, 2-HOB Sphere	2-Pentolite, 1-Nitro Methane	WSMR
35	MISERS GOLD	1989	1	2440T	Surface Hemisphere	ANFO	WSMR
36	MIDNIGHT HOUR	1989	2	1000 lb.	DOB Sphere	Nitro-Methane	WSMR
37	MINERAL FIND	1990	3	1000 lb.	HOB Sphere	HMX	WSMR
38	HURRICANE LAMP	1991	4	1000 lb.	HOB Sphere	3-HMX, 1-ATX-25R-M	WSMR
39	DISTANT IMAGE	1991	1	2650T	Surface Hemisphere	ANFO	WSMR
40	MIDDLE KEY	1991	3	1000 lb.	HOB Sphere	ATX-25R-M	WSMR
41	MINERAL FIND 6	1991	1	855 lb.		DET/Deta Sheet	WSMR
42	MINOR UNCLE	1993	1	2500T	Surface Hemisphere	ANFO	WSMR

Table 1. Major high explosive tests of the USA (Concluded).

FOREIGN

Item	Operation/Test	Year	Number of Shots	Charge Wt. Up to 75T	Charge Position	Explosive	Location of Test
43	STACK FRAGMENTATION	1980-91				NEQ TNT	Woomer, Australia

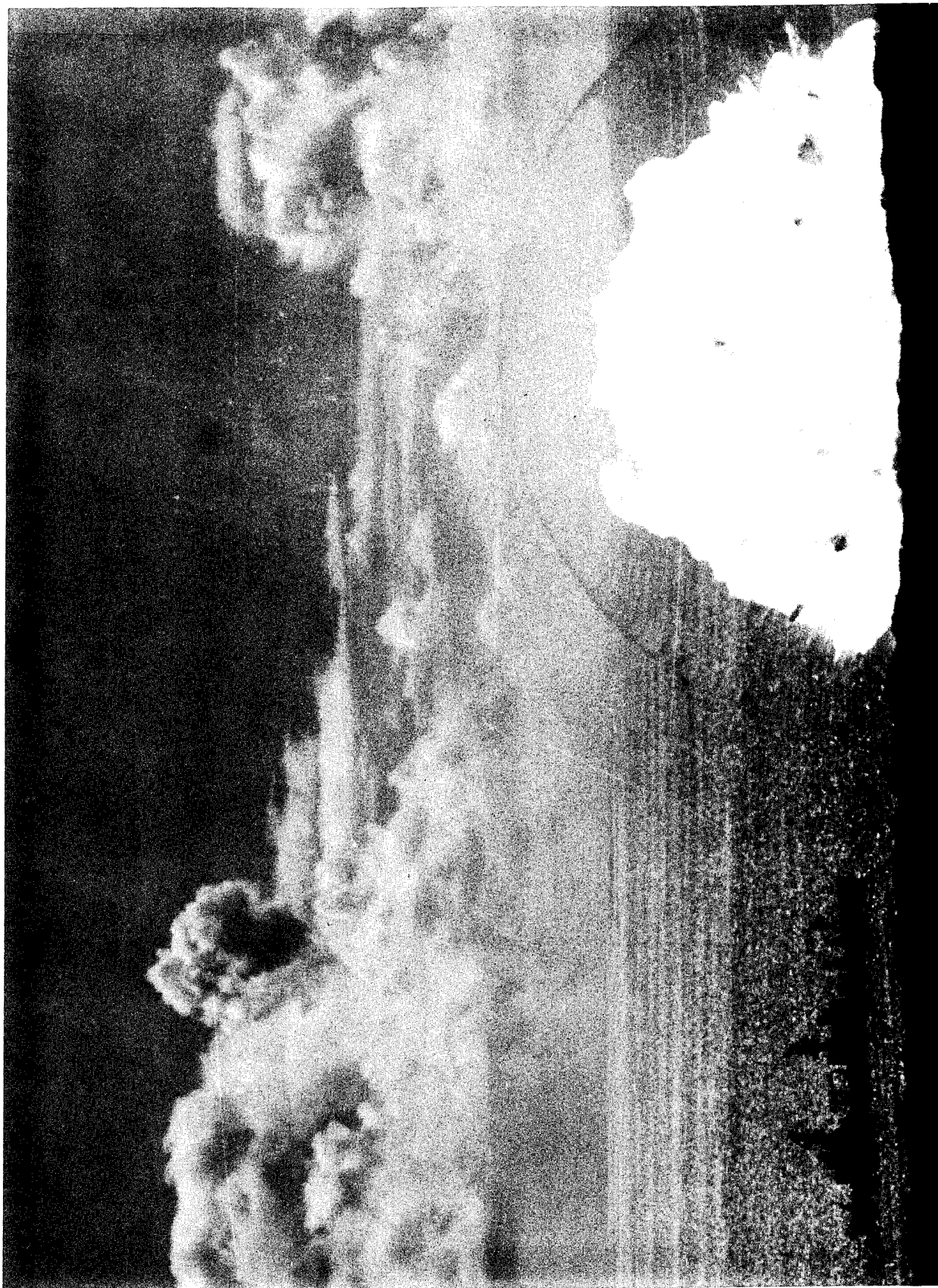


Figure 1. Multi-ton (500-ton) explosion.

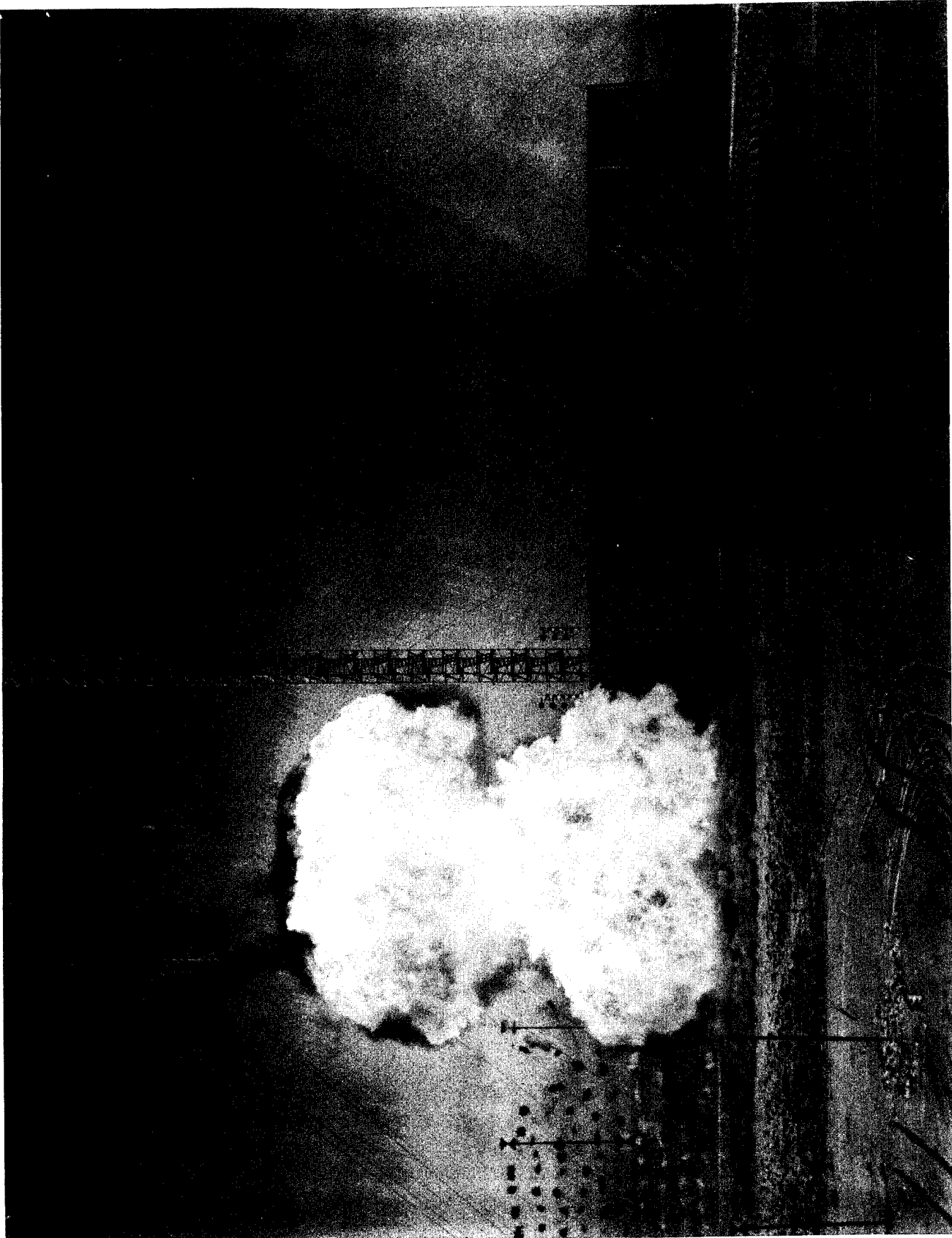


Figure 2. Multi-burst (two 1000-lb) explosion.

further. In the 60's, computer technology was developing and used to generate predictions of airblast phenomena. HE tests were used to verify and adjust such prediction techniques.

Some of the issues addressed by the testing in the high explosive era were: (1) target response, (2) height of burst, height of target, (3) dynamic pressure in high and low pressure areas, (4) Mach reflection, irregular Mach, (5) multi-burst, (6) precursor simulation, (7) blast in forest, and (8) dust entrainment. Instrumentation and measurement techniques to address these issues are discussed. These are summarized in Tables 2 through 6.

A layout of a multi-ton HE test bed is provided in Figure 3. Figure 4 presents a photograph of a multi-burst HOB HE test bed.

Table 2. Passive gages.

	<u>Gage</u>	<u>Country</u>	<u>Period</u>	<u>Charge Size*</u>
1	Bursting Diaphragm	Australia	80s to present	small to large
2	DPI (Dynamic Pressure Impulse)	Australia	60s, 80s, 90s	large
3	Cantilever Drag	Canada	60s, 90s	small to large
4	Cube Displacement	USA	60s, 80s, 90s	small to large
5	Jeep Vehicles	USA	50s to 80s	large
6	Lead Diaphragms	Finland	80s, 90s	small to large
7	Deformation Gage	Canada	60s	medium to large
8	Squirt Gage	Canada	60s	medium to large
9	Free Flight Drag Spheres	USA	60s, 70s	medium to large
10	Fiber Optic Bier Gage	USA	90s	large

* Large is defined as 500 tons or greater.
Medium is defined as 20 tons to 500 tons.
Small is defined as 1000 lbs. to 20 tons.

Table 3. Mechanical self-recording time gages.

	<u>Gage</u>	<u>Country</u>	<u>Period</u>	<u>Charge Size*</u>
	BRL Family of Gages	USA	60s	medium to large

* Large is defined as 500 tons or greater.
Medium is defined as 20 tons to 500 tons.
Small is defined as 1000 lbs. to 20 tons.

Table 4. Active devices: electronic sensors.

	<u>Sensor</u>	<u>Country</u>	<u>Era</u>	<u>Charge Size*</u>
A.	<u>Blast Switch</u>			
	ABTOAD	Canada	60s	small to medium
B.	<u>Reluctance Type</u>			
	WIANCKO 3 PAD	USA	40s - 60s	medium to large
	KAMAN K-1205	USA	60s	medium to large
	PACE P-7	USA	60s	medium
	CCC GAGE	USA	60s	medium to large
C.	<u>Resistive Type</u>			
	NORWOOD/DETROIT CONTROLS	USA	60s	medium
	DYNISCO	USA	60s	medium
	CEC (CONSOLIDATED ELECTRO DYNAMICS CORP.)	USA	60s	medium
	MICROSYSTEMS	USA	60s	medium
	SHAEVITZ-BYTREX BYTREX	USA	60s, 70s	small to medium
	HAT GAGE (BRL)	USA	60s	medium
	ENERTEC CZ 1023	France	80s, 90s	small
	ENDEVCO 8500	France	80s, 90s	small
	KULITE HK SERIES	USA, France, GBR	80s, 90s	small to medium
	STRAIN GAGES, MOUNTED ON ELEMENTS	USA	60s	small to medium
	STATHAM	USA	60s	small
D.	<u>Capacitance</u>			
	PHOTOCON DYNAGAGE	USA	60s	small to large
E.	<u>Piezoelectric</u>			
	KISTLER	European	70s - 90s	small to medium
	ATLANTIC RESEARCH	Canada	60s	small to medium
	LC33, CL60, BC33, CZ, LZP			
	SUSQUEHANA INSTRUMENTS	USA	60s - 80s	small
	PCB, PIEZOTRONICS	All	70s - 90s	small to medium
	ENDEVCO 2501	France	70s - 90s	small to medium
	UK-FQ11C, (B2) MQ10, MQ18, MQ20, MQ23	GBR	60s	small
	ZINC OXIDE CHIP	USA	80s	small to medium
F.	<u>Other</u>			
	BAR			small to large
	GEN ATOMIC QUARTZ	USA	60s	small to large
	SRI QUARTZ BAR	USA	60s	small to large
	WES Bar	USA	80s - 90s	small to large
	S ³ Bar	USA	80s - 90s	small to large
	NMERI Bar	USA	80s - 90s	small to large
	ST4 PIEZOELECTRIC	USA	50s - 90s	small to large
	CERF PIEZORESISTIVE	USA	70s	small to large
	PHOTOELASTIC SAPPHIRE	USA	90s	large
	DRES BETA DENSITOMETER	Canada	60s, 80s, 90s	small to medium
	HOT WIRE ANEMOMETRY	USA, GBR	60s, 80s	small to medium
	LASER VELOCIMETRY			
	VORTEX-SHEDDING ANEMOMETER			
	FREE FLIGHT CYLINDERS			

* Large is defined as 500 tons or greater.

Medium is defined as 20 tons to 500 tons.

Small is defined as 1000 lbs. to 20 tons.

Table 5. Gage systems using sensors noted in Table 3.

<u>System</u>	<u>Country</u>	<u>Era</u>	<u>Charge Size*</u>
KAMAN VORTEX SHEDDING ANEMOMETER	USA	60s	medium to large
SRI MAD GAGE (ULTRADYNE)	USA	50s - 60s	large
SC GREG GAGE (WIANCKO/ULTRADYNE)	USA	50s - 60s	large
SC SNOB GAGE (WIANCKO/ULTRADYNE)	USA	50s - 60s	large
BRL - BIAXIAL DRAG GAGE (SHAEVITZ-BYTREX LOAD CELL)	USA	60s	medium to large
H-TECH - SNOB GAGE	USA	80s- 90s	small to large
H-TECH - GREG GAGE	USA	80s - 90s	medium to large
CRC - SNOB GAGE	USA	80s - 90s	small to large
CRC - GREG GAGE	USA	80s - 90s	medium to large
BRL - DIFFERENTIAL GAGE (KULITE XCW-8WN SERIES)	USA	80s - 90s	small to large
BRL - CANTILEVER (STRAIN INSTRUMENTED)	USA	60s	small to medium
SRI - TOTAL DRAG PROBE	USA	60s	medium to large
SRI - BRL DRAG FORCE GAGE	USA	60s	medium to large
AFWL HIGH-PRESSURE GAGE	USA	80s	medium to large
NMERI SNOB PROBE	USA	80s	medium to large
BRL CANTILEVER	USA	60s	medium to large
INTERNAL STRAIN GAGE	USA	80s	medium to large
DRES DRAG CYLINDERS	CANADA	60s	medium to large
KKQ	USA	60s	medium to large
GR PITOT PRESSURE	GERMANY	80s	medium to large

* Large is defined as 500 tons or greater.

Medium is defined as 20 tons to 500 tons.

Small is defined as 1000 lbs. to 20 tons.

Table 6. Recording systems for blast measurements.

	<u>Recorder</u>	<u>Country</u>	<u>Era</u>	<u>Charge Size*</u>
A.	<u>Oscillograph</u>			
	CEC SYSTEM D	USA	60s - 70s	small to large
	CEC SYSTEM E	USA	60s - 70s	small to large
B.	<u>Oscilloscope</u>			
	RASTER OSCILLOSCOPE & CAMERA	USA	60s - 80s	small to large
	MILLER CATHODE-RAY-TUBE OSCILLOGRAPH	USA	50s - 60s	small to large
	OSCILLOSCOPE FIXED CAMERA	GBR	50s - 60s	small to large
	4-6 CH. CRT PHOTOGRAPHED BY REVOLVING DRUM	GBR, USA	50s - 60s	small to large
C.	<u>Magnetic Tape</u>			
	AMPEX	USA	40s - 80s	small to large
	WEBSTER-CHICAGO	USA	50s	small to large
	LEACH FM SYSTEM	USA	60s	small to large
	GENISCO	USA	60s	small to large
	PEMCO FM	USA	70s	small
	HONEYWELL 101	USA	70s - 90s	small to large
	SANGAMO 4784	USA	70s - 80s	small to large
	BELL & HOWELL VR 2800, 3300	USA	70s - 80s	small to large
	DAQ - PAC (GATX)	USA	60s	
D.	<u>Digital</u>			
	BSI DIGISTAR	Canada	80s - 90s	small to large
	PACIFIC INSTRUMENTS	USA	80s - 90s	small to large
	KAMAN NUCLEAR HARDENED SELF-CONTAINED	USA	80s	small to large
	WES HARDENED SELF-CONTAINED	USA	80s - 90s	small to large
	AVL INTEGRATED SINGLE-CHANNEL	Austria	90s	small to large
	DRI DAAS SYSTEM DRI	All	90s	small to large

* Large is defined as 500 tons or greater.
Medium is defined as 20 tons to 500 tons.
Small is defined as 1000 lbs. to 20 tons.

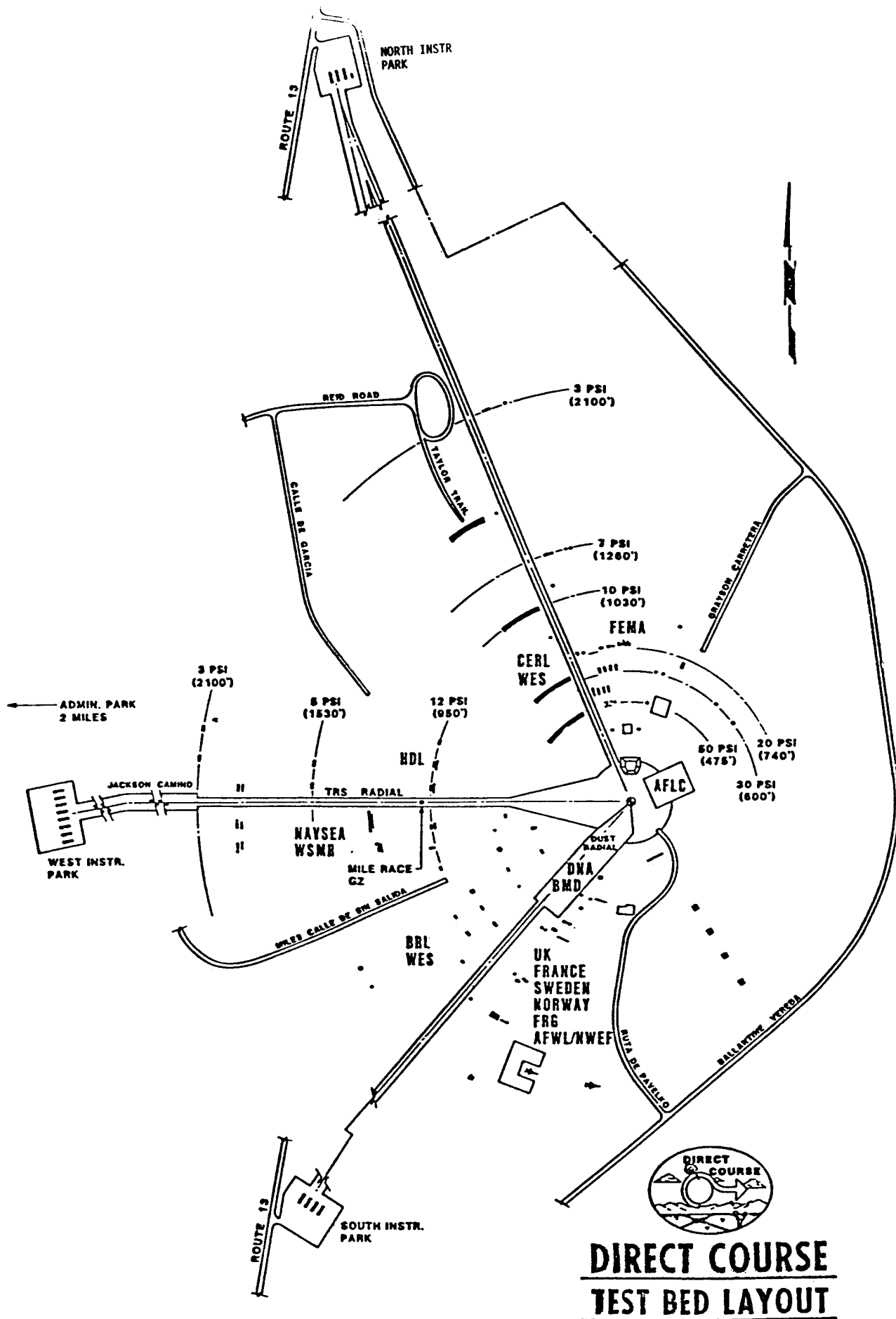


Figure 3. Test bed for multi-ton trial, Operation Direct Course.

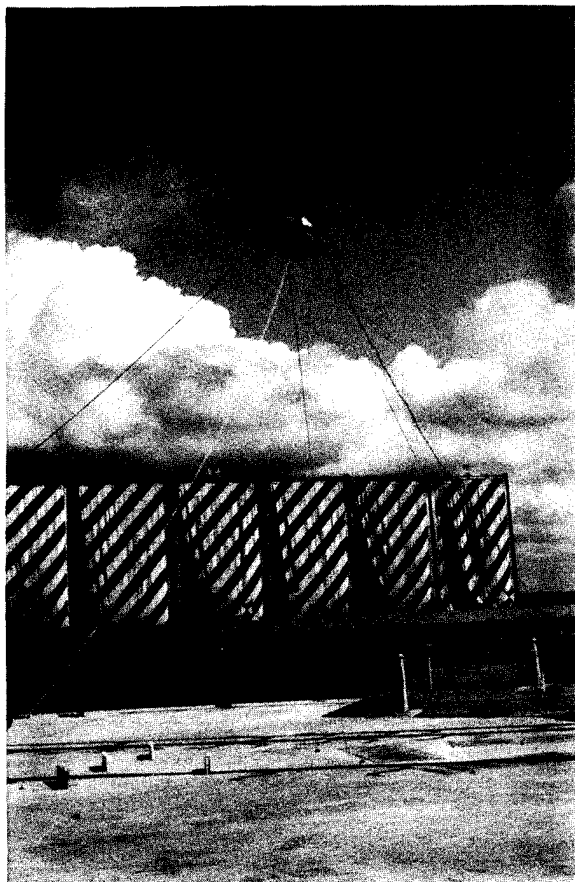


Figure 4. Test bed for 1000-lb HE trial.

SECTION 3

FREE-FIELD PASSIVE DEVICES, PRESSURE SENSING

3.1 DISPLACEMENT SYSTEMS.

3.1.1 Canadian Wire (Cantilever) Drag Gages (Canada) (1961).

Wire drag gages were first introduced by Canada in 1961 on a 100-ton HE test program. The gage saw little use after the 60s until the 90s when it was updated and deployed on many test programs.

The wire drag gage consists essentially of a heavy plate into which are clamped vertically six lengths of cylindrical solder wire. The wire used was 0.04-in. diameter Kester solid wire solder 50% tin, 50% lead. It extended 2 inches above the plate. The mounting plate is 18 inches long by 10 inches wide and 1 inch thick in the uniform central region. Two interlocking halves are bolted together to firmly clamp the wires in holes drilled in the line of separation of the two sections. A stand is used to support the gage 2 feet above the ground to avoid damage by dust and pebbles lofted by the blast.

These gages were designed as a simple and economical sensor that would respond to the dynamic forces of a blast wave. They would be used to give the approximate yield of an unknown charge, the direction of ground zero, and to test the symmetry of the blast wave around the charge. Figure 5 shows the standard gage and Figure 6 shows the standard wire gage after the blast.

The response of a cantilever to an impulse was determined by DRES and is quoted here:

"Consider an impulse I perpendicular to a simple cantilever of length $2L$. The moment of the impulse will equal the change of angular momentum:

$$\text{i.e. } IL = M$$

where M is the moment of inertia.

The initial kinetic energy of the cantilever is

$$\frac{1}{2} M \dot{\theta}^2 = \frac{1}{2} \frac{I^2 L^2}{M}$$

If the cantilever comes to rest after bending through an angle θ and the work done to bend the wire is W per degree of bending, then $\frac{1}{2} \frac{I^2 L^2}{M} = W\theta$ (neglecting the loss of potential energy due to the lowering of the center of gravity).



Figure 5. Standard wire gage on two-foot stand.

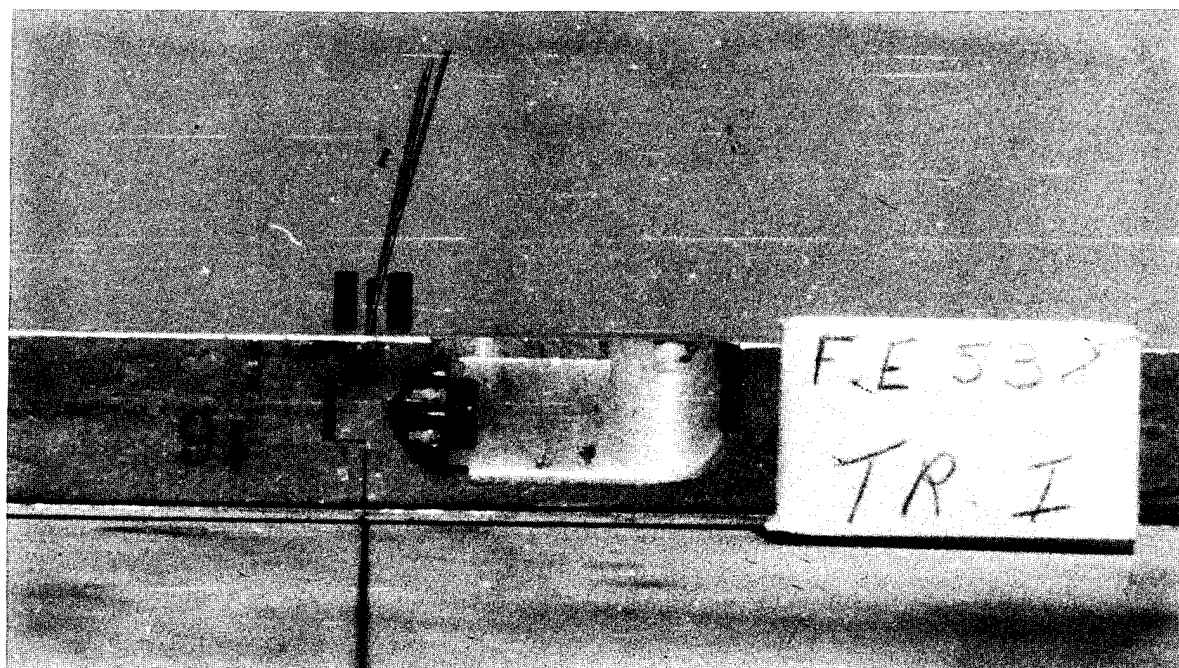


Figure 6. Standard wire gage after the blast.

i.e. Applied impulse is proportional to the square root of the angle of bending.

The assumption that the work done to bend the wire is proportional to the angle of bending is only valid if the stress-strain relationship for the wire can be idealized to a form shown in Figure 7, and if the strain to the elastic limit is small. Laboratory tests have shown that the wire ceases to bend elastically after approximately 8 degrees."

These gages were first used on tests involving charges of from 8 lbs to 20 tons in the early 1960s. Results confirmed that they could be used as a simple, immediately measurable and economical yield and GZ indicator.

Since this gage has a very limited pressure range, e.g. for 100-ton shot from 8 psi to 4 psi, it was postulated at that time that other cantilever gages could be developed for use at higher pressures.

Nearly 30 years later in the early 1990s, cantilever gages were studied and deployed on large (kiloton size) tests to cover a pressure range of 3-200 psi. These gages were made from materials that would either be permanently deformed after being strained beyond their elastic limit or be fractured if strained beyond a small amount. Each cantilever consisted of a rod or wire fixed at its base. Rods of a large diameter were fixed in concrete as shown in Figure 8. A post-shot view is seen in Figure 9. Solder wires were mounted on a platform stand as illustrated in Figure 10. Cantilevers of various materials, diameters, and lengths can be used. Recent tests used three different aluminum alloys, cold rolled steel 1018 and solder 50/50 tin/lead. The larger cantilevers were circular in cross-section and varied in diameter from 1 inch to 0.04 inches and in length from 5.6 feet to 0.8 inches. The smaller cantilevers had diameters which ranged from 0.06 inches to 0.04 inches and were supported on streamlined platforms 2 feet above the ground.

Brittle cantilevers were made of graphite pencil leads and were designed to break at certain levels of dynamic pressure depending on their length.

Results have shown that the wire solder cantilever can be modeled by using the rigid-plastic assumption. Those cantilevers which are constructed from aluminum and steel cannot use this assumption; these materials have other properties governing their response such as elasticity, strain rate hardening and strain hardening which the simple model does not take into account. Finite element techniques were developed taking these into account and used in the analysis. Results showed these gages provide reasonable estimates of peak dynamic pressure and peak dynamic pressure impulse.

Ref: Dewey, J., "Surface Burst of a 100-ton TNT Hemispherical Charge Wire Drag Gage Measurement," Suffield Tech. Note 80, 1962.

"DISTANT IMAGE Cantilever Gauges," DISTANT IMAGE Symposium Report POR 7379-5, 1992.

3.1.2 Australian DPI Gage (Australia) (1964).

The Australian DPI gage was deployed in 1964 and 1966 on large HE test programs. It was again used in 1993.

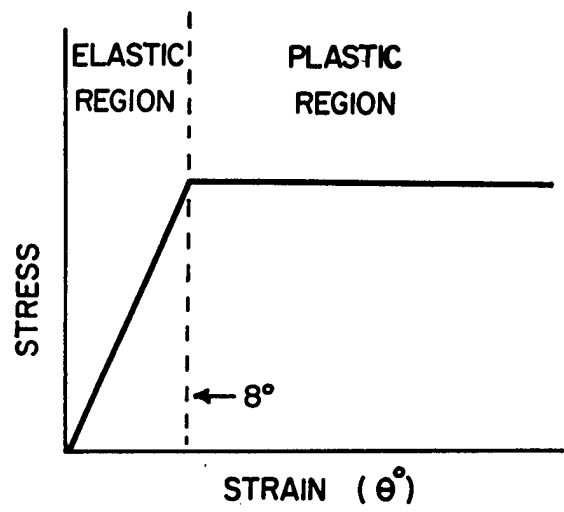


Figure 7. Idealized stress-strain relationship.

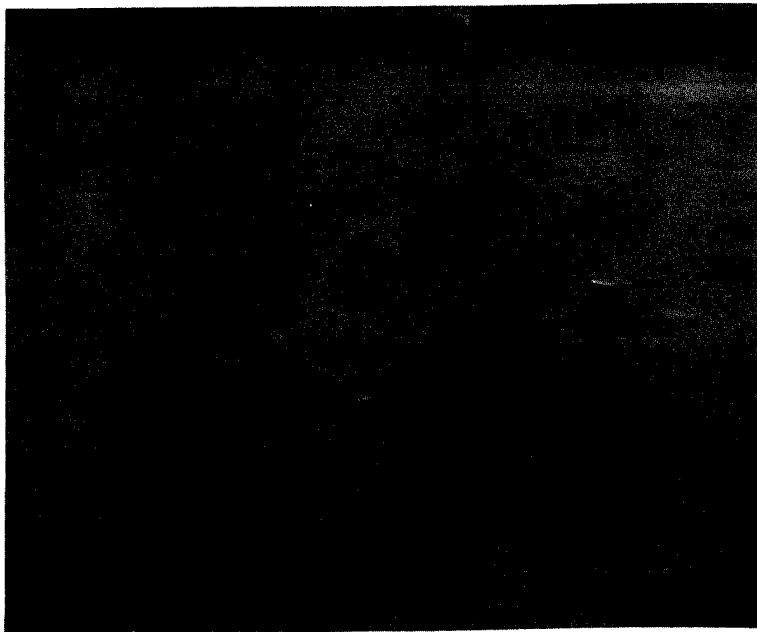


Figure 8. Ground-mounted steel and aluminum cantilevers.

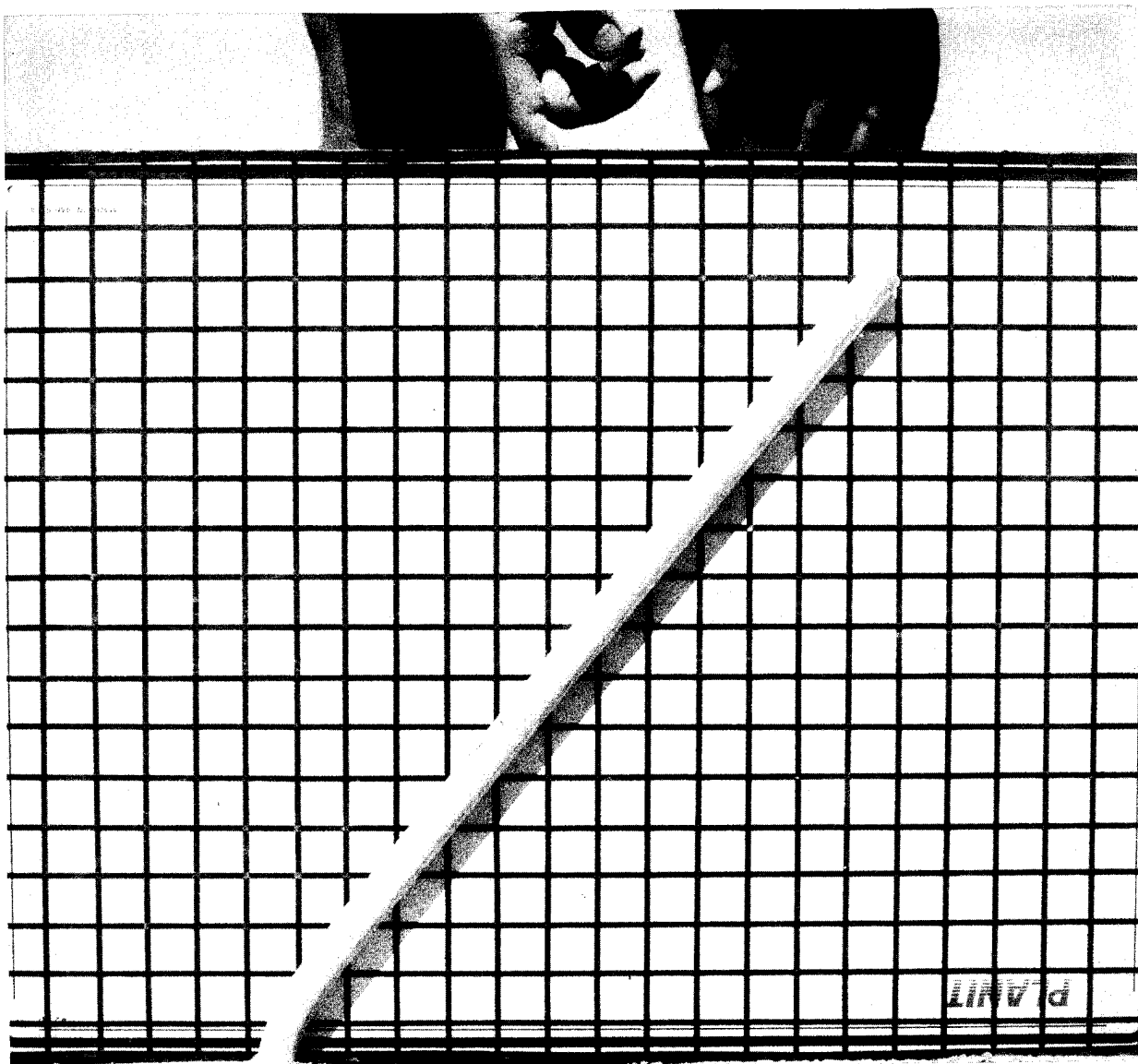


Figure 9. Deformed cantilever at a distance of 296 m showing that the majority of the bending occurs at the base.

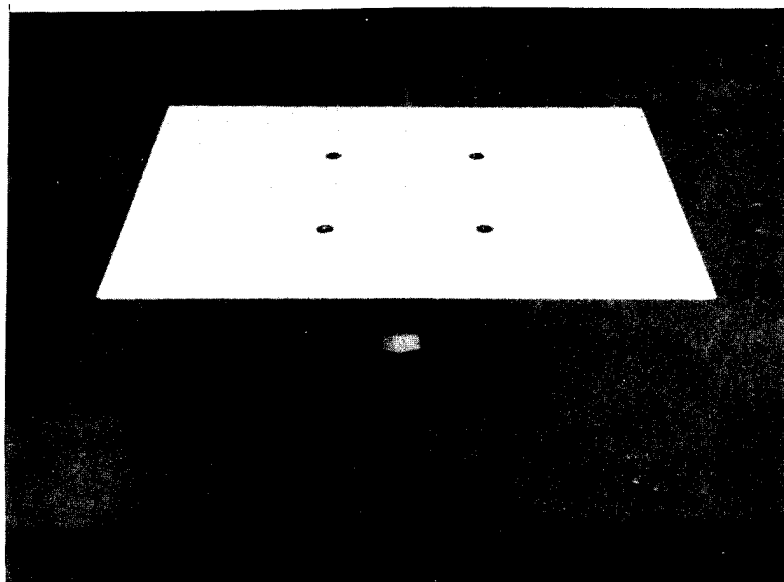


Figure 10. A set of platform-mounted solder cantilevers.

The gage consists of a rigid stem and a cylindrical head supported by a flexible aluminum strip or "hinge" at its base. When a shock wave passes the gage, it receives an impulse from the dynamic pressure causing it to deflect in the direction of particle flow until the energy imparted to the gage is lost in the plastic deformation of the aluminum strip. Hence, the permanent bend in the aluminum strip is a measure of the dynamic pressure impulse of the shock wave.

To make the gage sensitive to only the DPI, it was necessary to make the quarter period of the gage long compared with the positive phase duration of the blast wave so that the restoring force on the gage is small compared with the deflecting force and the gage velocity will be small compared with the air particle velocity during the major part of the DPI.

Gages have been used over a range from 16 to 400 psi-msec and with charges 500 tons to 100 lbs on Operations Blowdown and Distant Plain. The gage has been calibrated using wind tunnel shock tube facilities and the theoretical behavior verified. The range of the gage can be changed by the use of different frontal areas while keeping the mass the same. They can be used both in an upright or inverted position depending upon the most suitable mounting arrangement.

The gage is illustrated in Figures 11 through 13.

Ref: Williams, D. A., "A Deformation Gauge for Measurement of Dynamic Pressure Impulse of Shock Waves, Australian Defence Standards Laboratories, Technical Note 72. September 1964.

Keefer, J. H., "Australian Dynamic Pressure Impulse Measurements Note," Operation Distant Plain.

3.1.3 DRES Deformation Gage (Canada) (1960s).

The DRES deformation gage consisted of a deformable sheet metal cap installed over the open end of a short pipe; the other end of the pipe was closed. The metal used was a soft metal, usually aluminum or copper. Deformation of the cap was measured in terms of the volume of concavity rather than simply its depth. These gages were used to measure static overpressure/impulse.

To measure stagnation pressure/impulse, the deformable element was sandwiched between two orifice plates.

Brittle diaphragms constructed of cellophane or thin glass were placed in various housings to provide a "more than" indication of the overpressure level.

Calibration of these devices was made in a shock tube.

Ref: Muirhead, J. C., et al., "Some Self-Recording Pressure Indicators," DRES-TW-118, 63-0527, 1963.

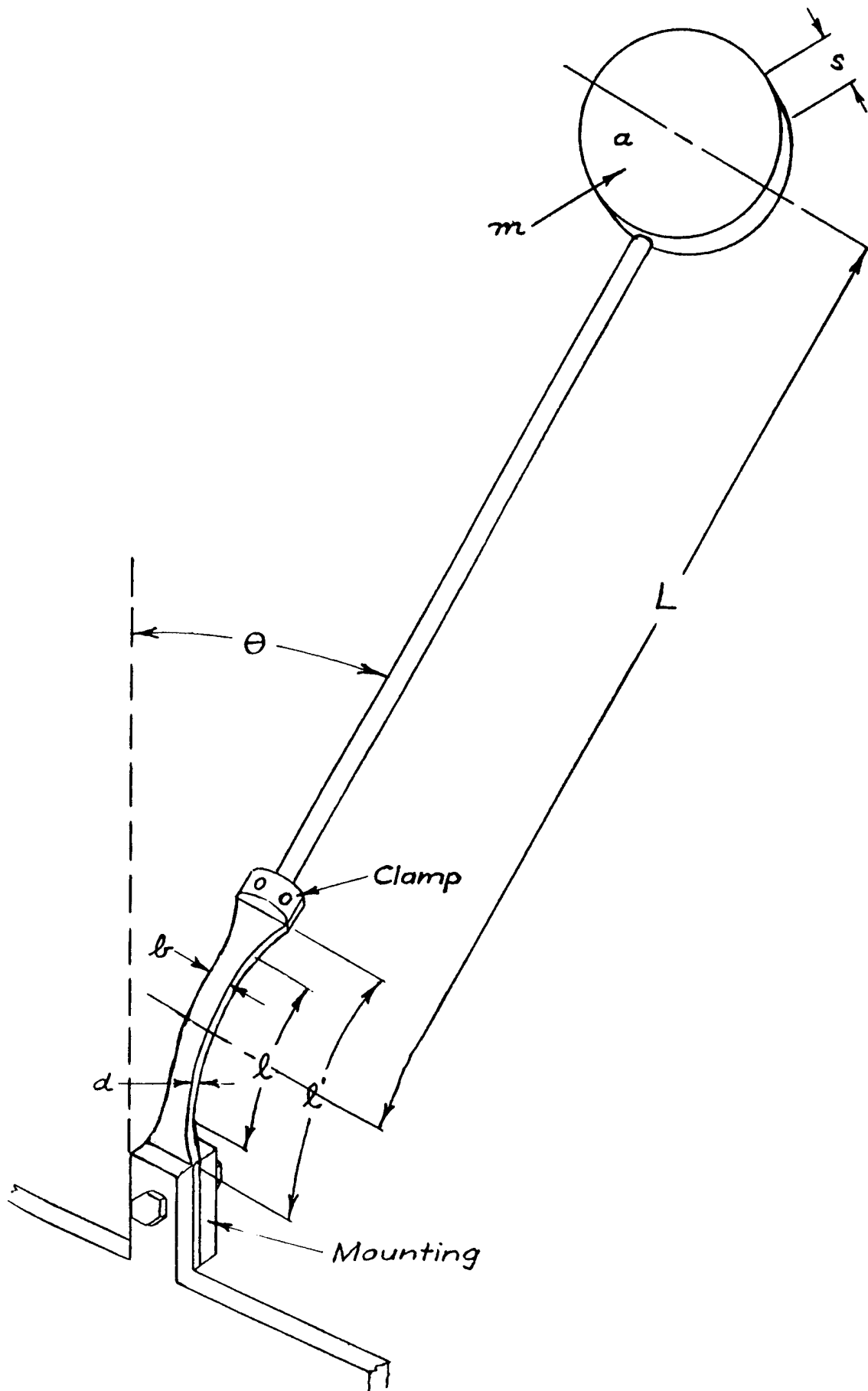


Figure 11. Schematic of DPI gage.

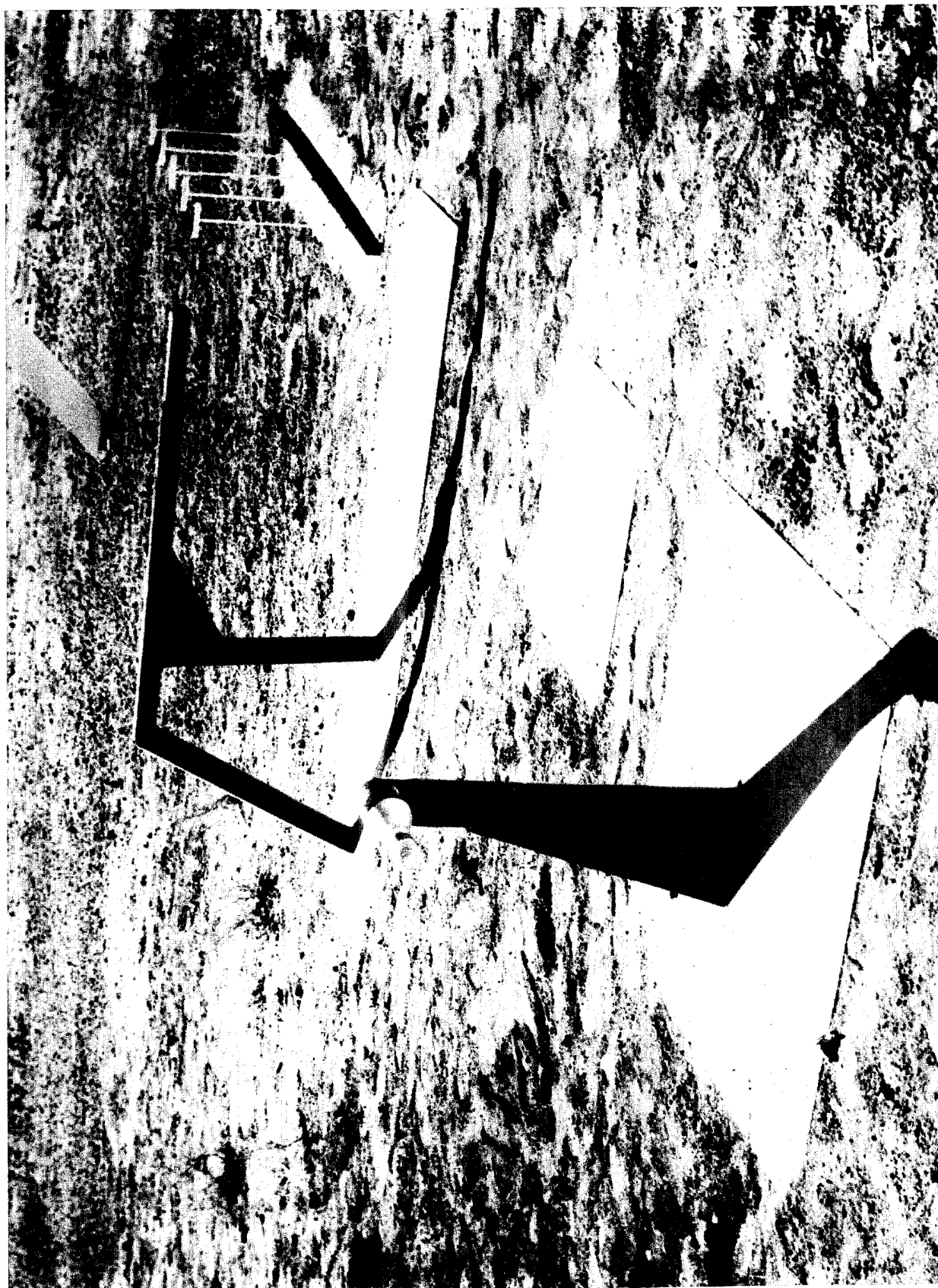


Figure 12. Pre-shot DPI gage installation.

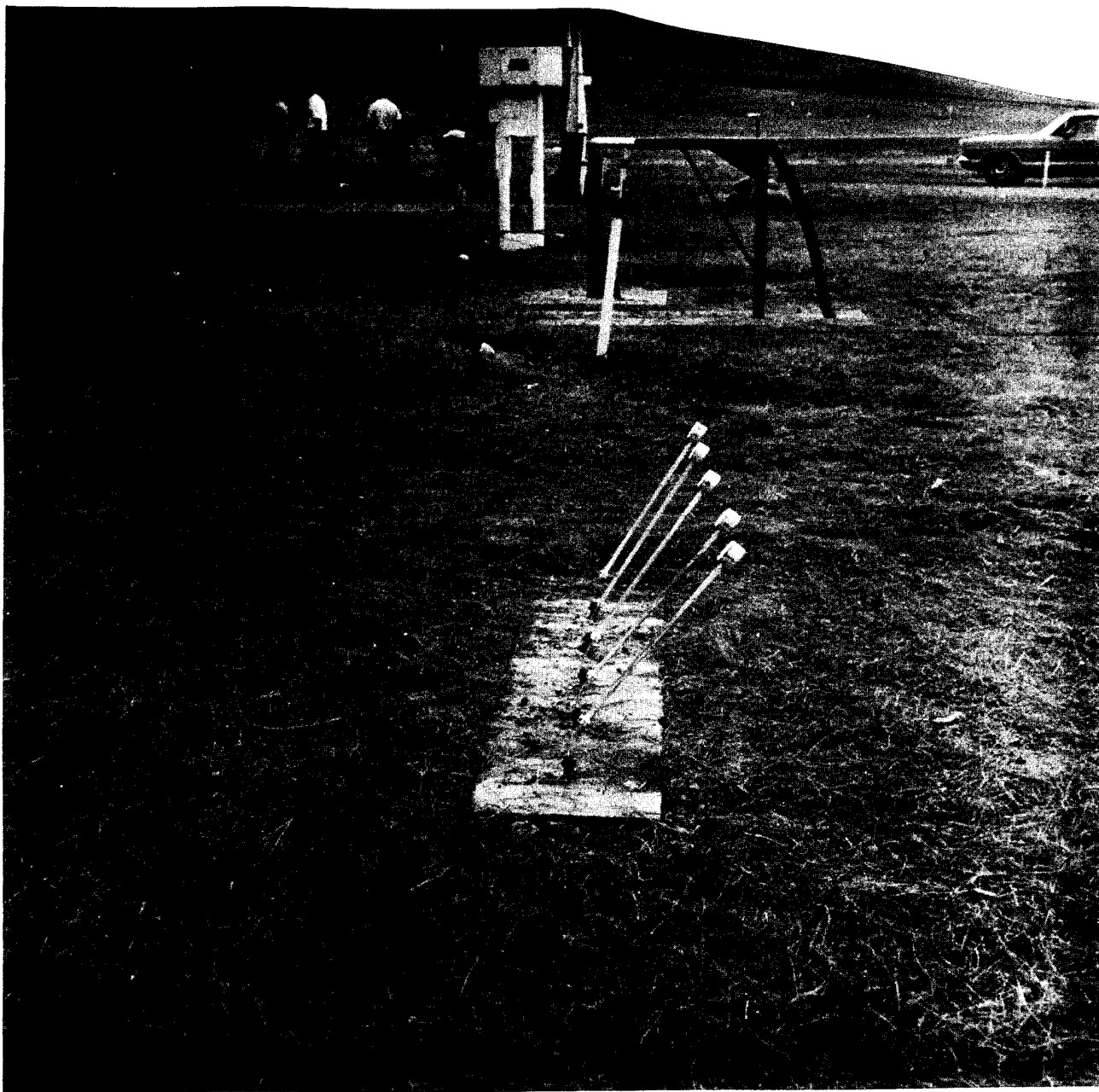


Figure 13. Post-shot view of DPI gages.

3.1.4 DRES Fluid Ejection (SQUIRT) Gage (Canada) (1960s).

The DRES fluid ejection gage consisted of an open-topped well containing the fluid (colored water) out of which extended a small diameter spray pipe, see Figure 14. The application of pressure to the fluid in the open top of the container caused a quantity of the liquid to squirt from the spray pipe onto a recording paper. The distance the stream reached and the quantity ejected provided an indication of the overpressure experienced.

The same principle described above was used in an ink jet gage labeled "squirt gage," see Figure 15. Ink was used as the liquid in the squirt gage.

For low pressure measurements, a mildly acidic water was contained in an open-topped metal tin whose thin walls were perforated by a ring of tiny holes, see Figure 16. The diameter of the holes varied around the ring. Surface tension of the water prevented any leaking of the water through the holes; when a blast wave passed over the gage, water would flow through all or some of the holes and be absorbed by a recording strip of litmus paper. The size of the smallest hole from which the water ran was correlated to the overpressure applied.

The range of the gage was 0.015-0.15 psi.

In another design, drops of mercury were contained in a ring of small reservoirs in a 0.25-inch steel plate, see Figure 17. Beneath the reservoir plate was an orifice disc with a ring of small holes, one for each reservoir. The holes around the ring varied in diameter over a small size range. Surface tension of the mercury prevented it from passing through the small holes until the overpressure of the blast wave acted on it. A lucite collector with a well for each reservoir was installed beneath the orifice disk to collect the mercury which passes through the orifice. As with the water tension gage described above, the size of the hole through which the mercury passed was a measure of the overpressure applied.

The range of the gage was 0.05-1.2 psi.

Problems noted with these gages were:

1. Moisture loss if in place for many days prior to the event.
2. Ink hardening in the spray pipe if extended hours occur before the event.
3. Contamination by dust or oxidation.

Ref: Muirhead, J. C., et al., "Some Self-Recording Pressure Indicators," DRES-TN-118, 63-0527, 1963.

3.1.5 Cubes (USA) (1986).

The displacements of cubes by blast have been used on both large and small-scale HE experiments and on an underground magazine trial to investigate uniformity of loading on an arc, effective flow direction, and impulse due to flow. The results are discussed in the referenced MABS13 paper, and some are summarized here. The cubes used were 1.75 inches (44 mm), 2 inches (51 mm), and 6 inches (152 mm) on an edge, and constructed of several types of wood, aluminum, and steel. Small 0.39-inch (10-mm) cubes have been used on some undocumented shock tube experiments.

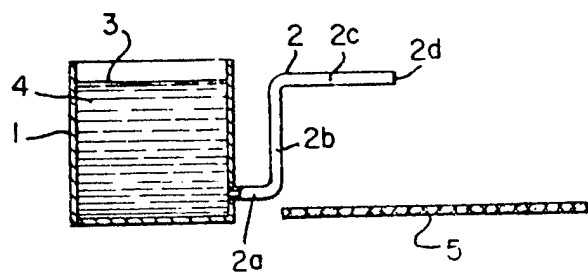


FIG. 5

Figure 14. DRES fluid ejection gage.

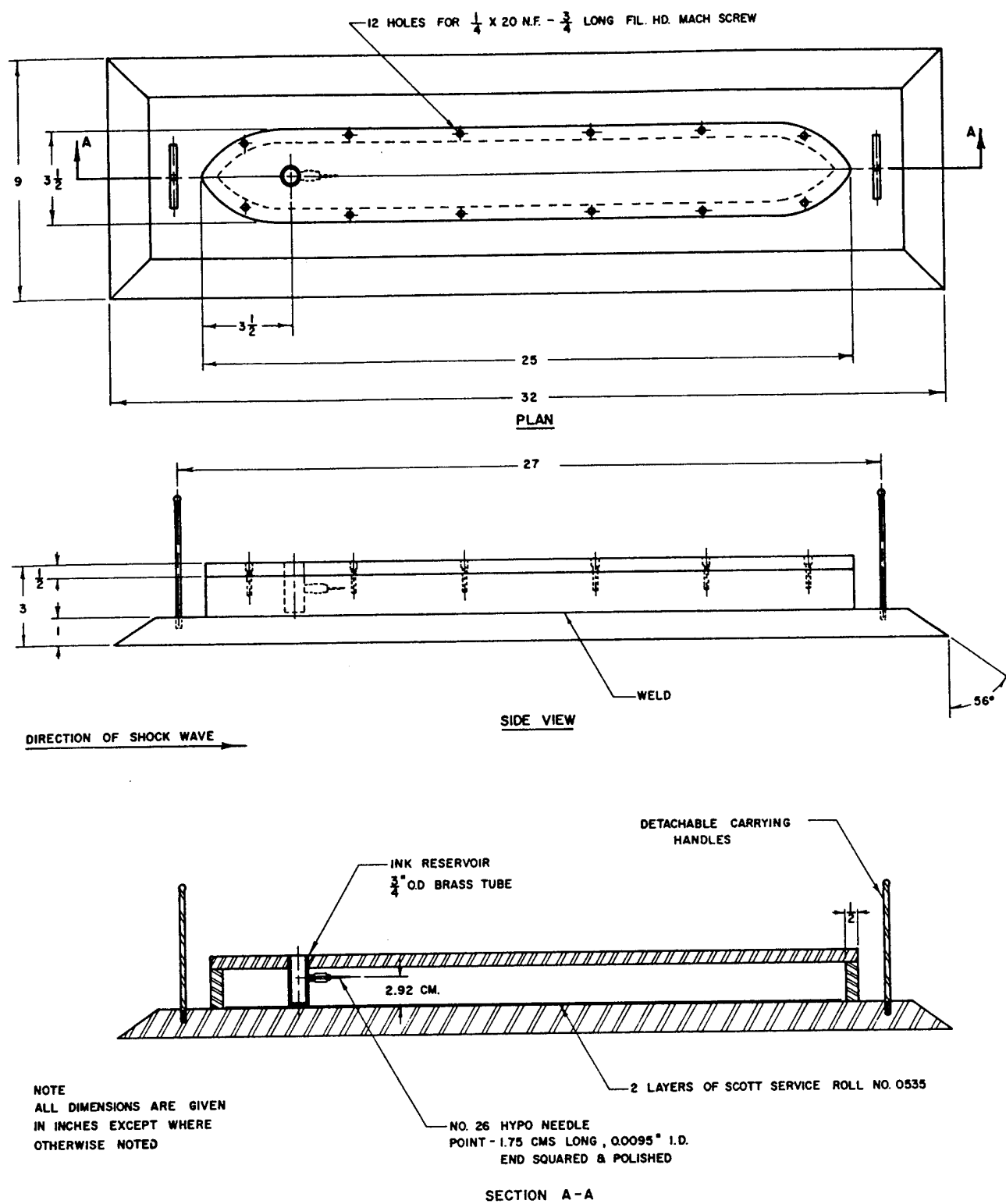
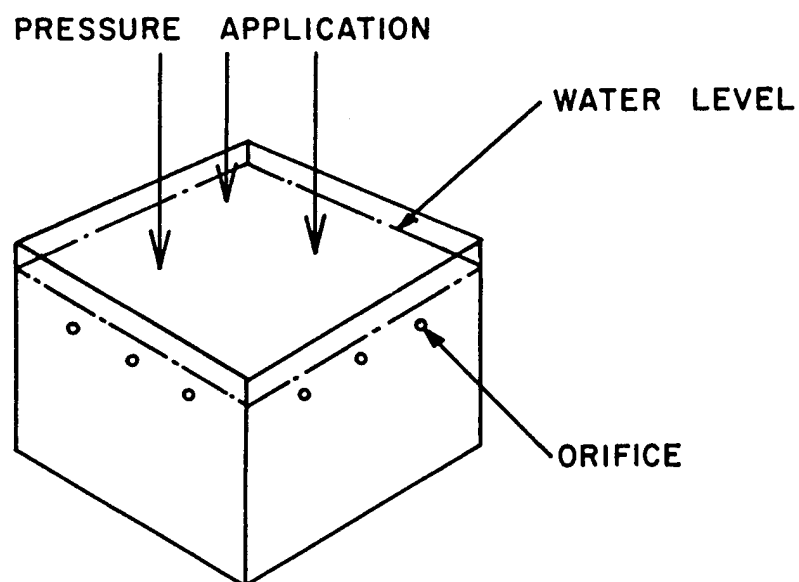
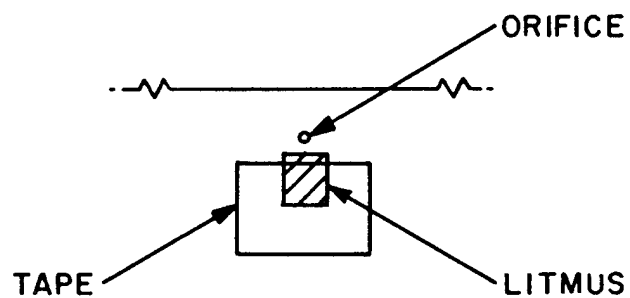


Figure 15. Squire gage.



BASIC ELEMENT OF SURFACE TENSION GAUGE



POSITION OF FIRST LITMUS DETECTOR

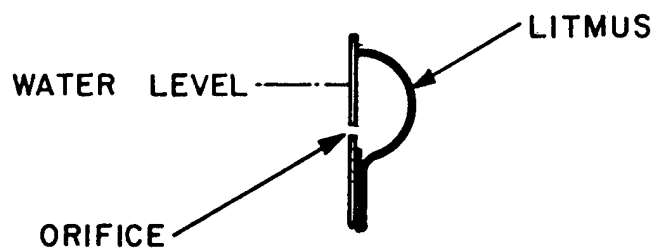


Figure 16. Low pressure fluid-ejection gage.

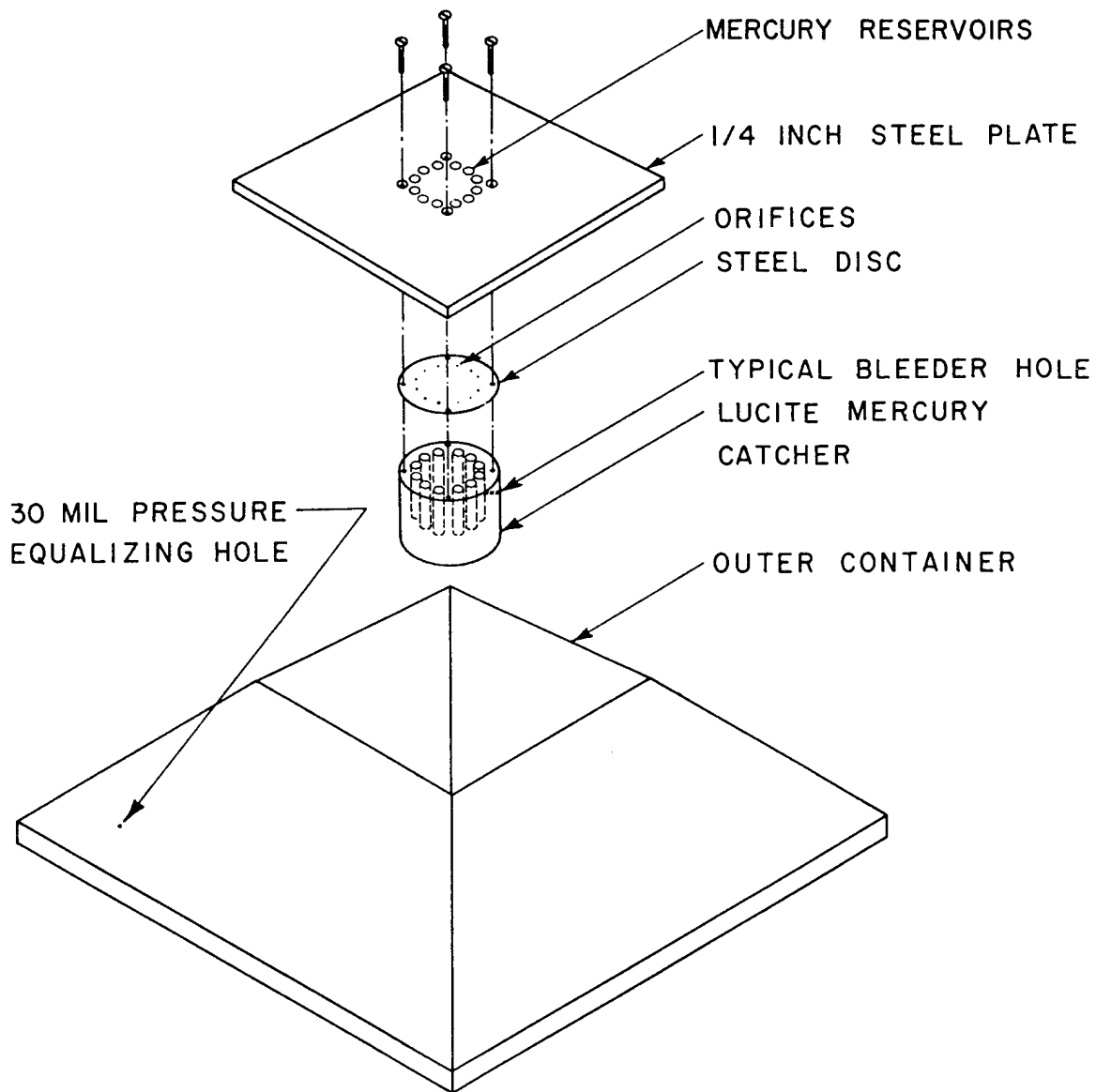


Figure 17. Field model of mercury surface tension gage (exploded view).

For use, the cubes are placed on the ground surface, free to move, with a face normal to the radius to the explosion source. The ground surface should be essentially planar, with no obstructions to movement away from the blast or obstruction to flow toward the blast. Typically four or five cubes of the same type are placed on an arc. Their initial positions are marked, and their final positions are recorded after the explosion. The total displacement and angular deviation from the radial direction of the line connecting the initial and final position is determined for each cube.

Uniformity of loading on cubes of the same size and mass can be evaluated by comparing their displacements. The displacement of a cube is approximately proportional to the square of the impulse received by the cube. Non-radial flow is shown by a significant non-random distribution of deviation angles.

Assuming the loading on a cube is delivered as an impulse, the initial velocity imparted to the cube by blast is

$$V = I_{\text{total}}/M$$

where V is the initial velocity, I_{total} is the impulse delivered by blast, and M is the mass of the cube.

Experiments were conducted to determine relations between total displacement over a hard-packed desert surface and initial launch velocity for several types of cubes. These relations were found to be power-law functions, and were inverted to obtain relations for initial velocity versus final displacement. They are as follows:

$$D = a V^{**b}, \quad V = c D^{**e},$$

where D is the total displacement of the cube, a , b , c , and e are fitted parameters, and $**$ denotes exponentiation.

For estimation of dynamic pressure impulse, I , the relation is

$$I = MV/(A C_d) = M c D^{**e}/(A C_d),$$

where A is the face area of the cube, and C_d is the drag coefficient, assumed to be 1.2.

Table 7 lists the cubes for which the experiments were conducted, and values of a , b , c , and e were determined.

For 450-kilogram HE charges fired above the surface the aluminum cube displacements provided good estimates of the dynamic pressure impulse measured by electronic gages at an elevation of three feet (0.914 meters). Cubes of less mass apparently were not truly impulsively loaded. However, power-law least squares fits were developed for predicting dynamic pressure impulse from the cube displacements. These are given in Table 8, along with the minimum shock overpressure where the functions apply for 450-kilogram charges. Figure 18 shows arrays of cubes deployed on a height-of-burst experiment at the Defense Research Establishment, Suffield, Alberta, Canada.

Table 7. Cube, cube mass, face area, coefficients, and exponents for the power-law functions $D = aV^b$ and $V = cD^e$ derived from experiments over the desert surface at the test site.

Cube	Mass (kg)	Area (m ²)	a	b	c	e
152-mm Steel	27.5	0.0231	0.06004	2.2501	3.4905	0.4444
152-mm Aluminum	9.68	0.0231	0.06934	2.1552	3.4496	0.4640
152-mm Oak	2.55	0.0231	0.08077	2.0395	3.4341	0.4903
152-mm Pine	1.664	0.0231	0.12800	1.8565	3.0262	0.5378
152-mm Balsa	0.636	0.0231	0.16784	1.7506	2.7718	0.5712
51-mm Steel	1.021	0.00258	0.07764	2.1367	3.3071	0.4680
51-mm Aluminum	0.350	0.00258	0.13063	1.9322	2.8674	0.5176
44-mm Oak	0.064	0.00197	0.24375	1.6341	2.3723	0.6120
44-mm Poplar	0.040	0.00197	0.22758	1.6198	2.4939	0.6174

Table 8. Fitted functions for dynamic pressure impulse versus cube displacement on 1000-pound (450-kilogram) charges.

Cube Type	Mass (kg)	Function (kPa-s)	Minimum Overpressure (kPa)
51-mm Aluminum	0.350	$I=0.325 D^{0.500}$	130
44-mm Oak	0.065	$I=0.097 D^{0.474}$	90
44-mm Poplar	0.040	$I=0.071 D^{0.488}$	45

Since the aluminum cubes apparently were impulsively loaded, the function listed should apply for smaller charges, provided displacements greater than about 0.6 meters are produced.

For the large-scale HE charges in the 2500-ton range, the dynamic pressure impulses estimated from the cube displacements varied with cube size, mass, and station overpressure level. Only values derived from the displacements of 6-inch (152-mm) steel and aluminum cubes at the higher overpressures agreed reasonably well with dynamic pressure impulses measured by electronic gages at an elevation of three feet (0.914 meters). Factors reducing impulses on the cubes were boundary layer effects and non-impulsive loading by the long-duration blast waves. A qualitative study of boundary layer

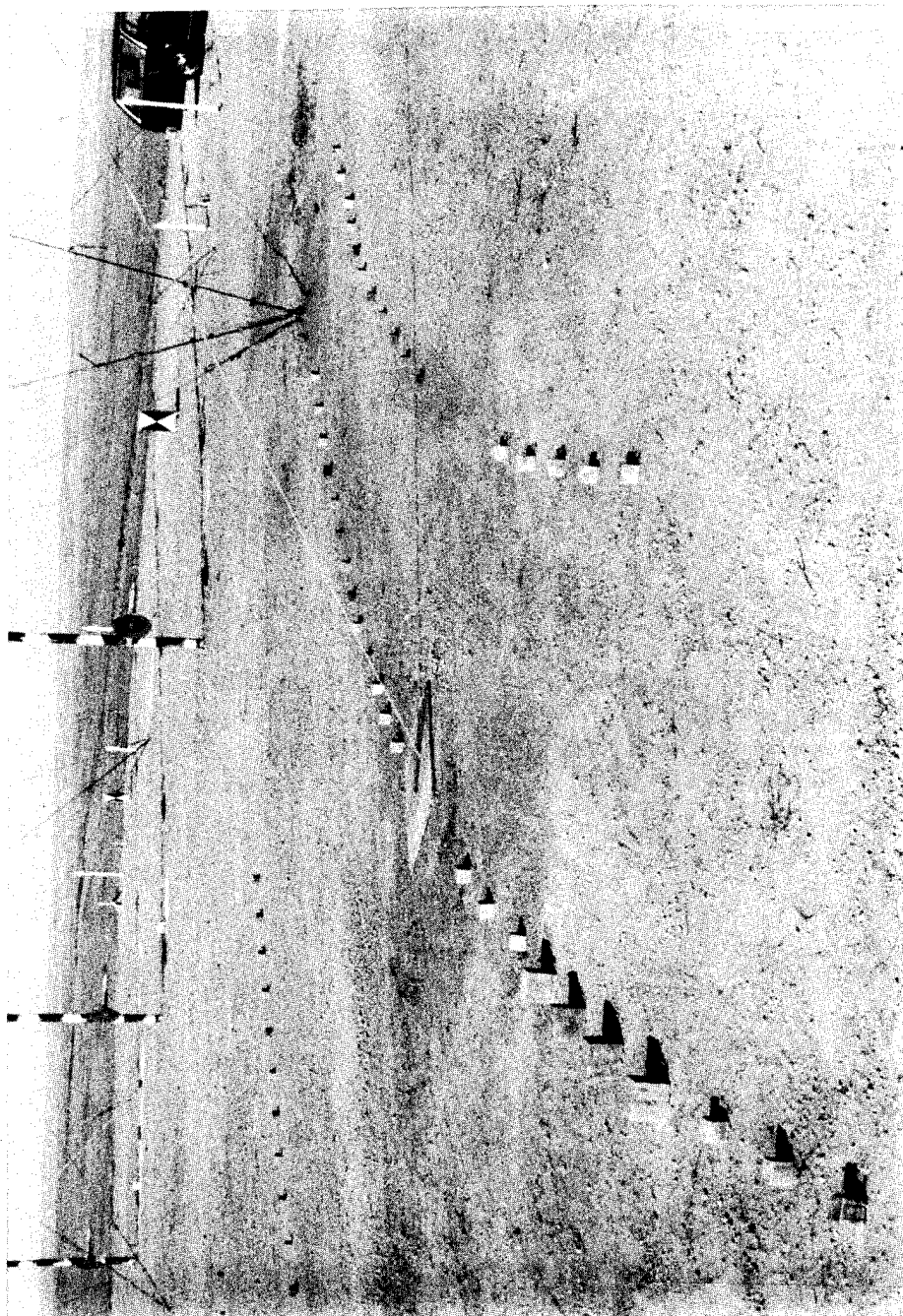


Figure 18. Cubes in position on west line.

effects conducted on the MINOR UNCLE event indicated that boundary layer effects were important only for the 2-inch (451-mm) and 1.75-inch (44-mm) cubes.

Power-law functions were developed for predicting dynamic pressure impulse out of the boundary layer as measured by electronic gages at a height of three feet (0.914 meters) from the displacements of cubes on the ground surface. The functions are listed in Table 9, along with the ground ranges and overpressure ranges for which they apply. The number of cubes at each station ranged from three to five, and the average displacements were used for the fits. The maximum difference of measured gage dynamic pressure impulse used for the fits from the power-law predictions using the observed average displacements is listed also. The prediction functions span the overpressure range from 60 psi (414 kPa) to 2 psi (14 kPa). The ranges for the cube types overlap, so that all or part of the total range can be covered by selecting the appropriate cube types. The 2-inch (51-mm) aluminum cube covers a wide overpressure range and is a convenient size and mass. A minimum of five cubes should be used at each station on future tests.

The use of cubes seems practical only for approximately level, planar, cleared surfaces. The relations for estimating initial velocities as a function of final displacements were derived from experiments over a hard-packed desert surface. The functions would be different for soft surfaces or very hard surfaces such as concrete. A drag coefficient larger than 1.2 may be appropriate for blast overpressures where much of the flow is near or exceeds Mach one. The debris produced by the large explosions may strike cubes and change their final position. Nevertheless, cubes have provided useful data on special experiments that would have been very difficult to obtain by other means.

Ref: Ethridge, N. H., and Flory, R. A., "Use of Cube Displacements as a Measure of Blast", Proceedings, Vol.I, 13th International Symposium on the Military Application of Blast Simulation, The Hague, The Netherlands, 13-17 September 1993.

Ethridge, N. H., Flory, R. A., and Keefer, J. H., "Cube Displacements", MINOR UNCLE Symposium Proceedings, Defense Nuclear Agency, Alexandria, VA 22310-3348, 1994.

- 3.1.6 Bursting Diaphragm Gage (Australia) (1984).
Thin Foil Pressure Gage (USA) (1972).
Anderson Blasgage (USA) (1986).

Thin Foil Pressure Gage. The thin foil pressure gage is an updated model of the foilmeter of 1945 which is discussed Volume I. This gage is shown in Figure 19. A topmost protective plate is used to prevent debris accelerated by the blast from puncturing the foil membranes. Aluminum foil, 0.005 inch, is sandwiched between 1/4 and 1/8 inch plates and is secured to the 1/4 inch plate with an epoxy adhesive. A small hole is made into the pipe chamber to allow for barometric and temperature changes.

A typical gage has membrane holes of 1/2 to 2 inches and an overpressure range of 5 to 100 psi. An accuracy of ± 10 percent was claimed.

Table 9. Fitted functions for dynamic pressure impulse versus average cube displacement for 2500-ton charges derived using data from MISERS GOLD, DISTANT IMAGE, and MINOR UNCLE.

Cube Type	Function (kPa-s)	Ground Range (m)	Over- Pressure Range (kPa)	Maximum Displace- ment (m)	Percent Deviation of Data	No. of Stations Used in Fits		
						MG	DI	MU
152-mm Steel	$DPI = 4.01D^{**0.373}$	202- 322	414-138	9-0.9	+ - 9	6	3	3
152-mm Aluminum	$DPI = 1.58D^{**0.405}$	270- 411	207- 83	46-1.8	+ - 6	7	2	2
152-mm Oak	$DPI = 0.406D^{**0.571}$	369- 767	103- 28	24-1.2	+ - 7	6	2	3
152-mm Pine	$DPI = 0.267D^{**0.627}$	450- 767	69- 28	16-2.2	+ - 9	4	0	2
51-mm Steel	$DPI = 2.21D^{**0.396}$	219- 369	345-103	36-1.6	+ - 5	0	2	3
51-mm Aluminum	$DPI = 0.81D^{**0.475}$	322- 767	138- 28	19-0.3	+ -10	6	2	4
44-mm Oak	$DPI = 0.162D^{**0.751}$	545-1227	48- 14	10-0.8	+ -12	6	3	1

Comments: DPI is predicted dynamic pressure impulse at gage elevation (0.914 meters).

D is average displacement in meters.

The two numbers under ground range are the nearest station and farthest station from which data were used for the power-law fits.

The two overpressures listed for each cube type are the nominal overpressures for the ground ranges listed.

The maximum displacements listed are the maximum displacements of individual cubes at the nearest and farthest stations.

The percent deviation of data is the maximum difference of measured gage dynamic pressure impulse used for the fits from the power-law predictions using the observed average displacements.

MG = MISERS GOLD, DI = DISTANT IMAGE, and MU = MINOR UNCLE.

35

Ref: Manweiler, R.W., et al., "Measurement of Shock Overpressure in Air by a Yielding Foil Membrane Blast Gage," Oak Ridge National Laboratory, ORNL-4868, 1973.

Australian Bursting Diaphragm Gage. The Australian bursting diaphragm gage was developed in 1984 and is very similar in design to the foil meter gages deployed in the late 40's and 50's. Presented in Figure 20 is a photograph of this gage. A diaphragm of a specified material is clamped between two plates covering holes of varying diameters. The diaphragm ruptures in response to the overpressure entering the pressure orifices (holes). Different diameter holes in the plates enables the gage to cover a range of pressure levels. Diaphragm materials are typically cellophane, aluminum foil, and Mylar. Calibration carried out in a shock tube was used to determine their pressure range. Mounting of the gage is made on a stand near the ground surface.

Anderson Blasgag. In 1986, a gage billed as the Anderson Blasgag (blast gage) was offered commercially by Anderson Effects, Inc., Mentone, CA. This gage, shown in Figure 21, uses standard copying paper covering ten different diameters: attention is directed by the supplier to look for the shearing of the paper at the edge of the hole. Only the edge shear is considered in reading. As shown in Table 10, if no hole shows such shears the peak pressure is less than 1.3 psi; if all holes show edge shear, the overpressure is over 6.5 psi.

Ref: Howe, John S., Personal Communications., Materials Research Laboratory, Department of Defence, Victoria, Australia.

3.2 FIBER OPTIC BIER GAGE (USA) (1992).

The Blast-Induced Emission of Radiation (Bier) Gage operates on the principle that a material such as quartz will emit graybody radiation when stressed by shocks in the tens to hundreds of kilobars peak pressure range. Two major components of the all-optical measurement system are the gage and the spectrometer. Transmission of the gage signal is made to the spectrometer by way of an optical transmission fiber. A three-optical-channel spectrometer shown in Figure 22 converts the content of the spectral signal to an electrical signal suitable for recording by digital recorders.

The gage itself is a fused quartz rod with one end drawn to a taper to facilitate coupling to a standard fiber optic cable. The current design, shown in Figure 23, has a rod approximately 12 mm in diameter with one end drawn to a fiber approximately 0.20 mm in diameter. The overall length of the rod can vary from 300 to 12 mm. The length of the drawn section is 50 mm. Rods are mirrored with aluminum on the sides and a protective coat of copper paint. A housing is provided for the gage to facilitate mounting and to give protection. Rifle gas gun and high explosive testing have shown the gage to be an effective totally passive optical gage with a pressure range of 20 to 110 kBar. It is purported to provide reliable performance in a small package with results in real time. More experiments are needed to understand and adequately characterize the gage response.

Ref: Del Frate, Renzo J., et al., "Optical Passive Shock (BIER) Gage Development Program," DNA-TR-93-23, 1993.

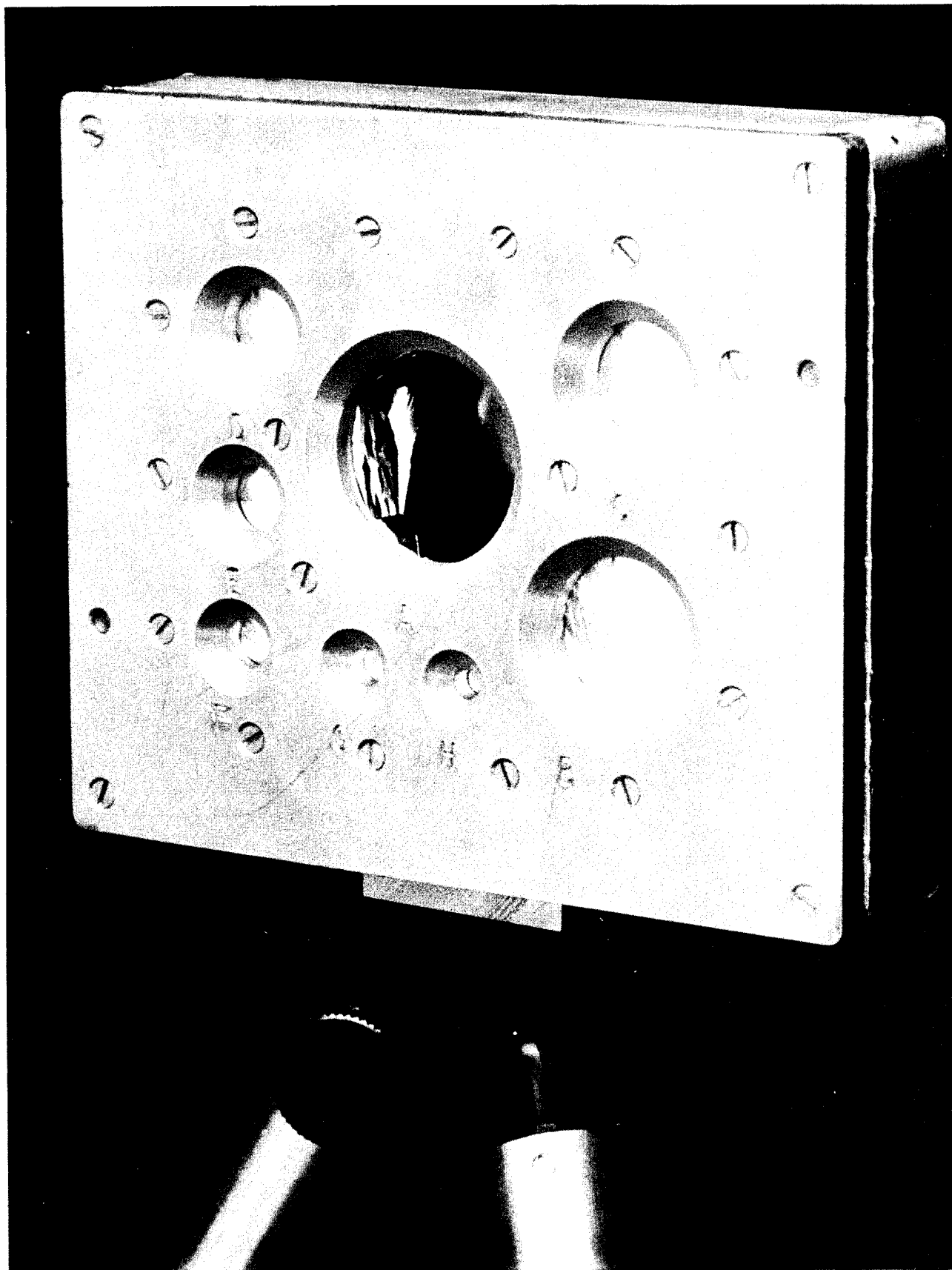


Figure 20. Australian bursting diaphragm gage.

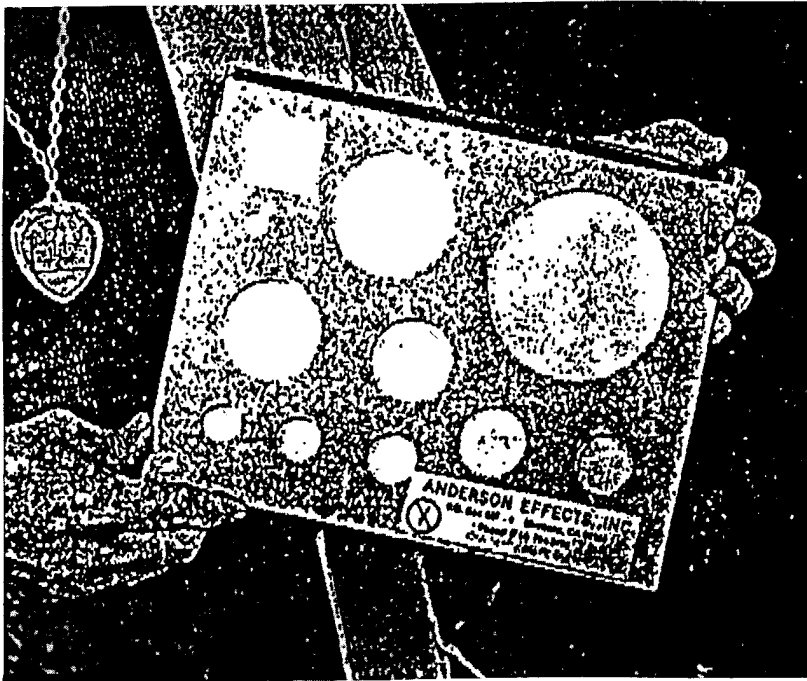


Figure 21. Anderson blasgag.

Table 10. Peak overpressure for Anderson blasgag.

If smallest hole to show positive shear of this diameter:		then the peak overpressure was between this minimum ... and this maximum:	
Zero (no shear)	Hole No. 0	000	to 1.3 psi
3.75 inches (3 3/4")	Hole No. 1	0.9	to 1.9 psi
2.50 inches (2 1/2")	Hole No. 2	1.3	to 2.4 psi
2.00 inches (2 ")	Hole No. 3	1.6	to 3.0 psi
1.675 inch (1 5/8")	Hole No. 4	2.0	to 3.7 psi
1.375 inch (1 3/8")	Hole No. 5	2.4	to 4.1 psi
1.188 inch (1 3/16")	Hole No. 6	2.7	to 4.9 psi
1.00 inch (1")	Hole No. 7	3.2	to 5.6 psi
0.875 inch (7/8")	Hole No. 8	3.7	to 6.5 psi
0.750 inch (3/4")	Hole No. 9	4.3	to 9.7 psi
0.500 inch (1/2")	Hole No. 10	6.5 psi or more ...	

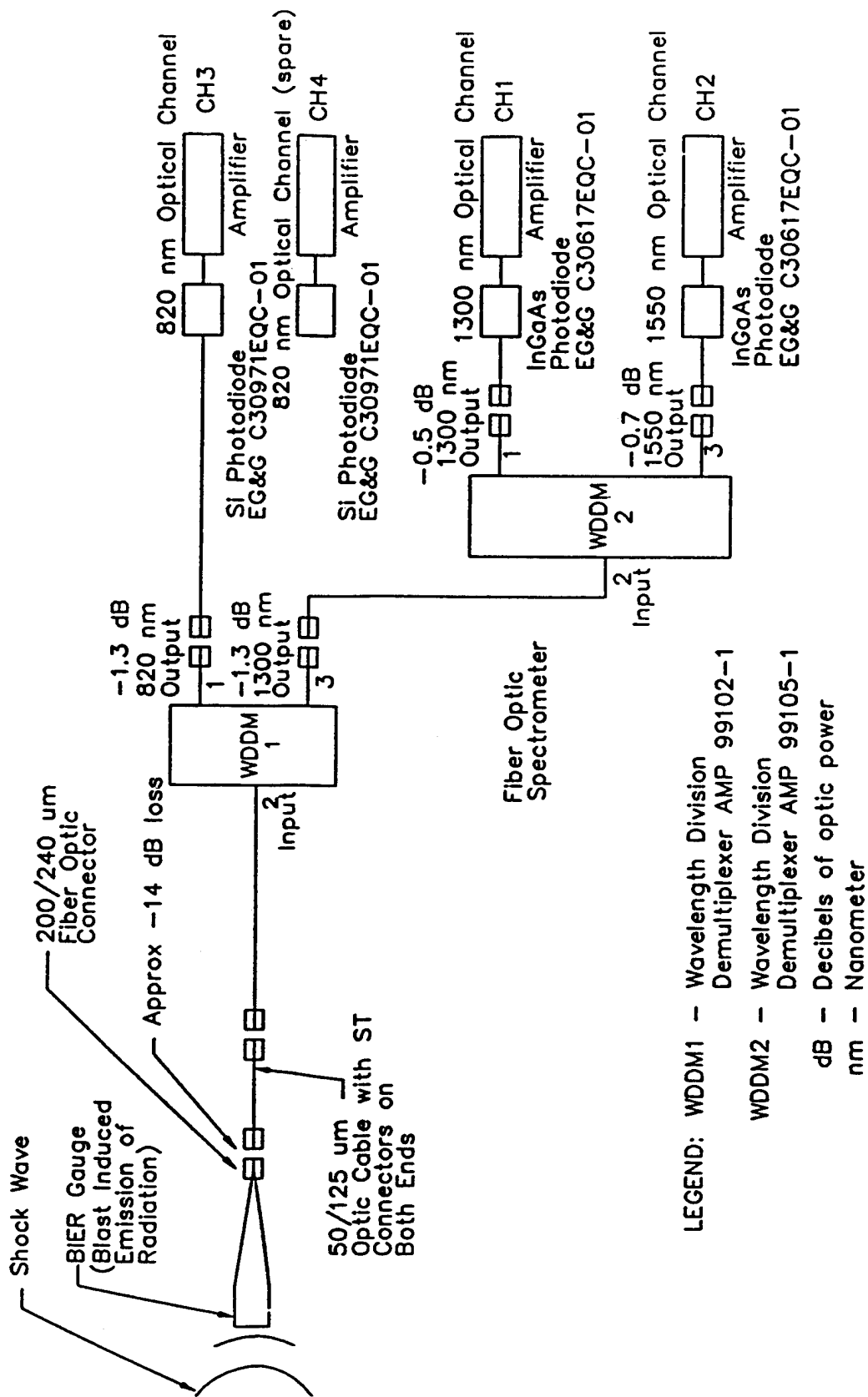


Figure 22. Production spectrometer design.

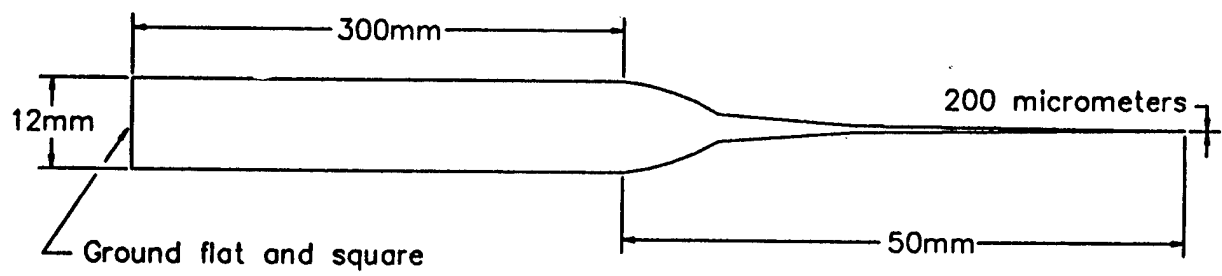


Figure 23. Drawn quartz rod.

SECTION 4

FREE-FIELD ACTIVE DEVICES, PRESSURE SENSING

4.1 PIEZO-RESISTIVE.

4.1.1 Kulite Pressure Gage (1980) (USA).

The Kulite pressure gage is a solid state device which incorporates a diffused four-arm wheatstone bridge on the surface of a silicon diaphragm. Manufactured by Kulite Semiconductor Products, Inc., the gages most popularly used were the HK series and the XT-190 series. The gages have internal temperature compensation for ambient temperature changes and may be excited with either a DC or AC power source. They are capable of DC response with a nominal output of 100 millivolts for full scale and a natural frequency of 725 KHz for 20 kpsi units to 70 kHz for 5 psi units.

A photograph of the gage is given in Figure 24. A screen labeled by the company as a "B" type screen covers the face of the gage. It consists of a 0.005-inch thick plate with 0.006-inch diameter holes positioned on a circle. The diameter of the circle is greater than the active diameter of the diaphragm. By using the screen, protection is given the sensing diaphragm from particles in the air flow. The screen is mounted in a screen holder which is installed on the gage housing in front of the diaphragm. A space of 0.005 inch exists between the screen and diaphragm.

The manufacturer notes in particular the high frequency, low hysteresis, and superior thermal and environmental performance characteristics of the gages. These features he says "are the result of the integrated silicon sensor and silicon force collector." Silicon was originally adopted because of its large piezo-resistive coefficient and compatibility with transistor fabrication techniques. Silicon has been found to possess excellent transducer characteristics.

The gages continue to be used today.

France (1993) uses the XCS and XCW series gages.

Ref: Kulite Semi-conductor Bulletin KS-1000D, Kulite Miniature 1S Silicon Diaphragm Pressure Transducer Catalog. 1985.

"PRE-DIRECT COURSE, Volume III - Results Report." DNA POR 7116-3.

4.1.2 Endevco Model 8510 (1975) (USA).

The Endevco Model 8510 gage employs a silicon diaphragm on which a four-arm wheatstone bridge is atomically bonded with a diffusion process. Compensation and balancing elements are contained within the gage case. An excitation voltage of up to 10 VDC can be used and a nominal voltage output of 30 mv/v full scale was experienced. The natural frequency for a 15 psi gage was 65 kHz.

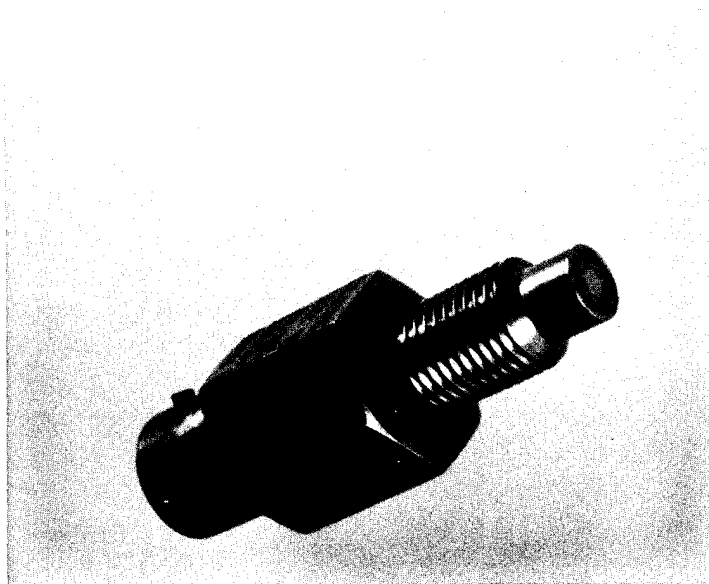


Figure 24. Kulite HK pressure gage.

France (1993) uses the 8500 series gages and Enertec CZ series, a gage similar to the Endevco model.

Ref: "Proceedings of the DICE THROW Symposium," Volume I, DNA 4377P-1, 1977.

4.1.3 Subsonic Differential Pressure Gage (1981) (USA).

The subsonic differential pressure gage was manufactured to specifications by the Kulite Semi-conductor Corporation, Inc., and used a piezo-resistive diaphragm as the sensing element. The configuration of the gage is shown in Figure 25. The outer configuration is that of a long cylindrical rod oriented parallel to the expected direction of air flow. A single pressure-sensing diaphragm is placed within the rod about one rod diameter from the nose. Stagnation overpressure is developed on one side of the diaphragm from the input port in the nose of the rod. The static overpressure is developed on the rear of the diaphragm by a connection of the internal volume at the rear of the diaphragm to static pressure inlet ports that are two-rod diameters to the rear of the nose. These ports are 12 cylindrical holes drilled perpendicular to the axis of the rod and spaced uniformly around its circumference. A metal screen with holes is placed immediately in front of the diaphragm to protect it from direct impact by particles in the air stream. The diaphragm is of silicon and contains an active wheatstone bridge. It is coated on both sides with an RTV compound. Figure 26 shows a gage installed in the field at an elevation of 5.5 feet (0.14 meters) above the ground.

An improved gage was developed in 1990-91. Figure 27 shows the configuration of this probe. The standard gage has a blunt nose. The improved probe has an interchangeable nose; one blunt, and one ogival in shape as shown in Figure 28. The plan was to test the two extreme shapes in a shock tube and select the best. The gages were delivered with the ogival shape too late for testing prior to use on DISTANT IMAGE, so the ogival shape was used in the field. Later, shock tube testing showed that the blunt nose was best.

The sensors in the probe are Kulite silicon diaphragms with four-arm strain bridges. The differential pressure sensor is about halfway between the nose tip and the inlet ports two diameters to the rear of the nose. These ports allow side-on overpressure to enter and load the rear side of the differential pressure sensor. The ports are 12 small holes spaced symmetrically around the circumference of the probe.

The diaphragm is protected by a Kulite B screen immediately in front of it, and by a second screen recessed about 0.05 inches (1.3 mm) from the nose. The holes in this screen are clustered around the center, rather than placed on the perimeter as is done with the B screen. This second screen near the nose reduces the magnitude of reflected pressure that loads the front of the differential pressure diaphragm.

The primary modification to the standard probe was to place a side-on overpressure sensor ten diameters to the rear of the nose. At this distance, the effect of the nose on the pressure at the side-on ports will be negligible, based on wind tunnel studies reported in the literature. For flow parallel to the probe axis, an accurate overpressure measurement should be obtained. The inlet ports are 12 small holes spaced symmetrically around the circumference of the probe.

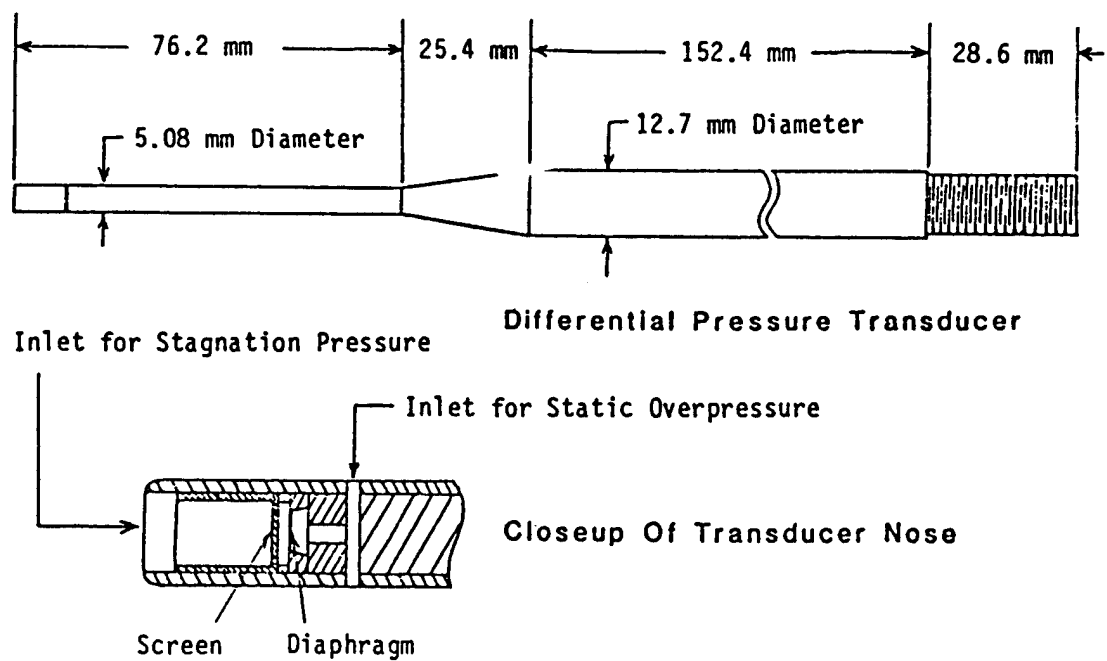


Figure 25. Configuration of the differential pressure gage



Figure 26. Differential pressure gage mounted in pylon 5.5 inches (0.14 meters) above the ground surface for the Mighty Mach IV test series.

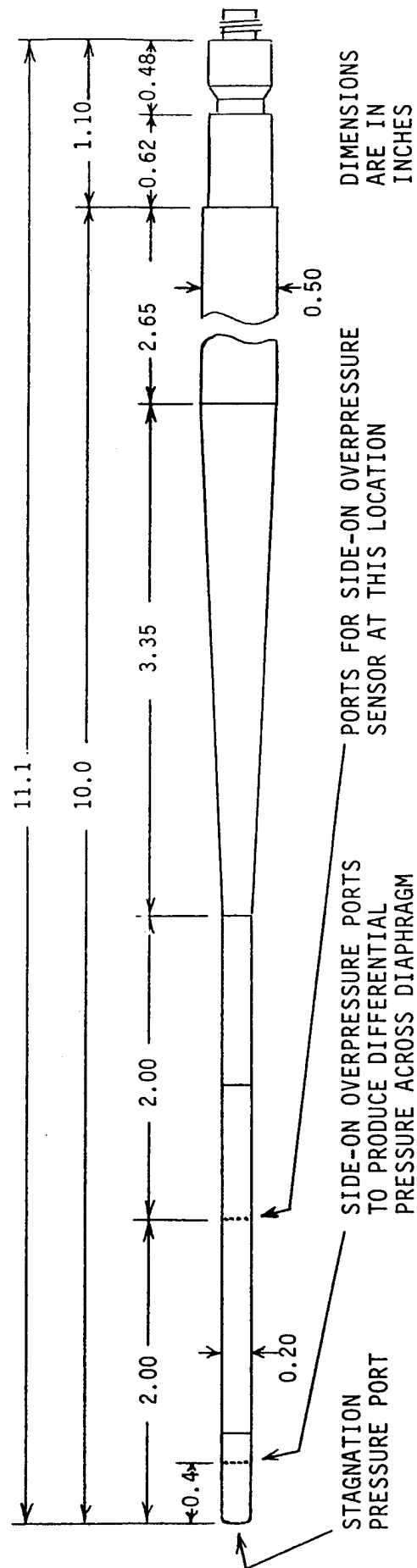


Figure 27. Configuration of the modified differential pressure probe with added side-on overpressure sensor. The probe is Model XCW-8-WZ-200, made by Kulite Semiconductor Products, Inc.

Original differential only

Differential with side-on

View of gage nose



View of gages with and without side-on ports



Figure 28. Differential pressure gage.

The probe was successfully manufactured in ranges of 100D/100G, 50D/50G, 30D/30G, 15D/15G, and 5D/10G, where the numbers refer to pressure rating in psi of the differential pressure element and the side-on overpressure element.

Mechanically, the gages are somewhat fragile in the sense that they can be easily bent if someone inadvertently backs into one. One was broken by falling debris on DISTANT IMAGE. However, they are no more fragile than the standard differential pressure gage.

Currently, the rear of the side-on overpressure gage has a bleed port to the atmosphere, so it is essential that the probe mounting isolate the bleed port from the blast wave.

At the lower pressures, the reflected shock pressures in the nose of the gage are large compared to the differential pressures that are to be measured. To avoid damage to the diaphragm, the use of the highest ranged gage that will yield an adequate signal is recommended. The sensors were found to be very stable when properly assembled. Calibrations did not change with time or with a large number of tests in the shock tube.

The response of the probe gages is limited by the fill times for the cavities to the front and rear of the differential gage and in front of the side-on gage. The settling time is about 0.2 milliseconds. The large oscillations that occur at earlier times are not valid data.

The DISTANT IMAGE test provided results that generally agreed very well with the other gages on the north radial. The blast wave was severely disturbed at three stations, so that identical records could not be expected.

The shock tube tests identified the blunt-nosed version as the preferred choice. For shock overpressure less than 25 psi (172 kPa) no correction function for nose shape is required in the equation used to convert the differential pressure read by the probe to the true dynamic pressure.

Field records from a 1000-pound high-explosive HOB test using the standard gage are shown in Figure 29. Records from a large-scale test using the improved gage are shown in Figure 30.

The gage is in use today.

France (1993) uses a similar gage of their own design using a Kulite differential sensor.

Ref: Ethridge, N.H., et al., "A Differential Pressure Gage for Measurement of Dynamic Pressure in Blast Waves," MABS-8 Proceedings, Volume I, 1983.

Ethridge, N.H. and Jackson, Willis F., "Dynamic Pressure Gage Development for Subsonic Flows," DNA-TR-92-109, 1993.

4.2 VARIABLE RELUCTANCE.

4.2.1 CCC (1965) (USA).

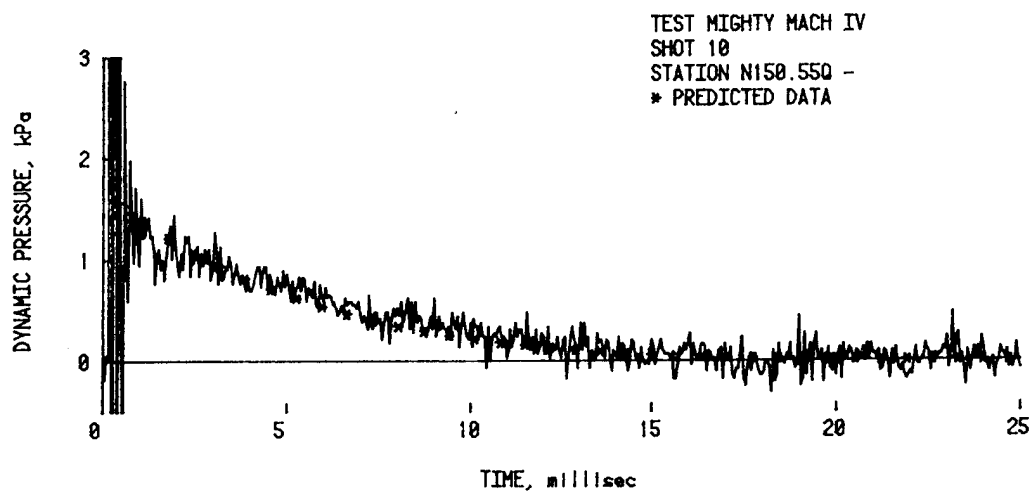
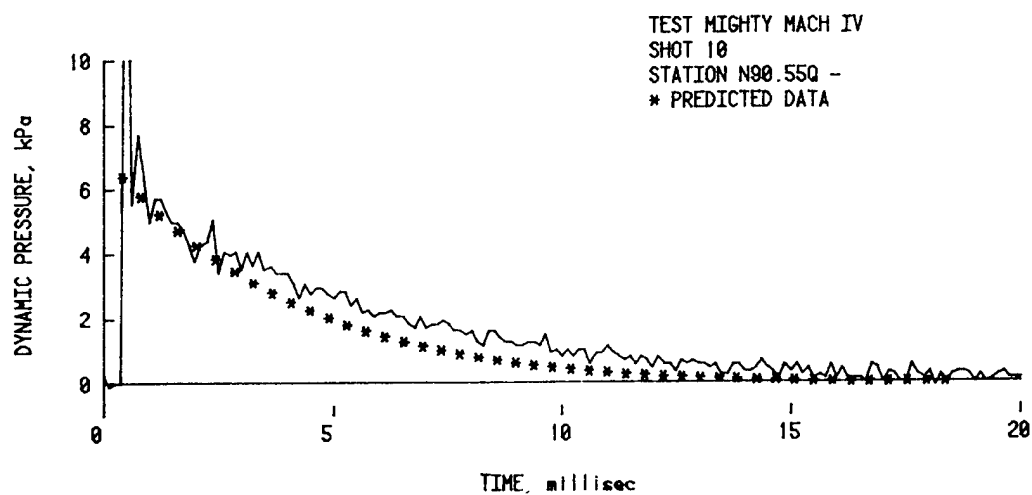
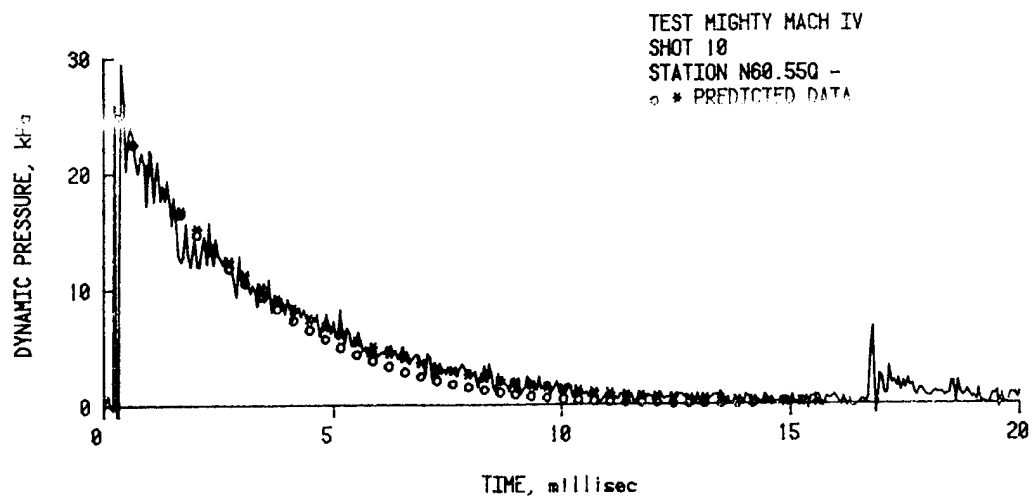
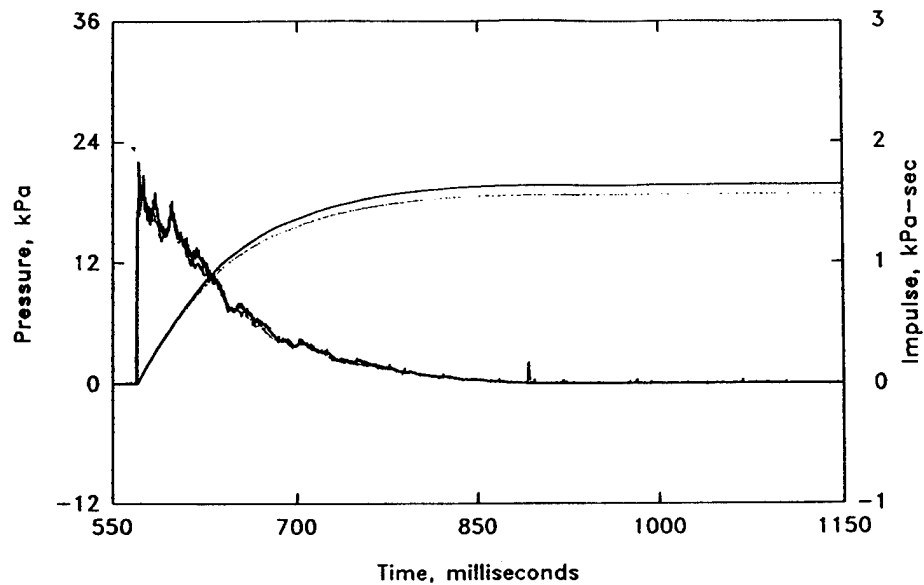
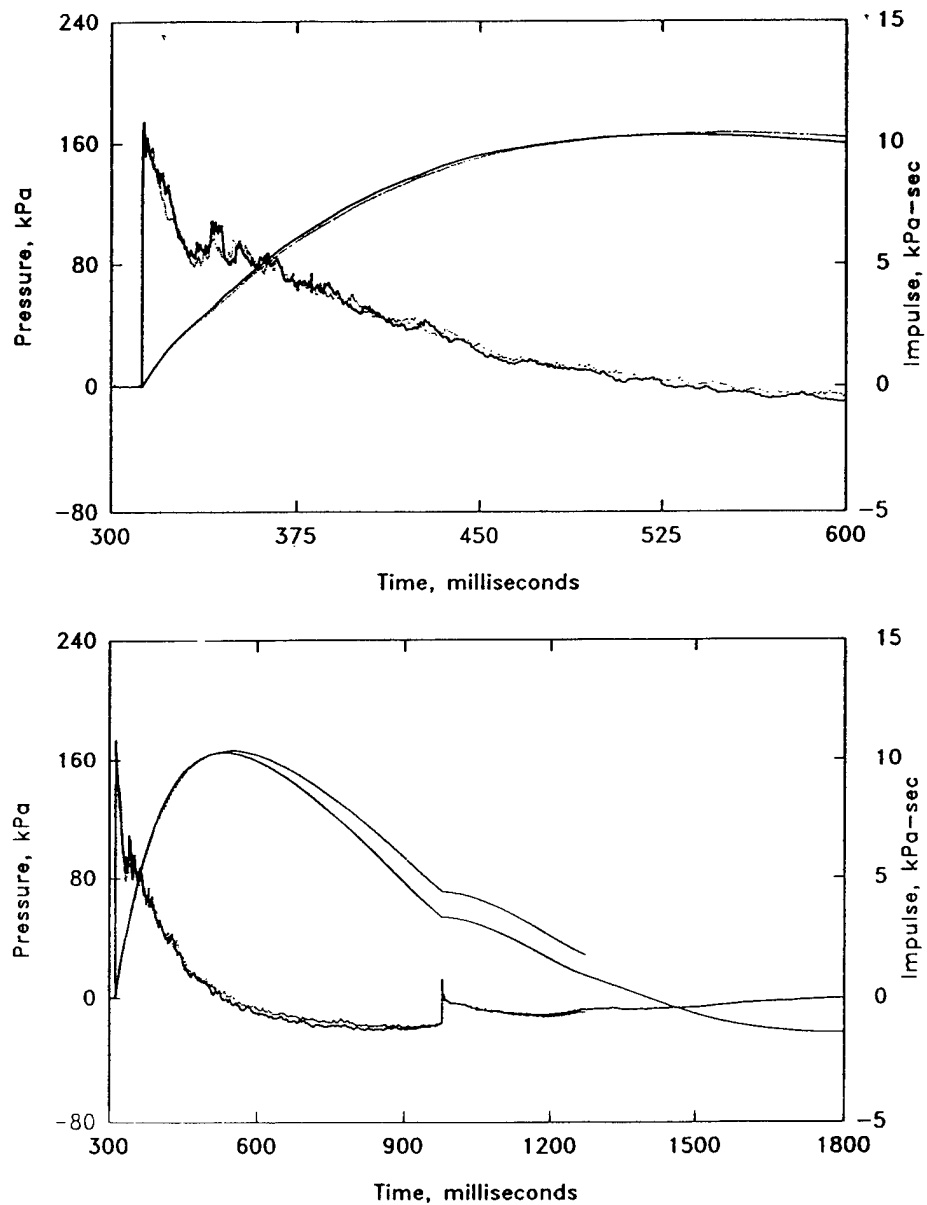


Figure 29. Comparison of the data from the differential pressure gage with predictions obtained by the flow-field reconstruction method - 1000-lb HE test.



(a) Comparison of the dynamic pressure records from the probe at the 10-psi station with that from the standard stagnation pressure and side-on overpressure gages. The solid curve is from the probe.

Figure 30. Differential pressure gage record comparison.



(b) Comparison of the overpressure record from the probe at the 20-psi station with the record from the standard gage in the baffle plate. The solid curve is from the probe.

Figure 30. Differential pressure gage record comparison (Continued).

The CCC gage uses the variable reluctance principle to sense the overpressure of the blast wave. Produced by the Consolidated Controls Corporation, overpressure is converted to frequency variation by use of a clamped plate diaphragm moving in a magnetic field. The gage was designed to measure pressures up to 300 psi.

The CCC gage was above average in its accuracy and reproducibility; it is easy to use and has valid static calibration. A shortcoming is non-linearity and a 2 kHz limit to a high frequency response.

Two problems were noted in field use. First, the gage occasionally exhibited a decrease in sensitivity, probably caused by mechanical changes in the diaphragm - coil relationship due to the corrosion resulting from a salt atmosphere. Second, since the gage measures a pressure difference across a diaphragm between chambers, conditions of blast loading may deform or displace the diaphragm and thus cause appreciable deviations of the pressure in the reference chamber. Deviations may thus become significantly greater than one percent for overpressures below five psi.

Ref: Pittman, J., "Free-Field Airblast Measurements," Operation SAILOR HAT, Project 5.2A, DNA POR 4056, 1966.

Rowland, R.H., "Blast and Shock Measurement State-of-the-Art Review," DASA 1986, 1967.

4.2.2 SRI MAD Gage, Ultradyne S-30 (1963) (USA).

The SRI MAD gage was designed for the measurement of air and dust (MAD) - a total pressure probe which measures the dynamic pressure of the air and the momentum flux of suspended dust. The basic element is a vented pitot tube about six inches long with ports for measuring the local pressure at two locations along the tube length. Shown in Figure 31 is a drawing of the MAD gage. Pressure is measured as near the forward end of the tube as possible and again as near the rear as possible. Static pressure is measured through taps in the well of the gage body. Venting of the pitot tube at the rear of the probe to avoid plugging with dust is controlled by a metering orifice.

As the stream of dust-laden air encounters the nose of the tube, the air phase decelerates almost immediately to the velocity of the metered airflow within the tube. The dust particles, being considerably more massive, decelerate gradually due to air drag, slowly transfer momentum to the air, and cause a corresponding increase in pressure with distance along the tube length. The pressures from the front and rear ports are transmitted through separate passages to variable-inductance pressure sensors, Ultradyne Model S-30. Data from the front port and the static port are used to compute the air dynamic pressure, while the difference in pressure between the front and rear port is a measure of the dust momentum flux. The assembled gage and its components are shown in Figure 32.

An inductive frequency-modulated-multiplex is used to transmit signals from the MAD gage. Each of three sensors in the gage (measuring front port pressure, incident pressure, and rear port pressure, respectively) consist of a diaphragm sandwiched between two coils, with a sealed cavity between diaphragm and coil on each side. As the cavity on one side is

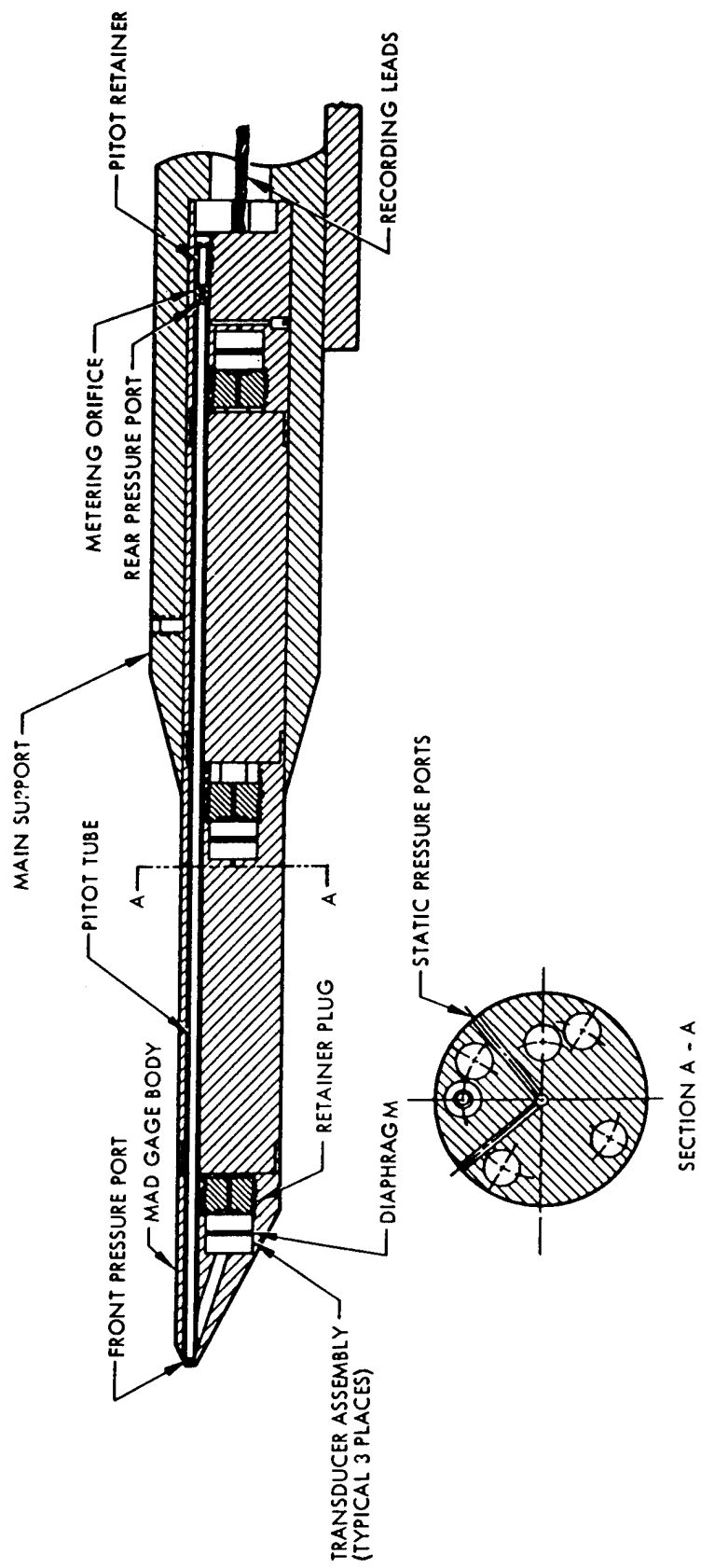


Figure 31. SRI-MAD gage.

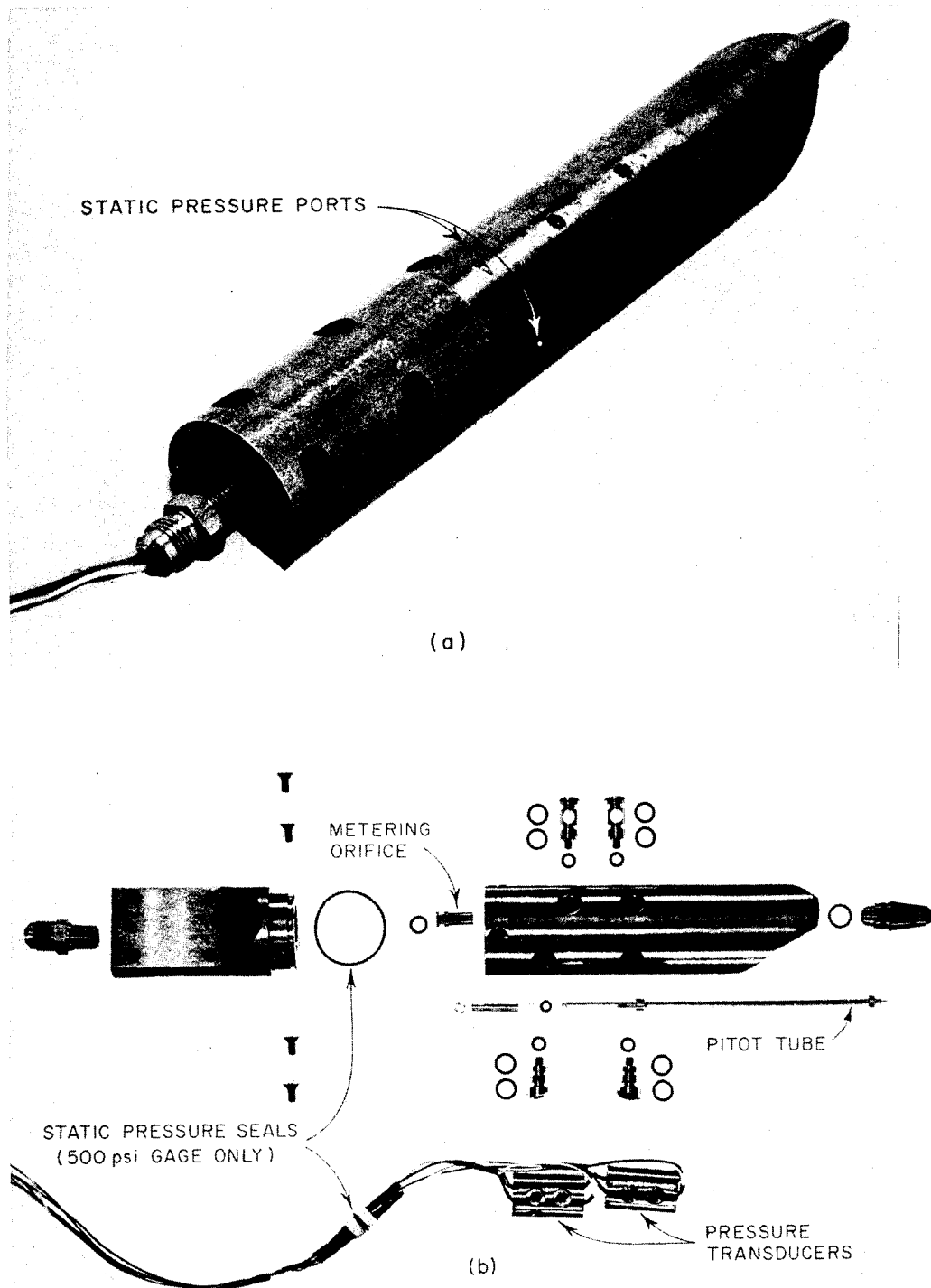


Figure 32. SRI-MAD gage: (a) assembled gage and (b) gage components.

pressurized, the diaphragm is displaced, causing a change in the inductance of each of the two coils - an increase in one and a decrease in the other. The coils are active members of tank circuits of two separate oscillators; therefore, as the inductance of the coils changes, the frequencies of the two oscillators also change, one increasing and the other decreasing. The oscillators' basic frequencies, when subtracted, provide a frequency which falls in one of the bands of a standard ± 4 kHz constant-bandwidth carrier system. This FM signal is combined with other FM signals in the carrier system and is transmitted to the data collection center on a single pair of wires. The composite signal is conditioned for the correct level and transmitted to a magnetic tape recorder. The signal-conditioning system is also capable of separating each band from the composite for quick-look evaluation.

The interpretation of data from the MAD gage requires a knowledge of the dust particle size. Therefore, a dust sampler is always used in conjunction with the MAD gage to obtain samples for laboratory determination of particle size distribution.

The dust sampler is a two-inch diameter tube 36-inches long with 1/4-inch thick walls. At the leading ends of the tubes the walls are tapered to a 15-degree wedge to permit the attachment of an oblique shock wave around the periphery.

Shown in Figure 33 is the dust sampler less the explosive closures.

"Pillow block" type clamps are provided at two points along the tube's length, one 12-inches aft of the leading end and one 12-inches forward of the trailing end. Grooves are provided at the points of attachment to enable the clamps to resist axial thrust of the tube. Two small bleed holes are provided under each clamp to permit venting before the tubes are opened for analyses.

Each of the two explosive closures in a dust sampler involves a detonator, a high explosive charge, and the containing hardware. When the advancing dust cloud interrupts a light beam, the devices fire simultaneously, pinching off a section of the tube and capturing a sample of the dust laden air. The initiation of the closure can be controlled to within ± 0.25 microseconds, and the completion of the closure to within ± 1 to 2 microseconds depending on the selection of the high explosive charge, i.e., whether the two charges were taken from the same batch. The time required for closure is about 30 microseconds.

The function of the sampler is to obtain a representative sample of dust for use in determining particle size distribution. This is needed for the MAD gage which examines the ratio of dust to air.

Ref: Witherly, T.D., "Instruments for Measurement of Dusty Airblast Effects in High Overpressure Regions," DASA-1433, 1963.

Witherly, T.D., "Field Testing of Instruments for Measurement of Dusty Airblast Effects," DASA-1671, 1965.

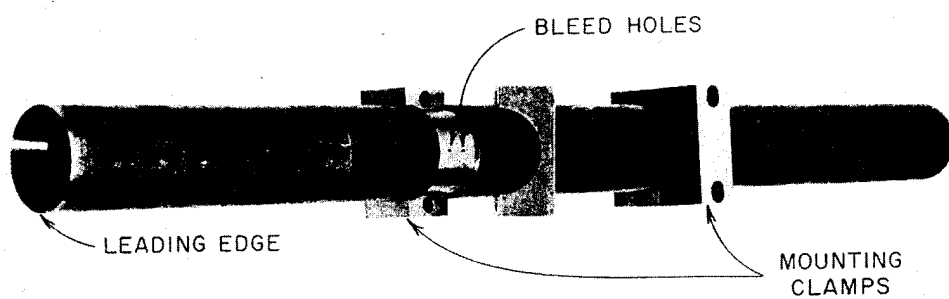


Figure 33. Dust sampler (explosive closures not shown).

4.3 STRAIN FOUR-ARM BRIDGE.

4.3.1 Schaevitz-Bytrex HFG Gage (1966) (USA). (Formerly Detroit Controls, subsequently Bytrex - 1966, then Tyco - 1973)

The Bytrex HFG gages have a four-arm wheatstone bridge with two active semi-conductor arms and two dummy arms. Semi-conductor strain elements are bonded to a force-summing column which is in turn attached to a force-collecting diaphragm; in the case of the low range transducers, the elements are bonded to the diaphragm. (This is an updated version of the Detroit Controls gage.) An orifice shield was placed over the sensitive area of the diaphragm to protect it from thermal radiation and damage by debris. The basic configuration of the unit is that of a 1 and 1/8-inch threaded cylinder, three-inches long. See Figure 34. The transducers are operated at a constant DC excitation of 20 volts. Nominal full scale output is 100 millivolts. The natural frequency of the gage varies from 30 to 80 kHz, depending upon its pressure range.

The Bytrex pressure gage became the transducer of choice through 1975.

Ref: Rowland, R.H., "Blast and Shock Measurement State-of-the-Art Review," DASA-1986, 1967.

4.3.2 Dynisco Gage (1964) (USA).

The Dynisco pressure gage introduced earlier in the 60's for nuclear testing was modified with an orifice plate installed in front of the diaphragm. The orifice plate provided protection from thermal radiation and damage from debris. Pressure entering through the orifice shield impinges upon the diaphragm, with the resultant force being sensed by a strain element mounted on the force sensitive member.

A drawing of the gage is presented in Figure 35.

The Dynisco pressure gage was used for blast measurements extensively throughout the period ending in 1967. In the years following, the gage was gradually replaced with the Bytrex gage.

Ref: "Operation DISTANT PLAIN Preliminary Report," Volume I, DASA 1876-1, 1966.

4.3.3 SRI Total Drag Probe (1964) (USA).

The SRI total drag gage uses an octagonal proving ring inside a hollow target cylinder. The basic design of the gage is illustrated in Figure 36. Support and alignment are provided the full length of the target cylinder. Two strain gages, one near each end of the sensing element, are used in series in each arm of a four-arm bridge. The hollow cylinder was three inches in diameter and three inches long and was the central element of a right circular mounting cylinder 33 inches in length. Natural frequencies of the probes which were built varied from about 4 kHz to 5 1/2 kHz. Overpressure ranges varied from 50 to 500 psi.

To minimize the influence of end effects on the sensing cylinder, the mounting cylinder was machined to the exact diameter of the target cylinder for a distance equal to about two diameters on either side of the target. Positioning of the target cylinder was achieved by

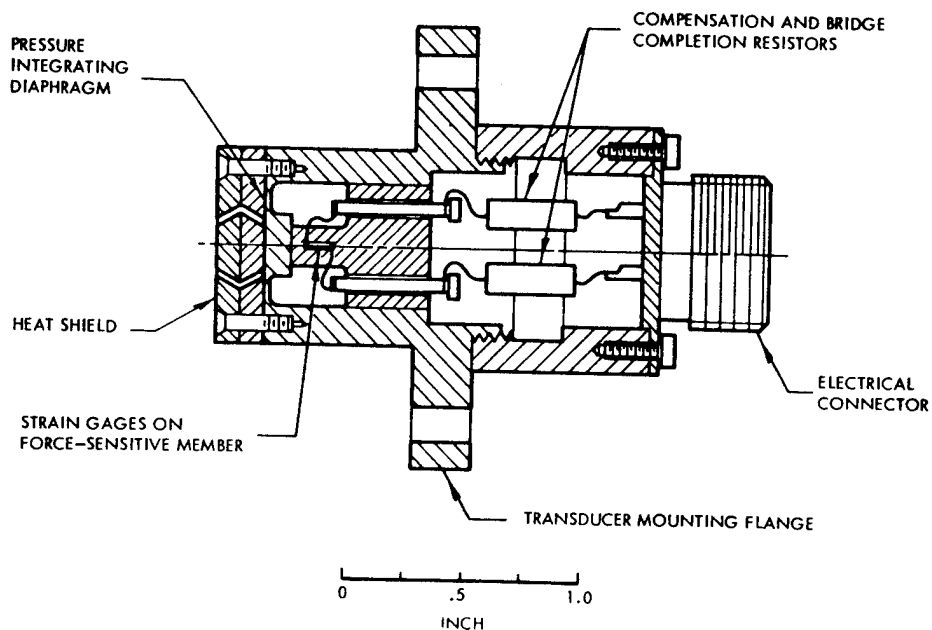


Figure 34. Drawing of Bytrex pressure transducer.

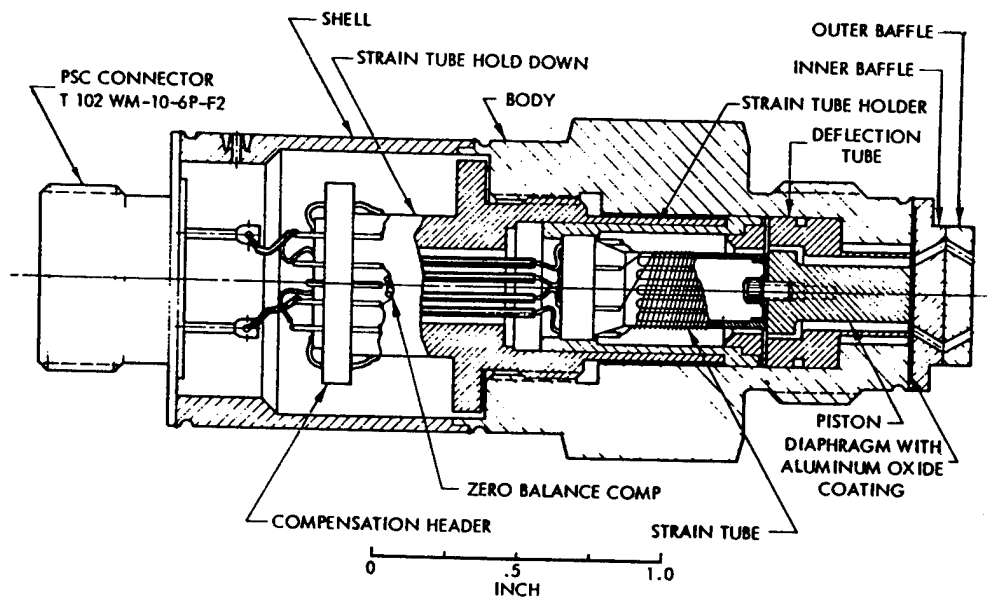


Figure 35. Drawing of Dynisco pressure transducer.

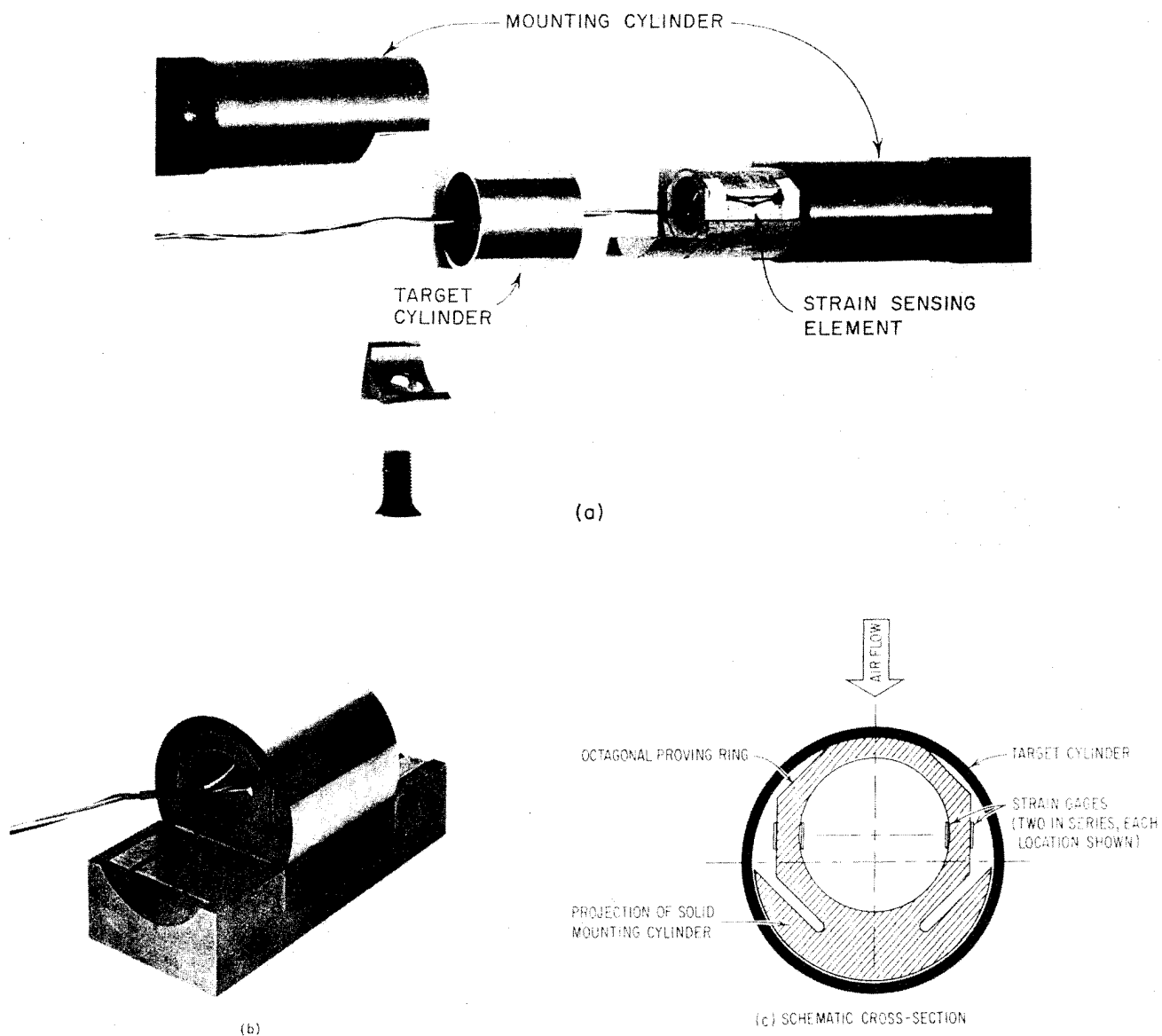


Figure 36. Total drag probe assembly. (a) exploded view - drag probe shown is for 50 psi overpressure region, (b) 500-psi probe shown on calibrating jig, (c) schematic cross-section.

set screws. It is mounted with its longitudinal axis horizontal and normal to the direction of air flow.

A report on testing in 1964 stated that the gages performed satisfactorily. The gages had a 1 millisecond rise time, were electrically stable with little evidence of zero shift, and ringing was not excessive.

Ref: Witherly, T.D., "Field Testing of Instruments for Measurement of Dusty Airblast Effects," DASA-1671, 1965.

4.3.4 SRI-BRL Drag Force Gage (1964) (USA).

A number of special cross-section drag gages that use the same sensing element as the SRI total drag probe were constructed and fielded. These gages are shown in Figure 37.

The sensing elements are strain gages attached to an octagonal proving ring located within the target item. The main design features were:

- (a) square cross-section where a cylinder of square cross-section replaced the cylindrical target of the total drag probe;
- (b) cubical target where a cube of the same edge dimensions as the cylinder of square cross-section was located at the end of the mounting tube; and
- (c) circular-plate target which is similar to the cubical gage except that an eight-inch diameter plate was fastened to the surface of the target facing the blast.

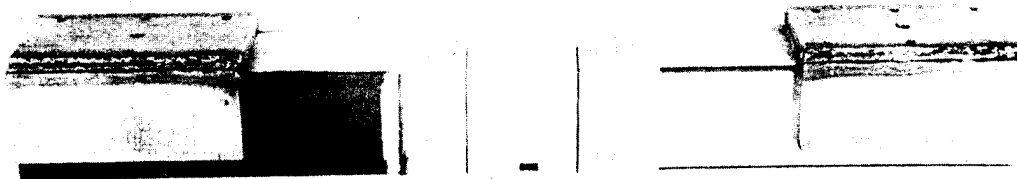
The cubical and circular-plate gages both were filled with a high viscosity silicone fluid to provide damping. Satisfactory performance was recorded by the project officer of those gages deployed on a field test. The adaptability of the octagonal ring sensing element to bodies of other shapes was demonstrated.

Ref: Rowland, R.H., "Blast and Shock Measurement State-of-the-Art Review," DASA-1986, 1967.

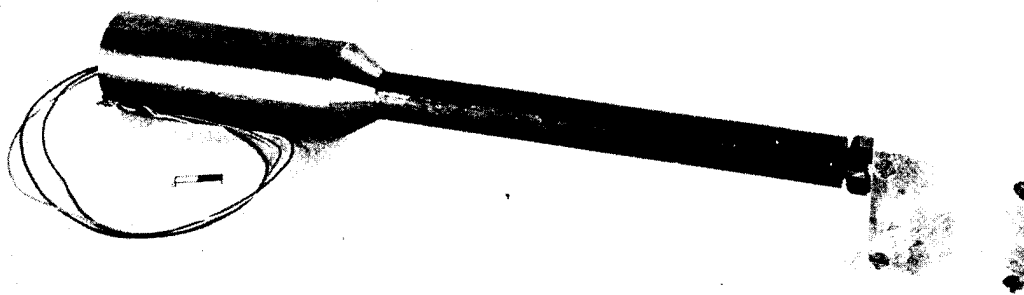
4.3.5 BRL Bi-Axial Drag Gage (1966) (USA).

The BRL bi-axial drag gage was designed and fabricated so the sensing area behaves like a section of a cylinder of infinite length. A load cell one-inch square by one-half-inches long that would sense forces in the two cross axes was manufactured by Schaevitz-Bytrex. The sensing elements of the load cell were strain sensors of the type used in the Bytrex gage. A cylindrical drag gage was designed around this load cell. Figure 38 is an assembly drawing of the completed gage and Figure 39 is an exploded view of the components.

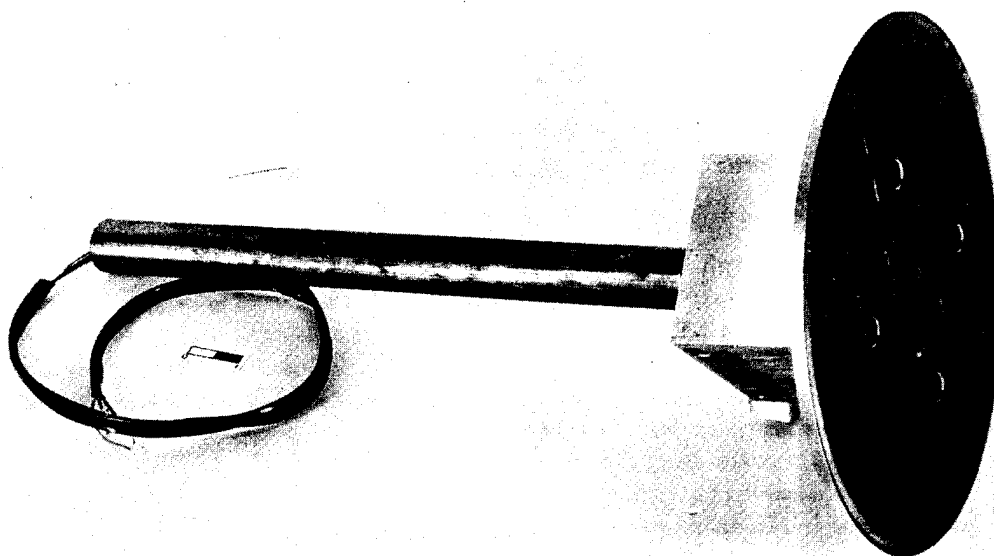
The conical base was designed to give rigid support to the active elements and to provide easy mounting in a three-inch O.D. by two-inch I.D. tube. The base is firmly held in the tube by a series of set screws bearing on the V groove. The bi-axial load cell is affixed to the base by four 10-32 screws. The center section encloses the load cell and provides support



a. SRI-BRL cylindrical drag force gage of square cross-section.



b. SRI-BRL cubical drag force gage.



c. SRI-BRL circular plate drag force gage.

Figure 37. Drag force gages.

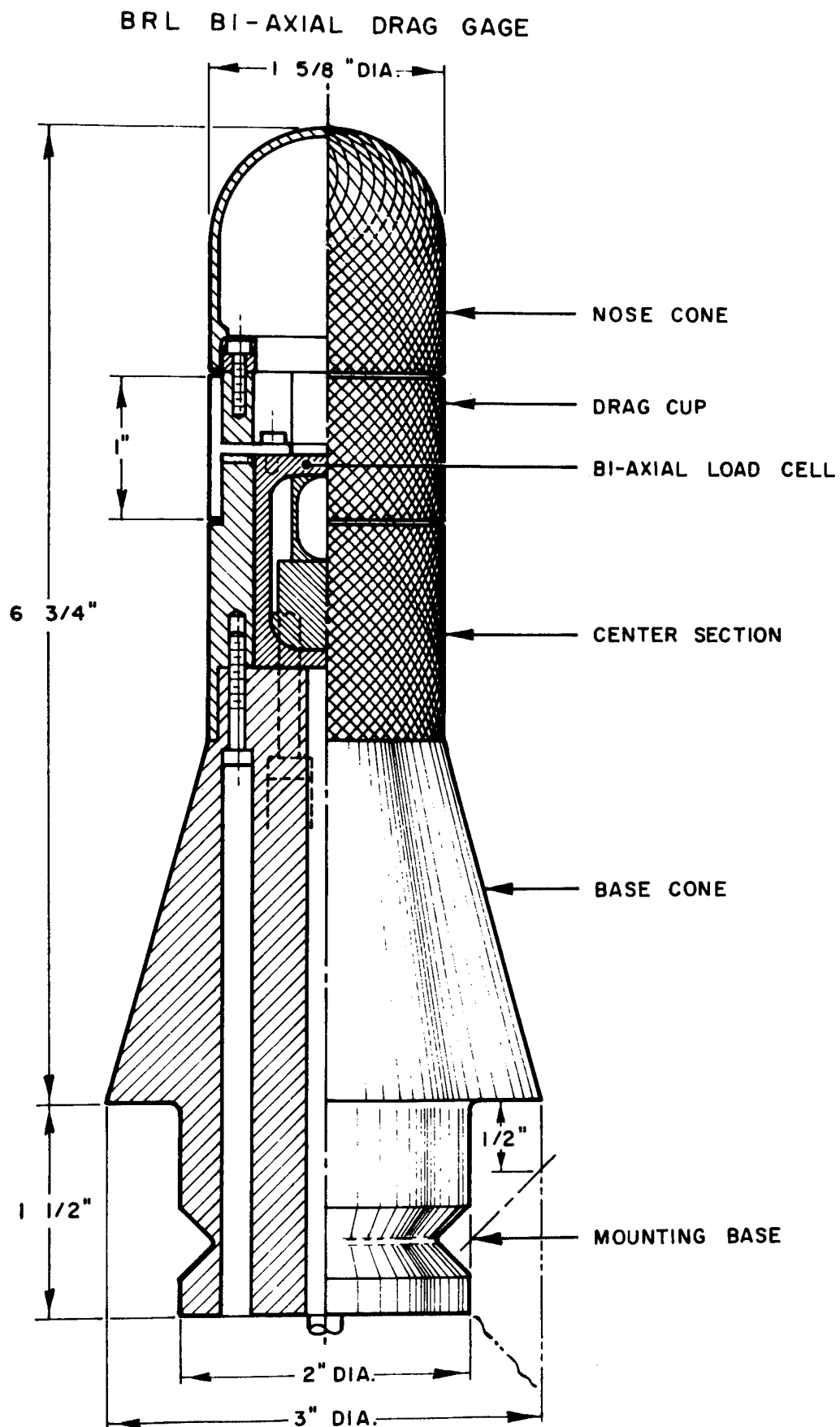


Figure 38. Assembly drawing of BRL bi-axial drag gage.

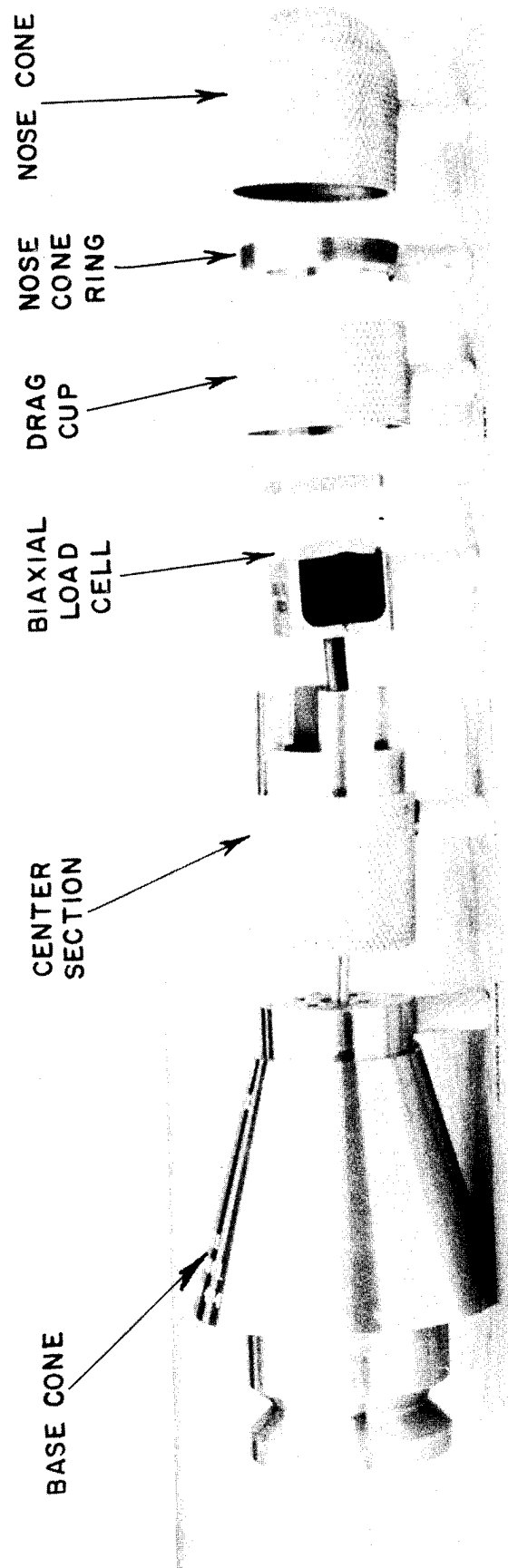


Figure 39. Exploded view of BRL bi-axial drag gage.

for the nose cone. A minimum clearance of 0.008 inches is allowed between the center section and the load cell to allow for the flexing of the cell. The drag cup is the sensitive section and provides a frontal area of 1 inch by 1 5/8 inch. Again a minimum clearance of 0.0008 inches is provided between moving and fixing elements. The central web of the drag cup is firmly screwed to the top (moving element) of the load cell. The four legs of the center section fit through clearance holes in the web of the drag cup. To these legs is mounted the threaded nose cone ring on which the nose cone is screwed on.

On the higher range of gages, 250-lbs force and above, all the components were made of a high strength aluminum alloy 7075T6. on the lower ranges, the base cone was of a milder aluminum alloy 2024T3, and the drag cup was made of magnesium. The magnesium drag cup had sufficient strength for the lower ranges of gages and being lighter, permitted a higher natural frequency of the moving elements to be realized.

The entire surface of the gage from the nose cone to the cylindrical center section was given a rough knurled finish. This was to promote turbulent flow about the body and minimize variations in drag coefficient in the transition region of flow.

Four ranges of bi-axial load cells were made; the ranges were 25, 50, 250, and 750 lbs. All ranges used solid-state strain patches giving the gages a high output signal of approximately 20 millivolts per volt full scale. They require a five volt input signal. With the drag cups mounted, the load cells had natural frequencies which varied with the rated range. These frequencies were determined by a simple laboratory setup where the gage was excited by a blow from a plastic hammer, with the hammer falling through a known angle. The oscillations were photographically recorded from an oscilloscope. The 25-lb gage had a natural frequency of approximately 2.5 kHz; the 50 lb, 3.5 kHz; and the 250-lb and 750-lb gages approximately 5 kHz. One would expect the 750-lb gage, naturally a more rigid member, to have a higher natural frequency than the 250-lb gage. The 750-lb element, however, is made of tool steel while the 250-lb element is made of aluminum alloy. The increase in mass of the steel element over the aluminum element apparently nearly cancels the advantage of the increase in spring rate, resulting in similar natural frequencies.

The entire gage must be assembled with extreme care to insure proper clearances between moving and static elements. A four prong feeler gage was made to aid in centering the load cell in the center section. After assembly, the gages were statically calibrated to 125 percent of rated load to insure that there indeed was sufficient clearance between the load cell drag cup assembly and the non-moving parts.

Typical field mounting of the drag gage is shown in Figure 40.

Ref: "Operation DISTANT PLAIN Preliminary Report," Volume I, DASA-1876-1, 1966.

4.3.6 H-Tech Snob Gage (1982) (USA).

The original H-Tech Snob gage used a pneumatic signal transmission line connecting an input plenum with a Kulite XT-190 transducer located a few inches from the plenum. However, while going over the design, it became evident that it was advantageous to eliminate the transmission tube and plenum by building a special piezo-resistive transducer

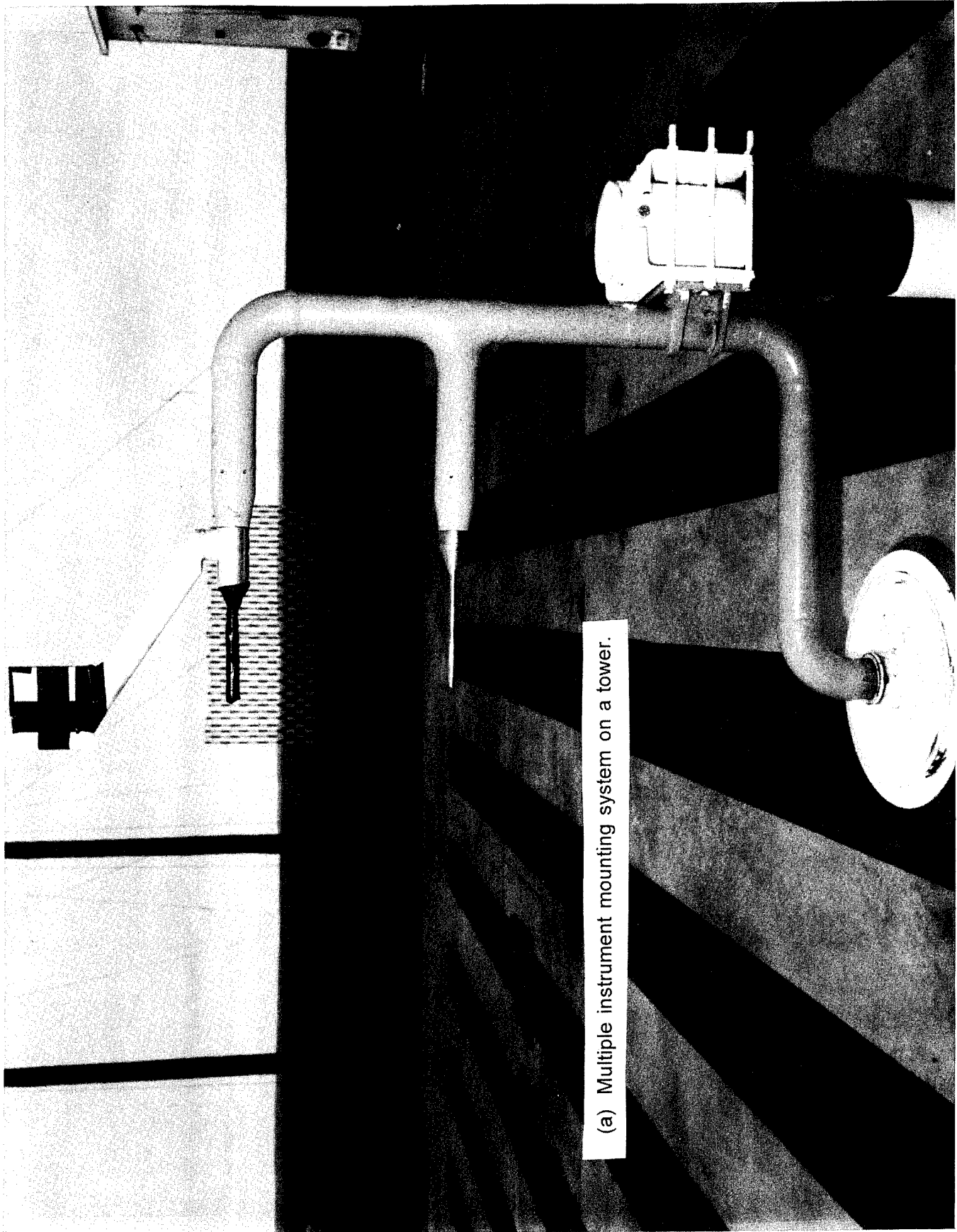


Figure 40. Typical gage mounting system.

(b) Ground surface instrumentation station.

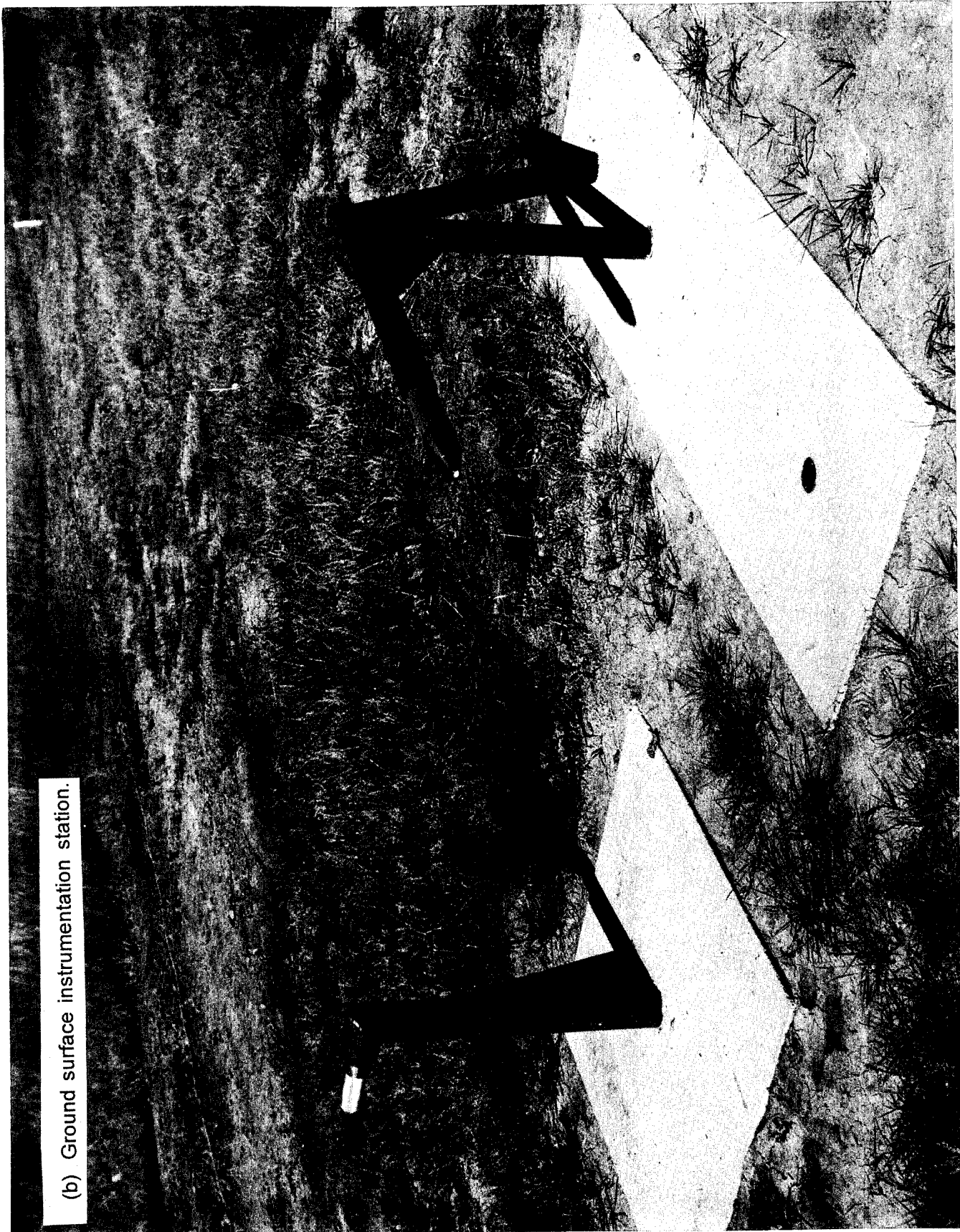


Figure 40. Typical gage mounting system (Continued).

that is similar to catalog designs but with a long threaded body. This design is shown schematically in Figure 41(a) and was labeled the direct-coupled Snob gage. This design was manufactured and deployed in the field.

Another design was developed as shown by the schematic in Figure 41(b). Known as the integrated Snob gage, it came about as an effort to improve the frequency response and reduce the frontal area of the gage by integrating silicon sensors directly into the walls of the Snob tube. A photograph of the gage is shown in Figure 42. Kulite CQ-140 pressure transducers were mounted directly into an enlarged gage tube. This design was limited to a stagnation pressure of approximately 100 psia because of the transducers.

The designers of the Snob gage believed that four transducers were needed in the gage to eliminate all uncertainties and ambiguities in interpreting the data. The front transducer measures the true stagnation pressure, the rear transducer located midway down the Snob tube monitors the pressure rise in the tube. (The magnitude of the pressure rise is indicative of whether particles are decelerated by impact or aerodynamic drag.) The third transducer, a dummy, is protected from the flow and is subject to the environment. This is used to ensure that no false signals are used in the interpretation of the data. A fourth transducer, an accelerometer, would measure the vibration experienced by the gage. Ultra-high strength steel was used in constructing the gage to ensure the gage was rugged enough to resist impact damage shock and vibration damage, dust contamination, and adverse heating effects.

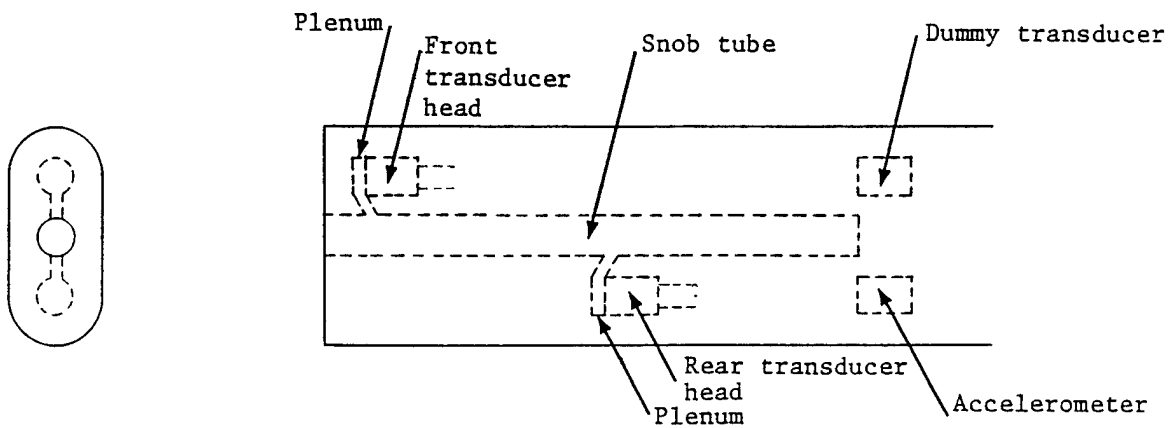
Four channels of recording assigned to one gage increases the overall cost considerably for a field test so selective use of adjunct transducers is advised.

Ref: "PRE-DIRECT COURSE Results Report," Volume I, DNA POR 7116-1, 1983.

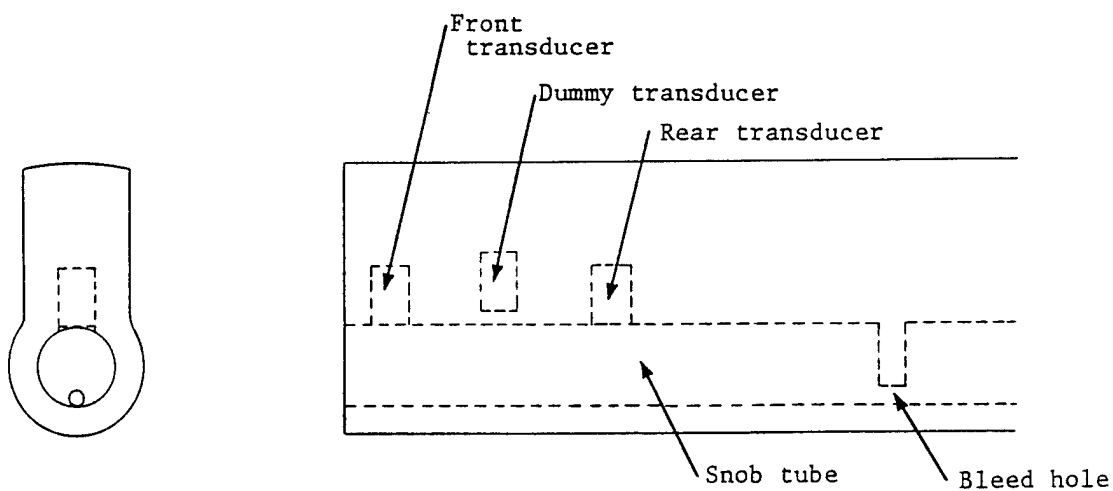
4.3.7 AFWL High Pressure Gage (1989) (USA).

The AFWL high pressure gage was designed to be placed very close to or directly beneath a large explosive charge. The gage uses a cylindrical assembly into which piezo-resistive strain elements are inserted. Kulite Semi-Conductor Products, Inc., manufactures the gage as the HKS-11-375 series. Transducers ranging from 500 to 10,000 psi have been deployed in the field in conjunction with an integrated conditioner/amplifier to form a sensor module. A diagram of a measurement channel is presented in Figure 43; a drawing of the sensor hardware is given in Figure 44.

The approach used to measure high overpressures was to use a shock and thermally hardened transducer mounted in a plug-in module that fits into a housing cast in concrete at the sensing location. The module fits into a cylindrical housing which has been cast into a large concrete mass. Contained in the sensor module were the transducer/integrated conditioner-amplifier subassembly, the container, T-disk, and M-disk. Two balsa-wood pieces were formed and installed over the ends of the electronic package. RTV silastic adhesive and o-rings were applied at interfaces to provide pressure seals and moisture barriers.



(a) Schematic of direct-coupled snob gage.



(b) Schematic of prototype-integrated snob gage.

Figure 41. Schematic of H-Tech snob gage.

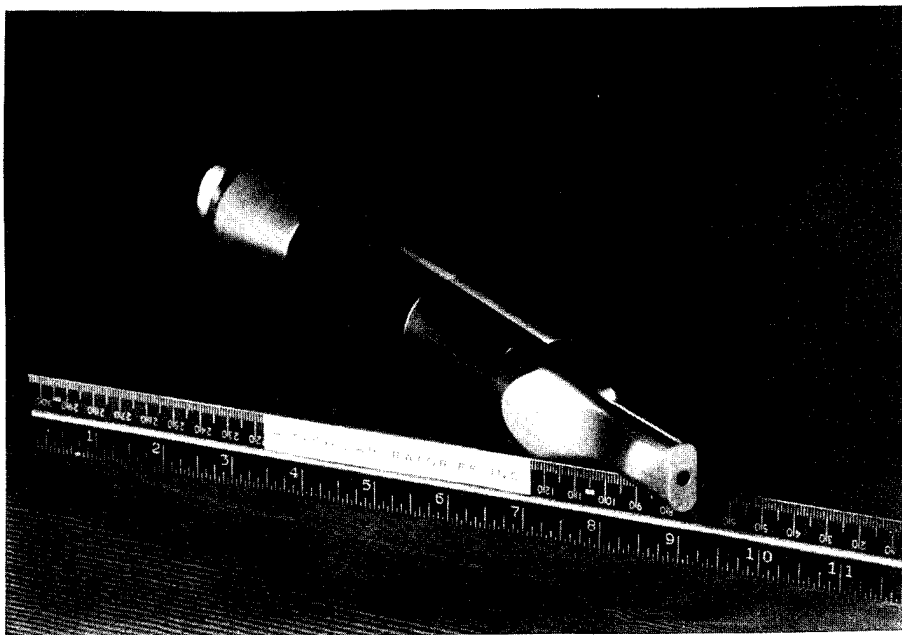


Figure 42. H-Tech snob gage.

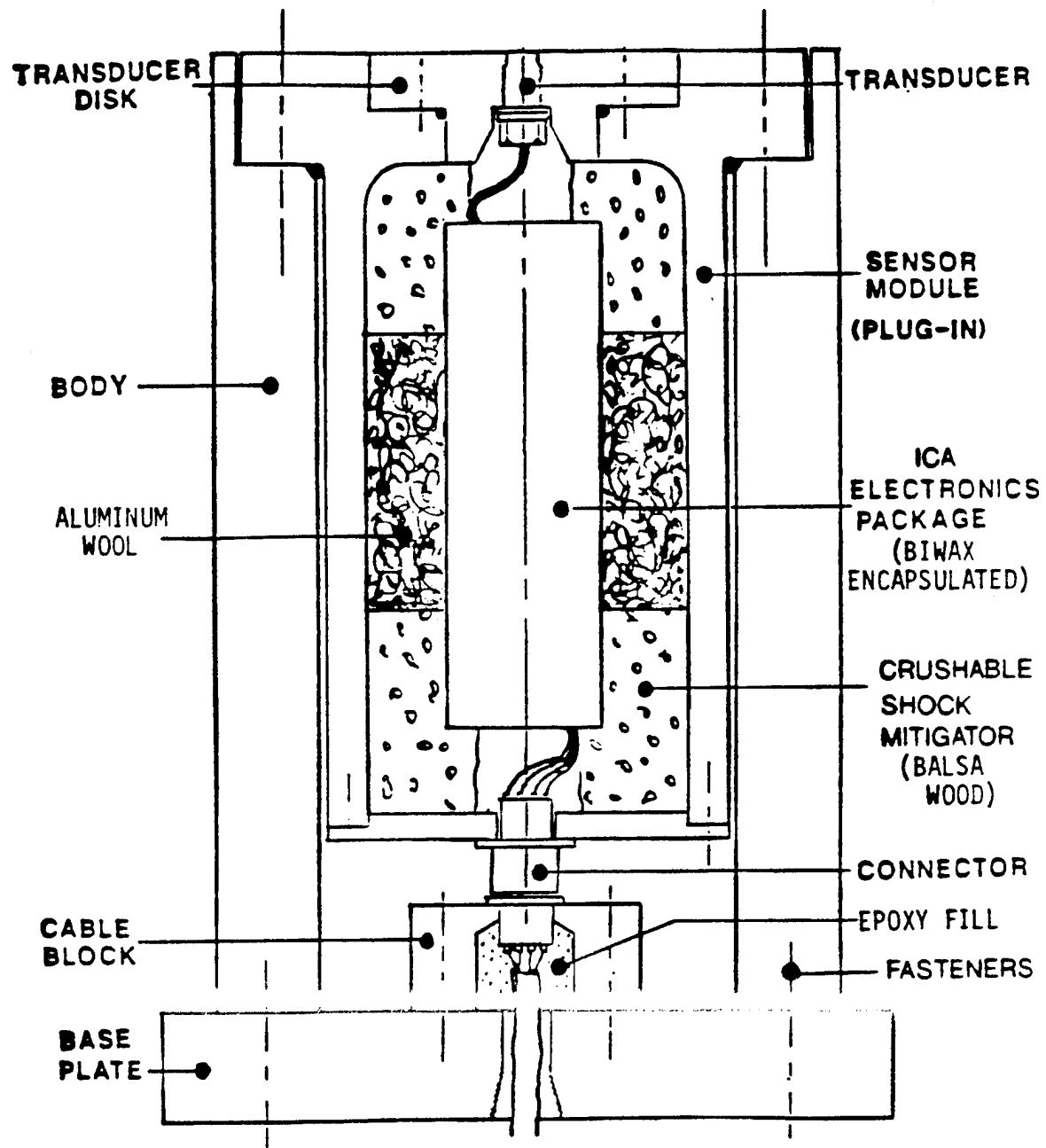


Figure 43. AFWL high pressure sensor hardware assembly.

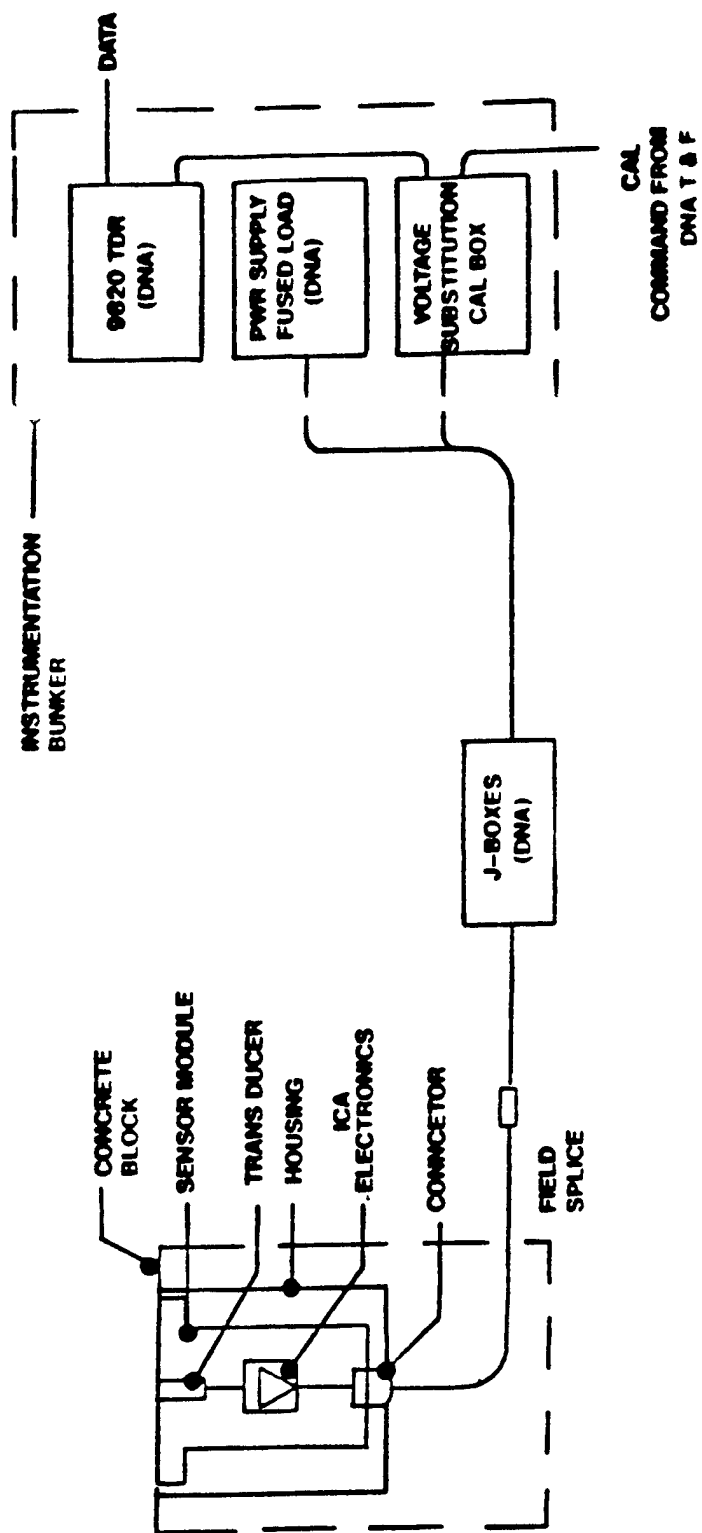


Figure 44. Typical channel for AFWL high pressure gage.

A 20 kHz bandwidth was quoted for the first model; later improved models were quoted as having a 100 kHz bandwidth.

Details of the pressure gage have not been published.

Ref: "DISTANT IMAGE Symposium Report," Volume I, DASA POR 7379-1, 1992.

Barth, P.W. and Wilson, J., "Ultrahigh Frequency Pressure Sensor-Novasensor," AFATL-TR-88-77, 1988.

4.3.8 CRC Snob Gage (1989) (USA).

The CRC Snob gage probe was designed and developed by the Carpenter Research Corporation using standard Kulite piezo-resistive sensors. The gage is shown in schematic form in Figure 45. It has a 0.4-inch shaft diameter with a 0.15-inch entrance diameter. A differential pressure sensor is used to measure flow Mach numbers of approximately 0.03 to 1.0. A static pressure is measured by a second gage. Dust particles of varying sizes pass through a throat in the gage to a chamber in the rear where the dust is captured for subsequent analysis.

Shown in Figure 46 is a snob probe in a forked shock tube fixture with a greg gage. The gage is aerodynamic in shape and has a slot in the top for access to the gage wires which is filled with epoxy prior to testing.

Gages deployed in the field were reported to be successful. The gages were located in the free field in a heavy dust environment and the record traces returned to zero at times which compare favorably to expected positive phase durations. Dust particles were collected in the back chamber; there was evidence of choking in the throat region. A response time of 1 millisecond was recorded.

Smaller miniature probes are currently being developed.

Ref: Carpenter, H.J., et al., "Snob/Greg Probe Characterization Analysis," DNA-TR-89-44, 1990.

Carpenter, H.J., Private Communication, 1993.

4.3.9 NMERI Snob Probe (1989) (USA).

A snob probe was developed by the New Mexico Engineering Research Institute and tested together with the H-Tech and CRC gages. Shown in Figure 47 is a schematic of the gage. It had a nose entrance diameter of 0.375 inch and used two piezo-resistive sensors which should give identical readings if the inlet flow is axially symmetric. A gage was tested in a shock tube but as far as is known, no gages were deployed in the field.

Ref: Carpenter, H.J., "Snob/Greg Probe Characterization Analysis," DNA-TR-89-44, 1990.

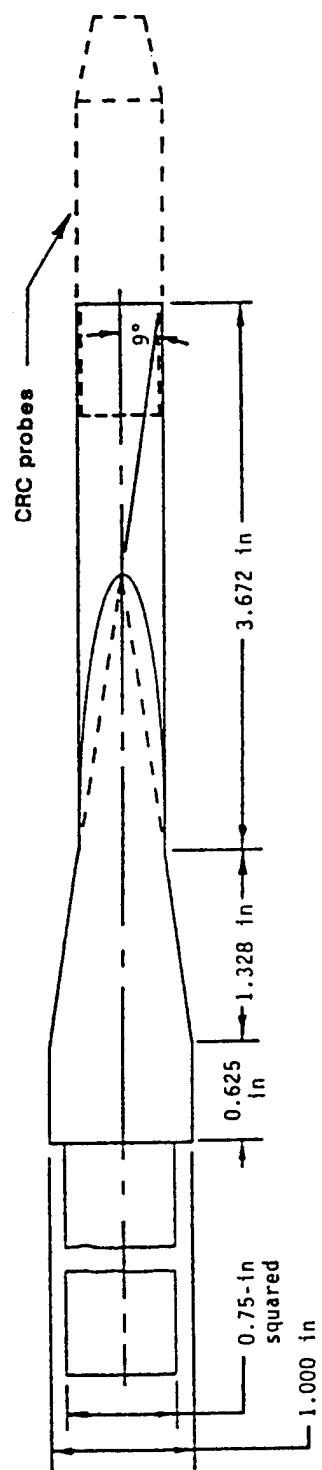


Figure 45. CRC snob probe.

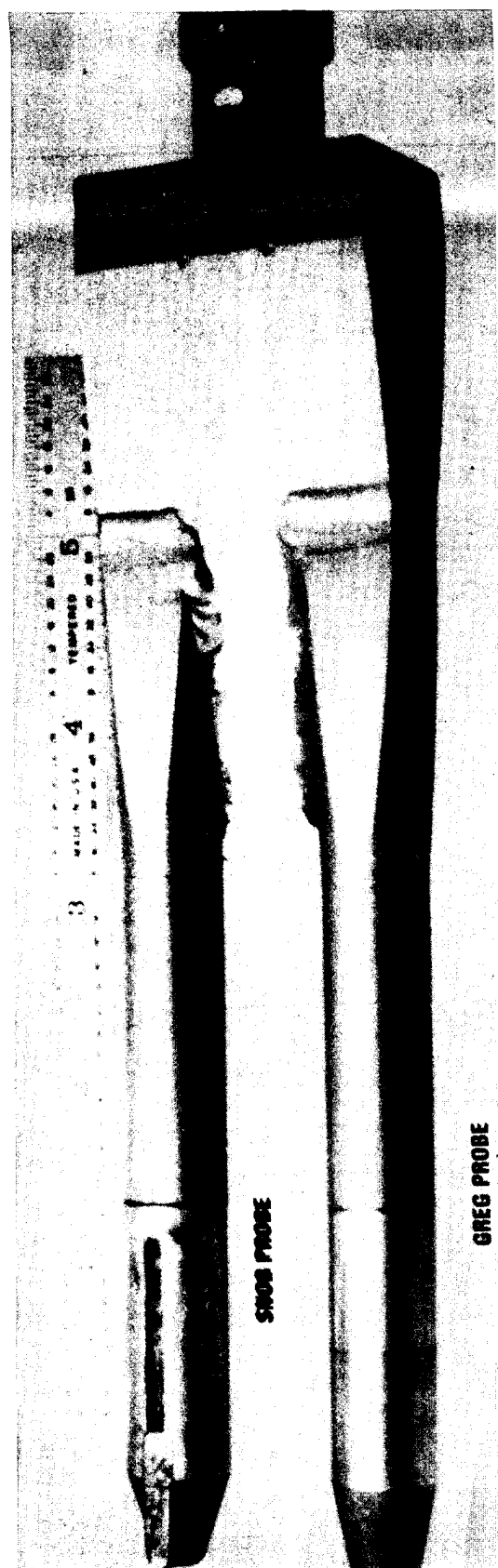


Figure 46. CRC snob/greg probe.

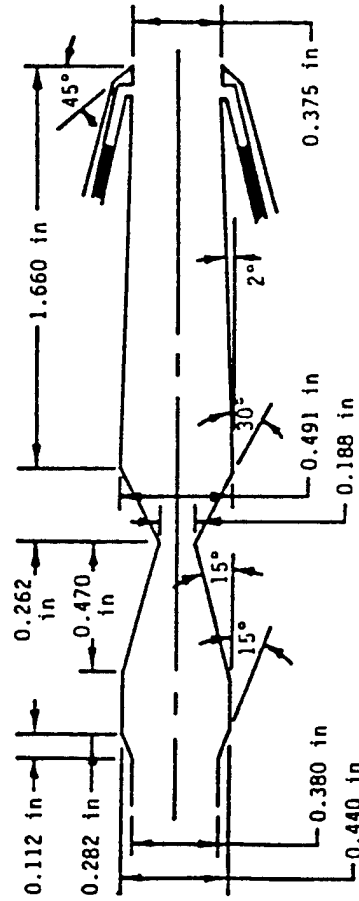
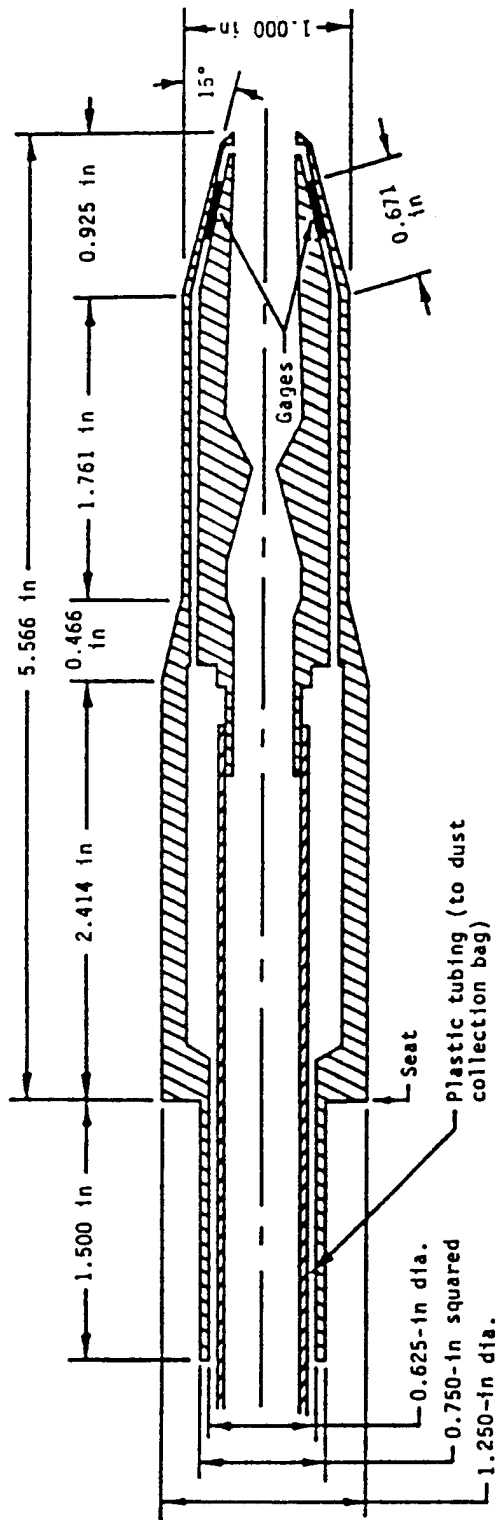


Figure 47. NMERI snob probe schematic.

4.3.10 BRL Cantilever (1961) (USA).

The BRL Cantilever gage was designed to determine the direction of flow and the time history of the dynamic pressure of the blast wave. An aluminum cylinder is capped at one end and instrumented near the base with four strain elements cemented at 90 degree intervals around the inner surface of the cylinder and oriented to measure longitudinal strain as shown in Figure 48. The clamped end of the cylinder is slit longitudinally at several locations about the cylinder circumference, with the slits extending from the base end of the cylinder to a point just below the effective length of the gage. The slits are to facilitate firm positioning and to prevent cocking of the cylinder when pressures are applied. The gage is assembled by inserting the cylinder into the smaller end of a tapered hole through a base plate until the slits are just below the surface. Through the other end of the base plate a tapered plug is threaded. This plug expands the slit end of the cylinder until the outer surface fits tightly against the inner surface, gripping the plug tightly.

Two gages were developed; one with a length of 12.9 inches with a frequency response of 500 hertz, and one with a length of 9.10 inches and a frequency of 1 kHz. The outside diameter of the cylinders was 2.250 inches and the inside diameter of 2.0 inches. The direction of loading can be determined by the proper orientation of the strain patches and by the polarity of the record.

Shock tube tests of the gage were made at subsonic flows of 10 and 30 psi. Results indicated that this omni-directional gage is practical and does have application in several aspects of blast instrumentation.

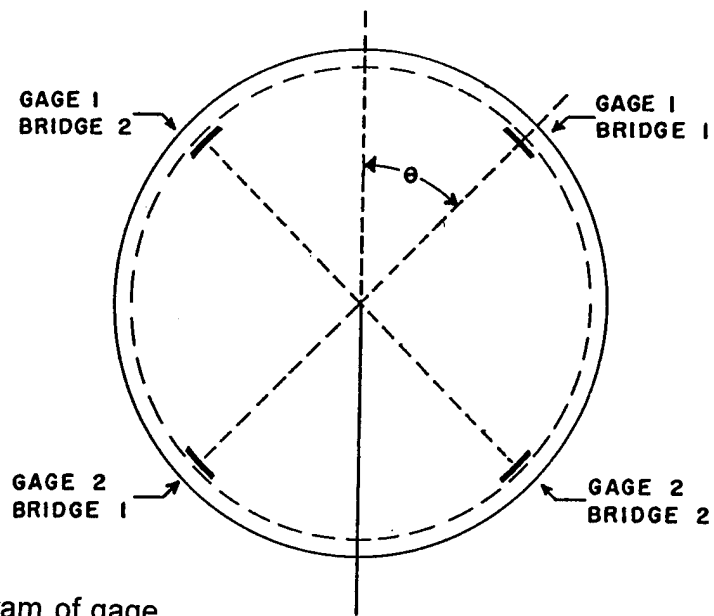
Ref: Johnson, O.T. and Ewing, W.O., "An Omni-Directional Gage for Measuring the Dynamic Pressure Behind a Shock Front," BRL Memorandum Report No. 1394, 1962.

4.3.11 Internal Strain Gage (ISG) Transducer (1987) (USA).

The ISG pressure transducer was designed to measure very high overpressures on the order of 10 kbar for the duration of the simulation. A mechanically rugged transducer, the sensor measures strain in a metal column through strain gages mounted on the inside of a small hole in the column. Shown in Figure 49, the cell in this assembly is the pressure transducer. The hardware was made from a cobalt-strengthened 18 percent nickel maraging steel. After heat treating, the metal has a nominal tensile strength of 350,000 lb/in².

Two 120-ohms foil matrix strain gages are bonded to the wall of the 0.156-inch diameter hole in the cell center to provide active axial gages. Two bridge completion resistors were placed in the cable splice module and encapsulated to soften the shock/acceleration environment on them. The gage operates like a compressive load cell so a substantial mount noted as the reaction plate is provided to react to the load on the exposed cell face and ring, and to lock the assembly firmly in position.

Field testing was conducted to a level of about 5 kbar. The hardware survived and data was favorable but limited in quantity and thus not conclusive. The gages deployed gave full duration pressure waveforms which appeared to be correct except for baseline shifts. When corrections were made for the shifts, the data agreed with other gage results.



(a) Diagram of gage.

(b) Unassembled gage.

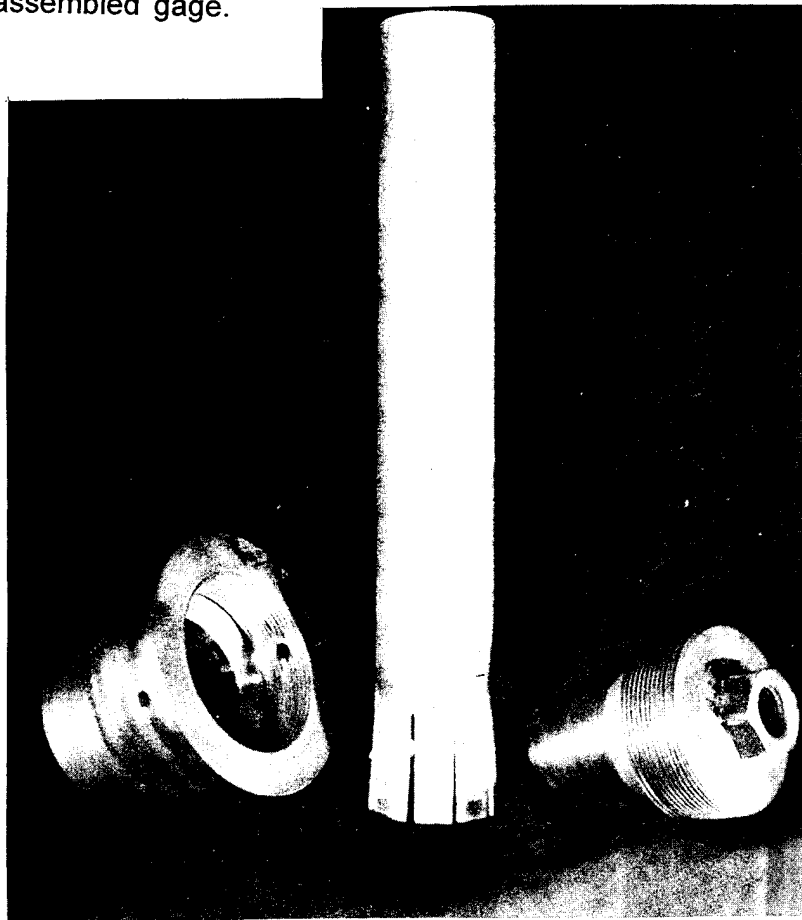
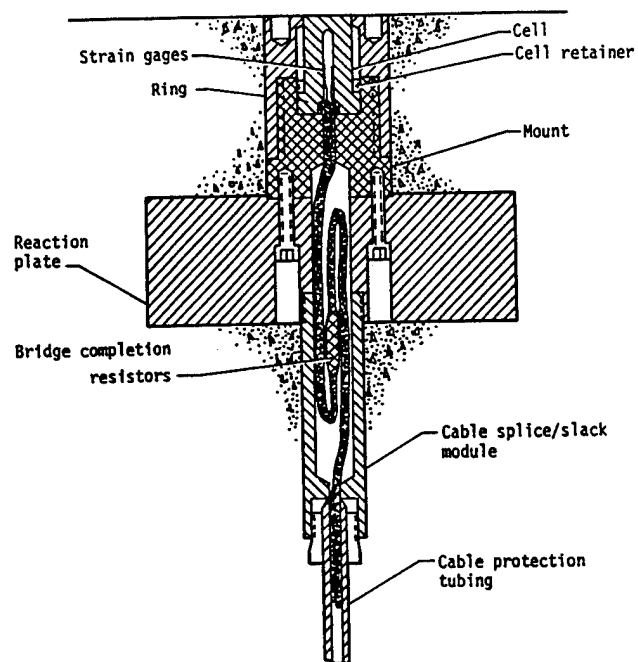
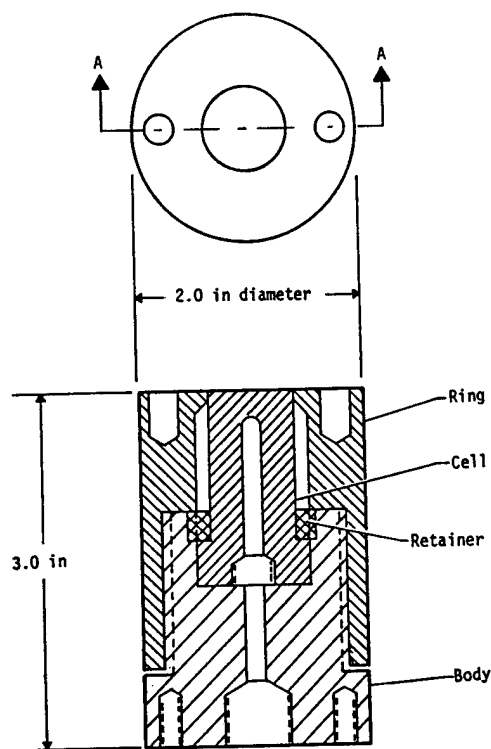


Figure 48. BRL cantilever gage.



(a) Mod N field assembly.



(b) Mod N.

Figure 49. Internal strain pressure (ISG) gage.

This gage is considered to be in the development stage and requires additional work to make it a useful transducer.

Ref: McCarson, Jr., T.D., "Internal Strain Gage (ISG) Airblast Pressure Transducer," AFWL-TR-87-77, 1988.

4.3.12 DRES Drag Cylinders (1968) (Canada).

Anchored cylinders measuring 3.5 inches in diameter were used to sense the drag pressure of the blast wave. Load bearing members were instrumented with strain gages and located inside the cylinders. In some cases specially shaped end caps were instrumented to sense the drag forces. Fins were added as seen in Figures 50 and 51 to simulate the presence of welded gussets at the attachment points of naval lattice masts constructed of cylindrical members.

Ref: Naylor, R. and Mellsen, S.B., "Unsteady Drag From Free Field Blast Waves," DRES-SM-42-71, 1973.

4.4 PIEZO-ELECTRIC.

4.4.1 LC33, CL60, BC33CZ, and LZF Gage (1960) (Canada).

Piezo-electric gages were deployed by the Suffield Experimental Station, now DRES, in the early 60's on a 20-ton and 100-ton HE event. These were a mix of commercially available gages and gages of their own design. It was stated in the report from DRES that "the commercially available pressure transducers of the 1950's apparently left something to be desired in terms of accuracy, frequency response, and insensitivity to acceleration and thermal effects, and this prompted the research agencies of that period to develop their own gages."

Canadian gages were:

- (a) The LC33 gage, made as a pencil model by the Atlantic Research Corporation. The sensitive element consisted of a short cylinder of lead zirconate titanate with a sensitivity of 120 pc/psi.
- (b) The LC60 gage, made as a flush mounted gage similar in principle to the LC33 gage described above.
- (c) The BC33CZ gage, made as a pencil model by the Atlantic Research Corporation. The sensitive element was barium titanate and had a sensitivity of 600 pc/psi.
- (d) The LZF gage was flush mounted and used lead zirconate as the sensitive element.

Recording of these gages was done by an FM Ampex 14-channel type recorder in the FM mode.

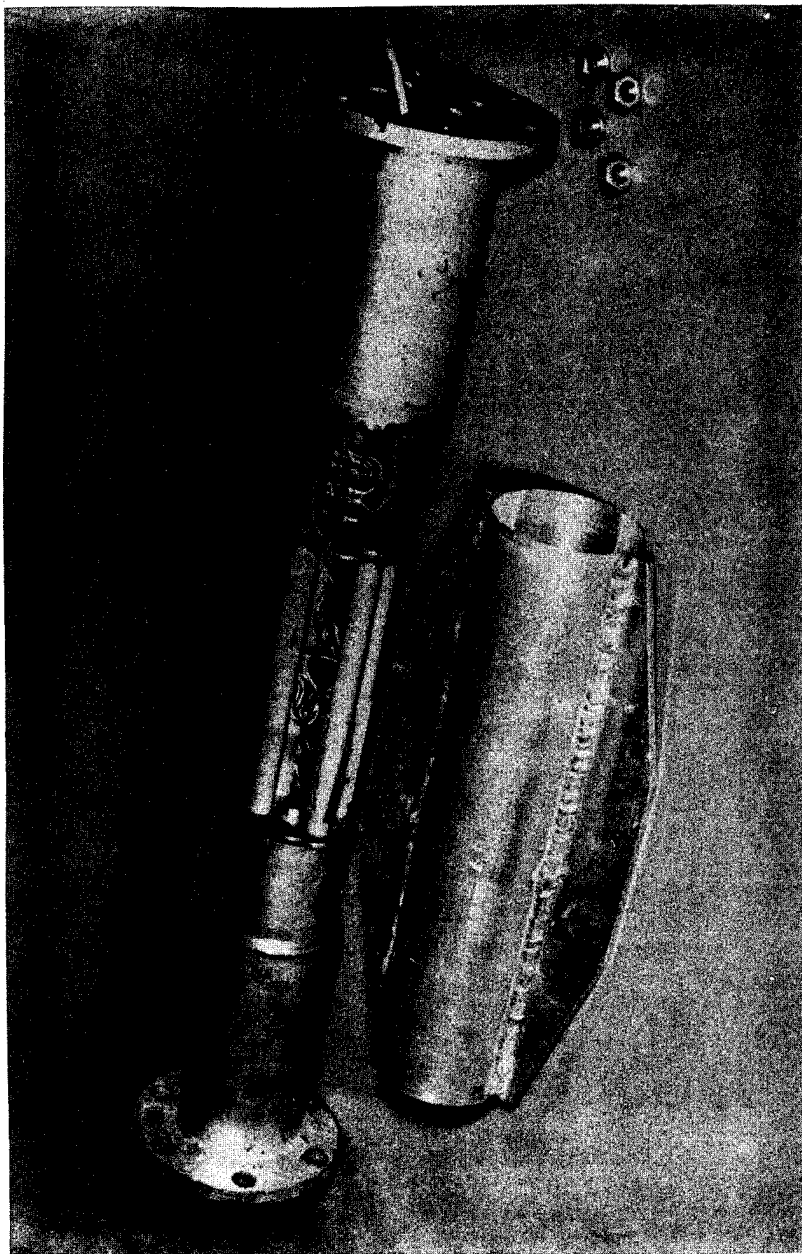


Figure 50. 3.5-inch finned drag force transducers.

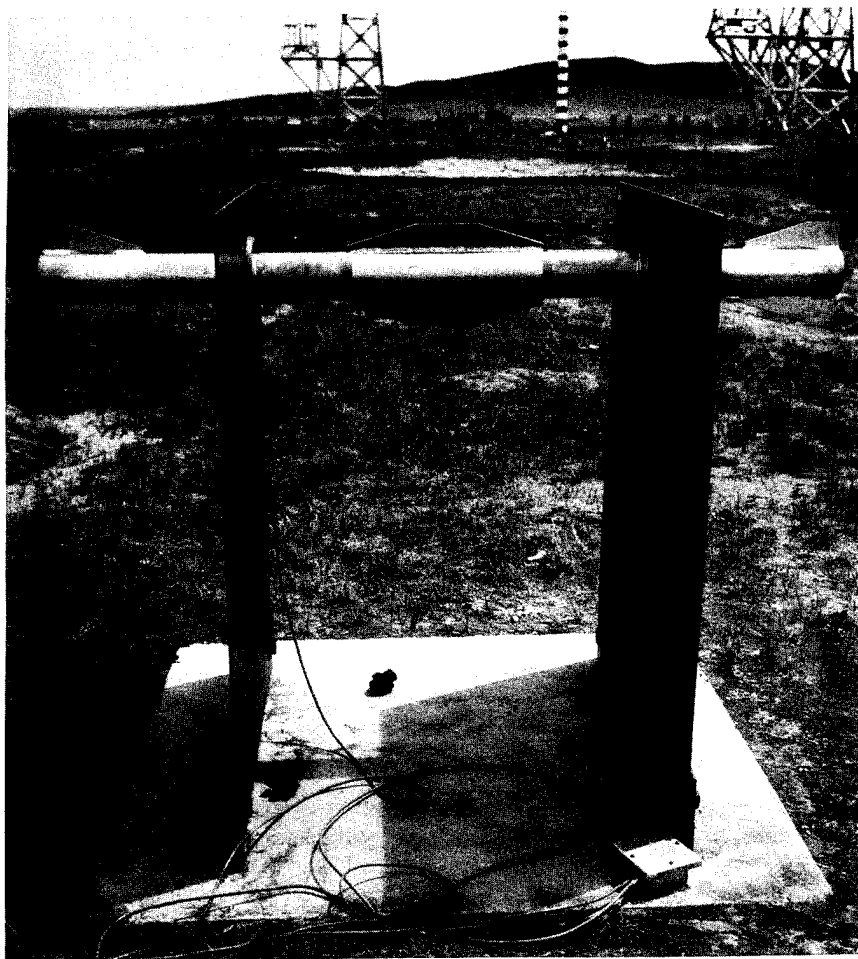


Figure 51. 3.5-inch finned drag force transducer in mount.

Gages were mounted in the field on stands as shown in Figure 52. Surface mounted gages were placed in a lead block as shown in Figure 53.

Pressure records from the LC33 and LC60 gages were not satisfactory. The BC33CZ gages yielded good results over the range of 4 to 17 psi. One good record out of three was realized by the LZF gages. In evaluating the piezo-electric systems in the early 60's, it was stated "that more time is needed to accumulate the necessary experience to produce a completely reliable system." The main difficulties appeared to be:

- (a) sudden changes in the pressure calibration of a channel;
- (b) zero drift of the recorded baseline;
- (c) changes in the wave shape which may possibly be due to the secondary effects produced by the mechanical stressing of the sensitive element or components of the gage.

Ref: James, D.J. and Rowe, R.D., "An Assessment of the Tripartite Pressure-Time Recordings from the 20-Ton and 100-Ton TNT Charges Detonated in 1960 and 1961 at the Suffield Experiment Station," AWRE Report E4/63, 1963.

"Scientific Observations on the Explosion of a 20-Ton TNT Charge," Suffield Report No. 203.

4.4.2 B2 (FQ11C) and MQ10 Gages (1960) (GBR).

The British piezo-electric gages used a quartz crystal in two configurations. One was labeled type B2 and was mounted in a hatched-shaped streamline baffle for recording free air pressure incident in the direction of the length of the baffle. This gage had a sensitivity of 100 pc/psi and was ranged for pressures 1 to 70 psi. The second gage was a type MQ10, a flushed-mounted version of the B2 gage. It also had a sensitivity of 100 pc/psi but was ranged for pressures 1 to 300 psi. The MQ10 gage was normally mounted in a concrete block flush with the ground surface.

Variations of these gages were the MQ18, MQ20, and MQZ3. Information concerning their characteristics are presented in Tables 11 through 15 and Figures 54 through 57.

Field results from these gages on a 20-ton and 100-ton event were very good and held by all the tripartite participants on the test to give the nearest approximation to the true pressure-time variations in the blast wave of all the type of gages deployed on the tests. This applied to a pressure range up to 230 psi.

Sample pressure records obtained with the MQ10 gage are presented in Figure 58.

The recording system for piezo gages, it was stated, was limited to durations of less than 150 ms owing to the finite time-constant of the line amplifier used. High levels of noise were expected from the high gain amplifiers when the cable lines were long and the overpressure low.

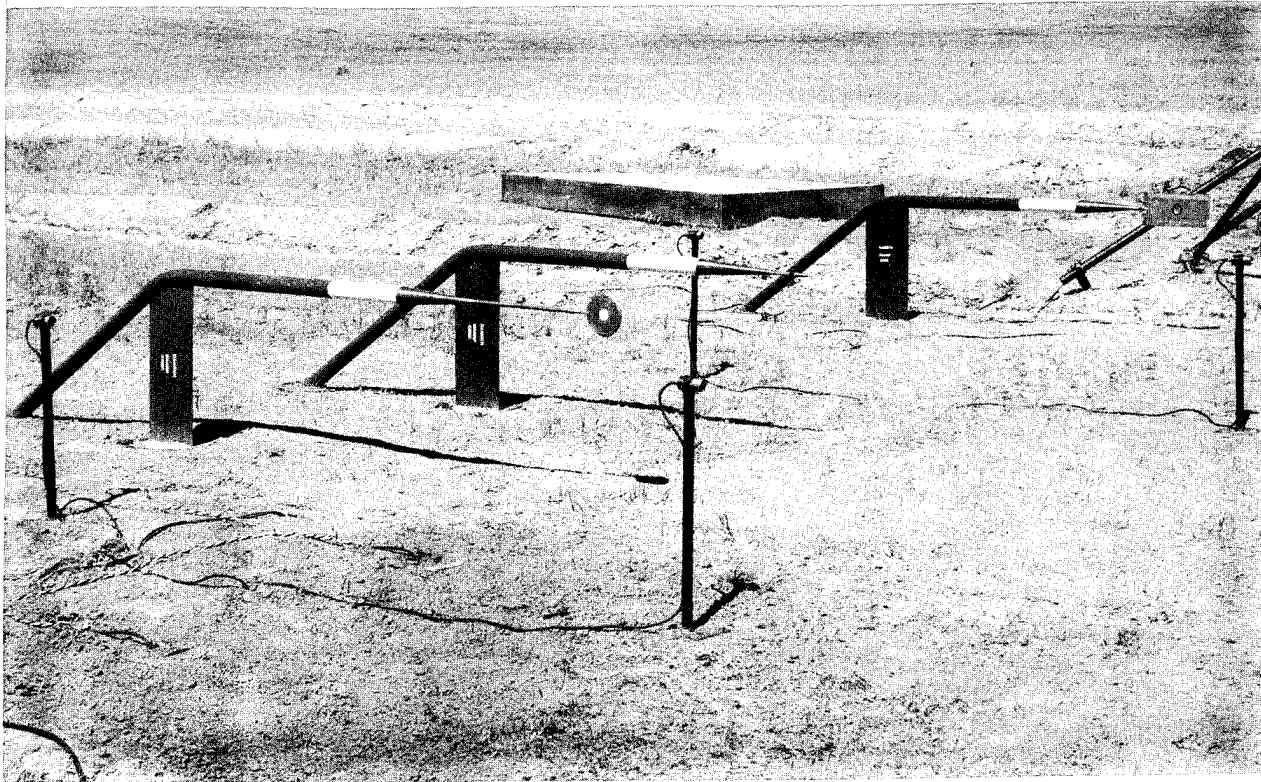
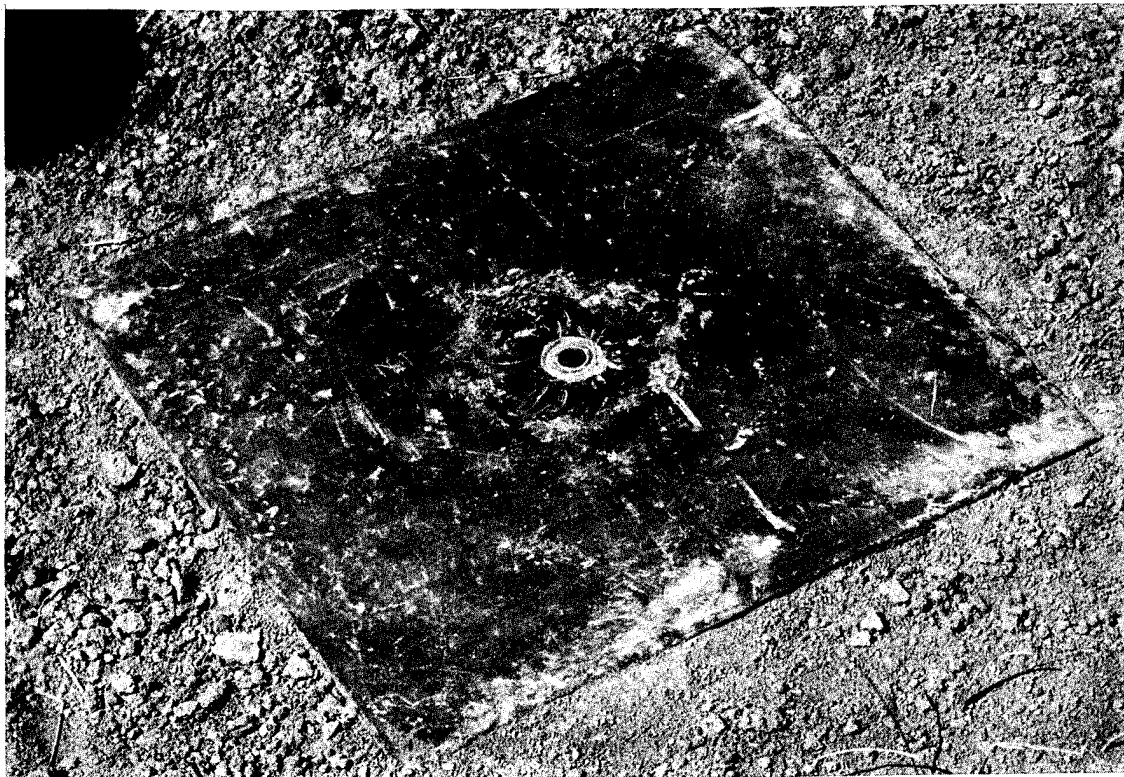
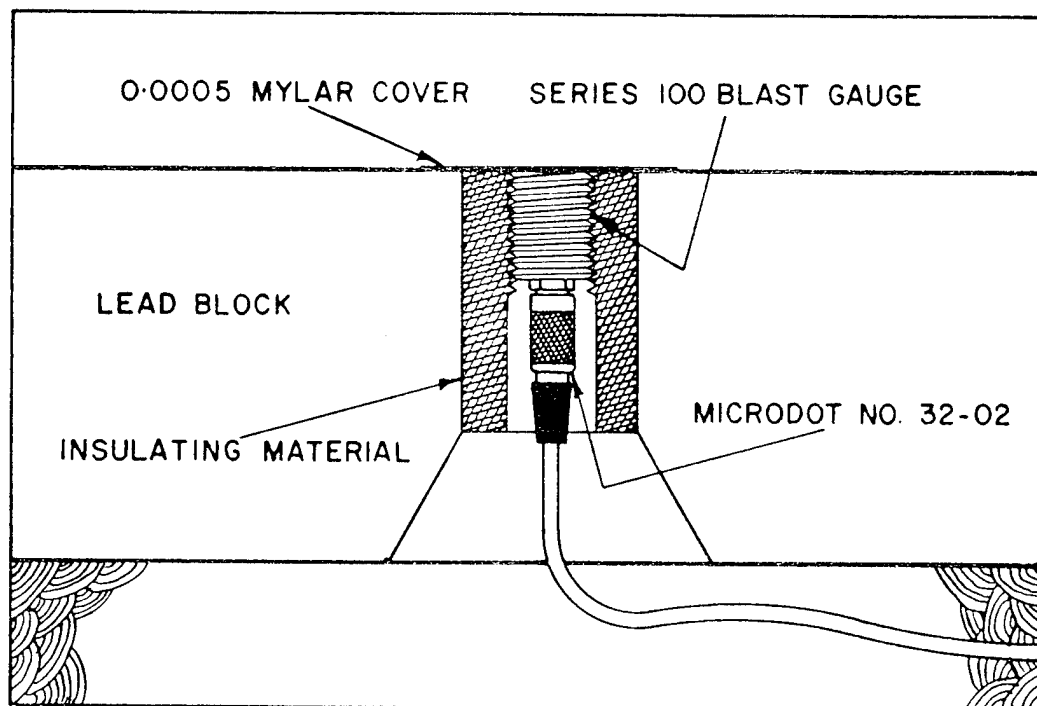


Figure 52. Gage stand setup for 20-ton trial.



(a) Gage installed.



(b) Diagram of gage installation.

Figure 53. Cross section of gage in lead block.

Table 11. Summary of properties of Foulness pattern standard piezo-electric transducers.

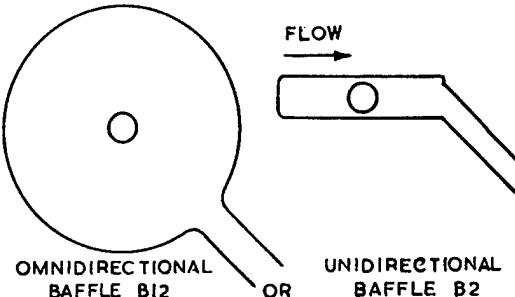
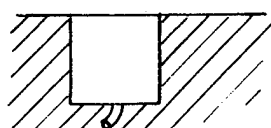
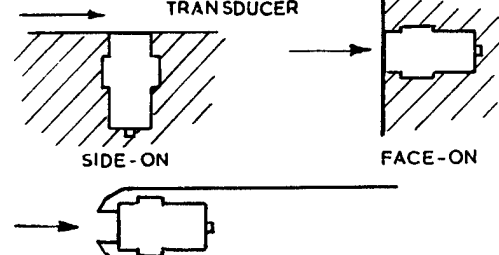
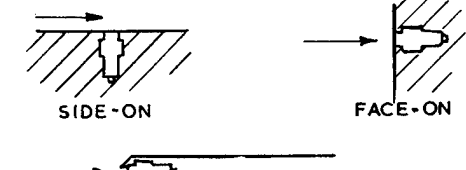
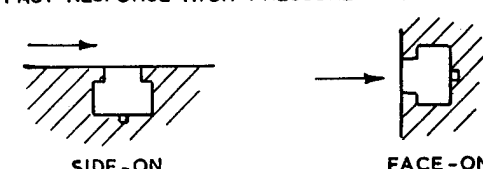
TRANSDUCER TYPE	MAXIMUM PRESSURE psi	SENSITIVITY pc/psi mv/psi WITH CABLE SUPPLIED		APPLICATIONS
FQ 11c PRESSURE INSERT	300	100	—	<p>FREE AIR MEASUREMENTS : MOUNTED IN</p>  <p>OMNIDIRECTIONAL BAFFLE B12 OR UNIDIRECTIONAL BAFFLE B2</p>
MQ 10	500	100	—	<p>SENSITIVE FLUSH MOUNTED TRANSDUCER</p>  <p>MAINLY USED FOR 'SIDE-ON' MEASUREMENTS</p>
MQ 18	300	24	300	<p>ACCELERATION COMPENSATED FLUSH MOUNTED TRANSDUCER</p>  <p>SIDE-ON FACE-ON</p> <p>TOTAL HEAD PRESSURE MEASUREMENTS USING BAFFLE BS2</p>
MQ 20	30000	0.5	2.5	<p>SMALL HIGH PRESSURE TRANSDUCER</p>  <p>SIDE-ON FACE-ON</p> <p>TOTAL HEAD PRESSURE MEASUREMENTS USING BAFFLE BS5</p>
MQ 23	20000	2.0	8	<p>FAST RESPONSE HIGH PRESSURE TRANSDUCER</p>  <p>SIDE-ON FACE-ON</p>

Table 12. Nominal MQ10 gage characteristics.

<u>DYNAMIC:</u>	
Dynamic Pressure Range	0-500 psi 0-36 kg/cm ²
Charge Sensitivity	100 pC/psi 14x10 ⁻¹⁰ C/kg/cm ²
Voltage Sensitivity with 6-ft Cable	180 mV/psi 2.5 V/kg/cm ²
Capacity	402 pF
Resonant Frequency	80 kc/s 80 KHz
Rise-Time (Face-On)	5 microseconds
Resolution	Infinite
<u>PHYSICAL:</u>	
Size	1 7/8" dia. x 2 1/8" 48 mm dia. x 53 mm
Weight	1 lb, 8 oz 670 g
Measuring System	Piezo-Electric
Measuring Element	12 Element Quartz Crystal Pile
Mechanical Preload	None
Body Material	Stainless Steel
Diaphragm Material	Metallised Neoprene
Mounting	See Diagram
Electrical Connector	Spike and Lock Screw
Connecting Cable	Low Noise Co-axial
Cable Capacity	21 pF 69 pF/m
Accessories Included:	Nil
<u>GENERAL:</u>	
Calibration	Semi-Dynamic
Insulation	> 10 ¹¹

Table 13. Nominal FQ11C gage characteristics.

<u>DYNAMIC:</u>	
Dynamic Pressure Range	0-300 psi 0-20 kg/cm ²
Charge Sensitivity	100 pC/psi 14x10 ⁻¹⁰ C/kg/cm ²
Voltage Sensitivity with 6-ft Cable	180 mV/psi 2.5 V/kg/cm ²
Capacity	420 pF
Resonant Frequency	80 kc/s 80 KHz
Rise-Time	Dependent upon shock velocity
Resolution	Infinite
<u>PHYSICAL:</u>	
Size	6 1/2"x 2 1/2"x 5/5" 16.6x6.2x1.6 cms
Weight	2 lbs, 8 oz 1125 gms
Measuring System	Piezo-Electric
Measuring Element	12 Element Quartz Crystal Pile
Mechanical Preload	None
Body Material	Stainless Steel
Diaphragm Material	Metallised Neoprene
Mounting	See Diagram
Electrical Connector	Spike and Lock Screw
Connecting Cable	Low-Noise Co-axial Cable
Cable Capacity	21 pF 69 pF/m
Accessories Included:	Mounting Butt and Box
<u>GENERAL:</u>	
Calibration	Semi-Dynamic
Insulation	> 10 ¹¹

Table 14. Nominal MQ18 gage characteristics.

<u>DYNAMIC:</u>	
Dynamic Pressure Range	0-300 psi 0-20 kg/cm ²
Charge Sensitivity	22 pC/psi 300x100 ⁻¹² C/kg/cm ²
Voltage Sensitivity with 6-ft Cable	50 mV/psi 700 mV/kg/cm ²
Capacity with 6-ft Cable	420 pF
Resonant Frequency	85 kc/s 85 kHz
Rise-Time (Face-On)	5 microseconds
Resolution	Infinite
Acceleration Sensitivity	< 0.05 psi/g
<u>PHYSICAL:</u>	
Size	1 1/4" dia x 1 3/4" 32 mm dia x 44 mm
Weight	5.2 oz 160 g
Measuring System	Piezo-Electric
Measuring Element	12 Element Quartz Crystal Pile
Acceleration Compensation	12 Element Quartz Crystal Pile
Mechanical Preload	Vacuum Assembled and Sealed
Body Material	Stainless Steel
Diaphragm Material	Stainless Steel
Mounting	See Diagram
Electrical Connector	Coaxial No. 10 UNF Thread Mates with Cable
Connecting Cable	Low-Noise Sub-miniature Cable
Cable Capacity	180 pF for 6 ft Complete with Connectors
Accessories Included:	(1) 6 ft (183 cm) sub-miniature co-axial cable terminated each end with number 10 UNF sub-miniature connectors. (2) Adaptor to system connector.
<u>GENERAL:</u>	
Calibration	Semi-Dynamic
Insulation	> 10 ¹¹

Table 15. Nominal MQ20 gage characteristics.

<u>DYNAMIC:</u>	
Dynamic Pressure Range	0-30,000 psi 0-2100 kg/cm ²
Charge Sensitivity	0.5 pC/psi 7x10 ⁻¹² C/kg/cm ²
Voltage Sensitivity with 6-ft Cable	2.6 mV/psi 37 mV/kg/cm ²
Capacity with 6-ft Cable	190 pF
Resonant Frequency	275 kc/s 275 kHz
Rise-Time (Face-On)	1.5 microseconds
Resolution	Infinite
Acceleration Sensitivity	< 0.01 psi/g
<u>PHYSICAL:</u>	
Size	7/16" dia x 7/8" 11 mm dia x 21 mm
Weight	0.28 oz 8 g
Measuring System	Piezo-Electric
Measuring Element	Quartz Crystal
Mechanical Preload	Vacuum Assembled and Sealed
Body Material	Stainless Steel
Diaphragm Material	Stainless Steel
Electrical Connector	Coaxial No. 10 UNF Thread Mates with Cable
Connecting Cable	Low-Noise Sub-miniature Cable
Cable Capacity	180 pF for 6 ft Complete with Connectors
Accessories Included:	(1) 6 ft (183 cm) sub-miniature co-axial cable terminated each end with number 10 UNF sub-miniature connectors. (2) Adaptor to system connector.
<u>GENERAL:</u>	
Calibration	Semi-Dynamic
Insulation	> 10 ¹²

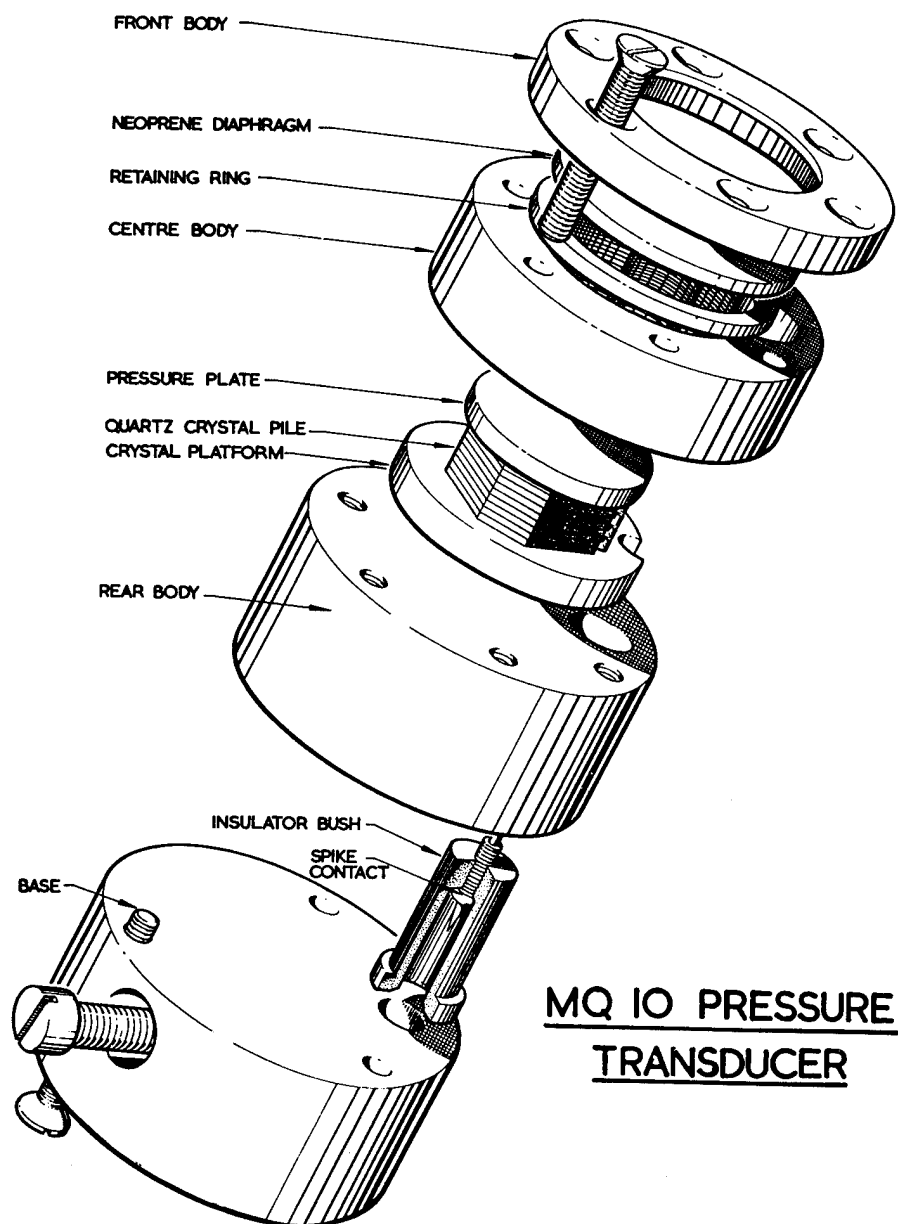
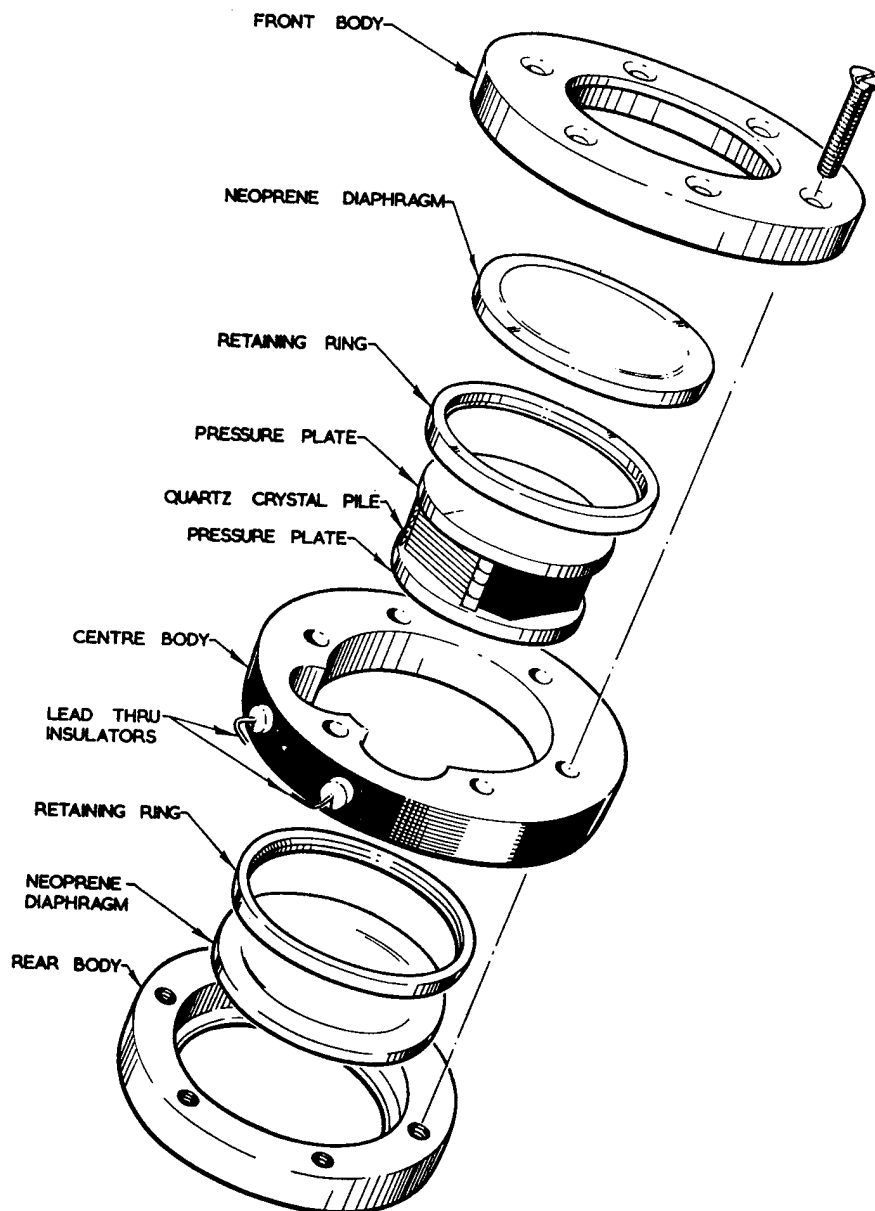
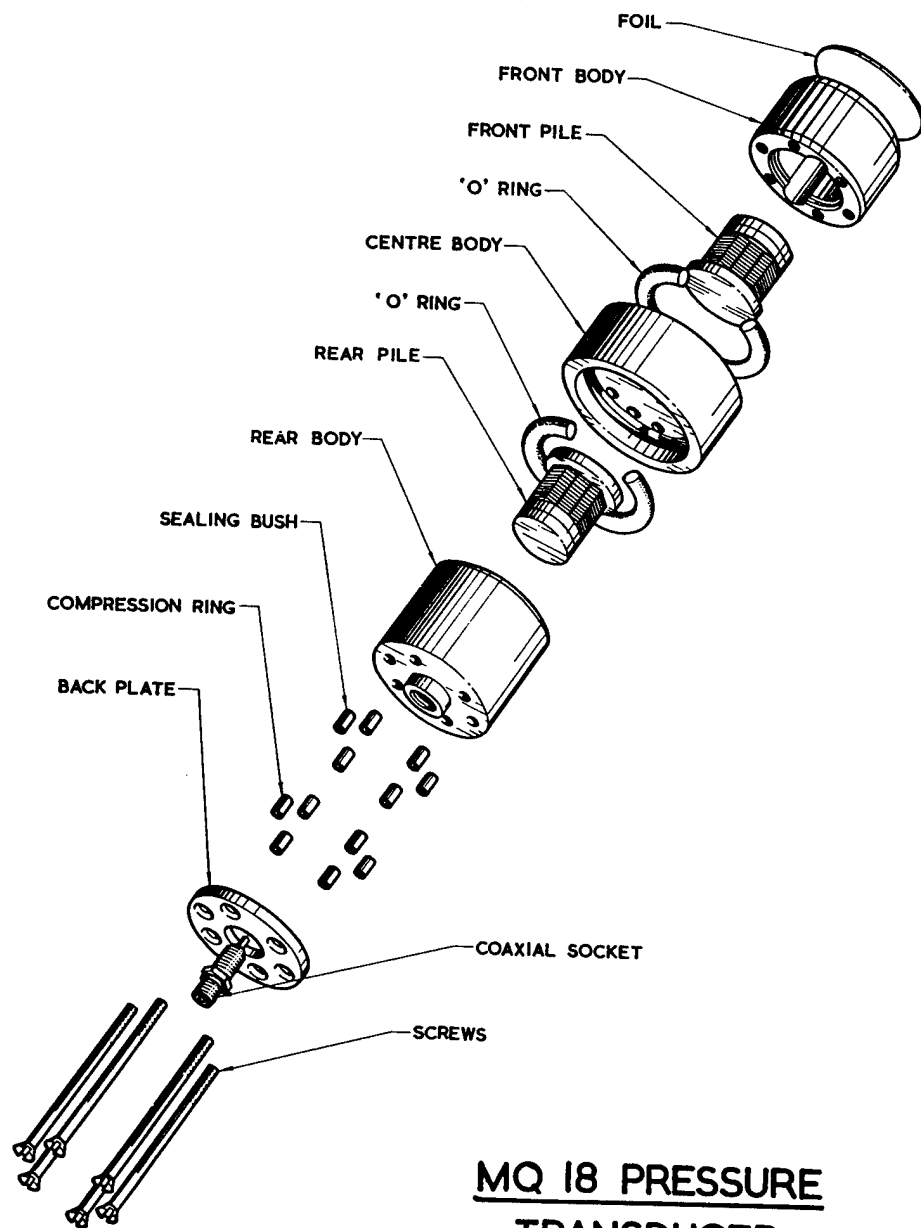


Figure 54. MQ10 pressure gage.



FQ 11c PRESSURE
TRANSDUCER INSERT

Figure 55. FQ11C pressure gage.



MQ 18 PRESSURE TRANSDUCER

Figure 56. MQ18 pressure gage.

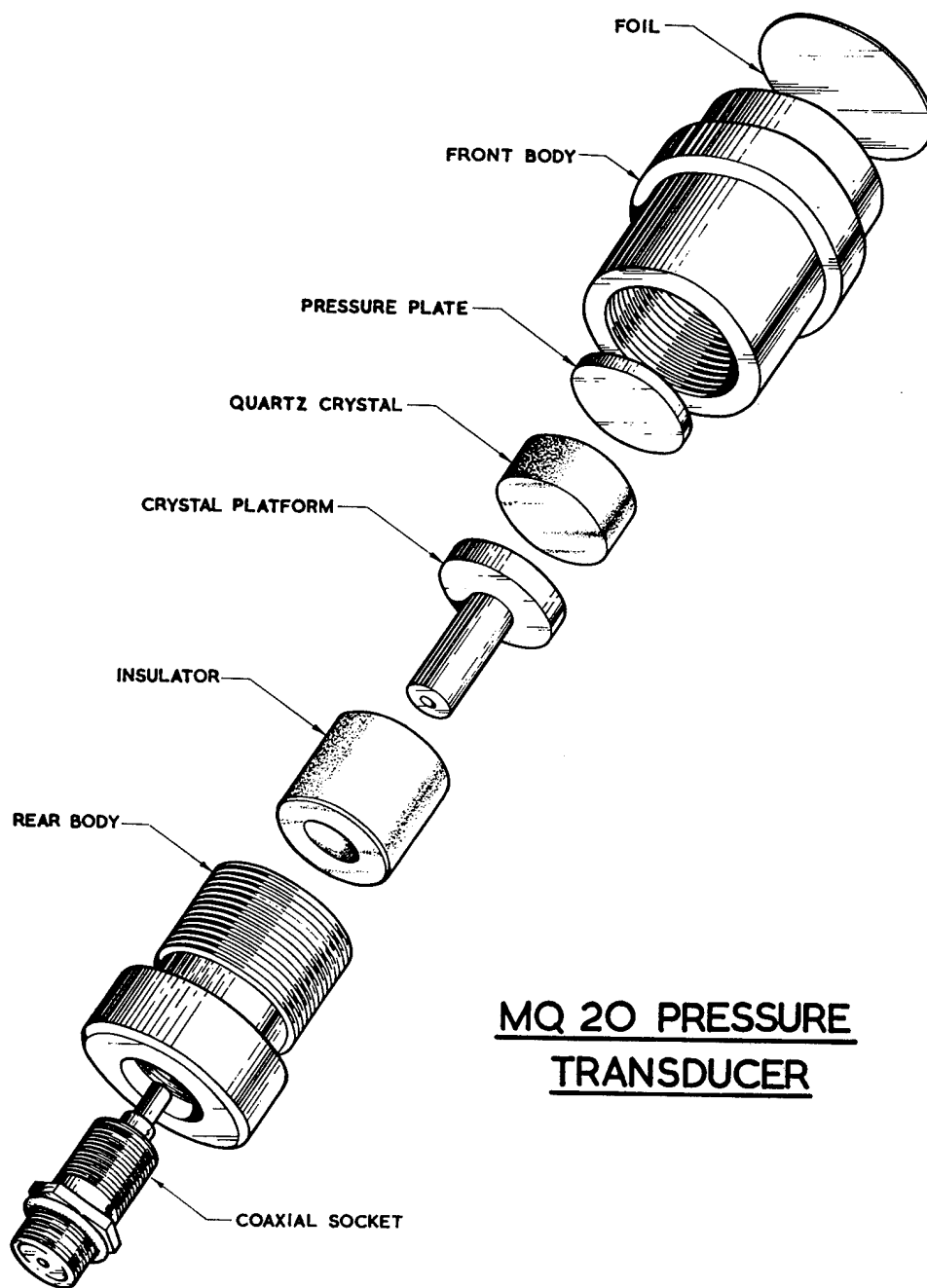


Figure 57. MQ20 pressure gage.

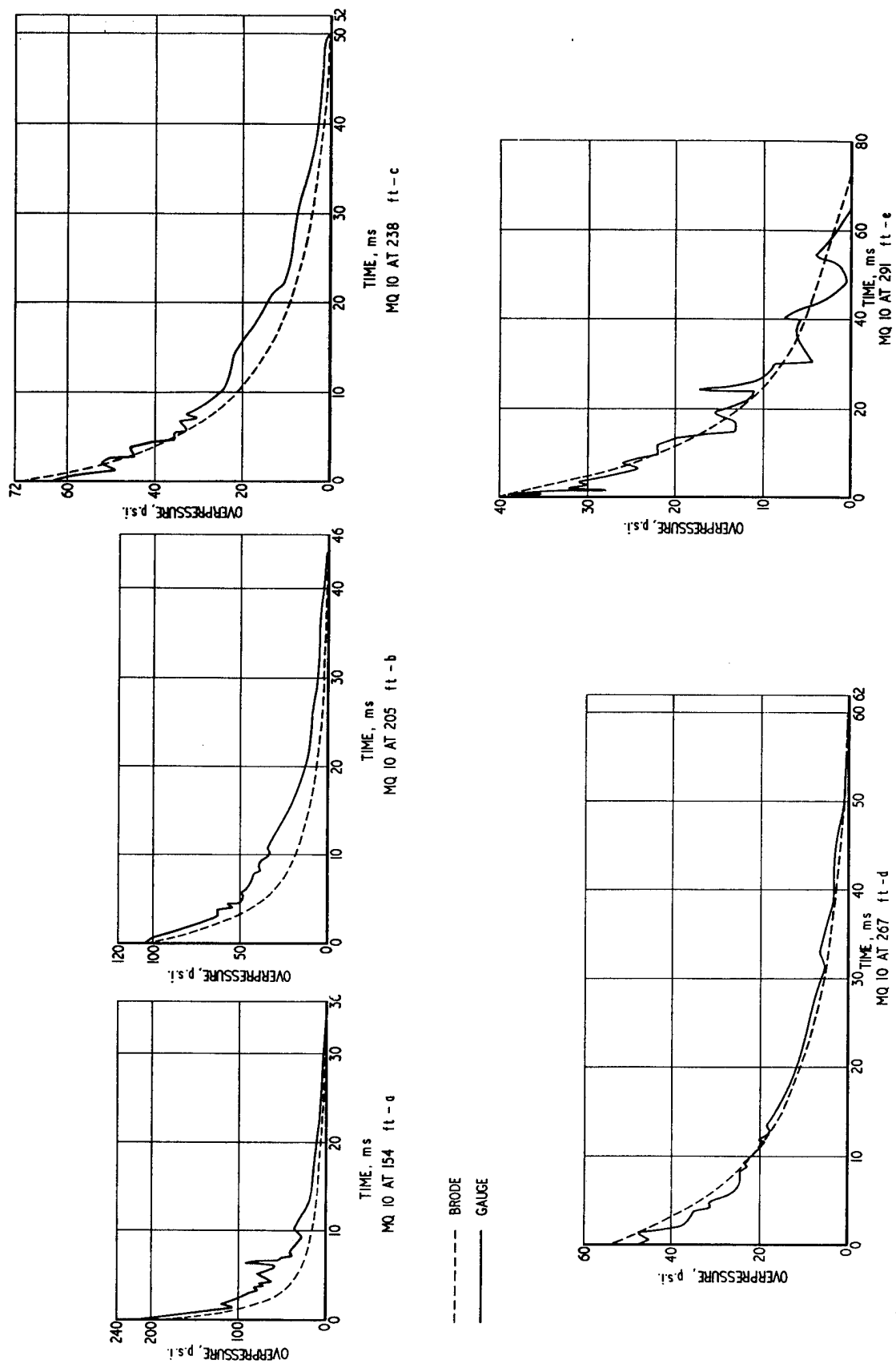


Figure 58. Comparison of UK MQ10 piezo-electric gage pressure time curves from SES 1961, 100-ton TNT trial with Brode's "point source" theoretical curves.

Ref: James, D.J. and Rowe, R.D., "An Assessment of the Tripartite Pressure-Time Recordings from the 20-Ton and 100-Ton TNT Charges Detonated in 1960 and 1961 at the Suffield Experiment Station," AWRE Report No. E4/63, 1963.

4.4.3 KKQ Gage (1960) (USA).

The KKQ gage uses piezo-electric elements as the sensing medium for measuring dynamic pressure. The basic principle was to difference the stagnation and side-on pressures before sensing and this was done by the use of a thin disc with side-on pressure led through a hole in the center of one side of the disc to the underside of a cap on a tube of piezo-electric material. Stagnation pressure was led to the other side of the cap. See Figure 59 for a schematic of the gage. Thus dynamic pressure was to be measured by the piezoelectric elements. Stagnation pressure was created by a thin baffle with a hole. The design objective was to measure small dynamic pressures from small charges.

Five gages were built by the Broadview Corporation. The first model was 2.5 inches in diameter, 5/16-inch thick with a baffle about 1/8-inches high. The second and succeeding gages were 2 3/16 inches in diameter and 3/16-inches thick.

Testing of the gage was made in a four-inch square shock tube. Results were very positive. Interest in direct dynamic pressure measurements at the time was not evident and the gage was not deployed on field tests.

Ref: Kaplan, Kenneth. "Reduced Ambient Pressure Explosion Testing in the VRS Shock Chamber," Military Applications of Blast Simulators, MABS-1, Vol 1, 1967.

4.4.4 BRL Piezo-electric Gages (1950) (USA) (Subsequently Susquehanna Instruments) (1968-1980) (Still later, PCB Piezotronics).

The BRL piezo-electric gages were developed in-house by the Ballistic Research Laboratory for use primarily in shock tube research. These gages were labeled types 1-4 and are outlined in Figures 60 through 63. The gage characteristics are given in Table 16. The type 2 and type 4 gages were deployed on several HE tests in the forefront of the 60's.

The gages were constructed in a stainless steel cylinder which for a type 2 gage was approximately 1/2 inches in diameter and 1/2 inches in length. The sensing element is essentially a flat disc of lead metaniobate about 1/4-inches diameter and 0.05-inches thick which produces an electrical charge proportional to the applied pressure. This element is embedded in a compound close to one end of the gage which is smoothed to a hard flat surface. The sensitivity of the transducer is 20 micro-micro coulombs per psi. When used as an overpressure gage at the ground surface, it was mounted into an adapter which isolates its housing electrically from ground.

The type 4 gage, later known as the Susquehanna ST-4 gage, employs a bar or what is labeled in the figure as an acoustic wave guide. The gage used tourmaline as the piezo-electric element. It was a high frequency transducer deployed in the field to measure shocks and had a rise time of one microsecond or less. Natural resonance of the crystal element is dissipated in the acoustic wave guide.

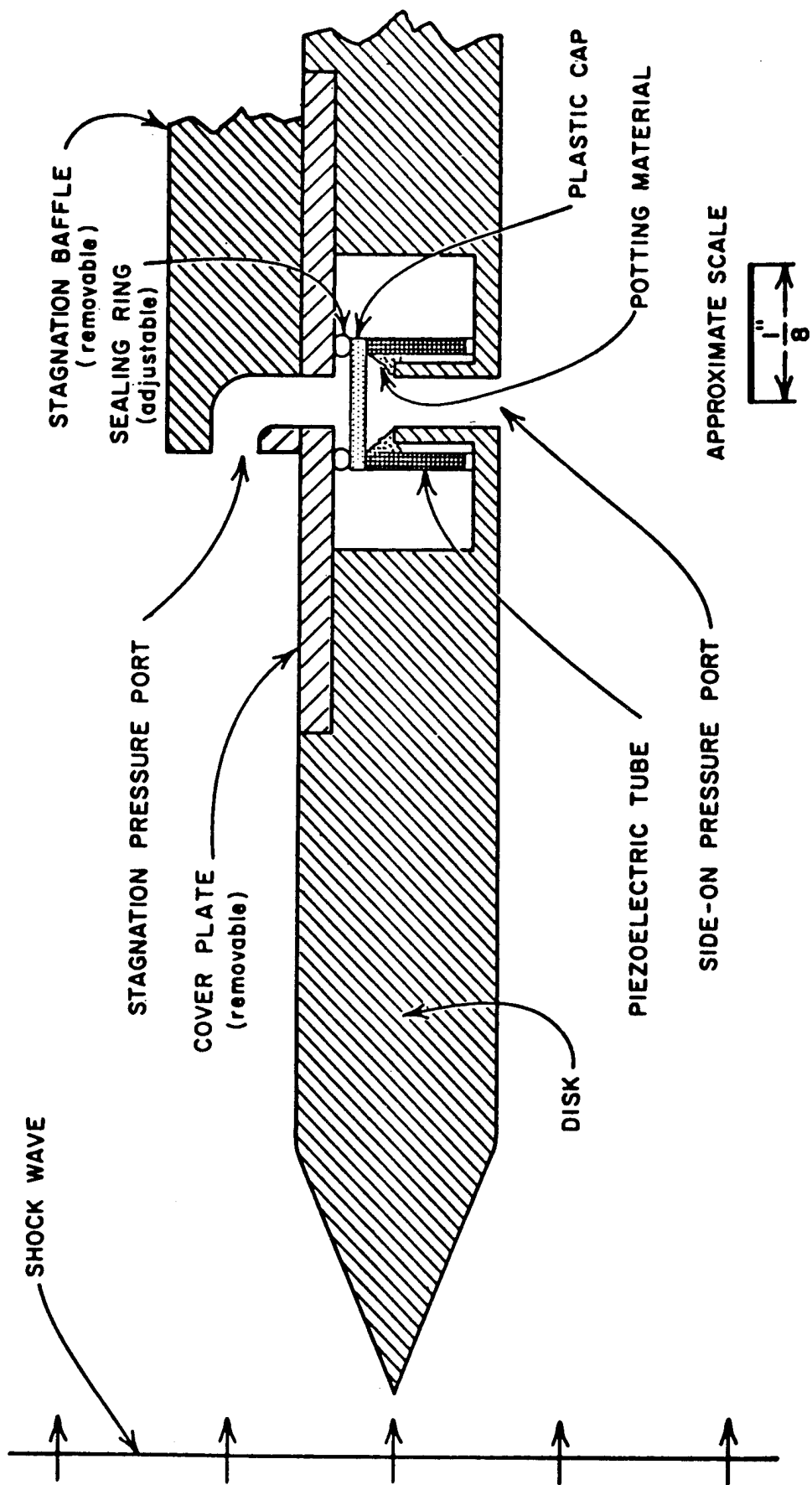
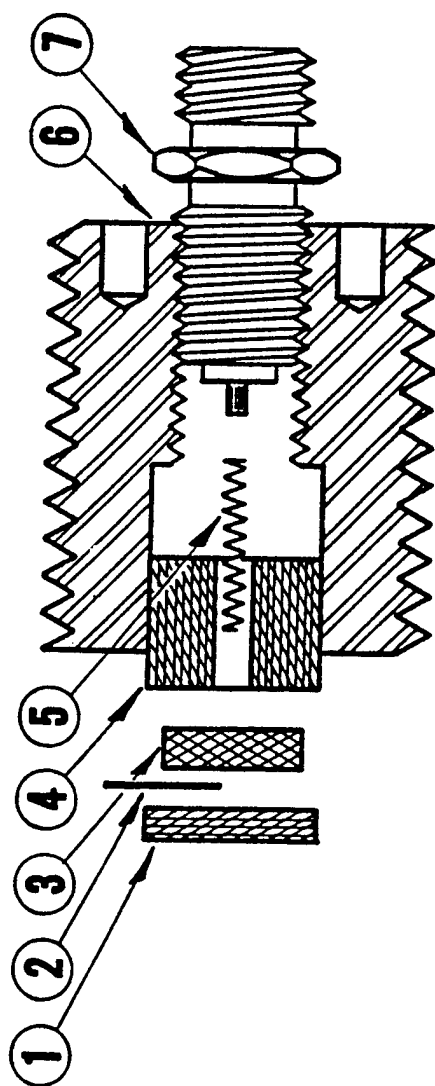


Figure 59. Schematic of KKQ dynamic pressure gage.



- 1 NYLON CAP
- 2 METAL FOIL GROUNDING TAB
- 3 CERAMIC PIEZO-ELECTRIC ELEMENT
- 4 NYLON INSERT
- 5 CONTACT SPRING
- 6 STAINLESS STEEL GAGE CASE
- 7 CO - AXIAL CONNECTOR

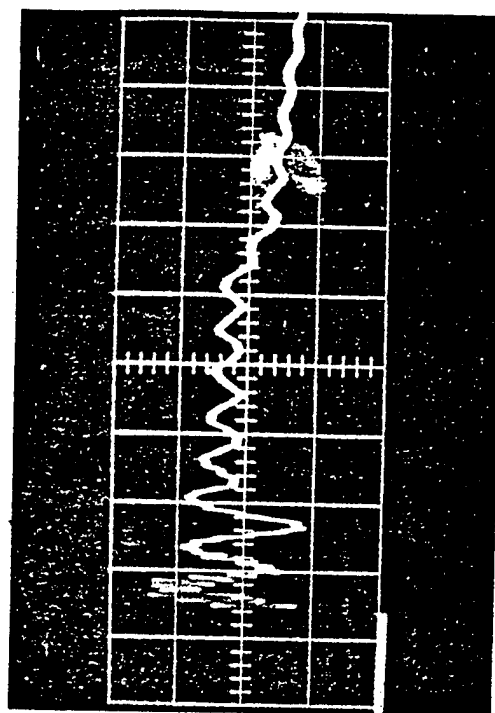
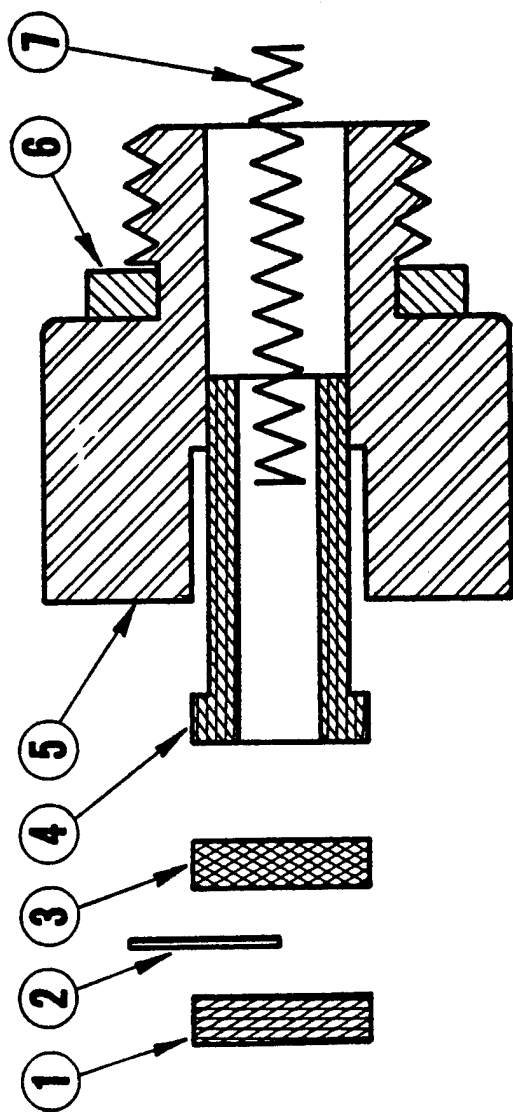


Figure 60. Type 1 piezo-electric gage.



- 1 NYLON CAP
- 2 METAL FOIL GROUNDING TAB
- 3 CERAMIC PIEZO-ELECTRIC ELEMENT
- 4 NYLON INSERT
- 5 STAINLESS STEEL GAGE CASE
- 6 RUBBER WASHER
- 7 CONTACT SPRING

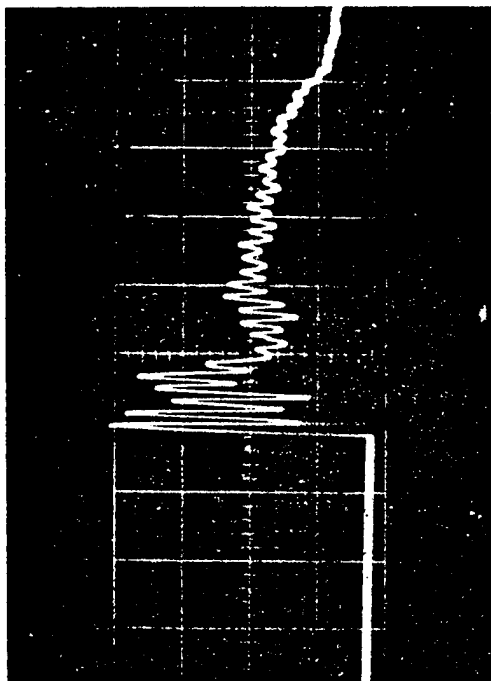
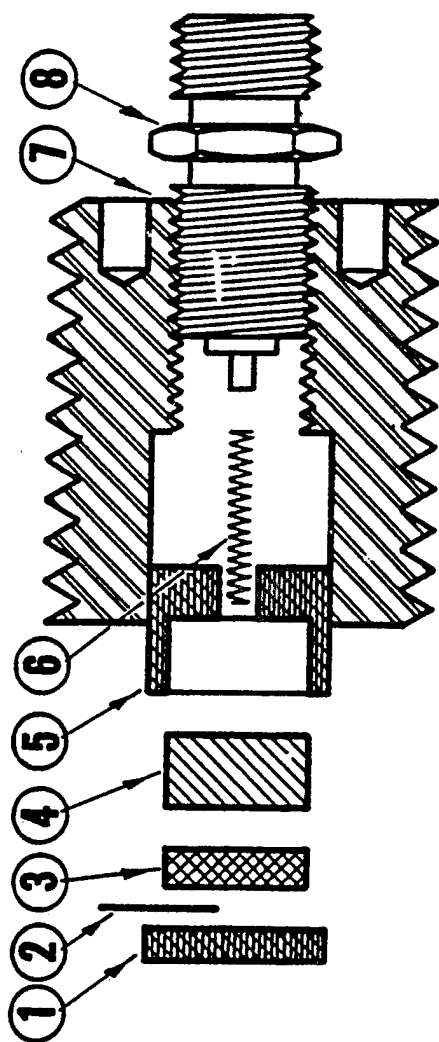


Figure 61. Type 2 piezo-electric gage.



- 1 NYLON CAP
- 2 METAL FOIL GROUNDING TAB
- 3 CERAMIC PIEZO-ELECTRIC ELEMENT
- 4 DISC
- 5 NYLON INSERT
- 6 CONTACT SPRING
- 7 STAINLESS STEEL GAGE CASE
- 8 CO-AXIAL CONNECTOR

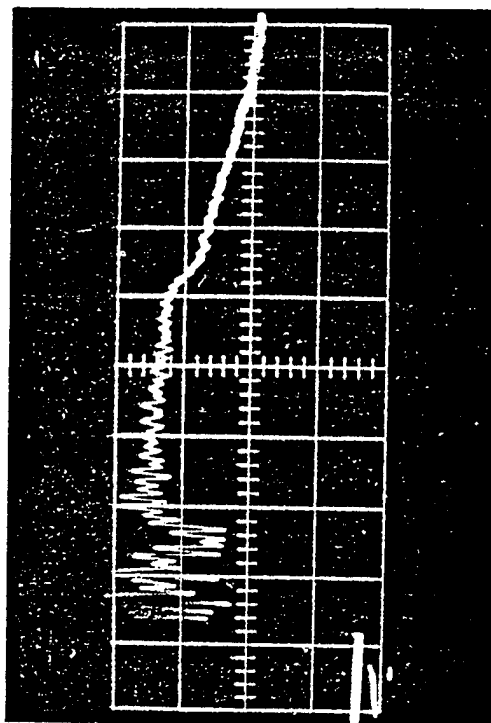
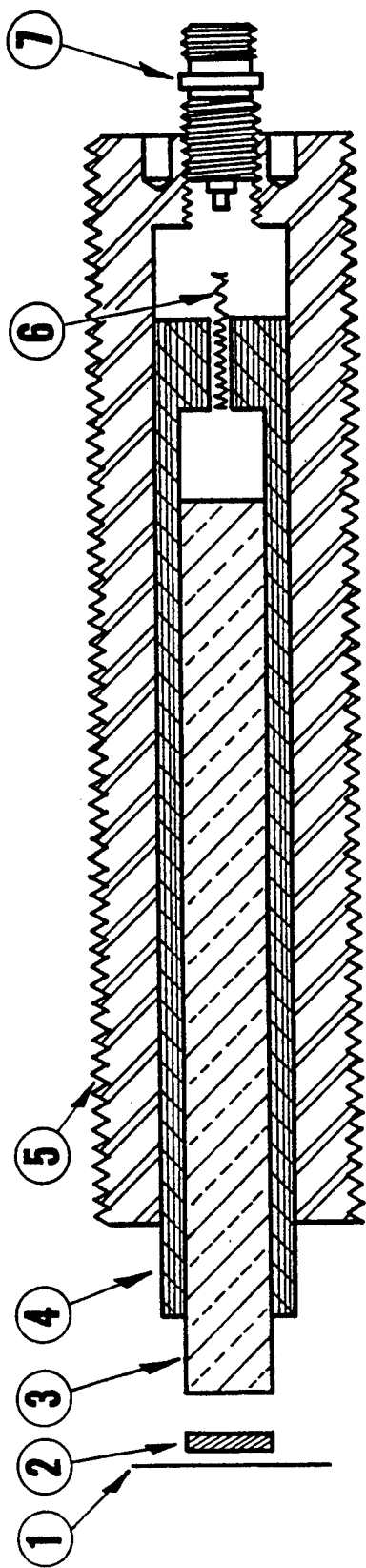


Figure 62. Type 3 piezo-electric gage.



- 1 METAL GROUNDING WIRE
- 2 PIEZO - ELECTRIC ELEMENT
- 3 BRASS ACOUSTIC WAVE GUIDE
- 4 NYLON OR TEFLON INSERT
- 5 STAINLESS STEEL GAGE CASE
- 6 CONTACT SPRING
- 7 CO - AXIAL CONNECTOR

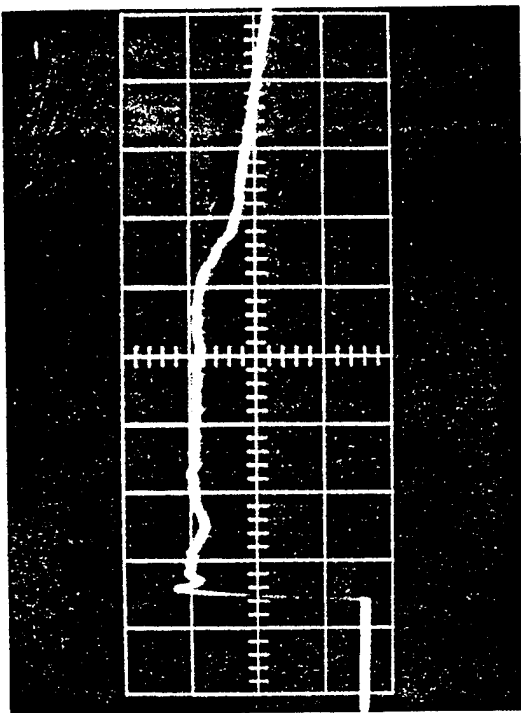


Figure 63. Type 4 piezo-electric gage.

Table 16. Characteristics of BRL piezo-electric blast gages.

	Type 1	Type 2	Type 3	Type 4	Type 4
Diameter, inches	1/2	1/2	1/2	1/2	3/4
Length, inches	1 1/8	5/8	5/8	1 9/16	3 1/4
Stainless Steel Case Thread, ASME	1/2-20	1/2-20	1/2-20	1/2-20	3/4-16
Piezo-electric Material	Tourmaline 0.150" dia.	Lead Metaniobate 0.150" dia.	Tourmaline 0.150" dia.	Tourmaline 0.125" dia.	Tourmaline 0.250" dia.
Natural Frequency, KC	100	250	450	2500	1500
Ringing Duration, microseconds	---	50	20	1	3
Rise Time, microseconds	3.0	0.8	0.4	<0.2	0.2
Temperature Range, °C	0-100	0-40	20-50	0-50	0-50
Accel Sensitivity, psi/g	<0.005	0.0005	---	0.005	---
Charge Output, pC/psi	0.200	15-20	0.150	0.130	0.450
Open Circuit Voltage, mV/psi	20	50	15	13	2
Pressure Range, psi	50,000	1-500	1-1000	10-10,000	10-2000
Linearity, Percent Full Scale	+0.001	+2.5	+1.5	+1.5	+1.5

Ref: Armendt, B.F., et al., "Project WHITE TRIBE: Air Blast From Simultaneously Detonated Large Scale Explosive Charges," BRL Report No. 1145, 1961.

Granath, B.A. and Coulter, G.A., "BRL Shock Tube Piezo-Electric Blast Gages," BRL Technical Note 1478, 1962.

Coulter, G.A., "Calibration of Pressure Transducers at the BRL Shock Tube Facility," BRL Memorandum Report 1943, 1967.

4.4.5 PCB 113A Gage (1978) (USA).

The 113A quartz piezo-electric pressure gage is manufactured by PCB Piezotronics, Inc., and was deployed on 1000-lb HE tests in 1978 after extensive shock tube testing. The gage has a resonant frequency of 500 kHz, a rise time of two microseconds, and a discharge time constant of 100 seconds. Integrated electronics provides for gage sensitivities of 1 to 50 mv/psi, a value which is fixed at the factory. The rigid structure of the gage contains the quartz element in a compression mode with an integral compensating accelerometer to reduce vibration sensitivity and suppress resonance effects.

The gage was configured for static pressure measurements in a 1/2-20 threaded case as illustrated in Figure 64, and given the number 102M. The same basic gage was used in a 1/2-inch total-head probe as shown in Figure 65.

The electronic system has the gage coupled through a line driver and signal conditioning to a Honeywell analog tape recorder. A block diagram of one channel of the system is shown in Figure 66(a) and 66(b).

The system was designed to have at least a bandwidth of 500 kHz so signals of one microsecond rise time could be recorded. The gages for static overpressure were either mounted in ground baffles, Figure 67, or one-sided rakes for elevated stations, Figure 68(a) and 68(b).

All gages used in the tests were connected by coaxial cables to PCB power units and line drivers located in an underground bunker near the test site. The line drivers were designed by TRW, Inc., as shown in Figure 66, to drive the RG-58 c/u coaxial cables running approximately 200 feet from the bunker to the recording van while providing bandwidths more than sufficient to record one microsecond rise time signals on Wide-Band II Honeywell 101 analog tape recorders. The coaxial cables were terminated in specially designed conditioner cards mounted in B&F 1-700 chassis. Calibration voltage steps were injected through these cards. The tape recorders were operated at the 120 inches per second speed to provide the necessary bandwidth.

Typical gage records obtained from two 1000-lb HE events in 1985 using these gages are presented in Figure 69. The explosive charge used for these events was the HMX-based cast spherical charge TPH-3342.

France (1993) uses the 113A20 gage.

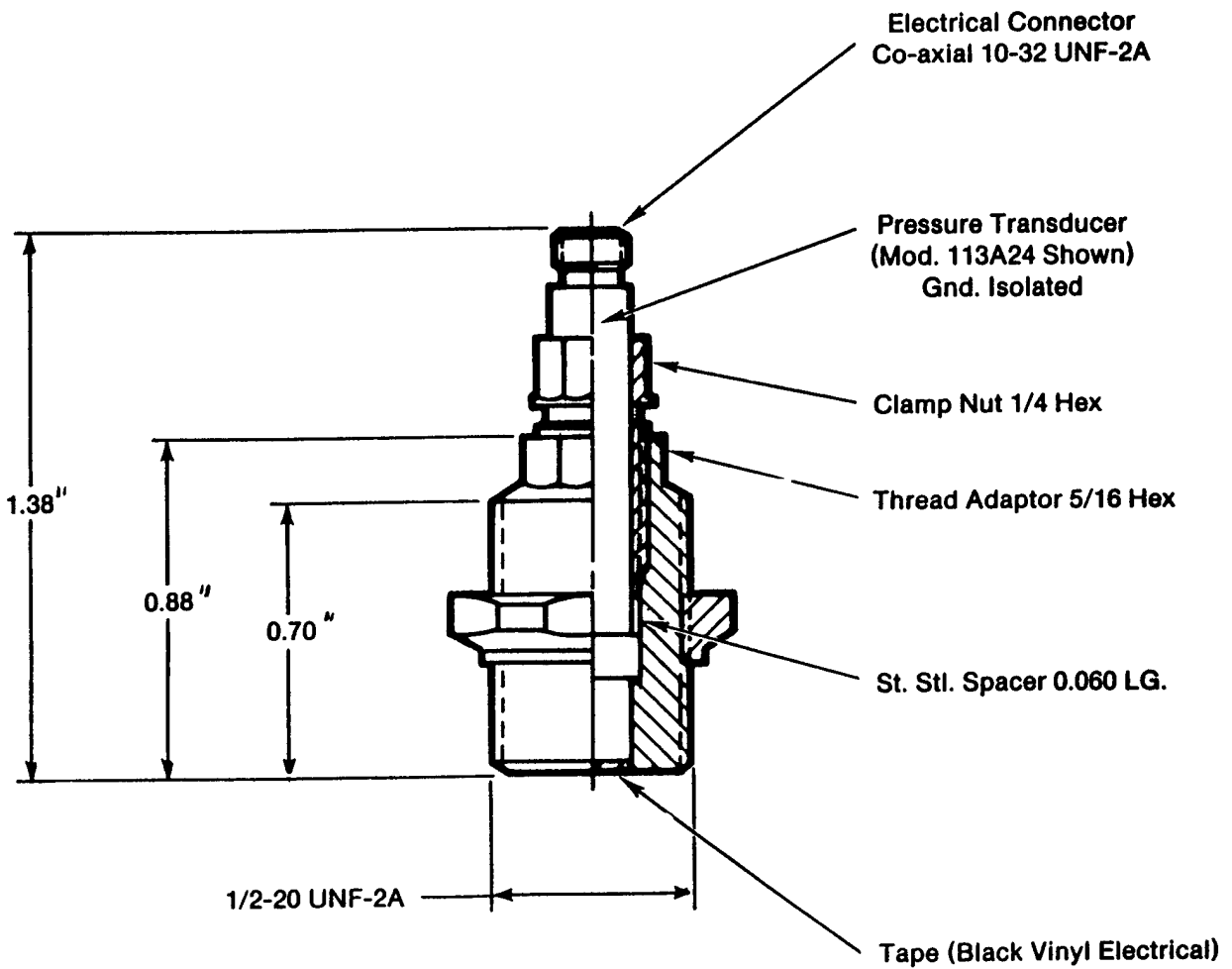
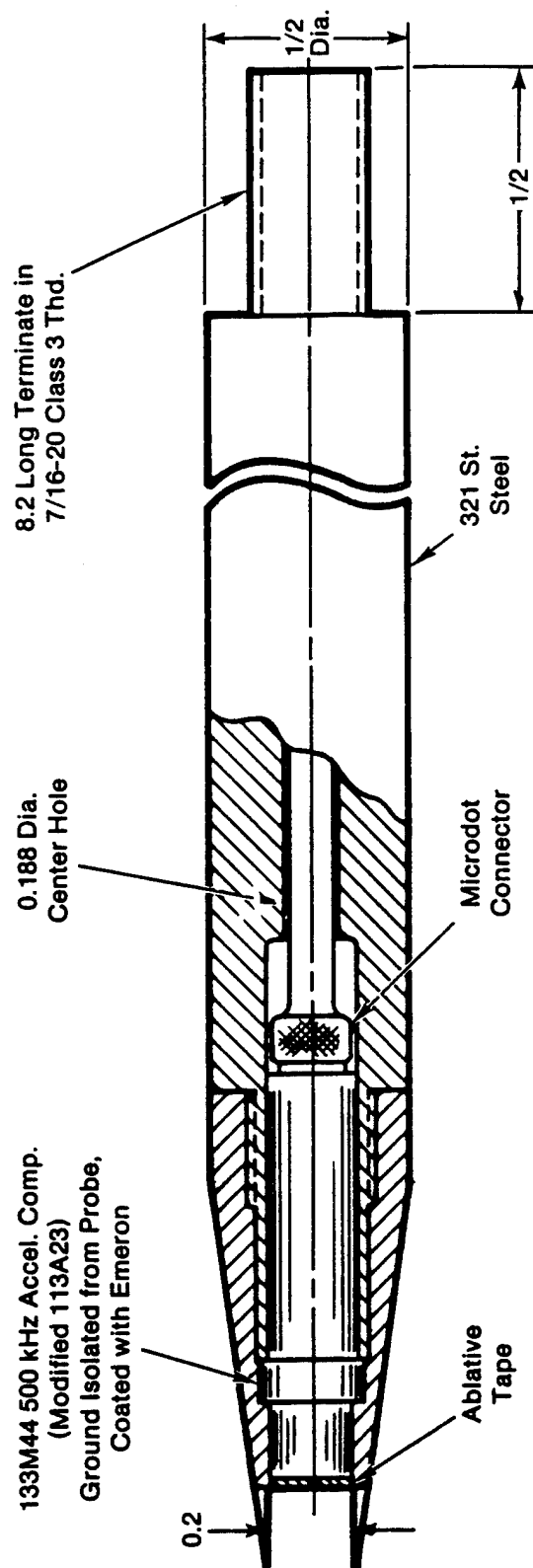
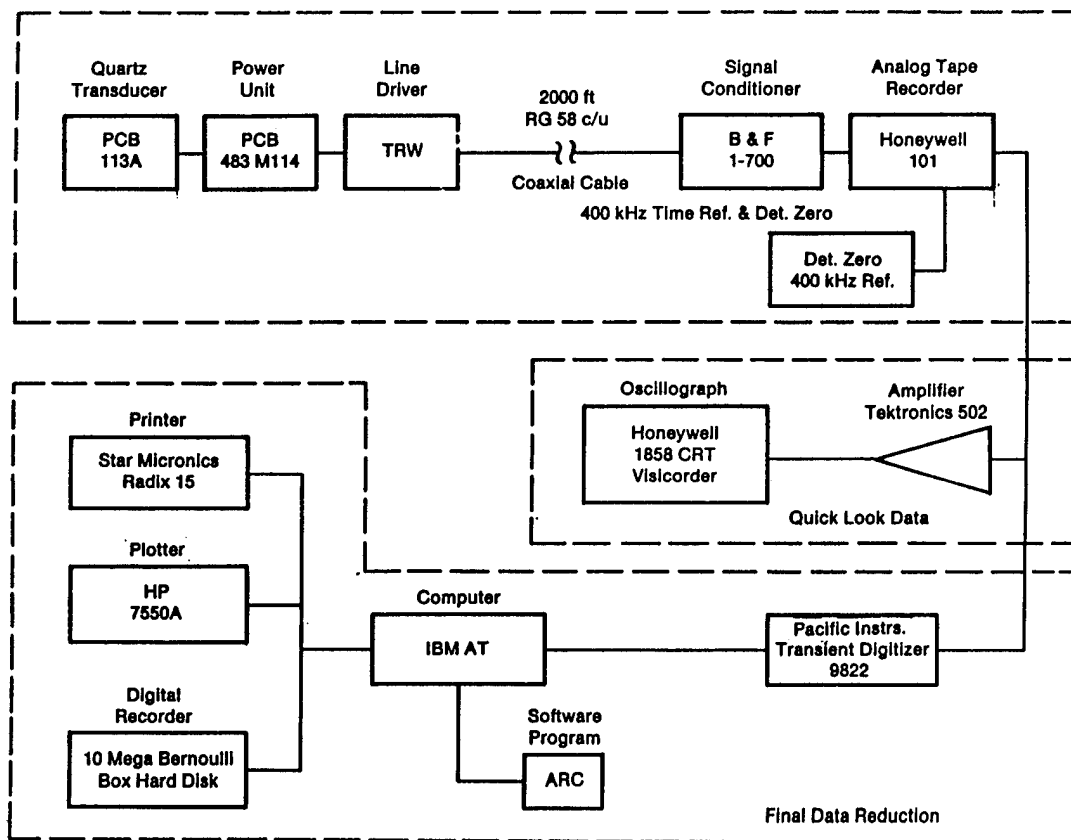


Figure 64. Diagram of static overpressure transducer housing.

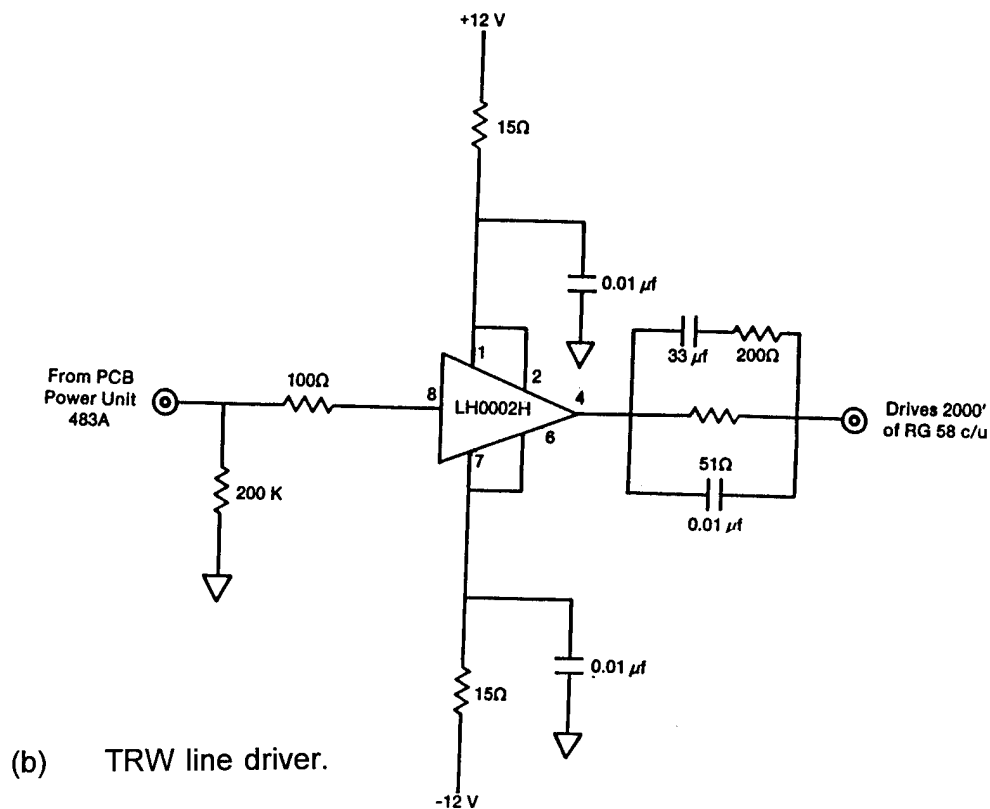


Dimensions in inches

Figure 65. Diagram of total head half-inch probe.



(a) Data acquisition system.



(b) TRW line driver.

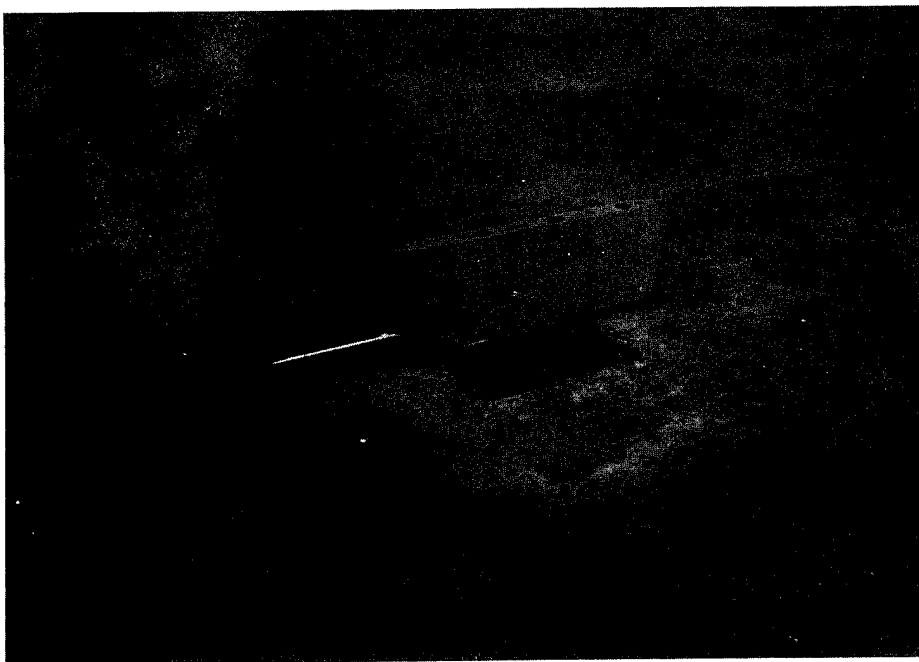
Figure 66. Schematic of piezoelectric gage recording system.



Figure 67. Photograph of ground baffles.

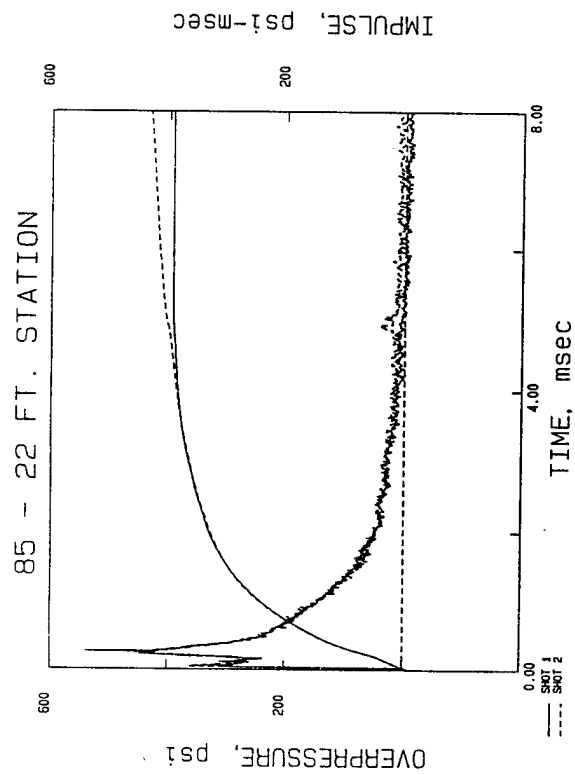
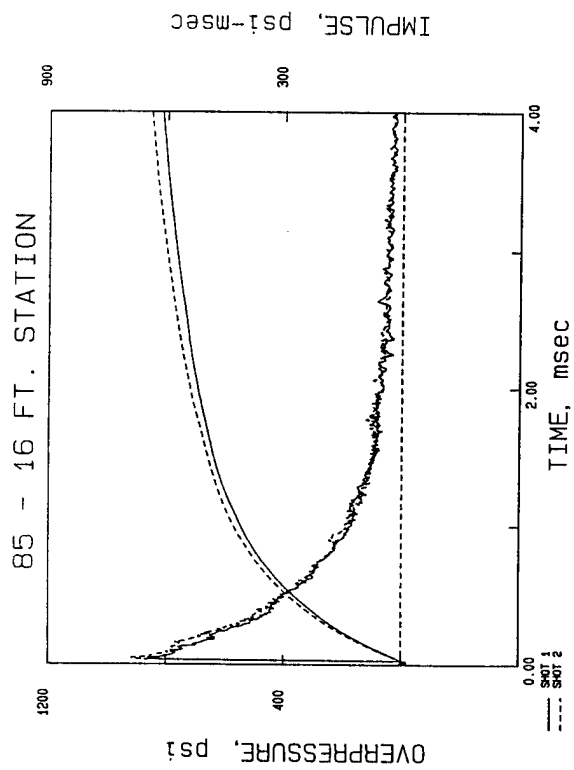


(a) Static pressure rake.



(b) Total head pressure rake.

Figure 68. Above the surface mounting of piezoelectric gages.



101

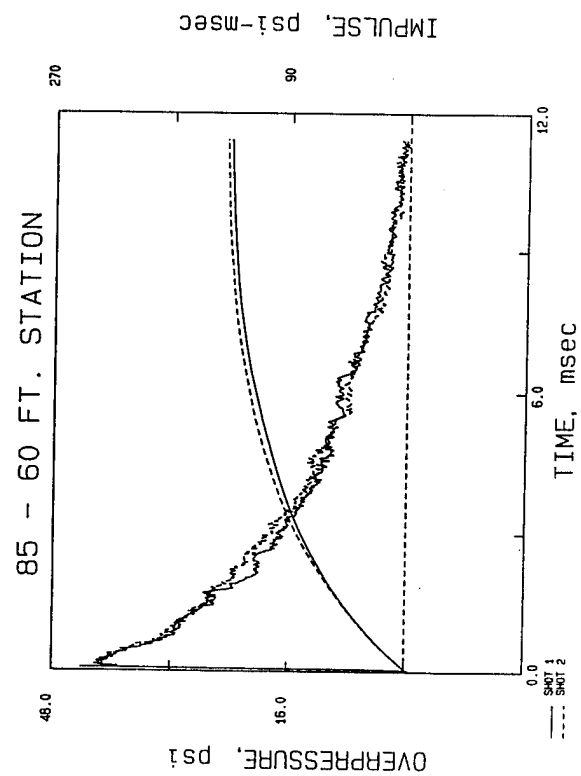
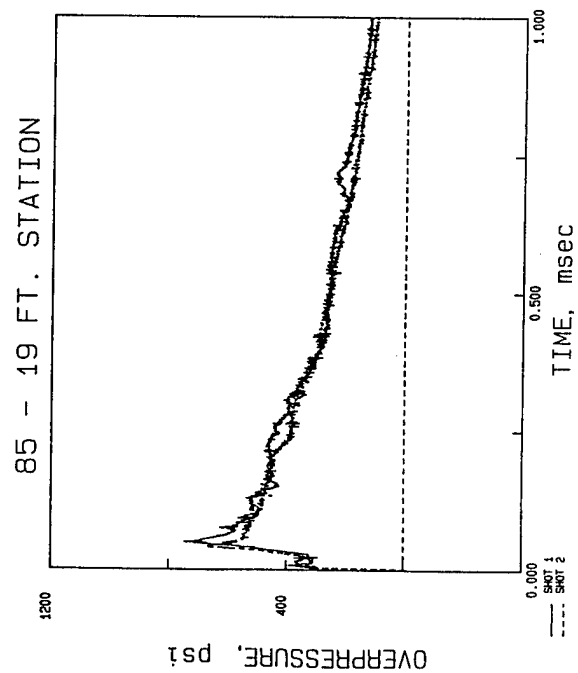


Figure 69. Piezo-electric field records from an HMX 1000-lb explosion.

4.4.6 H-Tech Greg Gage (1982) (USA).

The H-Tech Greg Gage incorporates a piezo-electric sensor which is placed normal to the dusty flow. Under such conditions, the sensor will be subject to impact damage. To protect against this, a force plate with grease pressure coupling was employed. The thickness of a force plate was determined to be 0.080 inches. Dow Corning silicone vacuum grease was used as the coupling material. RTV-511 was applied to the face of the force plate to give thermal protection and to provide a mechanical seal. The force plate was installed under a vacuum so as to exclude all air from the grease.

A schematic of the gage is shown in Figure 70, and a photograph is shown in Figure 71.

Ref: "PRE-DIRECT COURSE Results Report," Volume I, DASA-7116-1, 1983.

4.4.7 Piezo Zinc Oxide Chip (Developmental) (1988) (USA).

The design concept of the piezo zinc oxide chip pressure sensor is that of using the piezo-electric characteristics of zinc oxide coupled with electronics built into a silicon chip. A zinc oxide film is to be deposited on a silicon chip with signal amplification on the same chip. It was calculated that a resonant frequency of as much as 5.7 MHz could be achieved because thin piezo-electric layers on silicon use no diaphragm structure. Packaging for the piezo-chip configuration was felt to be more complex and several designs were developed as shown in Figures 72 through 74. In each design, the silicon chip is mounted on a thick stainless steel header where the sensor chip is electrically connected by gold lead wires and is covered by a 50 millisecond stainless steel diaphragm. Silicone oil is placed between the sensor chip and the steel diaphragm. The sensor head is connected to an electronics module for amplification; both are considered easily replaceable units. A range of 10,000 psi was postulated.

As far as is known, this gage was not deployed on field tests.

Ref: Barth, P.W. and Wilson, J., "Ultrahigh Frequency Pressure Sensor-Novasensor," AFATL-TR-88-77, 1988.

4.4.8 German Pitot Pressure Gage (GR) (1985).

A pitot pressure gage designed to measure incident and total head blast pressure was fielded by the Federal Republic of Germany. The gage as installed in the field is shown in Figure 75. Included were the pressure transducers and their mounts, the charge amplifiers, and a charge sensitivity calibration. A schematic of the system is shown in Figure 76.

The stations tested resemble the pitot tubes to measure stagnation pressure in steady flow fields. They consist of an axisymmetric housing with a blunt nose. The total head sensing element is located at the stagnation point. Incident overpressure gages were located on top of the horizontal tube. The stainless steel diaphragm of the piezoelectric head-on transducer was protected by a baffle plate consisting of a heat and debris shield with a small cavity between the plate and the diaphragm.

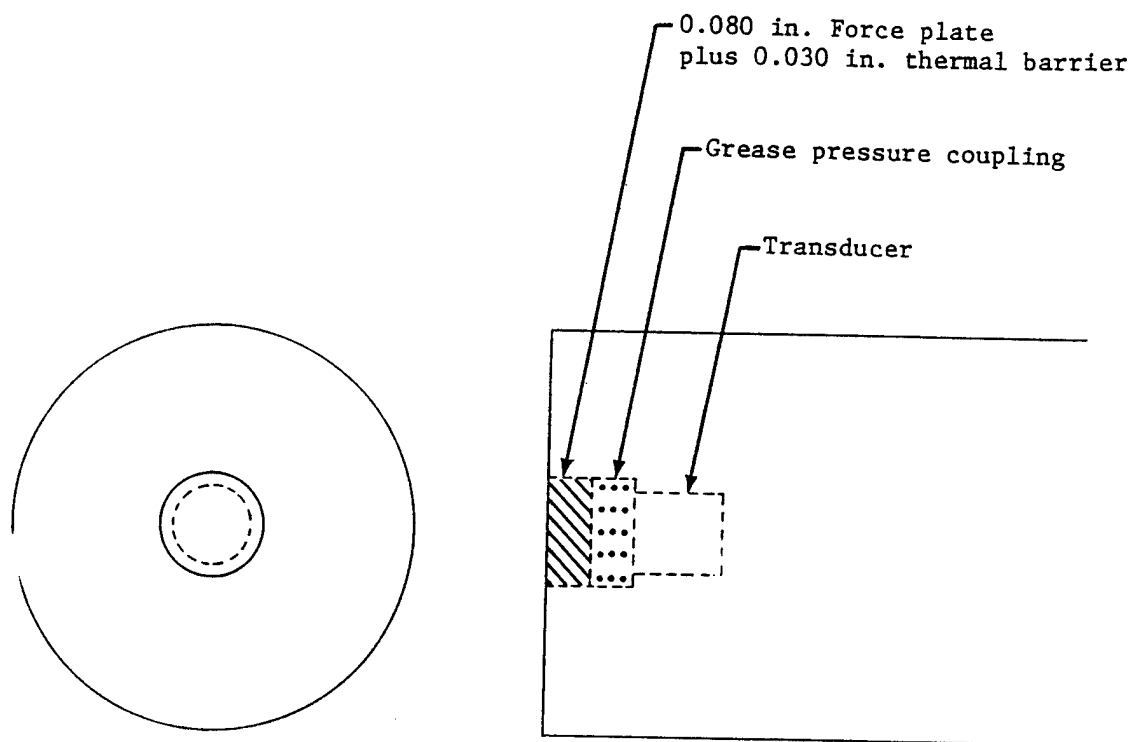


Figure 70. Schematic of H-Tech greg gage.

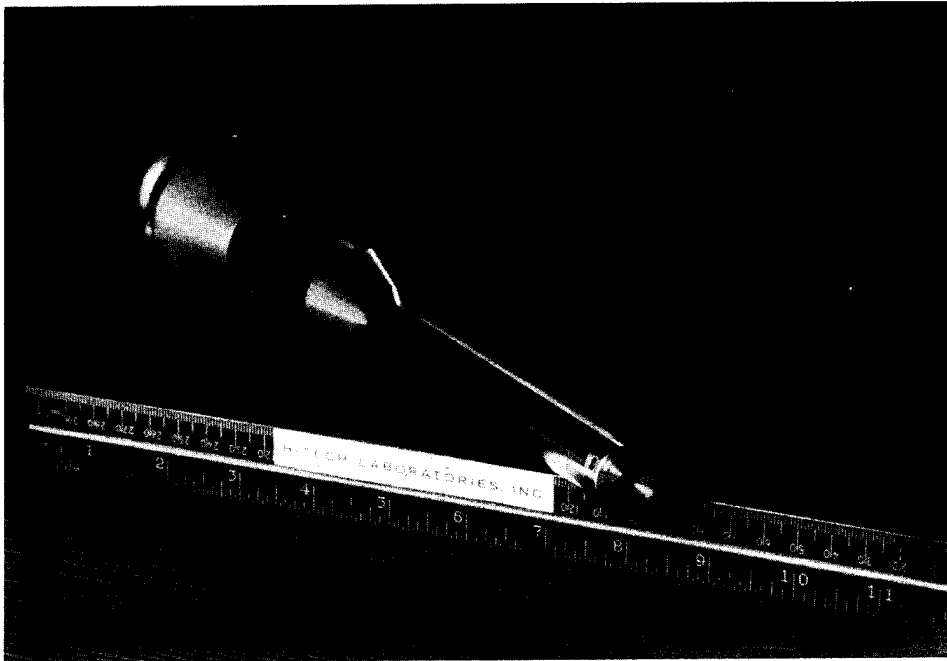


Figure 71. Photograph of H-Tech greg gage.

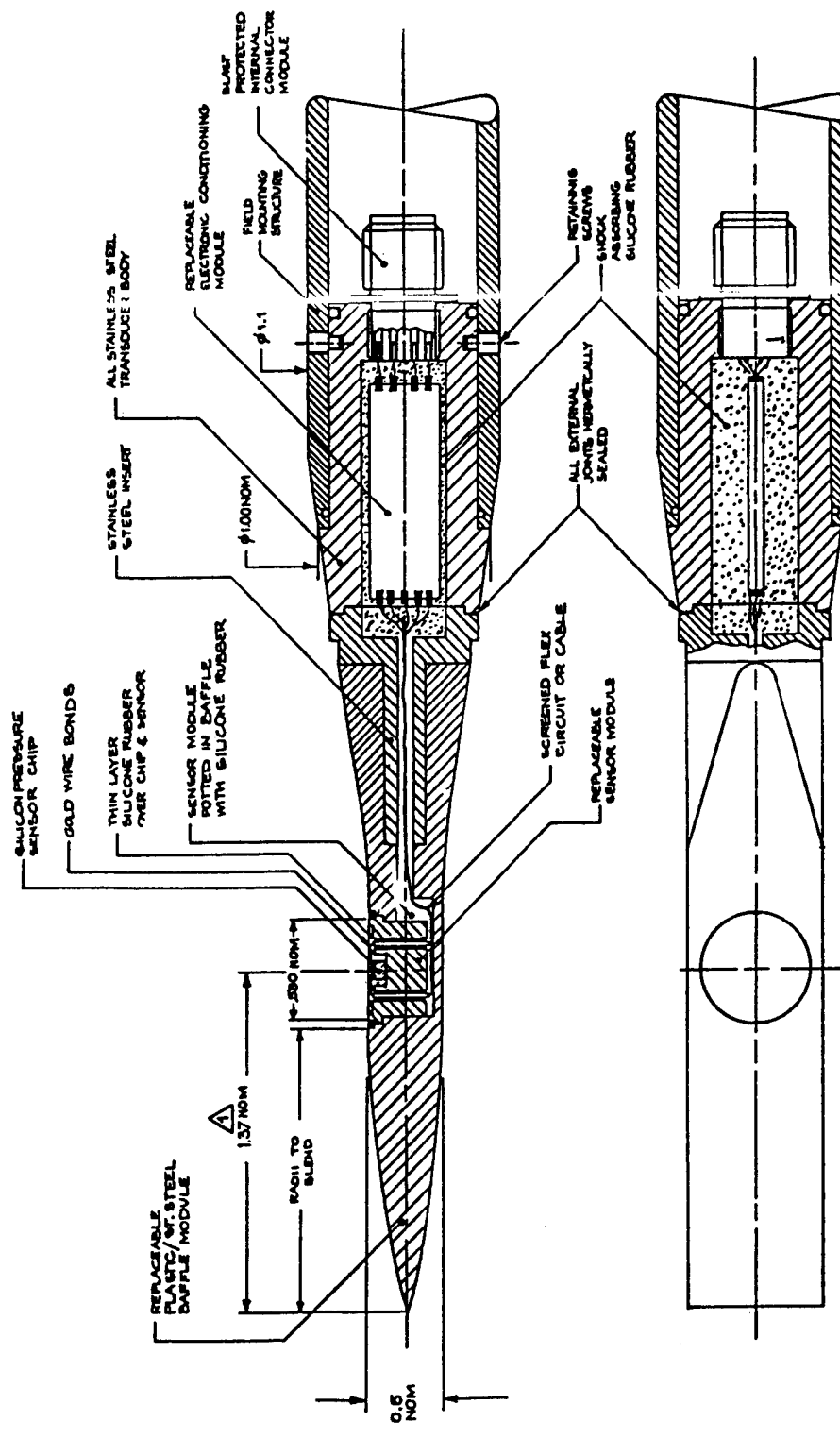


Figure 72. Proposed zinc oxide-silicon chip high pressure side-on gage.

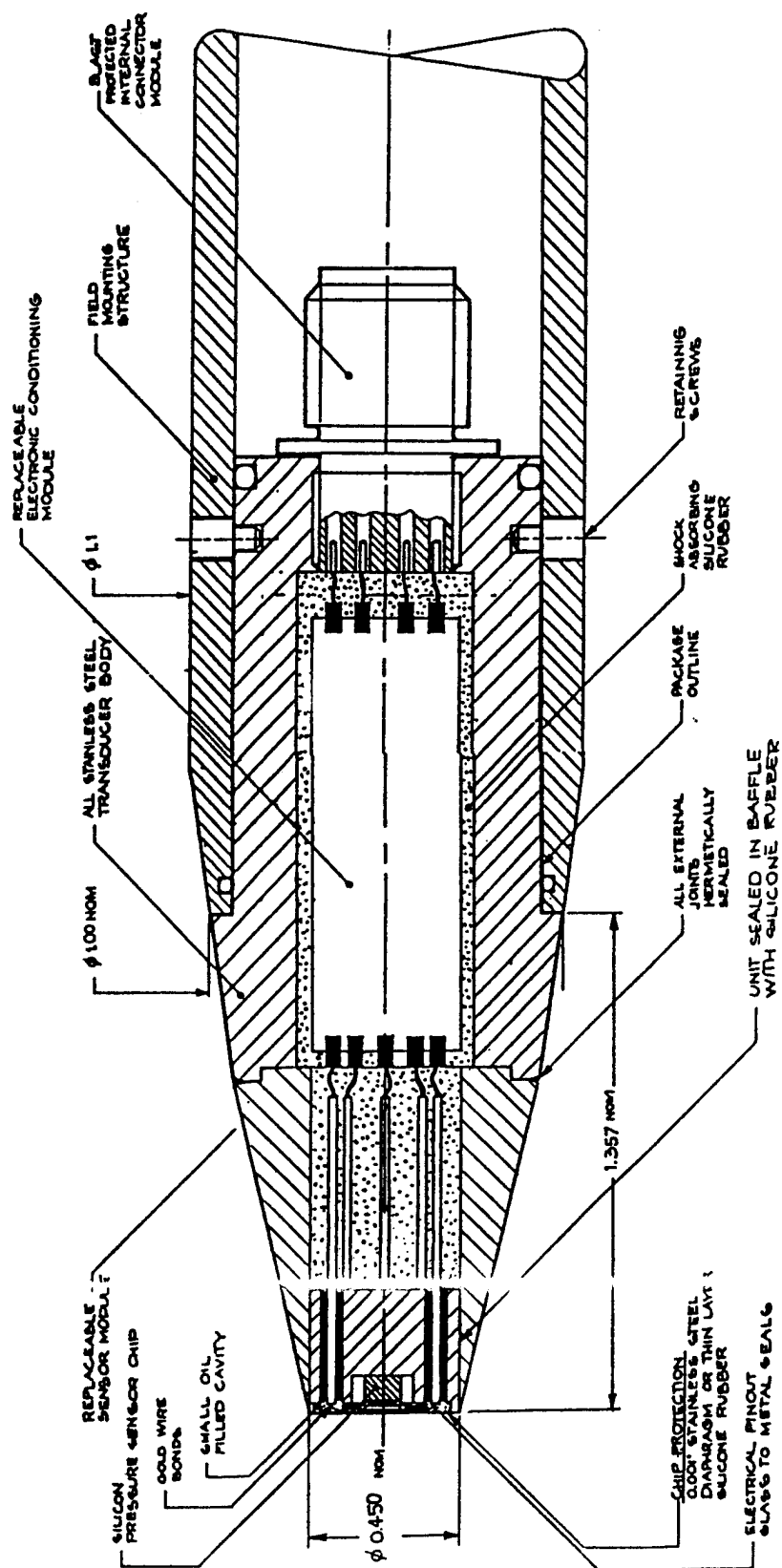


Figure 73. Proposed zinc oxide-silicon chip high pressure face-on gage, Design A.

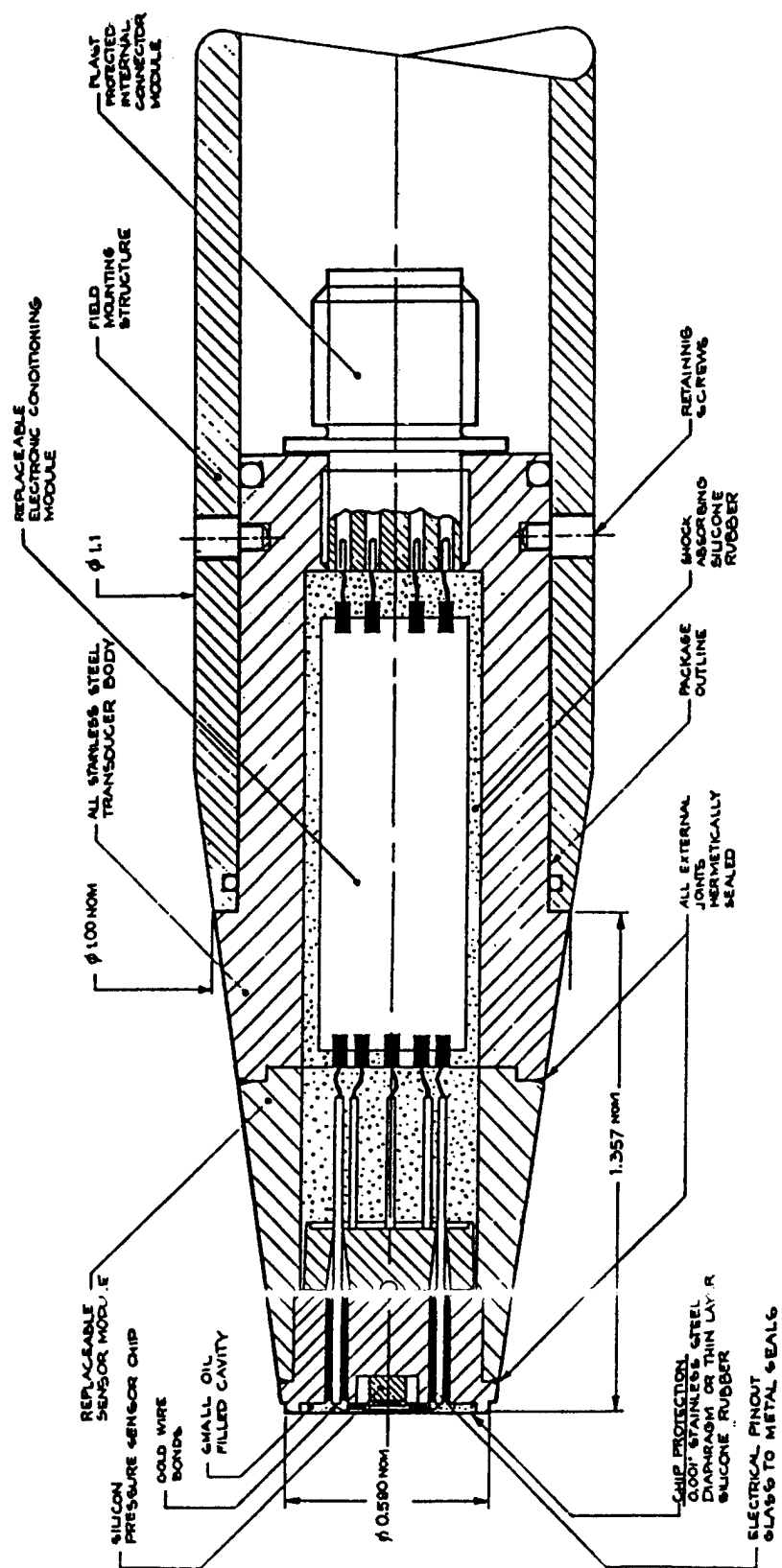


Figure 74. Proposed zinc oxide-silicon chip high pressure face-on gage, Design B.

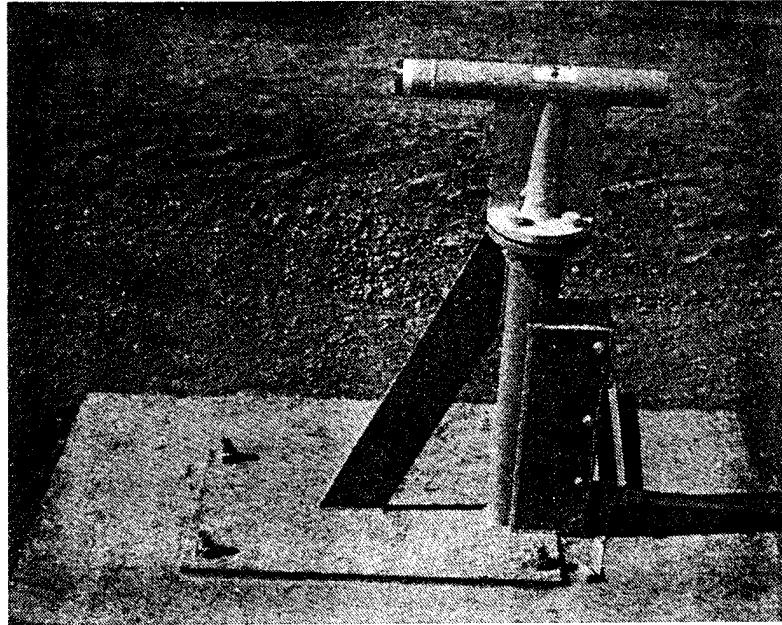


Figure 75. Federal Republic of Germany pitot pressure station.

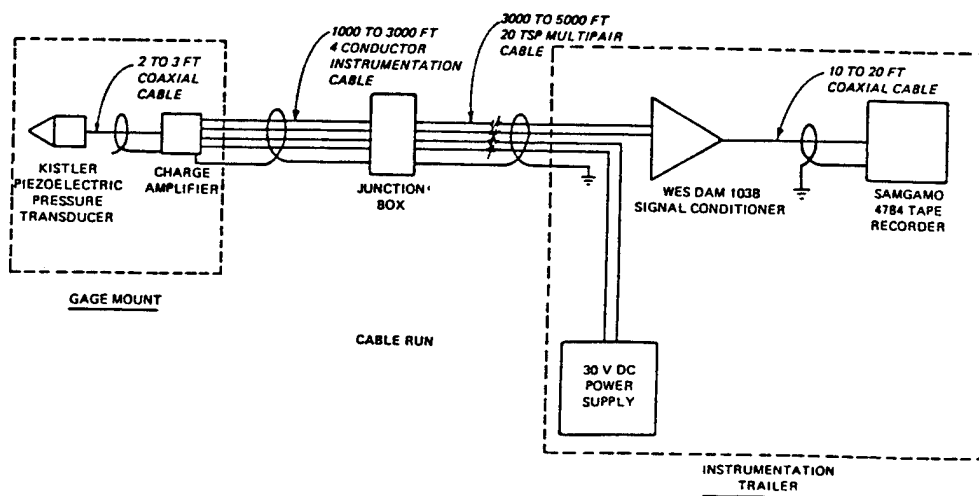


Figure 76. Schematic of electrical hookup for German pressure gages.

The transducer type employed was an acceleration-compensated quartz pressure design Kistler Model 7031. The main advantages of this transducer are high natural frequency and a rugged stainless steel diaphragm. The charge signal produced by acceleration due to the mass of the diaphragm was compensated by a signal from a built-in quartz accelerometer. The pressure unit had a sensitivity of about 55 pC/100 kPa. The nominal frequency is 80 kHz with an associated time constant of 10,000 seconds.

The charge amplifier for converting electrical charges into proportional voltages was a Kistler Type 5041 B with digital adjustment and a frequency range from quasistatic to 50 kc. The charge signal yielded by the transducer was converted into a proportional electric voltage of ± 10 volts. The power supply was ± 15 volts DC.

Ref: Ackerman, J., "Pitot Gages Test," Proceedings of the Minor Scale Symposium, POR-7158-4, 1986.

4.5 MECHANICAL SELF-RECORDING SYSTEMS.

4.5.1 BRL Self-Recording Gages (USA) (1960).

The BRL self-recording gage of the fifties was constantly evaluated, redesigned to make it smaller, and improved to increase its response and reliability. The basic principles utilized in the gage were maintained. These "new gages" were deployed on HE tests of the sixties.

Pressure sensors were changed from a capsule design to that of a single diaphragm. A single diaphragm, shown in Figure 77, was welded into a mounting ring for ease of interchange from gage to gage. An osmium-tipped stylus and its spring arm are attached to the diaphragm by means of a section of stainless steel tubing. As the diaphragm flexes, the movement of the tubing is restrained to one axis by a sapphire jeweled bearing. The characteristics of these sensors are set out in Table 17. These sensors are available in 15 ranges from 0.03 psi to 1,000 psi. The natural frequency is approximately four times that of the older sensors and rated deflection is about half. Hysteresis is generally within 1 percent and linearity well within an acceptable 5 percent for mechanical instrumentation.

Newer recording mechanisms were developed. One was a negator gage where the method of using a negator spring as both a drive motor and a recording medium were employed. See Figure 78. The stainless steel spring provides a constant torque as it unwinds from a supply drum, travels around the recording drum, and into its designed configuration on a take-up drum. The excursions of three styli are recorded; these excursions represent pressure, time base, and reference. These are recorded on the spring's microhoned surface as it travels around the recording drum. A balanced friction governor geared to the supply drum provides a spring travel rate of about 3 inches per second. A square-wave time base trace is supplied by a solenoid-driven scribe which receives a signal of 50 cycles per second from an electromechanical oscillator. A simple mechanism is provided for arming the gage and for cutting it off when the spring reaches the end of its travel. Two methods are used to initiate the gage; a solenoid on earlier models and a more rapid explosive piston actuator on newer models, both triggered by an externally supplied relay circuit closure. In each case the motor is given a spring-driven "kick" in order to decrease the time required to bring the spring travel rate up to constant speed.

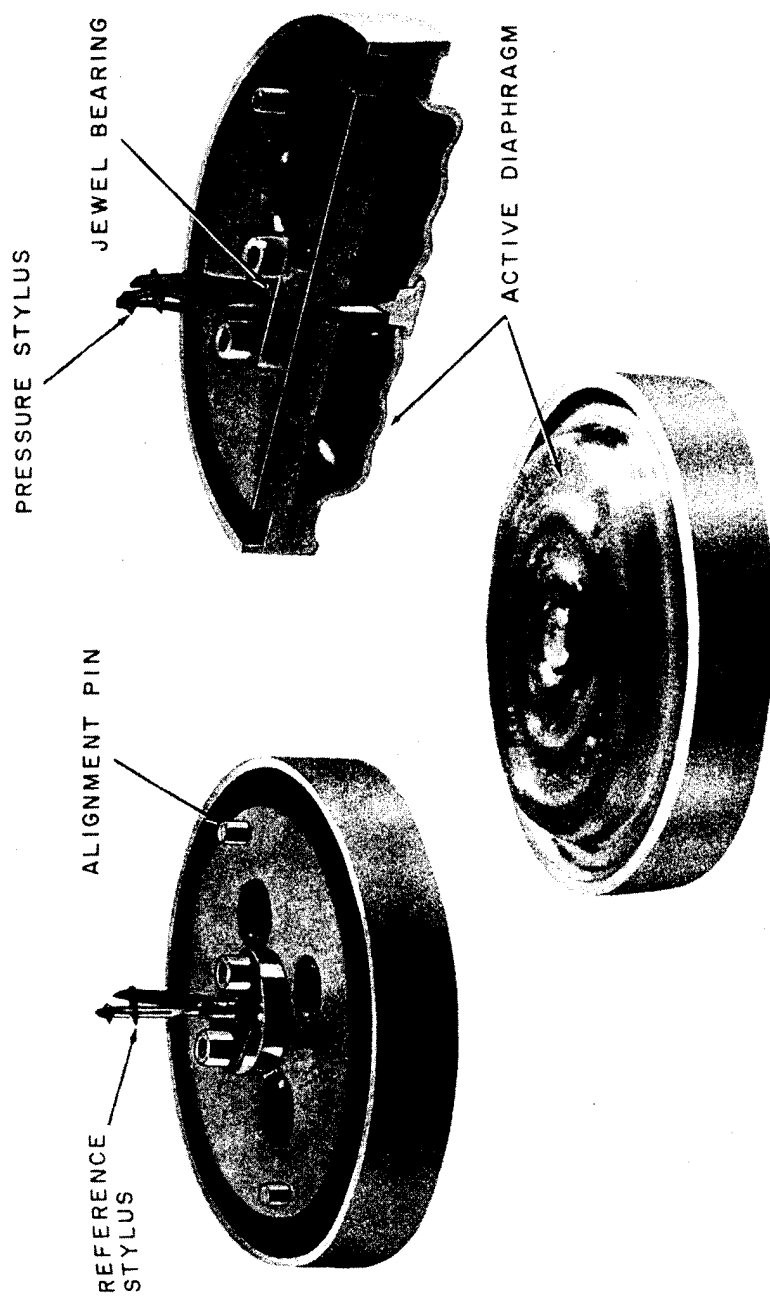
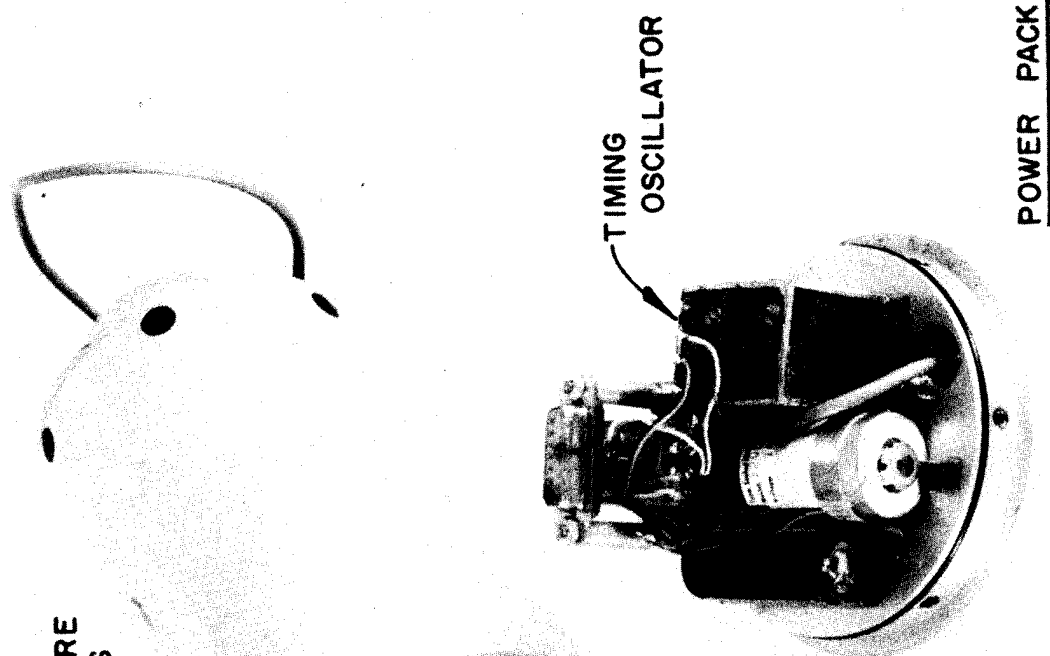


Figure 77. Single diaphragm self-recording gage pressure sensor.

Table 17. BRL self-recording sensor characteristics.

Sensor Range (psi)	Nat. Freq. (Undamped) (cps)	Deflection at Rated Pressure (mils)	Hysteresis (%)	Linearity (Terminal Based) %
0-1000	6990	20.10	0.59	0.45
0-600	5955	20.82	0.62	2.16
0-400	5105	23.17	0.86	3.75
0-200	4351	31.35	0.73	3.57
0-100	3615	28.60	0.35	0.87
0-50	2995	24.20	0.30	2.40
0-20	2726	23.90	0.20	0.70
0-10	1895	26.80	0.67	2.69
0-5	1570	20.20	0.00	1.60
0-2	1085	19.60	0.87	1.68
0-1	820	15.30	0.70	1.60
Experimental				
0-0.5	430	18.15	0.55	1.70
0-0.125	250	17.40	0.60	4.90
0-0.030	250	18.20	1.10	4.20
0-10 Negative	1915	25.70	0.20	0.70

ASSEMBLED GAGE



POWER PACK

NEGATOR
SPRING



ARMING
SCREW

INITIATOR
ASSEMBLY

GOVERNOR

MOTOR ASSEMBLY

REFERENCE
SCRIBE

TIMING SCRIBE

SENSOR SCRIBE

CUT-OFF
ARM

MOTOR

ARMING
SCREW

TAKE-UP
DRUM

RECORDING
DRUM

SUPPLY
DRUM

Figure 78. BRL negator pressure gage.

A second new recording mechanism is that shown in Figure 79 which employs a stainless steel microhoned disk as the recording medium driven by a smaller D.C. motor. A time trace is supplied by a system identical to that used on the negator gage.

A modification of this disk gage was made to conform to the special requirements of a dynamic pressure gage. A similar microhoned disk records both total and side-on pressure histories for probes used in supersonic and subsonic flows. The gages are shown in Figure 80.

Experimental gages tested included a nondirectional side-on pressure gage, a negative pressure gage, a standard disc gage with a zero-time adapter, a modified standard negator pressure gage, a very low pressure gage, and a miniature blast pressure gage. These gages are described briefly in the following sections.

Nondirectional Gage System. The first experimental unit is a standard negator gage mounted within a preformed sphere. Figure 81 is a schematic of a non-directional system which was designed to measure side-on overpressure where gage orientation is a problem, such as suspension from a balloon. The test mount consists of a suspended cable from which the gage hangs freely (see Figure 82). Non-directional measurements were made at the 10 and 25-psi ranges.

Negative Pressure Gage. The second experimental unit was a negative pressure sensor designed to measure accurately the negative phase in a high pressure region. The sensor was modified to restrict the positive deflection of a 10-psi diaphragm but allow full travel in the negative direction. One of these units was used at the 400-psi level. The recording medium used was a disc gage, and the field mount was the same as other gages.

Standard Disc Gage with an Arrival Time Indicator. An arrival time system, Figure 83, consists of a standard disc gage with a zero-time adapter for scribing a fiducial mark on the recording disc. The scribe is attached to an explosive piston actuator which is triggered by a simple photo cell device shown at left. This device was designed to record more accurately the arrival time. It was tested at the 90 and 125-psi ranges in a ground surface mount.

Modified Standard Gages. Two late models of the standard negator gage were tested in the 55 and 65-psi ranges. These gages are equipped with an explosive piston actuator in place of the solenoid initiator, and the 50-cycle-time oscillator was replaced with a 100-cycle generator. The higher rate time trace was the primary test item.

An experimental damping medium was tested on the standard negator gage at the 15 and 10-psi levels. The conventional aperture which separates the sensor diaphragm from the incident pressure was replaced with a porous metal damping disc. This damping material is made by compressing sintered stainless steel into a mass of varying density. Damping is expressed in percent density where 100 percent is solid metal.

The photo cell assembly was designed for use as a zero-time initiator for the BRL mechanical gages. It was tested at five different ranges, along with the two arrival time systems described above.

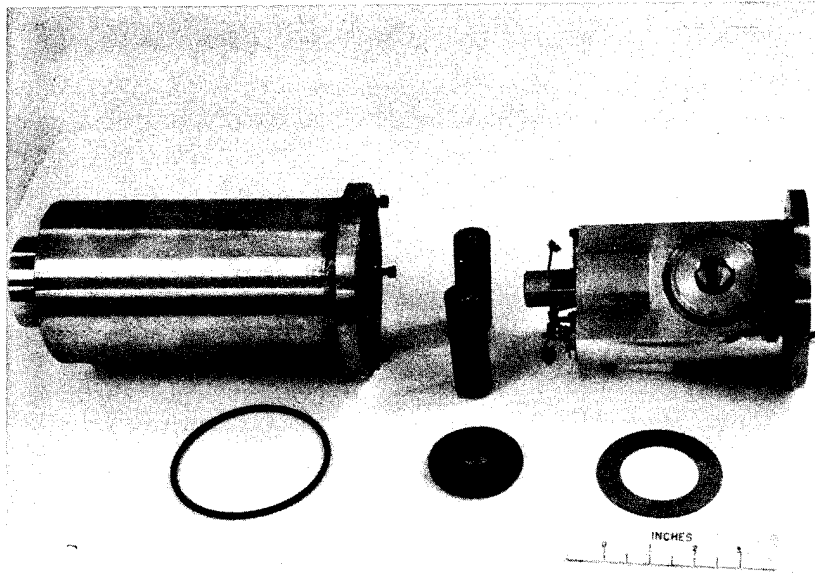


Figure 79. Standard disc pressure gage.

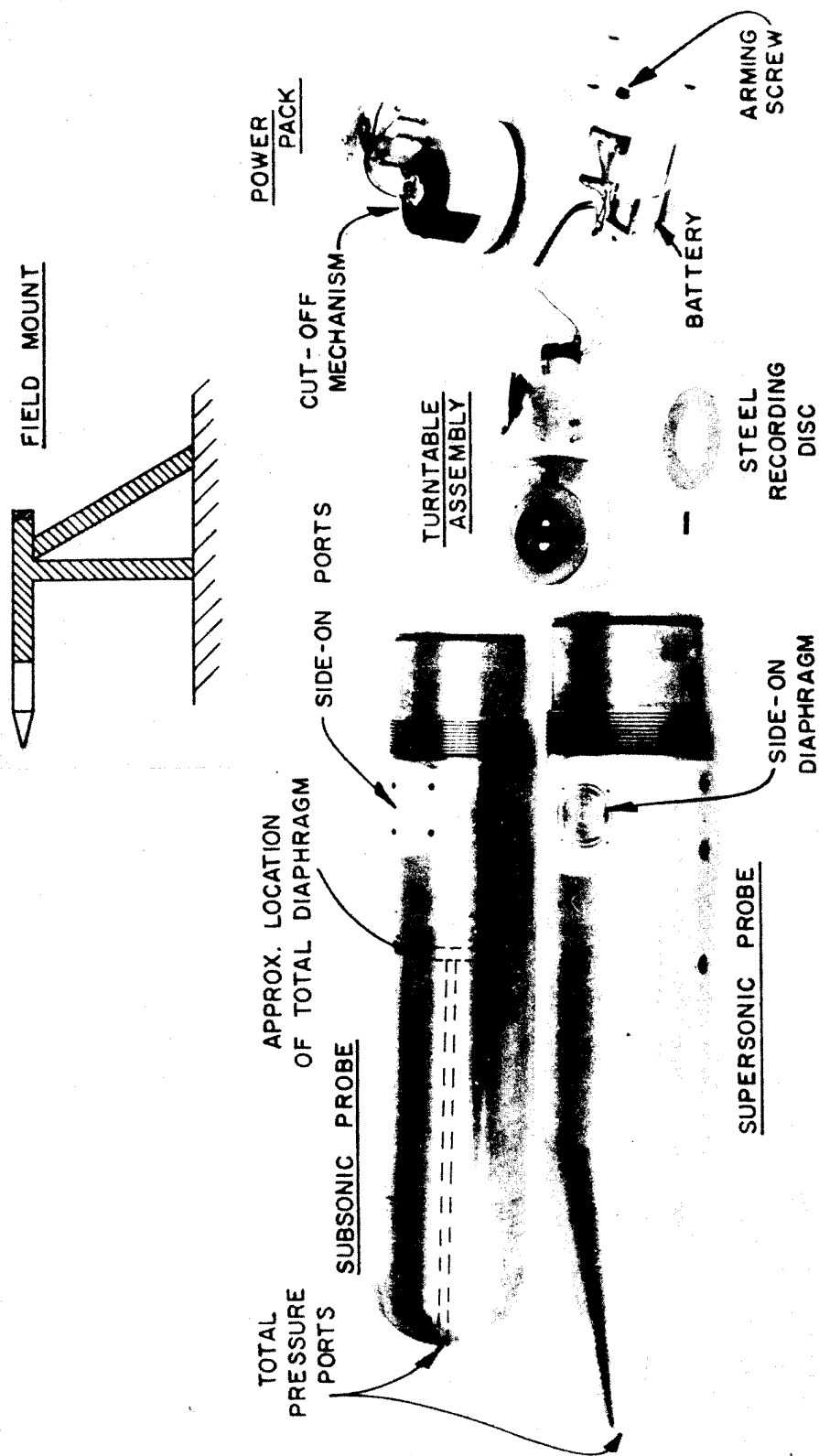


Figure 80. Self-recording dynamic pressure gage.

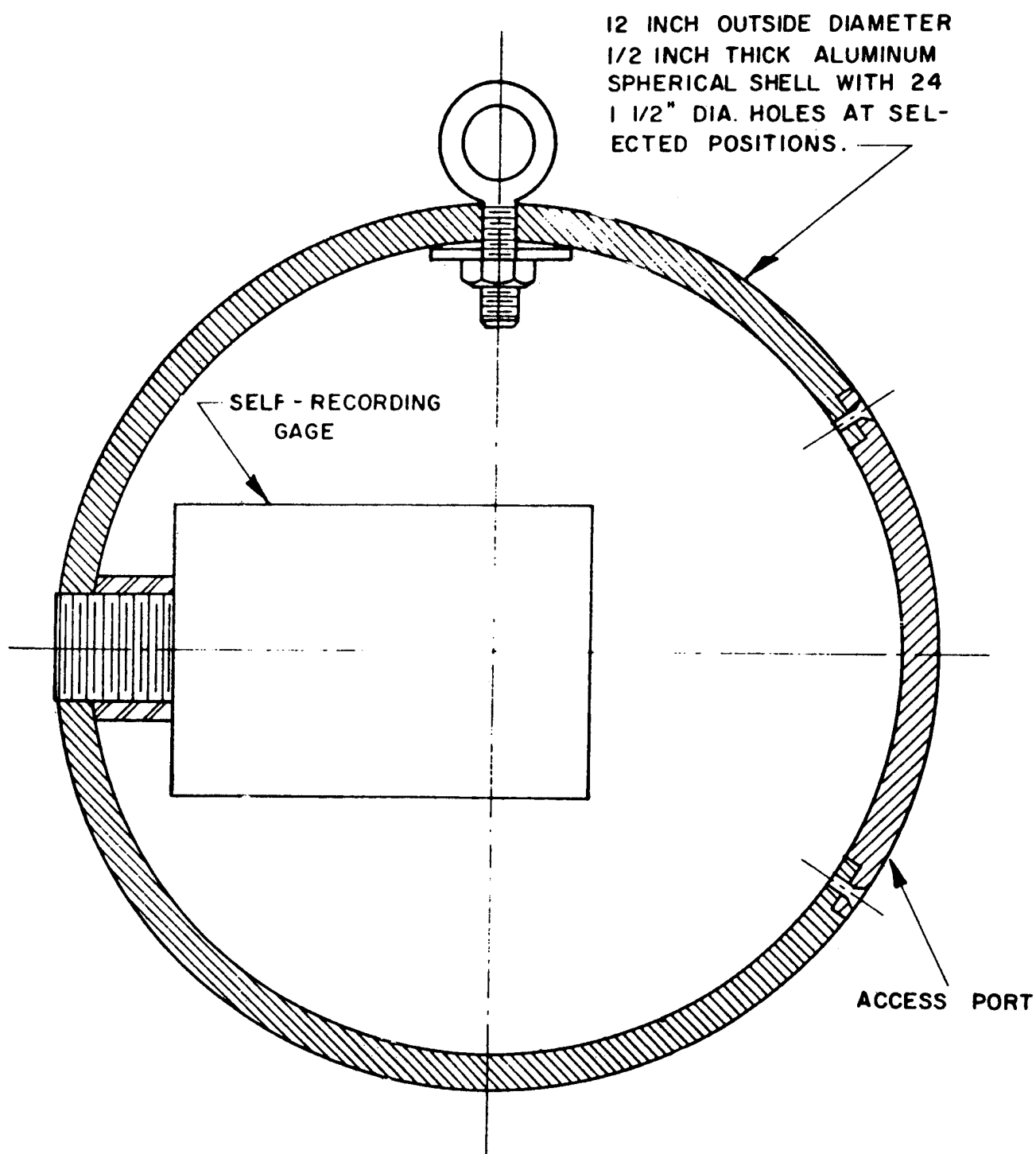


Figure 81. Nondirectional system.

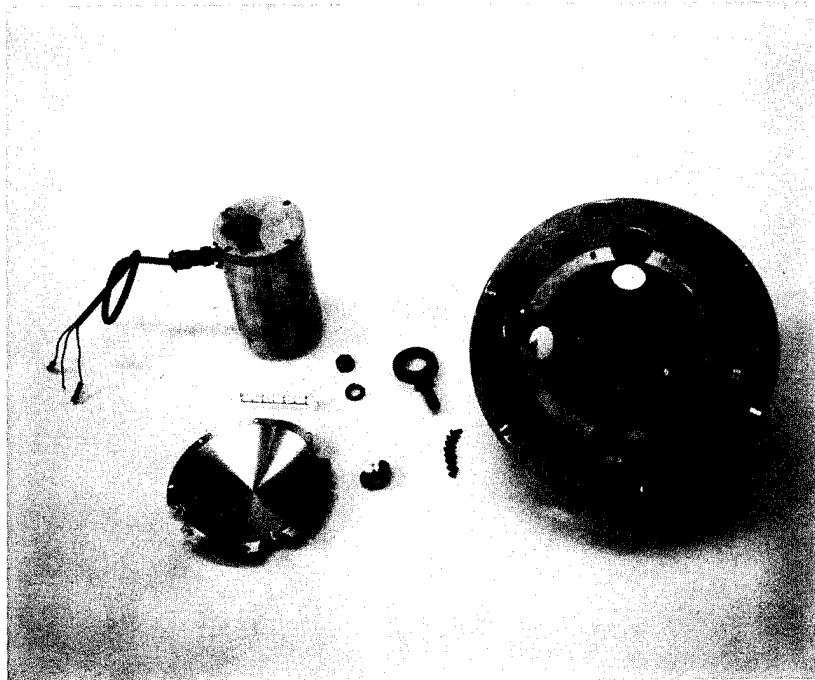


Figure 82. A nondirectional self-recording system.

DISC
GAGE

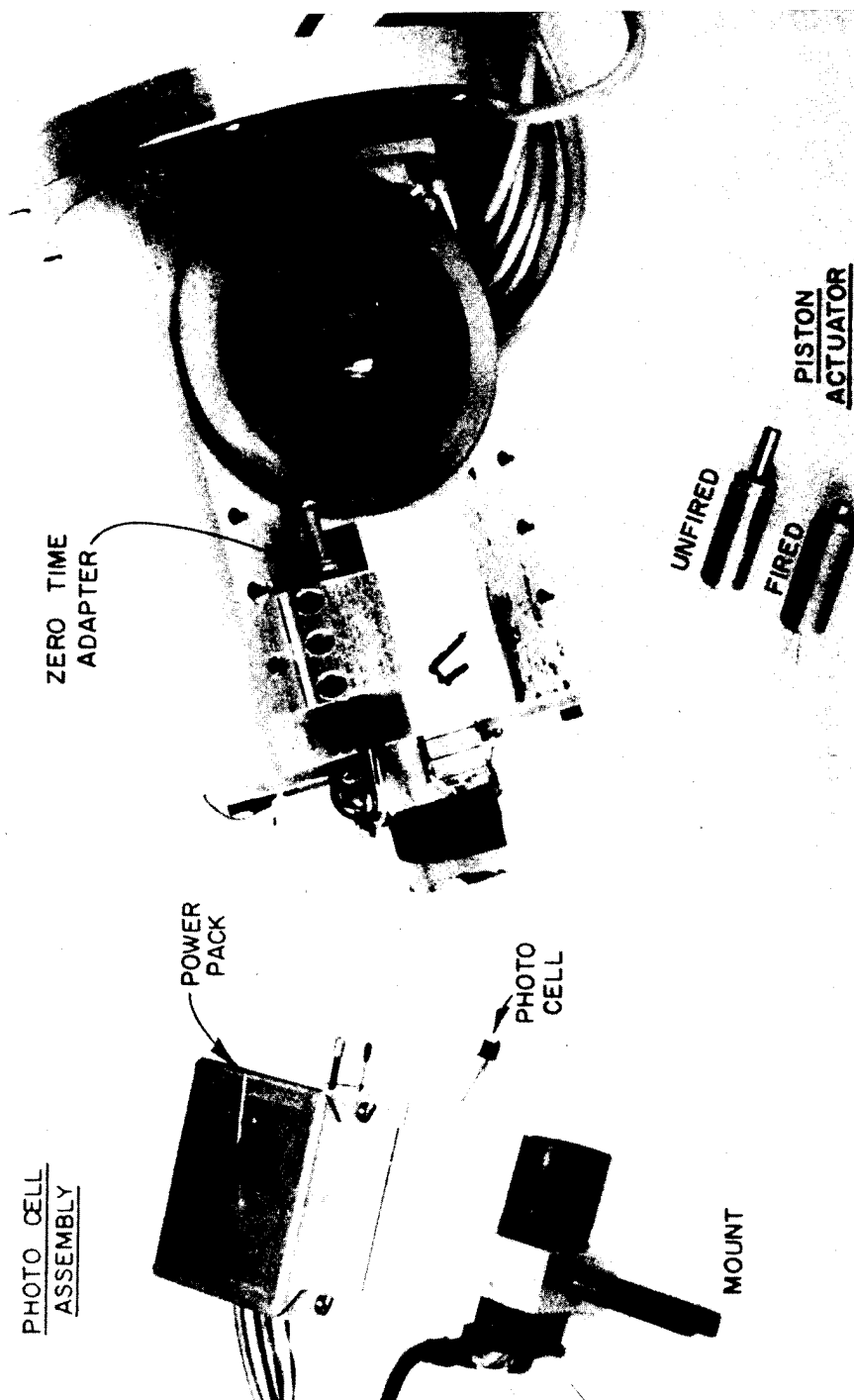


Figure 83. Arrival time system.

Very Low Pressure Gage. Figure 84 is the experimental very low pressure (VLP) gage (first major design change). It has three interchangeable sensors, 0.5, 0.125, and 0.03 psi. The natural frequency has been increased by a factor of five with a corresponding decrease in response time. The combination of a stainless steel gage case and a pressure equalizing system has helped solve the problems associated with internal pressure changes in earlier models which were caused by changing temperature conditions outside the gage.

The gage is essentially a standard negator gage adapted for use with the very low pressure diaphragm as shown in Figure 85. The addition of an explosive piston actuator both activates the gage and supplies a "kick" to the motor and governor, replacing the spring "kicker" used on the standard gage. This improvement has decreased the spring motor start-up time from 20 msec to about 5 msec. Three VLP gages were tested in the 0.5, 0.1, and 0.01 psi ranges. No prepared mounting facility is required.

Prototype Pressure Gages. Three miniature blast pressure gages were field tested.

The blast gage uses the pressure sensor shown in Figure 77. There are three major departures from the standard negator gage: the physical size of the motor unit was reduced by 50 percent, see Figure 86), the new recorders were considerably smaller than previous units, and the frames were more rigid. The negator spring was retained for the power source only, a separate tape being provided for the recording medium. The new recording tape was 0.001-inch thick by 3/8-inch wide, type 410 stainless steel (magnetic) strip with one side vapor-honed to provide a matte-finish recording surface. As a new feature, to help stabilize the tape (i.e., prevent shifting) during shock, the magnetic tape was given a 270 degree wrap around a magnetized recording pulley (an idler) located between the supply drum and the take-up drum. The separation of the tape functions simplified installation and replacement of the recording tape, a particular advantage in field service. Two explosive piston actuators connected to redundant initiation circuits were provided for accelerating the recorder motor to normal speed within five milliseconds.

A research study showed that a pure fluid time marker operating at frequencies up to 1000 cps was feasible. The first models were designed to operate at approximately 500 cps. The assembly consisted of a bistable fluid amplifier operated as an oscillator by diverting part of the fluid flow from each of the two output channels through delay lines of appropriate length, back to the control ports. The remainder of the flow from one of the output channels was directed to a diaphragm which deflected in response to the pulsating output pressure. A stylus attached to the diaphragm scribed the oscillating deflections on a moving tape. Tests on a typical oscillator built for use in a self-recording instrument confirmed frequency stability with respect to variations in gas supply pressure and temperature. It was shown that a relatively small change in frequency occurs with a ± 5 psi variation in gas pressure supply. The actual change in frequency with temperature is considerably less than the theoretical worst case based on the relationship that frequency is proportional to the square root of the absolute temperature. A compact assembly was fabricated operating on a fluid flow of about 0.3 standard cubic feet per minute at 15 to 25 psi, capable of scribing a 450 to 475 cps time mark on a moving tape with an accuracy of $\pm 1\%$ at constant temperature, see Figure 87.

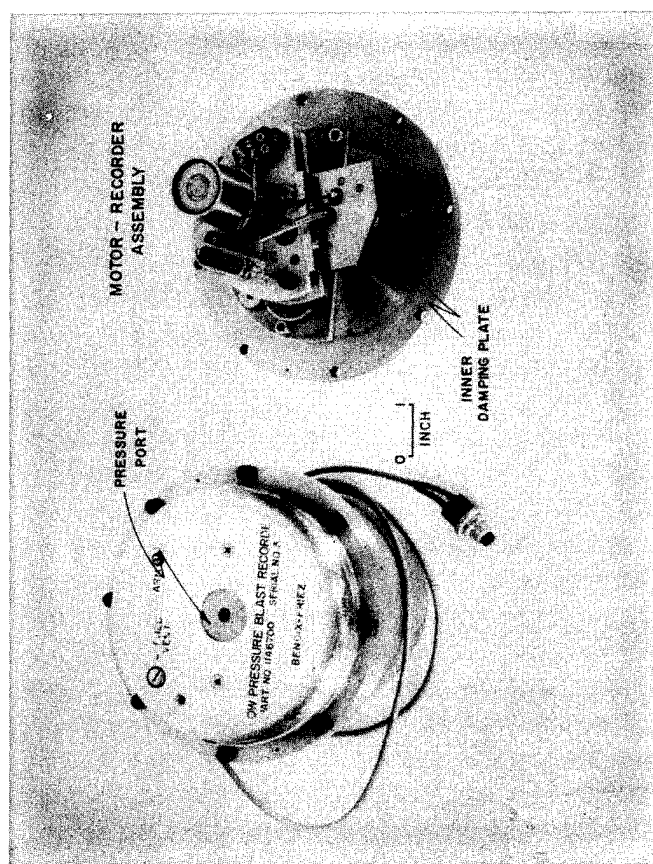


Figure 84. Very low pressure gage.

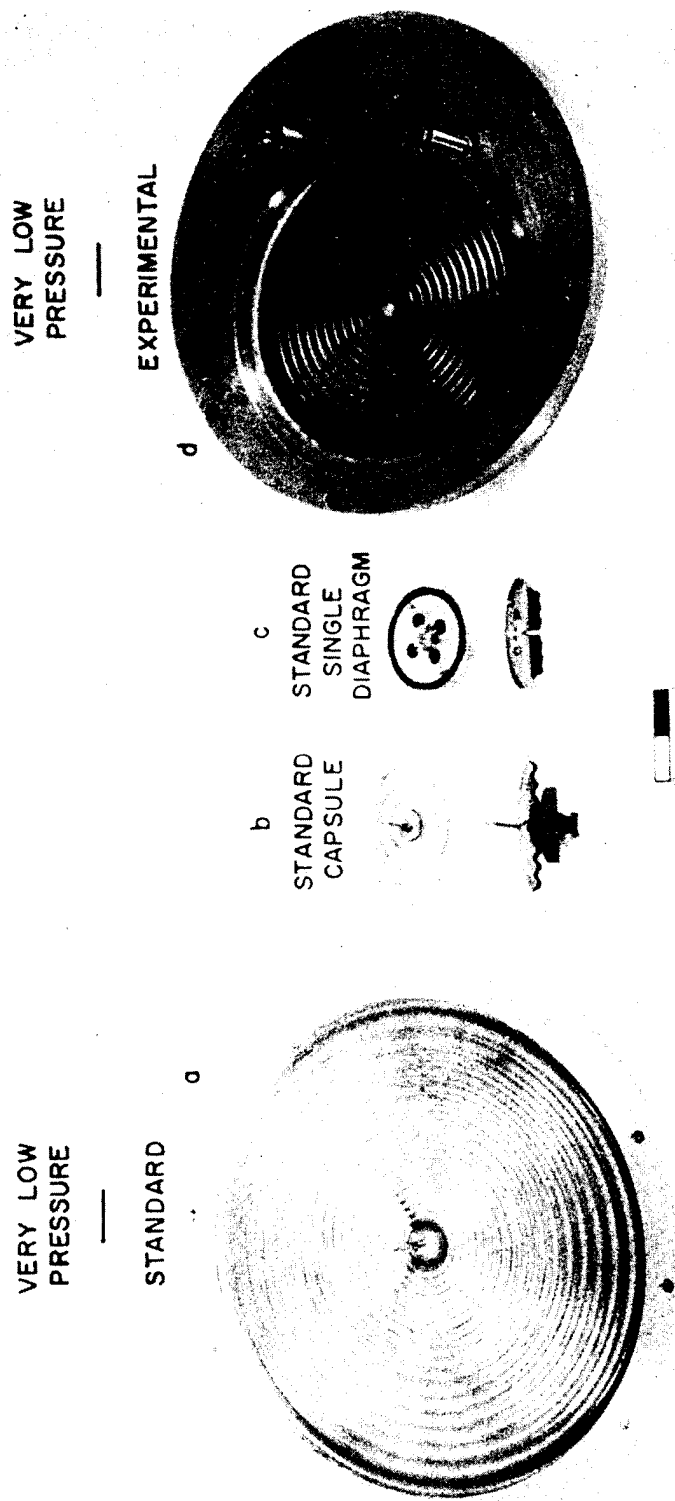


Figure 85. BRL pressure sensors.

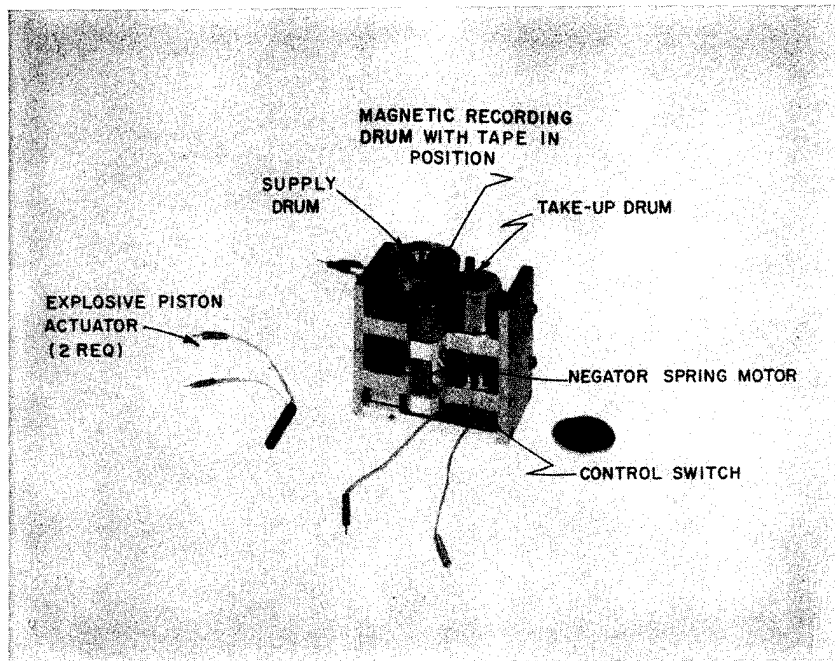


Figure 86. New tape recorder, Exline Model 245.

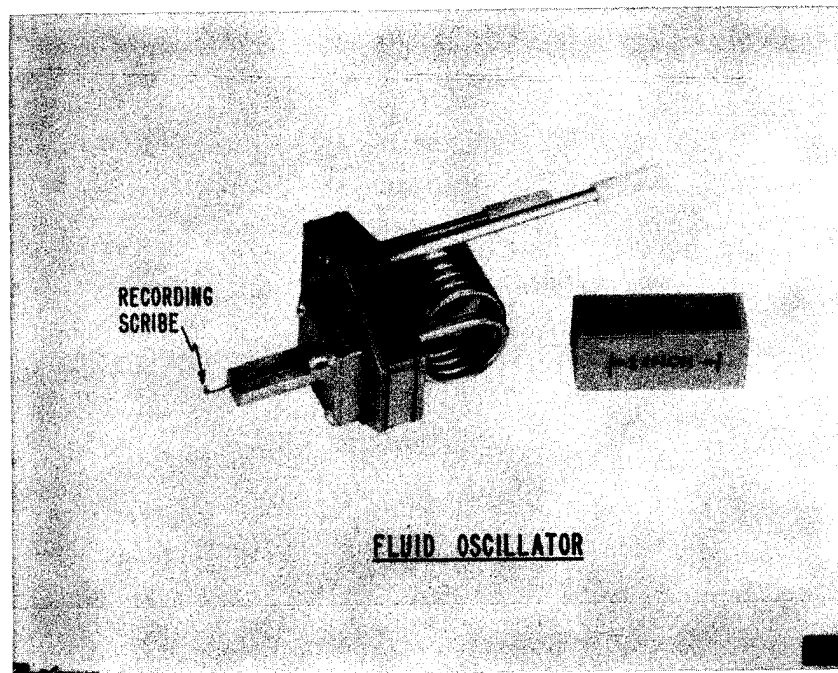


Figure 87. Fluid time marker.

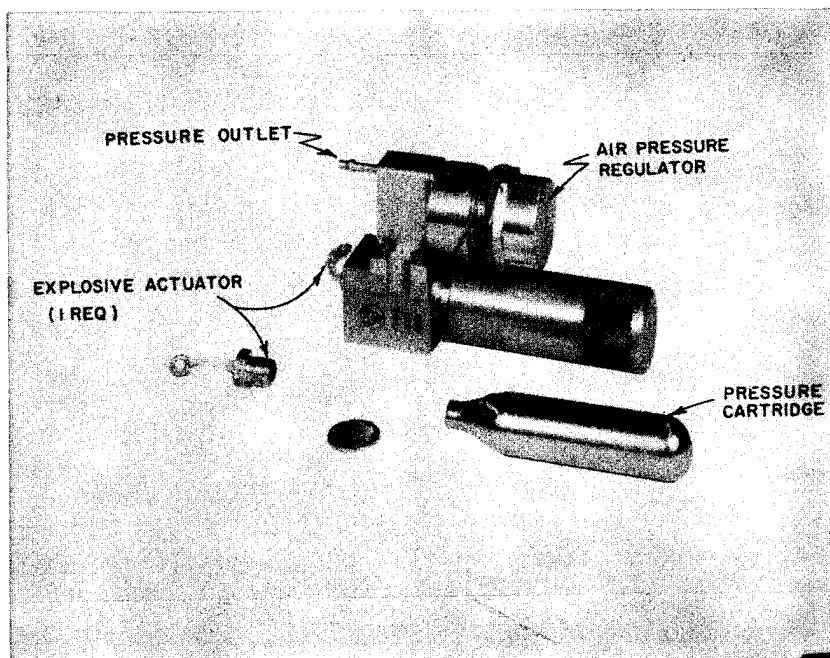


Figure 88. High pressure fluid supply and pressure regulator.

The pure fluid time markers require a source of fluid for operation. For the field tests, a container enclosing a supply of compressed gas at 2000 psi and a pressure regulator was provided. When the time marker was redesigned to operate at a lower flow rate, a much smaller assembly consisting of a container of nitrogen at 5000 psi and a pressure regulator to supply the gas at 0.3 standard cubic feet per minute at 20 ± 5 psi was developed. Figure 88 shows the assembly made by the Pneu-Hydro Valve Company which includes an explosive actuator in the regulator to initiate flow on command.

Samples of records obtained on HE tests using the self-recording gage of the same type as used on nuclear tests are presented in Figures 89 and 90.

Ref: LeFevre, D. P., "Evaluation of New Self-Recording Air Blast Instrumentation," Project 1.3b, Operation Snowball, BRL Memorandum Report No. 1815, 1967.

Wells, H. S., "Development and Test of Prototype Miniature, Rugged, Self-Recording Air Blast Instrumentation," Report No. E.I.R. 700, Bendix Environmental Science Division, Bendix Corporation, 1966.

4.6 FIBER OPTIC SENSORS.

Fiber optic pressure sensors are in the design-concept stage. No sensors of this type have been deployed on field test programs to the knowledge of the authors.

4.6.1 Optical Fabry-Perot Resonator Pressure Sensor (1988) (USA).

The optical Fabry-Perot (F-P) resonator pressure sensor uses the characteristic found in the F-P resonator in that its optical reflectivity is strongly dependent on the cavity thickness. By using a diaphragm as one reflector in the resonator, the deflection of the diaphragm in response to pressure can be measured optically.

The proposed sensor head is shown in Figure 91; the optical circuit is shown in Figure 92. A schematic of a Fabry-Perot optical resonator is shown in Figure 93.

A silicon diaphragm/optical fiber assembly is the center piece of the sensor head. It was designed to be disposable; achieving a low cost by a simple design and using the capability to mass produce micro-machined silicon components.

It was stated that "an important aspect of the design is that the reflectivity of the resonator is measured at several wavelengths. By ratioing two of these measurements, it is possible to compensate for intensity variations in the optical system. Such compensation is an important requirement for a practical optical sensor." The system would be able to be calibrated in the field for response.

In the optical circuit, Figure 92, broadband light from a light-emitting-diode is sent to an optical coupler which is coupled to the sensor head with optical fiber. Light modulated by the deflection of the diaphragm and reflected is transmitted back to the coupler. Here the signal is transferred to a five channel wavelength division multiplexer where it is separated into a number of spectral channels. Two of the five channels are coupled to high bandwidth

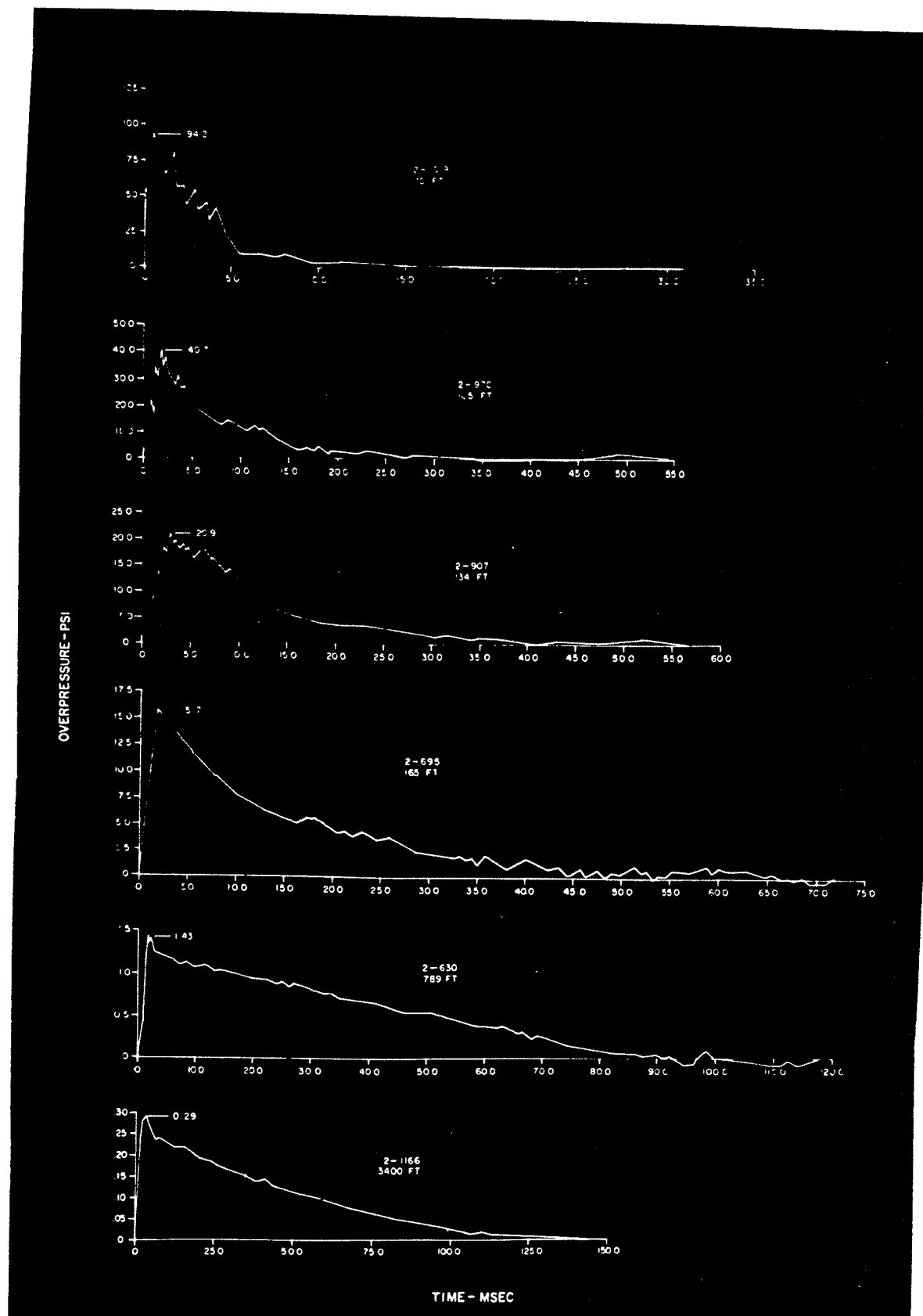


Figure 89. Sample plots of pressure-time records from HE field tests.

HE RECORDS

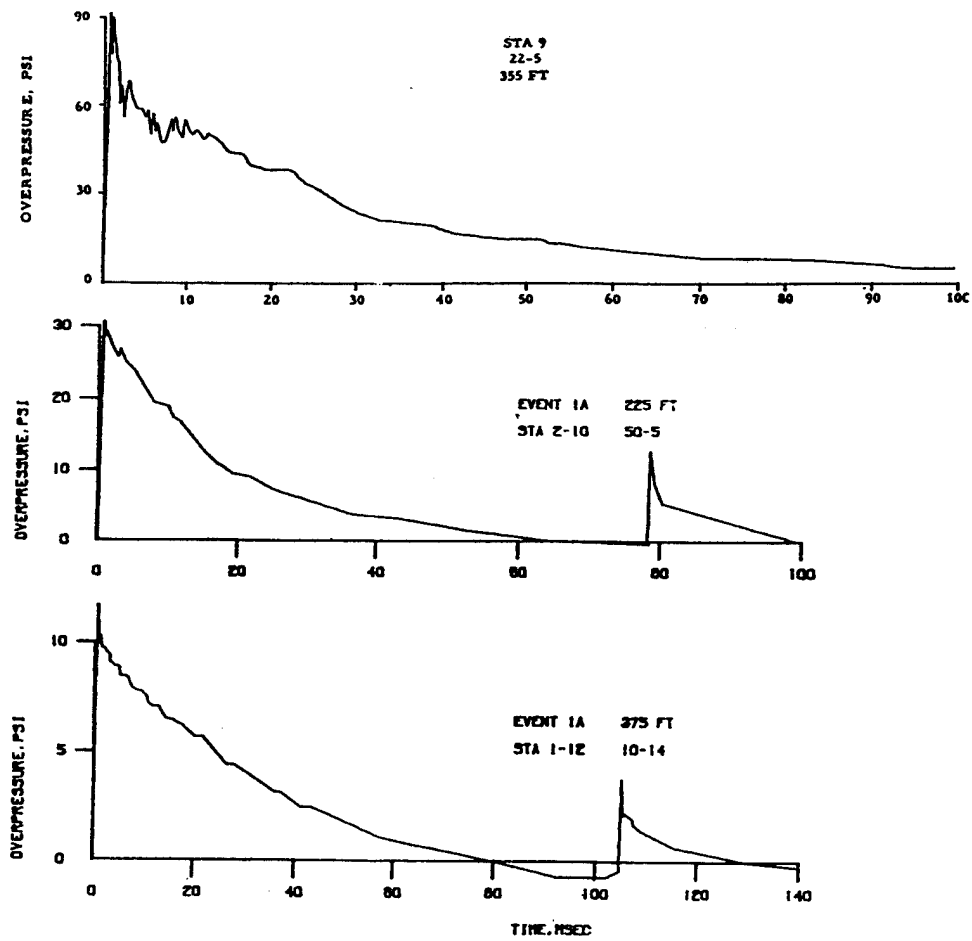


Figure 90. HE field records from self-recording gages.

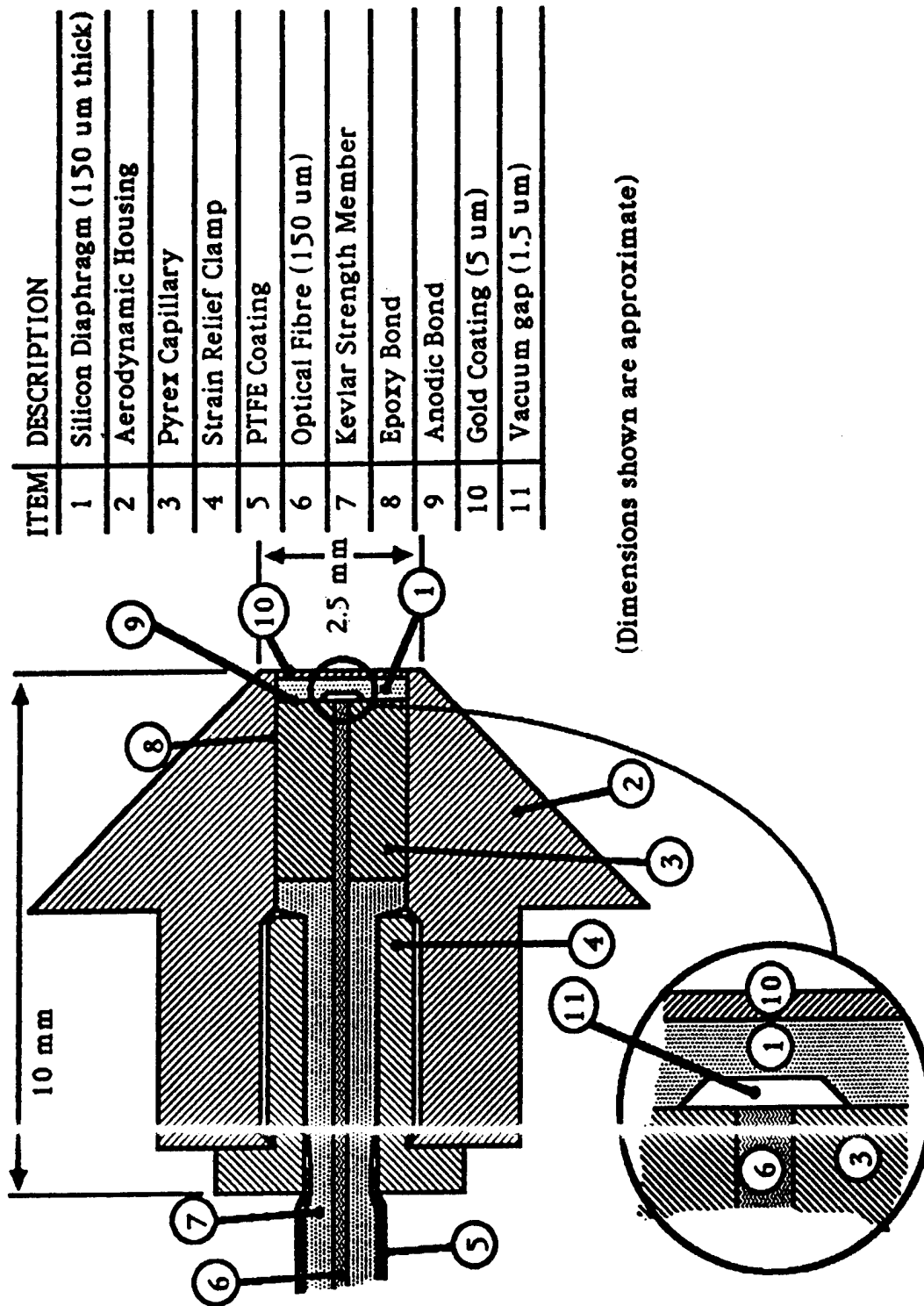


Figure 91. Fabry-Perot resonator sensor head design.

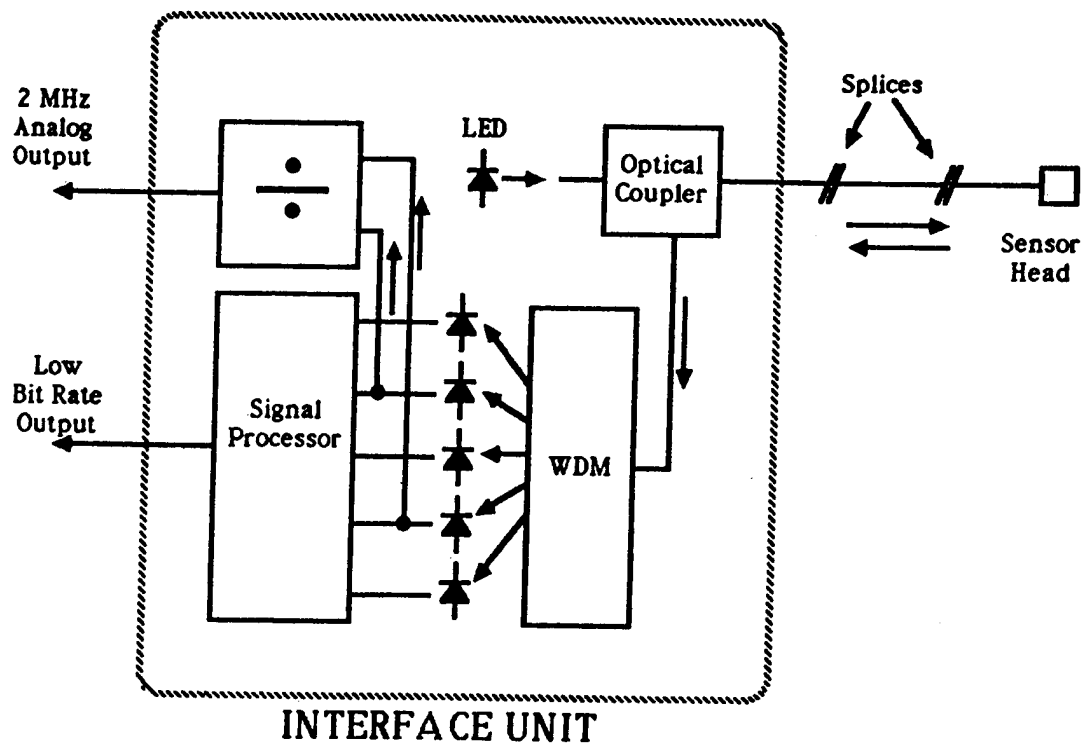


Figure 92. Optical circuit for a Fabry-Perot resonator sensor.

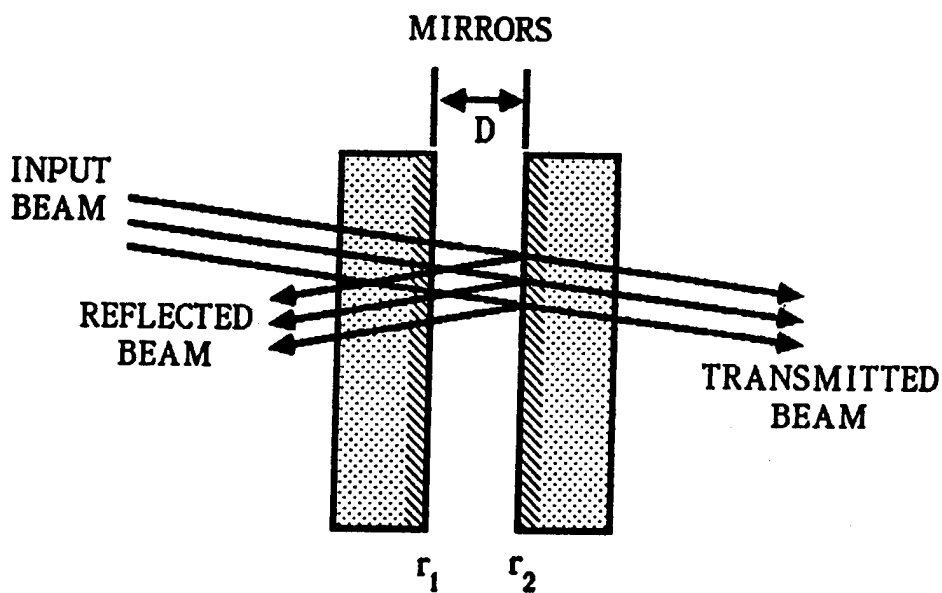


Figure 93. Schematic of a Fabry-Perot optical resonator.

detectors of two MHz. These two channels provide inputs to generate the normalized signal. The remaining three channels are used to calibrate the system.

The design goal of this sensor was a selected range in the 0 to 10,000 psi category and a frequency response of two MHz. A summary of predicted characteristics is presented in Table 18.

Ref: Barth, P.W. and Wilson, J., "Ultrahigh Frequency Pressure Sensor - Novasensor," AFATL-TR-88-77, 1988.

4.6.2 High Bandwidth Fiber Optic Sensor (USA) (1988).

A high bandwidth fiber optic pressure sensor was proposed by Geo-Centers, Inc. The sensor is based on the photoelastic effect in glass and has a range of 0 - 10,000 psi. The useable measurement bandwidth is DC - 2 MHz with a natural resonant frequency of more than 10 MHz. The unit is compatible with fiber optic data transmission lines. The gage output is immune to source light intensity variations, to EMI, to optical fiber microbending losses and to radiation fiber darkening.

A schematic of the optical configuration of a photoelastic pressure sensor is shown in Figure 94. The conceptual design of the sensor is shown in Figure 95. Experimental results with components of the sensor demonstrated its sensing range and rise time.

Ref: Nelson, Bruce N., "High Bandwidth Fiber Optic Air Blast Pressure Sensor," Geo-Centers, Inc., Newton Centre, MA. Paper presented at the Fifth State-of-the-Art Blast Instrumentation Meeting, Volume I, 1988.

4.7 BAR PRESSURE GAGES.

Adaptations of the Hopkinson Bar have been made to obtain a bar gage for the measurement of high pressures on the order of 1-8 kilobars (about 116,000 psi). Bar gages operate on the principle of conducting the pressure pulse down an elastic bar to a sensor which is shielded from the environment affecting the bar. Shown in Figure 96 is a schematic of a bar gage installed for a high pressure measurement. Schematics of generic bar gages are shown in Figure 97.

The bar gage appeared in the sixties, but it was not until the last decade and a half that the gage found extensive use. The measurement of high blast pressures carries with it a very harsh environment which must be dealt with to obtain a bonafide pressure record. A way to overcome such an environment was to remove the sensor, locating it on the bar at a desired point away from the surface environment. When a blast wave passes over the bar, a stress wave is induced in the bar that propagates at the longitudinal wave speed in the bar. The input pressure must not exceed the yield strength of the bar and the bar must remain elastic. When the stress wave reaches the sensor, the magnitude and wave form are related to the input pressure. A water jacket is used to encase the gage housing to impede the housing surrounding the bar from collapsing on it due to the blast. The water jacket keeps the bar from experiencing any shear stresses along its lateral surface.

Table 18. Summary of predicted sensor characteristics.

SENSOR HEAD:	
Resonant Frequency	3-5 MHz
Full-Scale Pressure	10,000 psi
Resolution	1% FSD
Accuracy (estimated)	2% FSD
Temperature Coefficient	0.005% FSD/C
Operating Temperature Range: Continuous Transient	-55 to +125 C -55 to +200 C
Shock (1000 G, 1 us)	0.03% FSD
OPTOELECTRONIC INTERFACE UNIT:	
Operating Temperature Range (other characteristics not evaluated)	-30 to +70 C

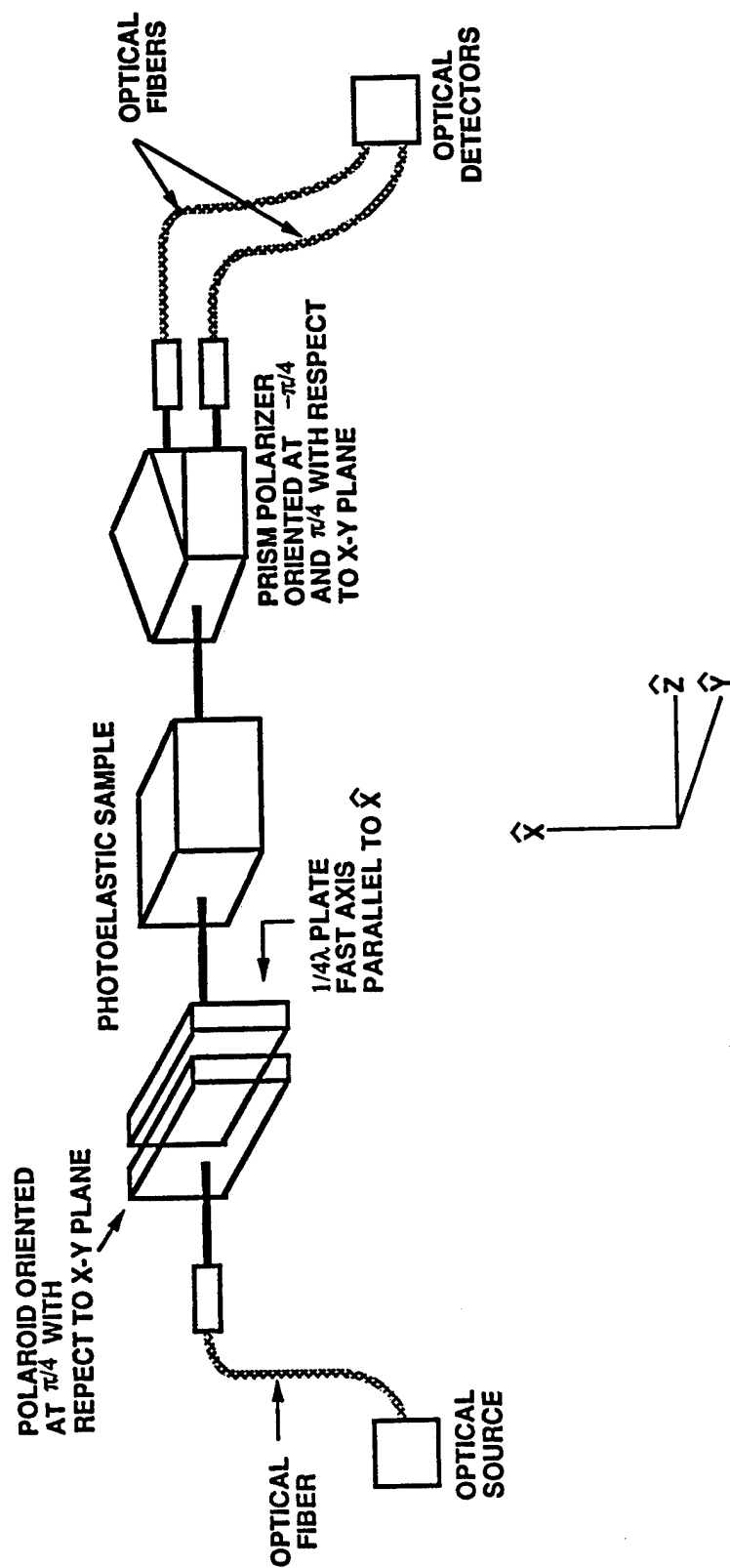
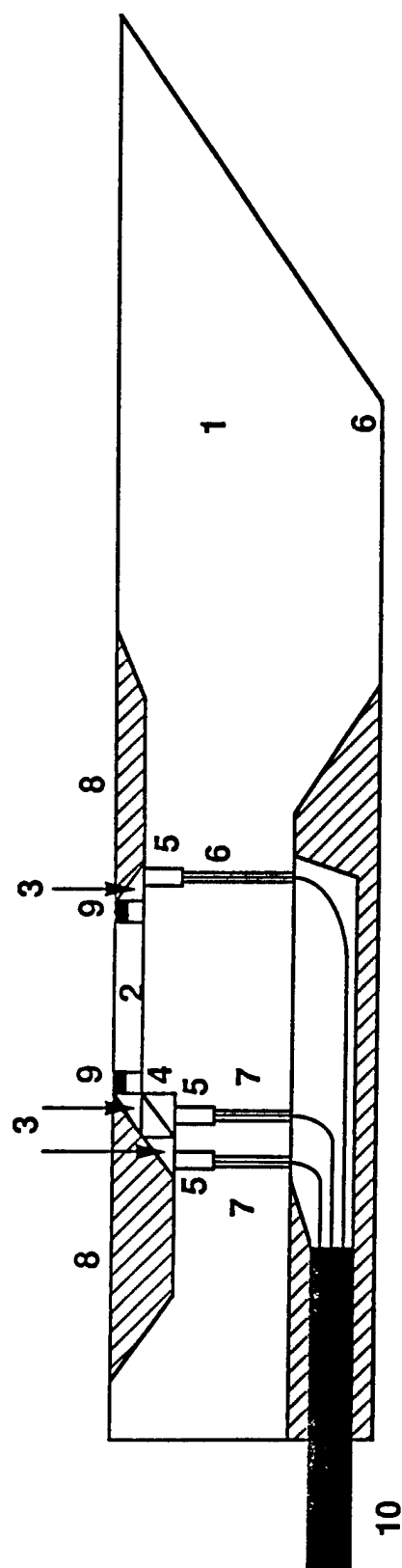


Figure 94. Schematic of the optical configuration of a photoelastic pressure sensor.



1. STRUCTURAL HOUSING
2. PHOTOELASTIC MATERIAL
3. RIGHT ANGLE PRISM
4. POLARIZING BEAM SPLITTER
5. GRIN ROD LENS
6. INPUT FIBER
7. OUTPUT FIBERS
8. STRUCTURAL SUPPORT
9. EPOXY
10. JACKET FOR INPUT / OUTPUT FIBERS

Figure 95. High bandwidth fiber optic airblast pressure sensor, conceptual design.

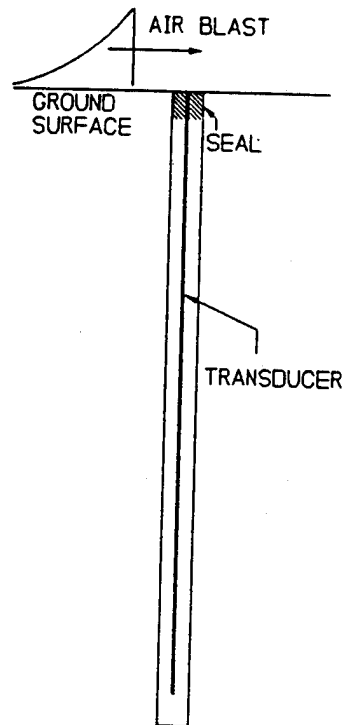


Figure 96. A high-pressure bar gage.

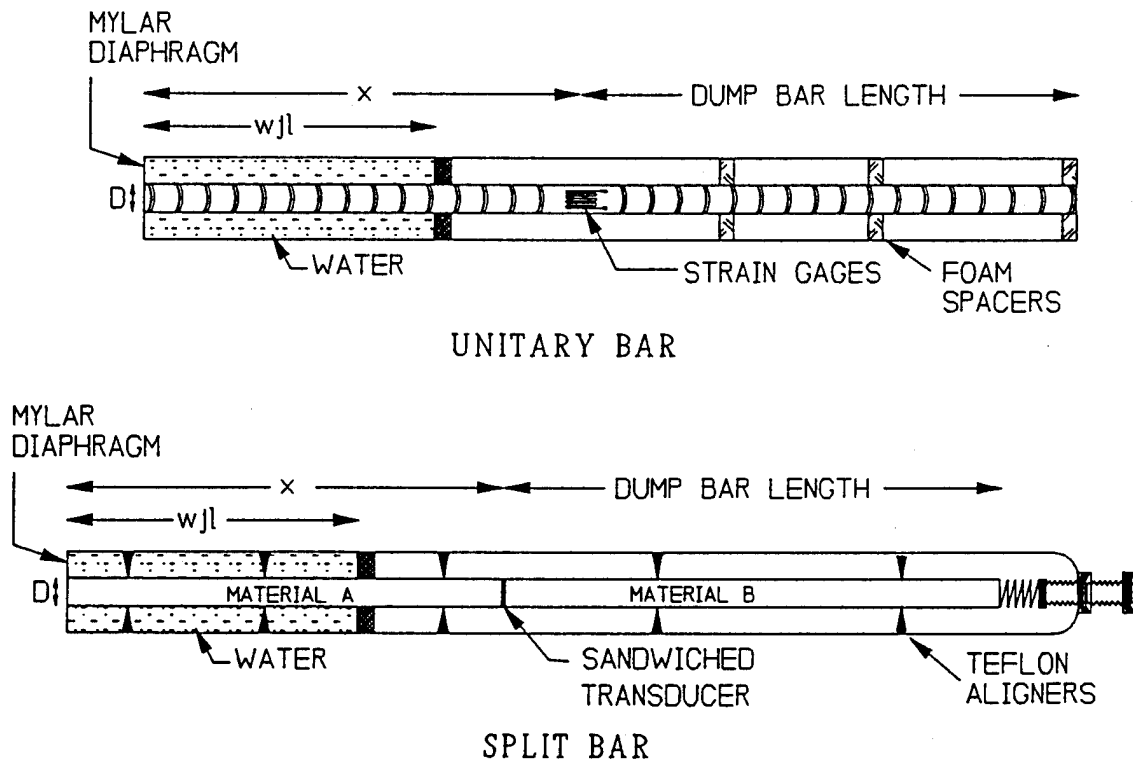


Figure 97. Generic high-pressure bar gages.

4.7.1 General Atomics Quartz Bar Gage (USA) (1961).

General Atomics Corporation introduced a bar gage having two rods 1/4 inch by 24 inches cemented together. The pressure pulse induces strain in a tungsten rod which is sensed by a quartz sensor. Just beyond the sensor is a magnesium rod. According to theory, the contrast between the acoustic impedances of the two rods causes the stress applied to be much lower in the tungsten rod thus the quartz sensor does not become overloaded and shatter. The duration which the gage could measure was 260 microseconds. When tested, the gage exhibited a fast response of about 3 microseconds; however, it was reported that there was a slower rise in the signal above the initial jump to a peak about 80 percent higher in 80 microseconds. It was first thought that the overshoot was due to an impedance mismatch between the quartz crystal and the tungsten. When an aluminum rod was substituted the overshoot was not eliminated. Some people thought the speed of loading could cause oscillations and produce overload.

To the authors knowledge, the gage was not deployed on a field test.

Ref: Rowland, R.H., "Blast and Shock Measurement State-of-the-Art Review," DASA-1986, 1967.

4.7.2 SRI Quartz Bar Gage (USA) (1961).

The Stanford Research Institute (SRI) proposed a bar gage similar to the General Atomics gage but capable of yielding a longer duration. This design would use a continuous rod with one or more sensors located four feet from the sensing end and six feet of rod beyond the sensors. The design would allow an operation time of 750 microseconds. Two types of sensors were planned; a piezoelectric and a strain sensor. Rise times of about 10 microseconds were postulated.

As far as can be determined, no gage was ever fielded.

Ref: Rowland, R.H., "Blast and Shock Measurement State-of-the-Art Review," DASA-1986, 1967.

4.7.3 ST-4 Piezoelectric Pressure Bar Gage (USA) (1962).

The ST-4 piezoelectric pressure bar gage was developed for high response measurements in shock tubes but was used on a very limited basis in HE field tests. Developed by the Ballistic Research Laboratory, now commercially available from PCB Piezotronics, the gage uses a piezoelectric sensor located on the input end of the pressure bar (see Figure 98). The pressure bar is acoustically matched to the sensor and is embedded in an absorptive material to dissipate the stress pulse into the surrounding material. A thin silver plating placed between the exposed face of the sensor and the gage case completes the electrical circuit. When properly used, the gage has a rise time of 0.2 microseconds. It has little overshoot and essentially no resonance; it is however very temperature sensitive and for this reason saw little use in field programs.

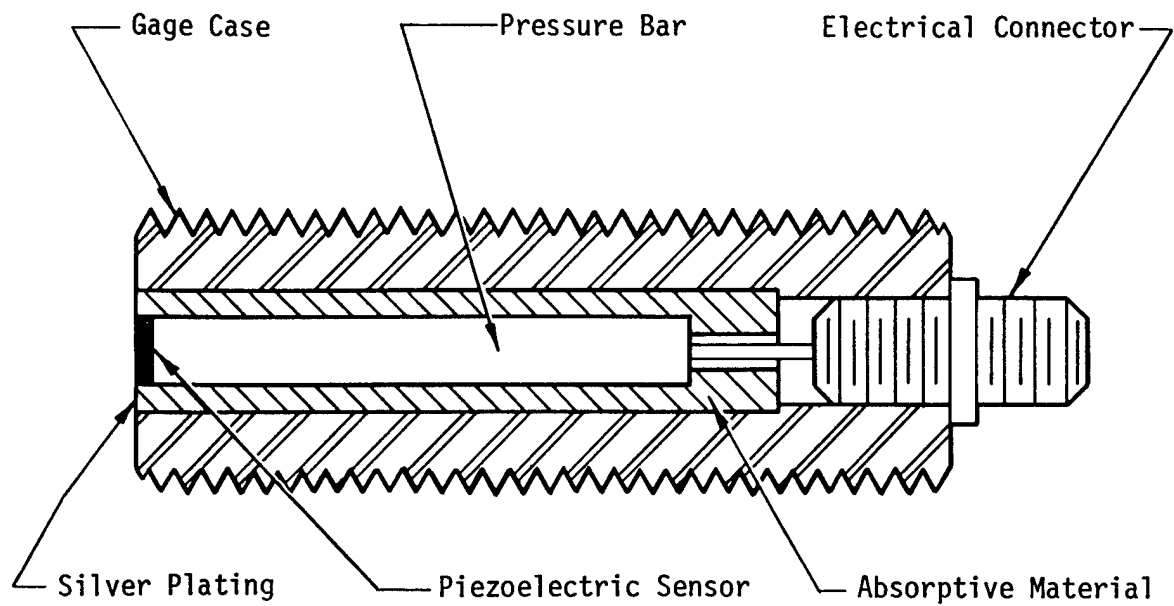


Figure 98. Piezoelectric pressure bar gage, Model ST-4.

Ref: Granath, B.A. and Coulter, G.A., "BRL Shock Tube Piezo-Electric Blast Gages," BRL Technical Note 1478, 1962.

4.7.4 CERF Piezoresistive Bar Gage (USA) (1975).

The Civil Engineering Research Facility, University of New Mexico, conducted an effort to develop a piezo-resistive bar gage which would overcome the problems inherent with piezo-electric sensors but retain the advantages of the pressure bar. The original gage, as shown in Figure 99, used a bar machined from gray cast iron in an attempt to take advantage of the internal mechanical damping characteristics of the material. A hard epoxy was cast around the bar to absorb the stress pulse as it propagates down the bar. Two longitudinal and two circumferential piezo-resistive sensors were mounted on the bar close to the pressurized end and connected into a full bridge for temperature compensation.

Tests of the gage indicated drift problems after several seconds. It was thought that the drift was due to creep within the epoxy compound encasing the bar.

A redesign resulted in the addition of a pressure relief ring which essentially eliminated the drift which was present in the first model. Beeswax was added under pressure to encase the bar. Test results indicated that good damping had been achieved by this process. The gage is illustrated in Figure 100.

The effective range of the gage was 30,000 psi with an over-range capability of about 100,000 psi. The gages were used with reasonable success on the Dynamic Air Blast Simulator (a large expendable shock-tube type of field test).

Ref: Simmons, K.B., "Development of Piezoresistive Bar Gage," AFWL-TR-76-65, 1976.

4.7.5 WES Bar Gage (1984) (USA).

The heart of the WES Bar gage is a 2.54 cm (one inch) diameter high strength steel astroloy bar with four semiconductor strain gages installed in a full bridge configuration at a prescribed location down the length of the bar. A detailed cross-section of a typical bar gage is shown in Figure 101. The lengths of typical bar gages vary according to the measurements desired, from 2 to 7 meters. Semiconductor strain gages are placed on machined flats on the bars at locations typically ranging from 0.6 to 2 meters from the top end of the bar. The bar itself is placed inside a 3-inch diameter PVC pipe to temporarily protect the bar from lateral loadings produced by the explosion. Wooden spacers are used to center the bar within the PVC pipe.

At the bottom end (or dump end) of the bar gage, a stack of alternating disks of styrofoam and wood are placed for the bar to rest on to simulate a free end condition at the dump end causing almost all of the pressure pulse to be reflected back into the bar. An annular column of water is added shortly before testing to the top of the gage extending from the top end of the bar to a short distance above the strain sensors; typically 61 cm long.

This is called the water jacket and is employed to prevent high velocity gases from propagating along the bar gage and destroying the strain sensors and cabling.

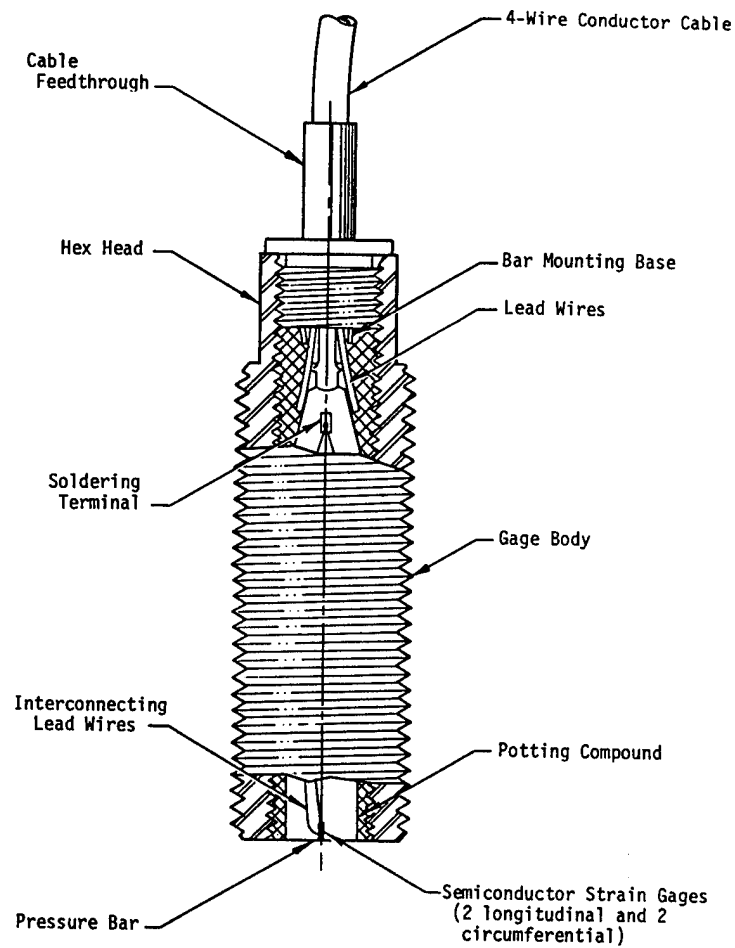


Figure 99. Redesigned piezoresistive bar gage modified for extrusion-filling process.

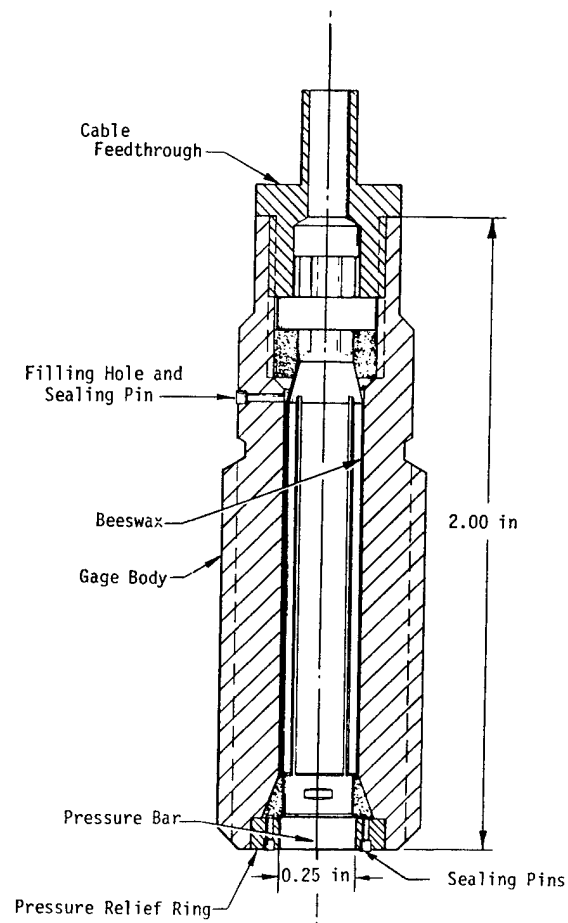


Figure 100. Original piezoresistive bar gage.

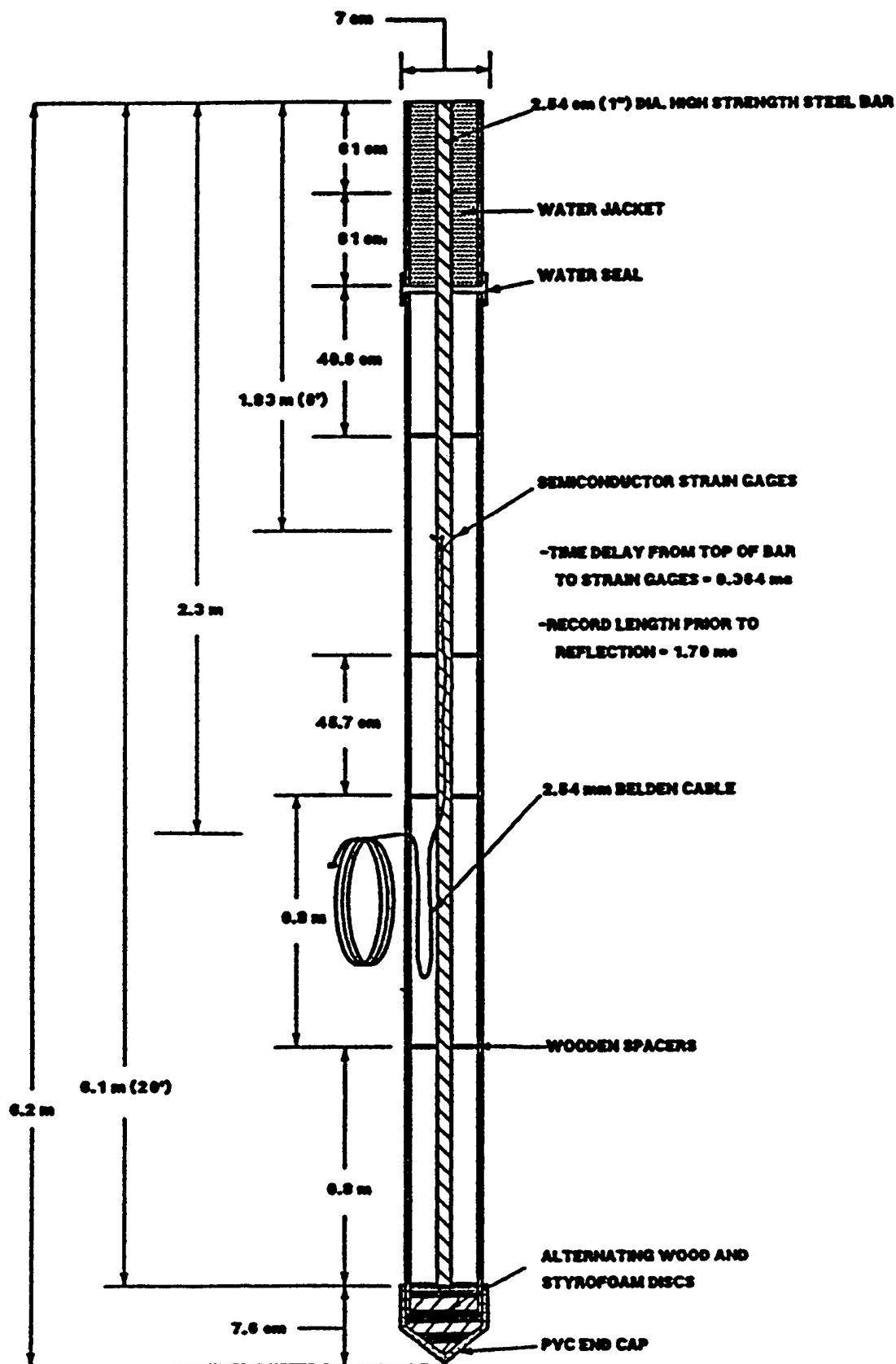


Figure 101. Detailed cross-section of a typical bar gage.

Instrumentation cables are routed through a hole in the PVC pipe and on to a recording center with care taken to ensure that they have protection from any damage resulting from the explosion.

A typical installation of the bar gage is presented in Figure 102. The gage is buried in the soil testbed with the measurement end exposed to the blast loading. As the blast wave strikes the components of the installation at the same time, the pressure wave travels rapidly down the steel bar, about 16,720 ft/s (5090 m/s); less rapidly through the water jacket, about 5009 ft/s (1525 m/s); and still more slowly through the soil at about 305 m/s to 1525 m/s. The result of this is that any lateral inputs to the bar from the water jacket or the ground shock are delayed until after the initial arrival of the stress pulse at the strain gage location.

Bar gages have a limited recording time depending upon the length of the bar. Extending the length of the bar will increase the recording time, however, there are practical limits on the bar length. Decreasing the distance from the top of the bar to the sensors is limited by the water jacket; also it is undesirable to place the strain sensors less than 10 to 20 bar diameters from the top of the bar. Unfolding the bar gage record has been tried with some success to gain more of the gage record.

The range of the gage is typically 1-8 kbars.

Figures 103 and 104 show various stages in the installation of the WES bar gage.

Ref: Rickman, Denis D., "MISERS GOLD High-Pressure Airblast Measurements," Waterways Experiment Station, Technical Report SL-91-1, 1991.

Ohrt, Alan Paul, "Analysis of D'Alembert Unfolding Technique for Hopkinson Bar Gage Records," Waterways Experiment Station, Technical Report SL-92-12, 1992.

4.7.6 NMERI Bar Gage (1984) (USA).

The NMERI bar gage follows the unitary bar gage design principle as illustrated in Figure 97. It has been deployed in several lengths and with different materials constituting the bar.

The "short" bar gage uses a high strength steel bar of astroloy 0.5 inches (127 cm) in diameter and 7.5 feet (2.3 meters) in length. Foil strain gages are placed at a distance of 3.61 feet (1.1 meters) from the input end of the bar on a cleaned, curved surface. The water jacket is 3.25 feet (0.99 meters) in length and is a PVC pipe container. A data time of 457 microseconds and a water jacket time of 448 microseconds is noted for the gage with a frequency response of 31.5 kHz. A diagram of the gage is shown in Figure 105.

The "long" bar gage also uses a high strength steel bar of astroloy 0.5 inches (127 cm) in diameter but the length is 12.8 feet (3.9 meters). Foil gages are placed at a distance of 6 feet (1.8 meters) from the input end. The water jacket is 1.5 meters in length and is a steel pipe container. A data recording time is noted as 762 microseconds, a water jacket time of 690 microseconds, and a frequency response of 27.5 kHz. A diagram of a typical long bar is presented in Figure 106.

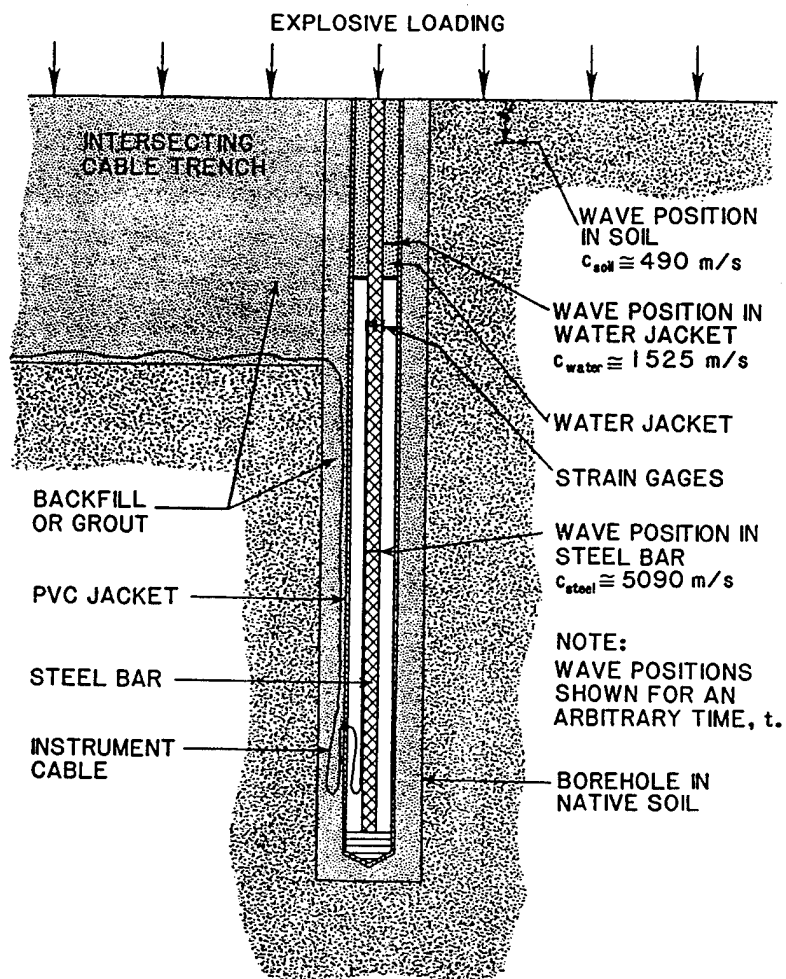


Figure 102. Typical installation techniques for a bar gage.

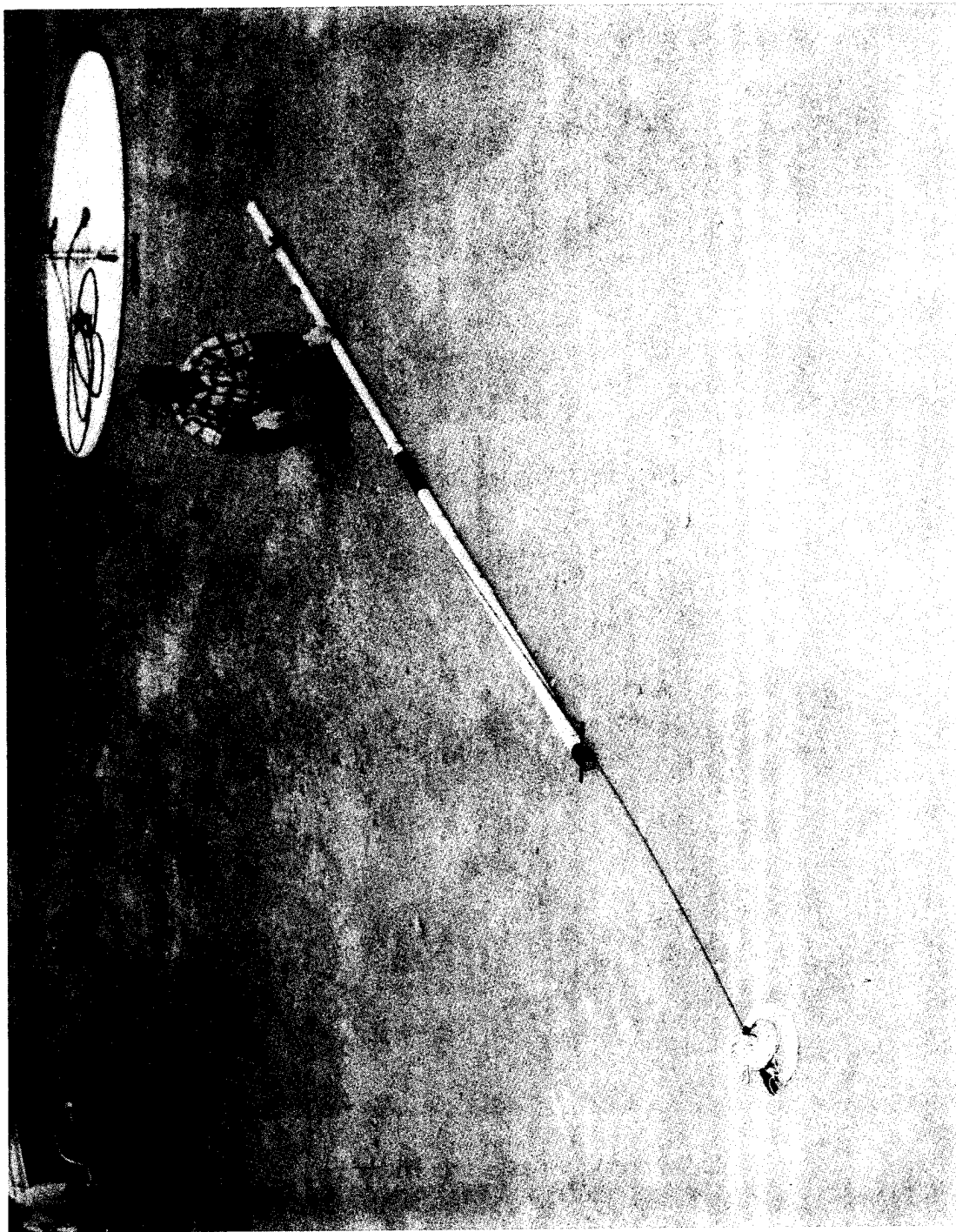
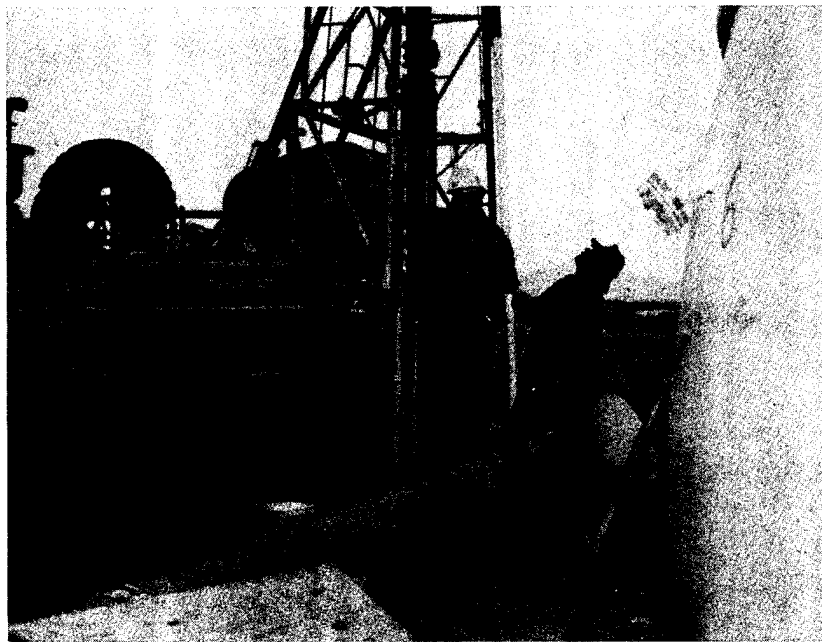


Figure 103. WES bar gage ready for installation.



a. Preparing bar gage for placement.



b. Lowering bar gage into borehole.

Figure 104. WES bar gage installation sequence.

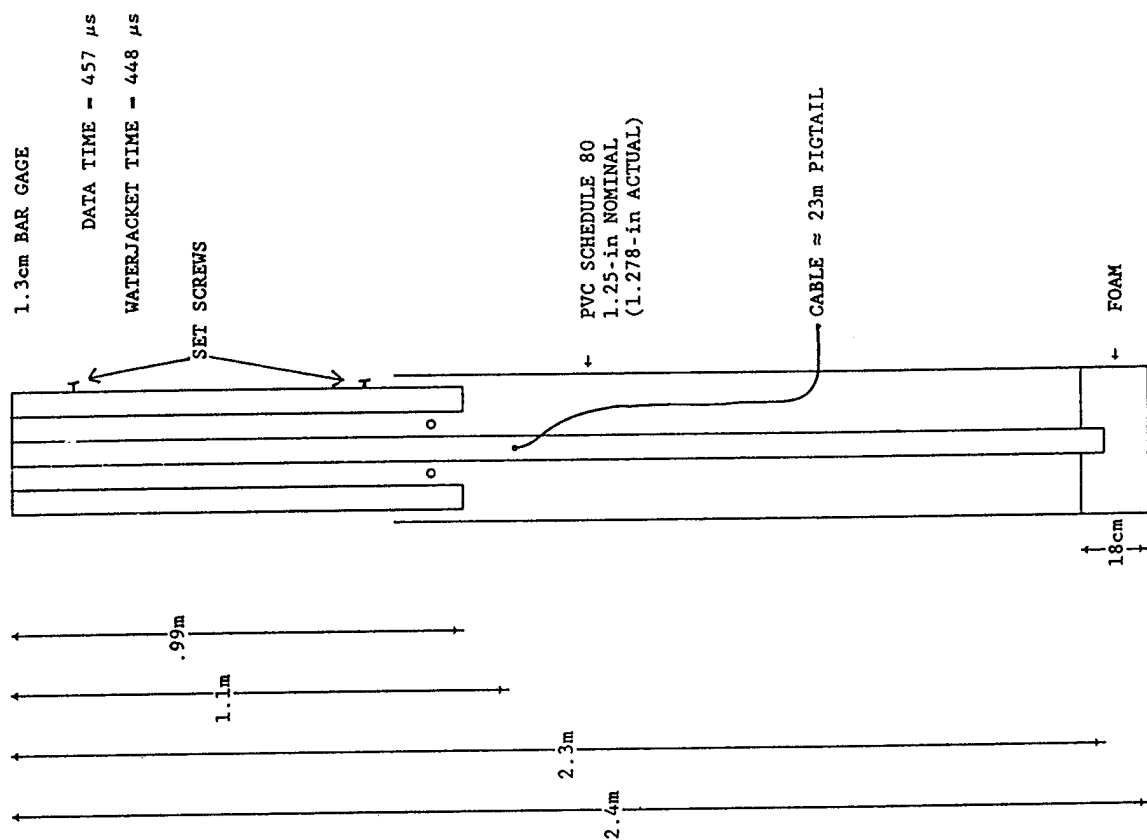


Figure 105. NMERI short bar.

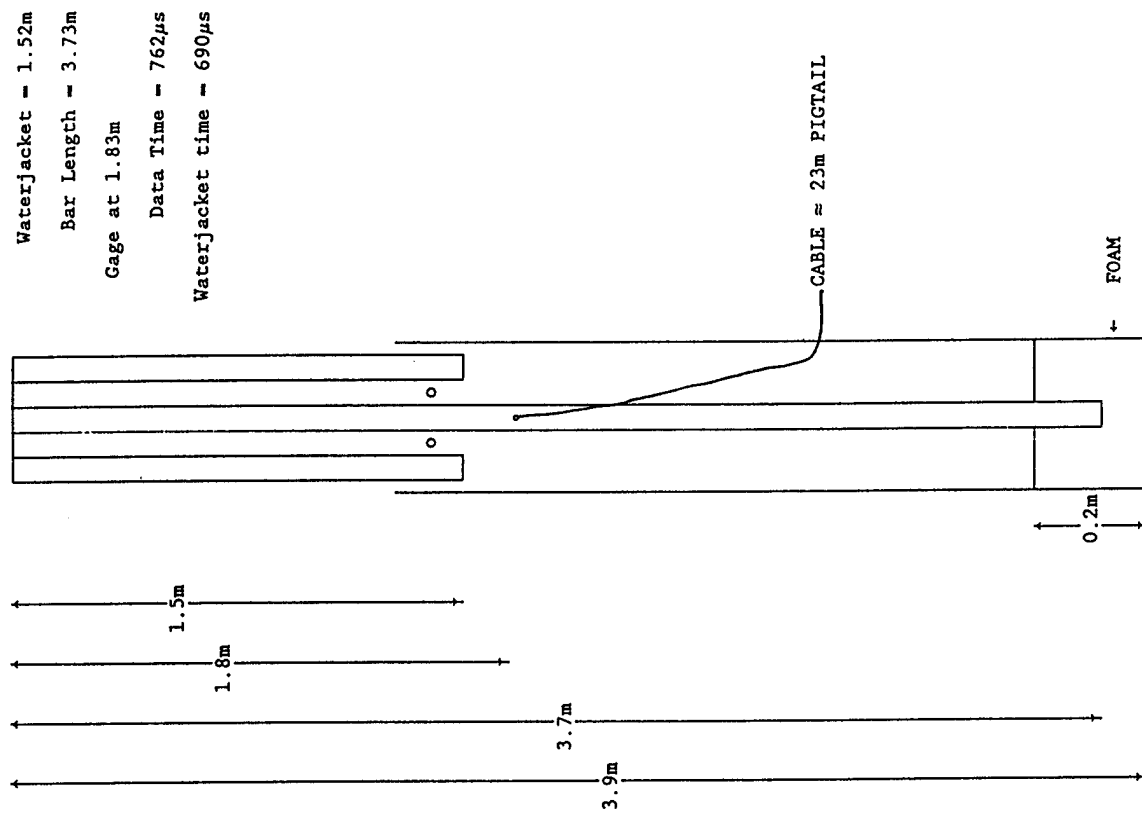


Figure 106. NMERI long bar.

Other NMERI bar gages are:

1. **The "FAT" Bar.** This bar was 20 feet (6.1 meters) in length with the foil strain gages located at 5 feet (1.5 meters) from the end and a water jacket 4 feet (1.2 meters) long. The bar was made of astroloy (0.5 inches (127 cm) in diameter).
2. **The "SKINNY" Bar.** This bar was 40 feet (12.2 meters) in length with the foil strain gages located at 9 feet (2.7 meters) from the end and a water jacket 8 feet (2.4 meters) long. The bar was made of astroloy 0.5 inches (127 cm) in diameter. A diagram of the skinny bar is shown in Figure 107.
3. **The "Air Jacketed" Bar.** This bar has the same basic design as the fat bar or skinny bar with the exception that the water jacket has been replaced with an air jacket. This configuration is depicted in Figure 108. Gage protection is achieved by a tight clearance between the bar outside diameter and the drill bushing inside diameter.
4. **The Ceramic Bar.** This bar gage was made out of high purity alumina (99.8 percent) and was 3/8 inch (9.53 mm) in diameter. Full bridge constant strain gages were located 10 inches (25.4 cm) from the end of the bar. Total bar length was 3 feet (91.4 cm) and the water jacket was 8 inches (20.3 cm) long. This dimension was chosen to optimize the length of the bar and eliminate the water jacket effect. The wave speed was 10 km/s and the predicted rise time was 2.2 microseconds. High frequency recording electronics were used to maximize the frequency response. The gage is shown in Figure 109.

Ref: Baum, Neal, et al., "The High-Pressure Bar Gage, Volume 1 - High-Pressure Bar Gage Designs," DNA-TR-92-160-V1, 1993.

4.7.7 S-Cubed Bar (1977) (USA).

The S-Cubed bar is one that typically uses the split-bar principle and appears in many varying sizes and lengths. The developers of the gage have chosen the split bar for two reasons: (1) the strain at the sensor can be adjusted by varying the mechanical impedance of the input and dump bar, and (2) transducers such as quartz or ytterbium can be used in the split. The signal generated by these transducers is sizeable, much greater than that generated by strain gages. Foil strain gages are frequently mounted on the dump bar to provide a redundant measurement .

S-Cubed bars were also developed using the unitary principle. These gages were 0.5 inches (1.27 cm) in diameter and used hardened steel for the bar. Short bars were 7.5 feet (228.6 cm) in length with foil strain gages mounted on a clean, curved surface 2.7 feet (83.8 cm) from the input end. A soft water jacket container of PVC pipe surrounds the bar for a length of 2 feet (61 cm). Long bars were 12.4 feet (378.5 cm) and had two sets of foil strain gages; one mounted at 2.7 feet like the short bar, and a second set mounted at 42 inches (106.7 cm). The water jacket was the same in both the short and long bar. A diagram of these gages is shown in Figure 110.

A good frequency response is achieved by positioning the gage sensor close to the input end of the bar. Some bars had strain gages plus either quartz or ytterbium sensors. Using

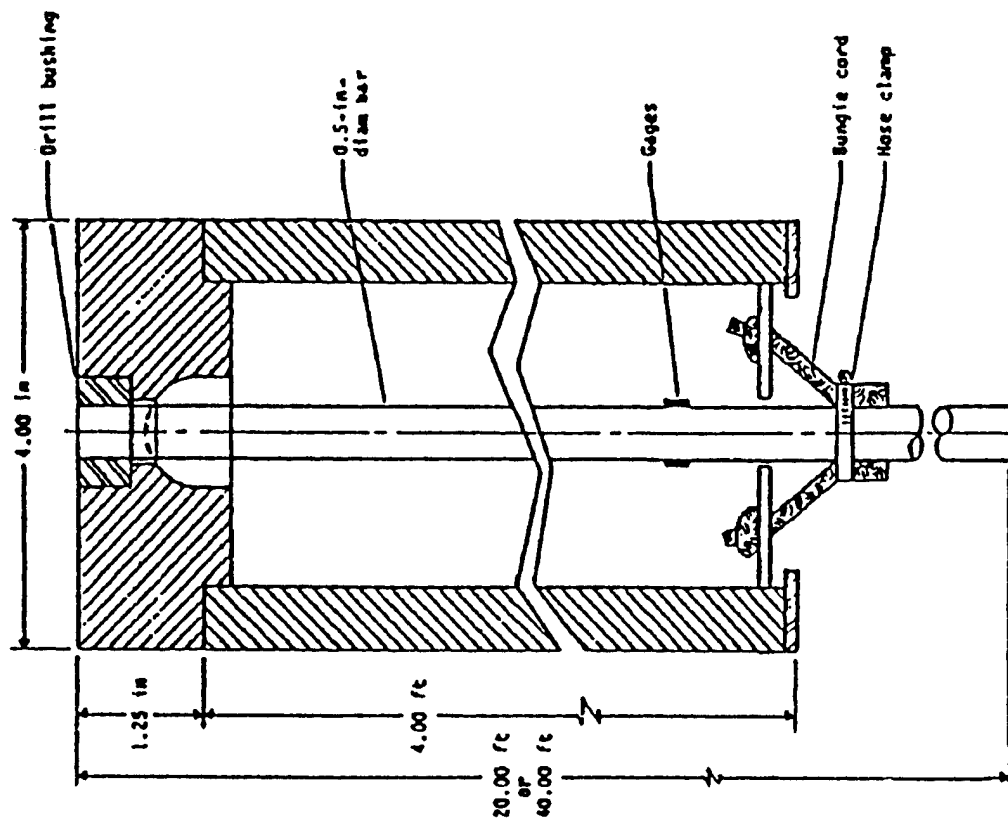


Figure 108. Air-jacketed bar.

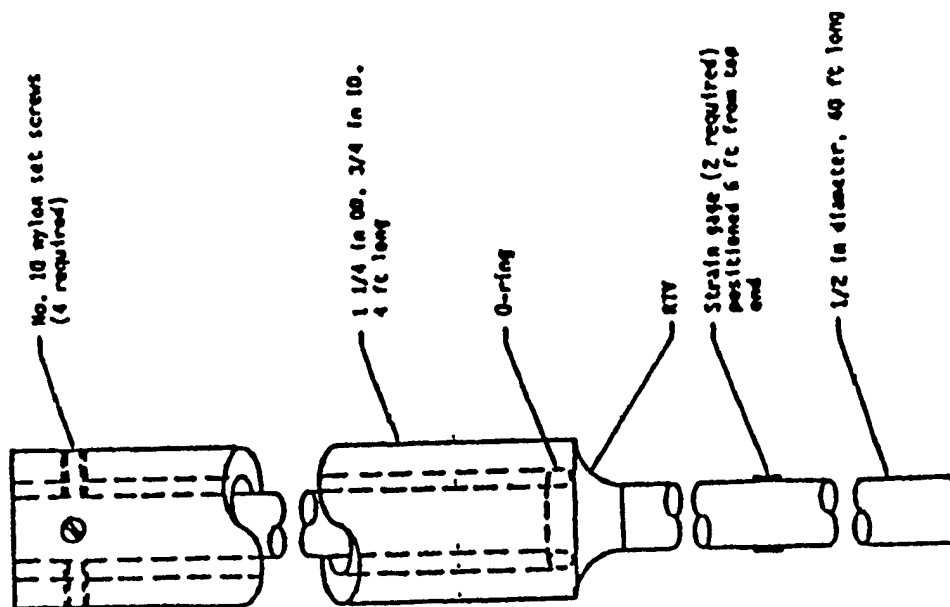


Figure 107. Skinny bar gage.

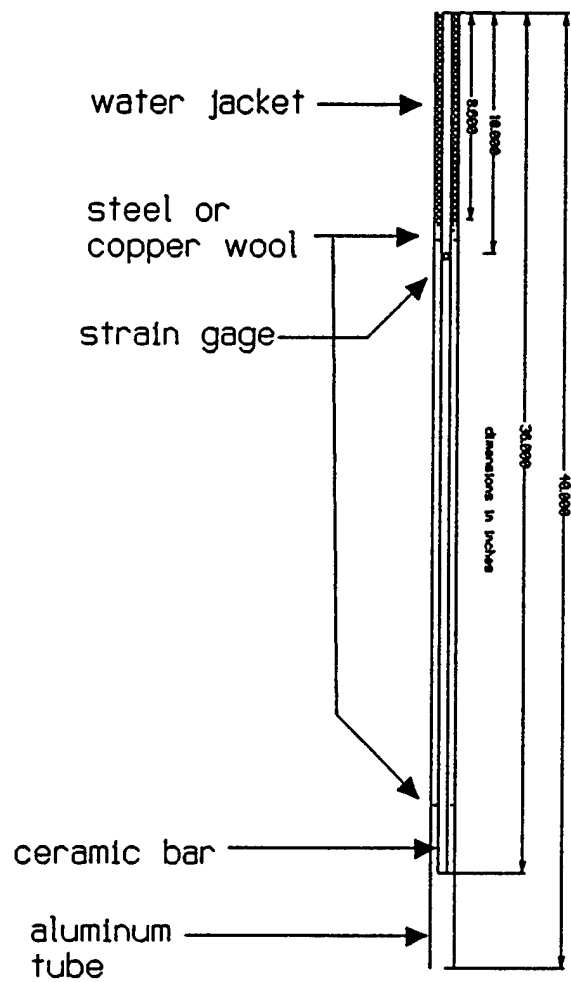


Figure 109. NMERI ceramic bar.

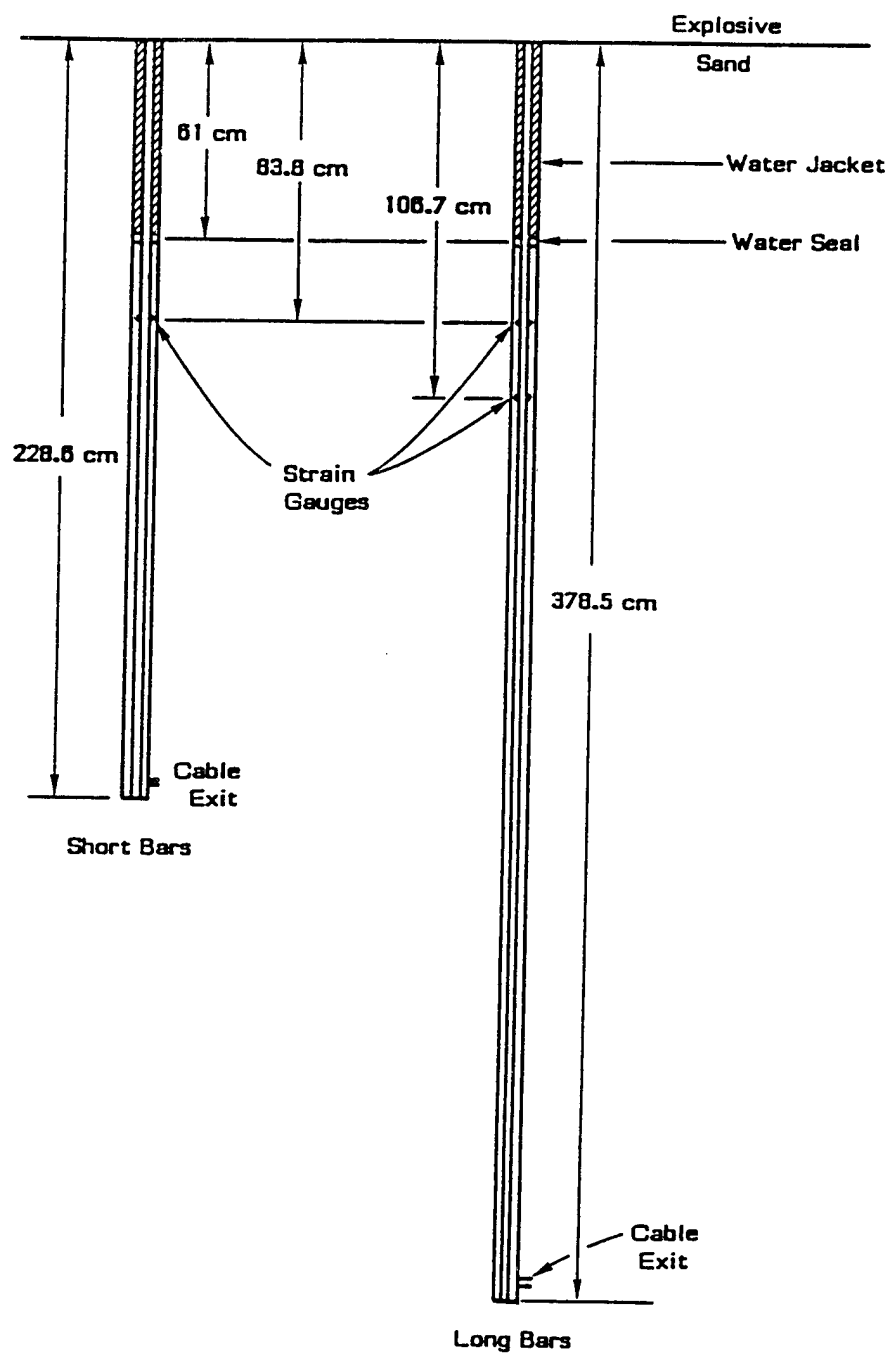


Figure 110. S-Cubed bar gage design.

quartz or ytterbium sensors require the split bar assemblies. Users have indicated that the split bar is more complicated to field than the unitary bar.

A "fast" S-Cubed bar was developed which uses a 1/8 inch (3.2 mm) bar of steel or one of tungsten carbide. Strain sensors were located 3 feet (91.4 cm) down the bars.

A modification was made to the gage as shown in the diagram of Figure 111. A hardened steel surround was placed on the input end. The idea was that this would keep the bar from penetrating any surface material and reduce the shear on the sides of the bar gage. A larger diameter bar, 1/4 inch (6.4 mm) was used. The modified gage was labeled the S³ armored bar.

Another modification made was simply to increase the size of the bar. It was 3/8 inches (9.5 mm) in diameter. The gage developed was a tungsten carbide bar and was labeled the S³ unarmored bar gage. It is depicted in Figure 112. The input bar was 3 feet (0.9 meters) long and had a 3 foot (0.9 meters) long steel dump bar. The gage was enclosed with an annulus water jacket made of aluminum 0.1875 inches (4.8 mm) in diameter.

An attempt was made to extend bar gage recording time by using the dump bar to absorb the pressure wave. This has been labeled a damped bar gage and is illustrated in Figure 113. An absorbing material used as an attenuator surrounds a tapered dump bar. A constant acoustic cross-section is maintained. The attenuators used have been different types of epoxies. Results were encouraging but the effort was halted because of lack of support.

A free-field static overpressure bar gage was developed and HE shock tube tested on a limited basis. The gage is a mercury-coupled bar gage shown in Figure 114. The literature describes this gage as follows.

"The gage is mounted so that the point is directed to the flow source. The point acts as a streamlined guide for the shock and gas flow along the cylindrical portion. The point is shock-isolated from the cylindrical body by means of a fiberglass-epoxy sleeve configured so that compressional stress is transmitted only by shear in the epoxy. The pressure pickup location is ten diameters from the transition shoulder. Pressure is applied to a mercury-filled cavity which includes the input end of the input bar. A piston with an o-ring confines the mercury and transmits the side-on pressure to the mercury cavity. The outer surface of this piston is contoured to match the outside surface of the probe. An o-ring in a specially designed retaining groove seals the input end of the input bar into the mercury cavity. A small diameter pin prevents the bar from being forced into the mercury cavity by a compression spring at the dump bar end. The spring force also assures bar contact where joints are not bonded. Such slip joints are a requirement in long gauges which are designed to provide long-duration read times and a low sensitivity to flexure waves in the bar.

The response time of a fluid-coupled gauge is minimized by the use of a fluid with low compressibility and by a fluid cavity with short length, which requires

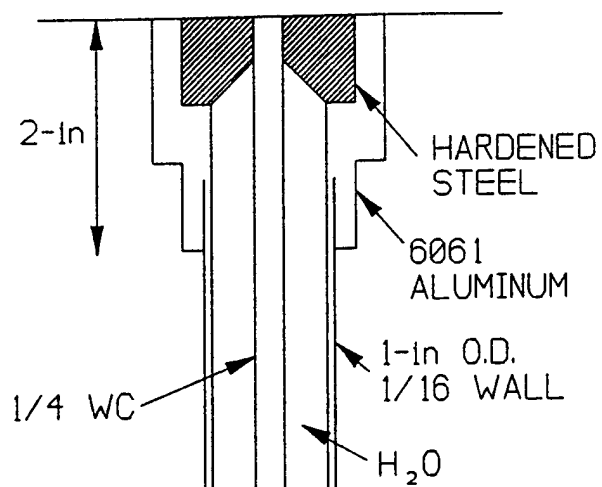


Figure 111. The S-Cubed armored bar.

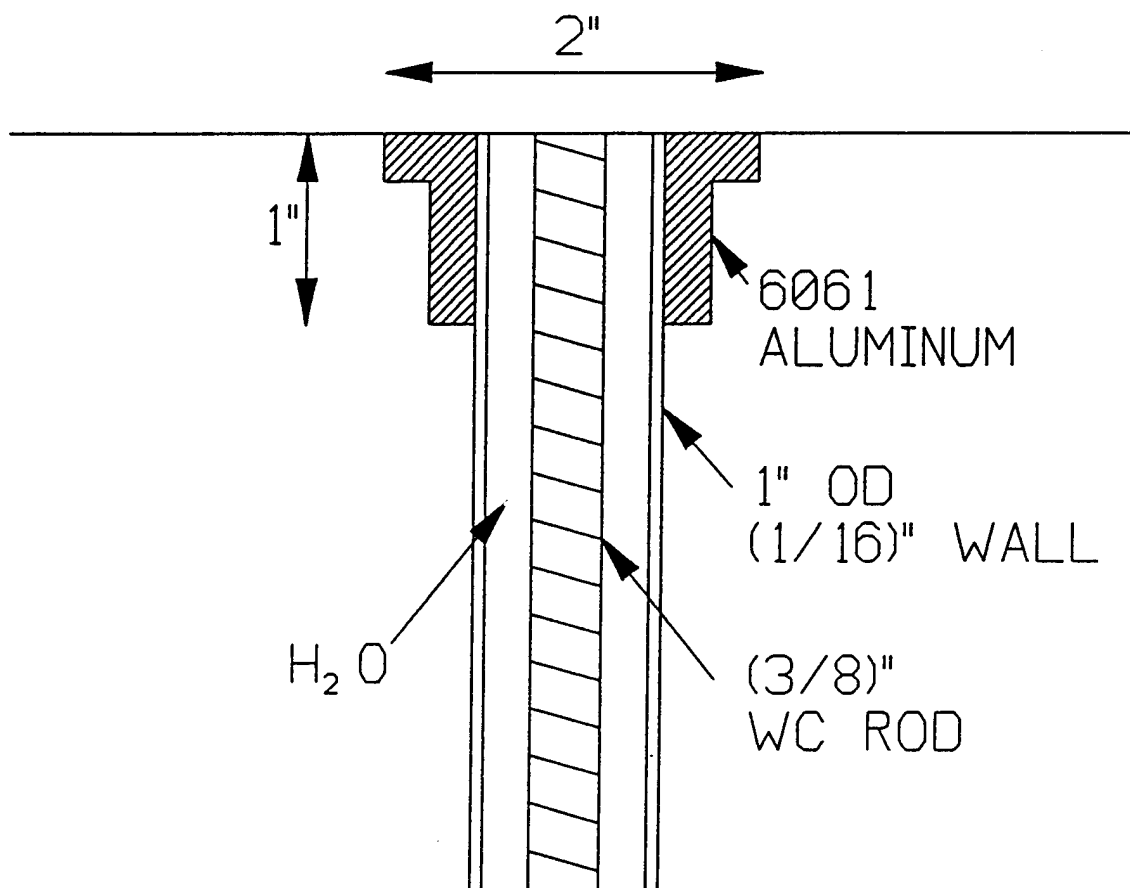


Figure 112. The S-Cubed unarmored bar gage on HURRICANE LAMP 3.

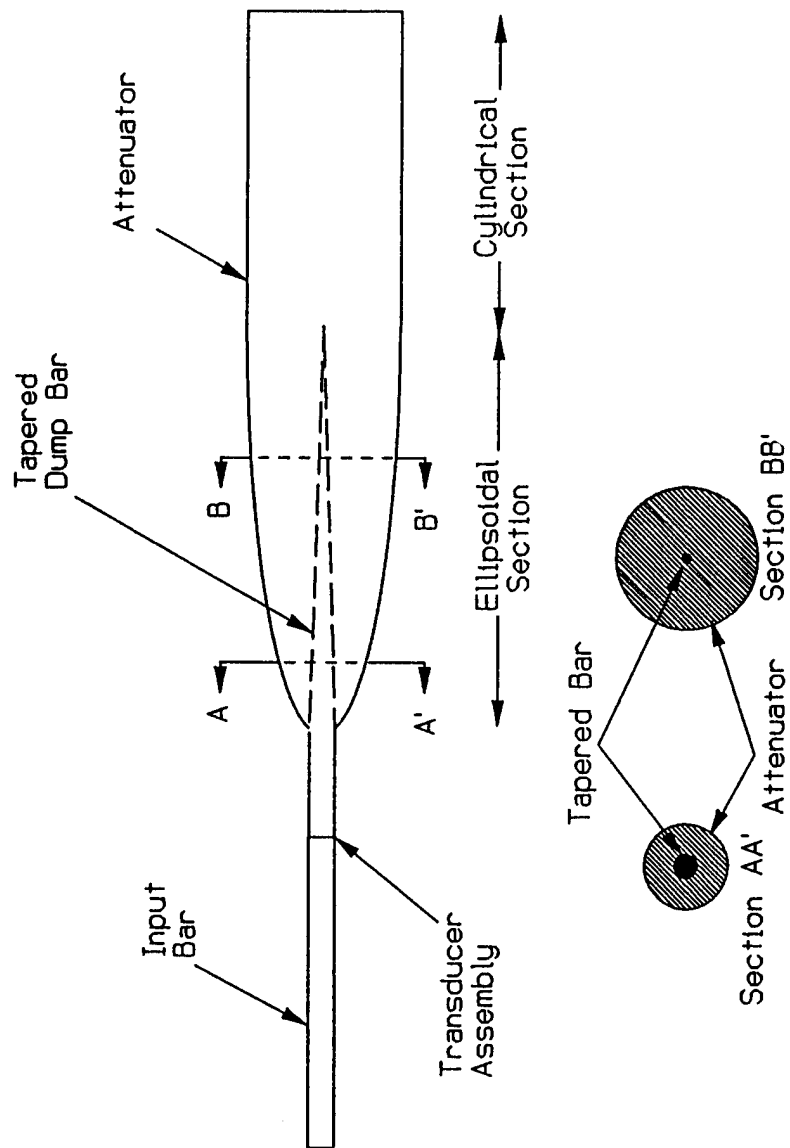


Figure 113. The S-Cubed damped bar gage.

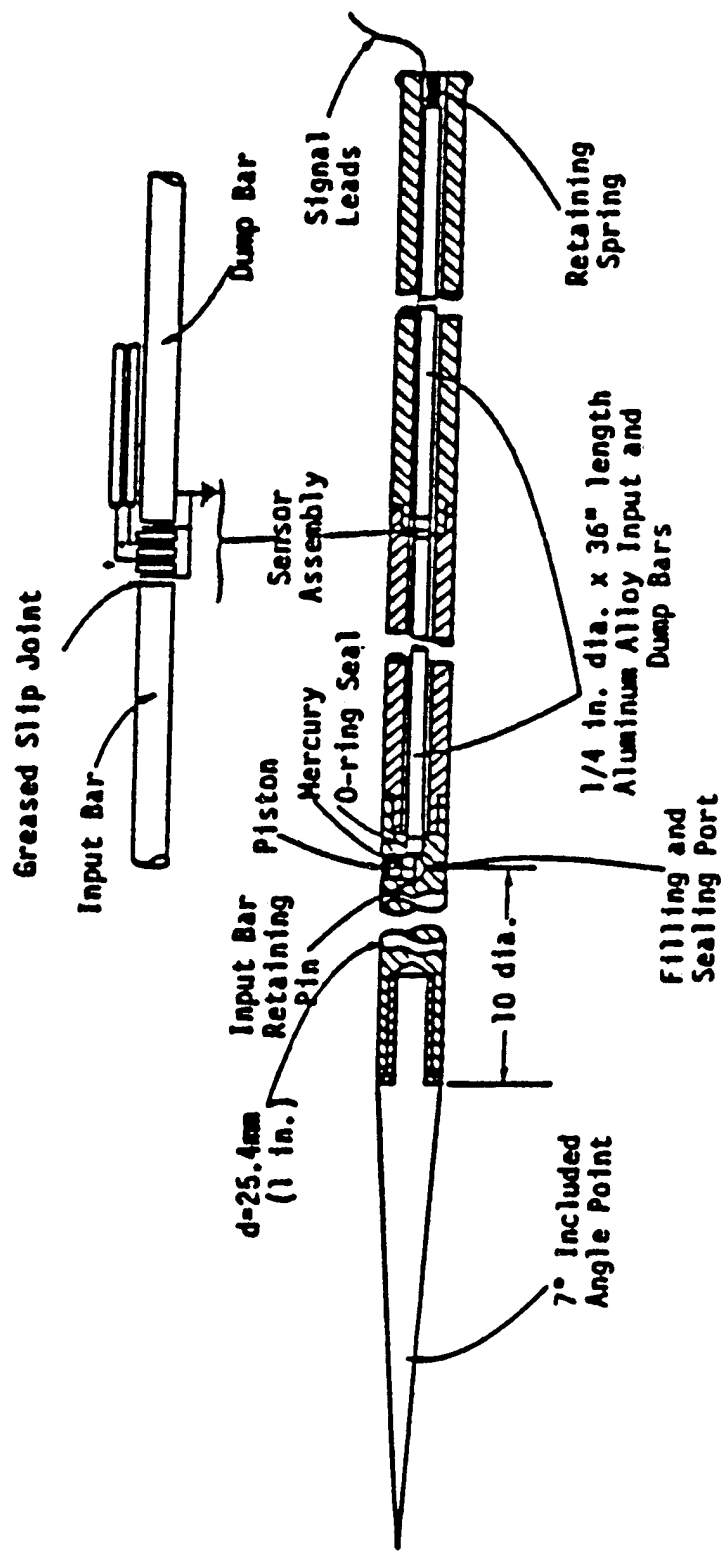


Figure 114. Side-on mercury-coupled-bar static overpressure gage.

a small-diameter input bar for the bar gauge. To insure that the theoretical limit on risetime is approached, the design and fluid-loading procedure must minimize the gasket movement around the input bar and eliminate any trapped air and/or other highly compressible materials. Mercury is the least compressible of available fluids. In the current design, vacuum removal of air to 1 part in 10^4 is a part of the assembly procedure. Evacuation of the cavity and the mercury supply for a period of 30 minutes or more is advisable to remove any moisture as well as air from the system prior to pouring the mercury into the cavity. Once the cavity is filled with mercury, the vacuum pump is shut down and atmospheric air pressure is applied to the mercury supply. The small filling port is sealed with a setscrew-driven stainless steel ball: the filling port is submerged in mercury during the sealing operation to insure that no air is carried into the cavity.

The input end of the input bar is capped with a thin-wall steel shell for compatibility with mercury. The outside diameter of this shell is 0.260 inches and it is 0.6 inches long. The sensor consists of three x-cut quartz crystals stacked to produce a differential signal arrangement so that equal lead noise pickup is canceled and the signal is double that of a single crystal."

Ref: Baum, Neal, et al., "The High Pressure Bar Gage, Volume 1 - High Pressure Bar Gage Designs," DNA-TR-92-160-V1, 1993.

Coleman, P.L., "Mini-Jade Instrumentation," DNA-TR-86-320, 1986.

4.7.8 Photoelastic Sapphire Bar (1991) (USA).

The Photoelastic Sapphire Bar is a development technique that employs an optical system which takes advantage of the photoelastic effect exhibited by sapphire. The system is diagrammed in Figure 115.

Baum, et al., describe the system; "The photoelastic effect of sapphire means that its birefringence is relatable to its state of stress. The retardation of the polarized vector is a function of the stress. The most common use of the effect is with white light and crossed polarizers. The varying states of stress in a large sample will cause colored patterns of light to appear. In this case, a polarized monochromatic light source is used. The quarter-wave plate is used to change this to circularly polarized light. It exits the sample in an elliptically polarized state that depends on the state of stress. This is passed through an analyzer (the half-wave plate), then one counts the fringes as the stress changes."

A path length of 9.784 mm through the sapphire bar is used. Rise times of 0.5 microseconds have been observed at pressures up to 5.7 kbars.

Ref: Baum, Neal, et al., "The High-Pressure Bar Gage, Volume 1 - High-Pressure Bar Gage Designs," DNA-TR-92-160-V1, 1993.

Johnson, D. and Gaffney, E., "One Microsecond Rise Time Birefringent Hopkinson Bar for Nuclear Airblast Measurement," K-Tech TR-91-15, 1991.

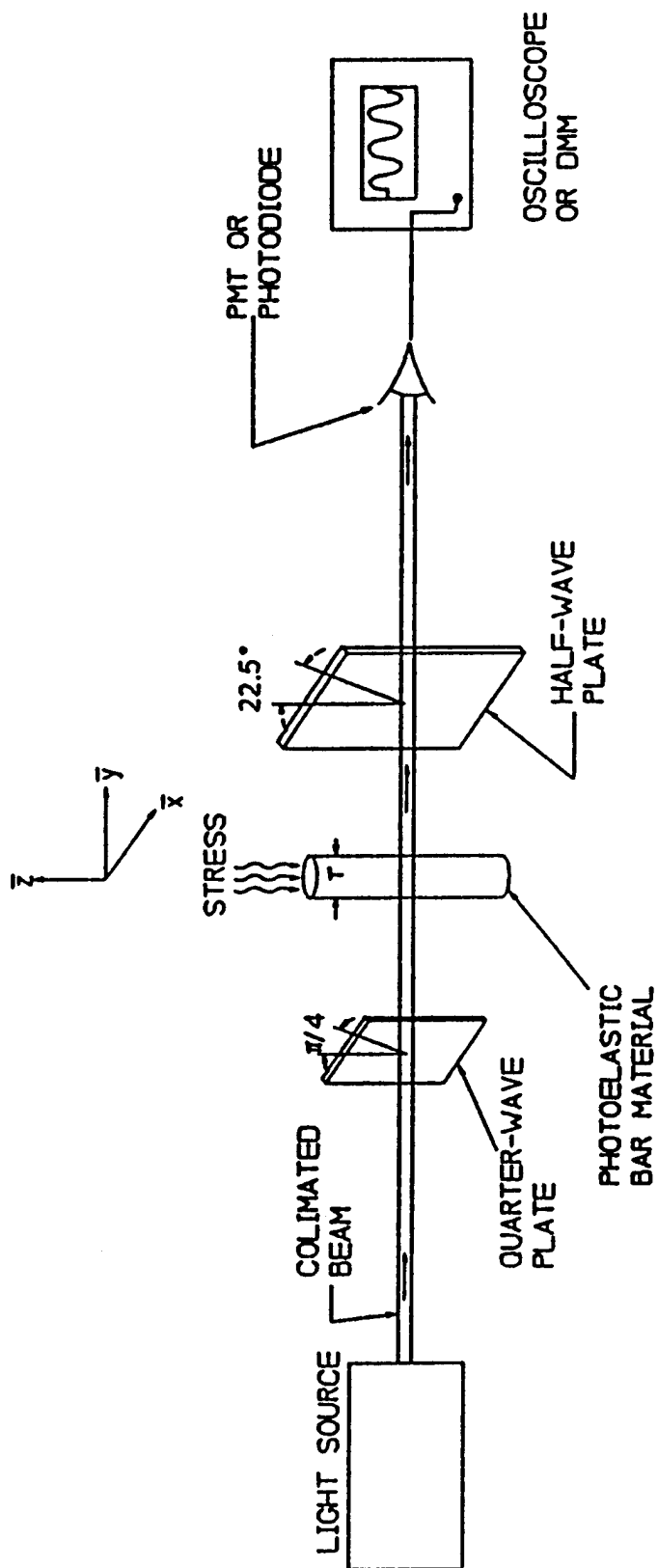


Figure 115. The photoelastic sapphire bar gage technique.

4.8 OTHER SYSTEMS.

4.8.1 DRES ABTOAD Gage (Canada) (1959).

The DRES ABTOAD gage, Air Blast Time of Arrival Detector, is a simple blast switch used to determine the velocity of the blast wave and, in turn, calculate the blast pressure. As illustrated in Figure 116, the ABTOAD was a simple, inexpensive system which required only one instrumentation wire pair for multiple gages placed on a given radial of a particular test. Shown in Figure 117 is a line of gages deployed on a large HE test.

The ABTOAD was constructed of a short length of brass tubing over the top of which was secured a conductive metal foil or Mylar cap. The passage of the blast wave would bend the conductive cap material such that it touched a central conductor, a brass rod, to complete an electrical circuit. Thus a connection was made for a brief moment between the outer brass tube and the brass center conductor.

Each gage was fitted with a simple capacitor-diode bleed resistor circuit and was connected across the single instrumentation wire pair in parallel with the other gages on that line. A small DC voltage was applied across the wire pair so when the blast wave passed each successive gage and momentarily connected the two instrumentation wires, a discrete voltage spike appeared on the recorded output.

Ref: Muirhead, J. C., and D. W. Lecuyer, "Development of Expendable Gauges for Detecting the Arrival of Shock Fronts, I. A Pressure Contractor with Mylar Element," DRES-TN-33, 59-0903, 1959.

Clink, W. L. et al., "A Progress Report on the Development of a Pressure Switch System for Detecting the Arrival of a Shock Front," DRES-TN-112, 63-0646, 1963.

4.8.2 DRES Blast Gage Station (1982) (Canada).

The DRES blast gage station is a single station which includes instrumentation for measurements of static pressure, density, shock velocity, and total head pressure. The key component is the densitometer which operates on the principle that beta radiation is attenuated in a well defined relation by the total mass between source and detector. A densitometer, as shown in Figure 118, was developed and fielded in the 60's. A suitable beta radiation source was located and incorporated in the housing with a photomultiplier tube, an electronics package, and a durable but sensitive detector window. Despite successful deployment of the gage, it was shelved until 1982.

Major improvements were made at that time in the overall design; reducing its bulk, incorporating static and total-head gages, and making use of a better packaged, stronger source and a hardened photomultiplier tube. This new source is shown in Figure 119 with a sketch of the overall design of the head. Two static pressure gages, the Kulite XT-190, are used; one is downstream of the other such that shock speed can be resolved based on the relative times of arrival of the blast front. A third Kulite gage is located out of line with the first two to allow two-dimensional resolution of the shock velocity.

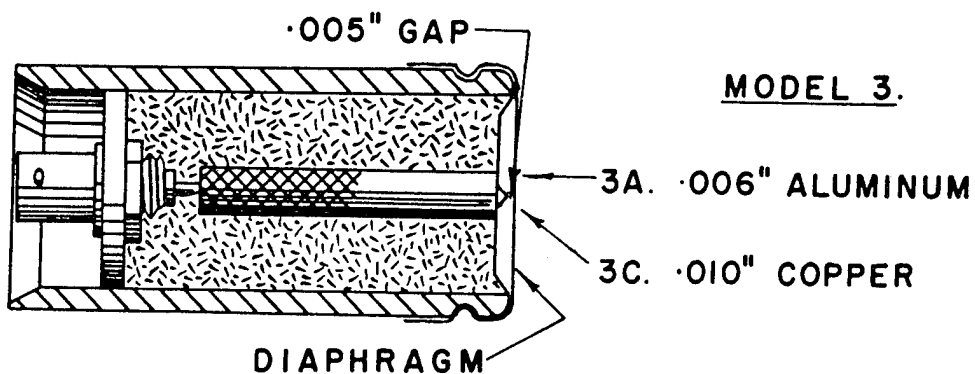
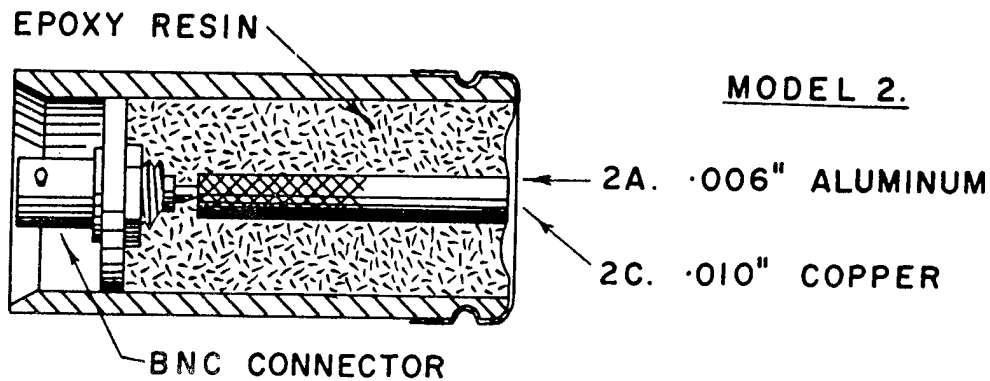
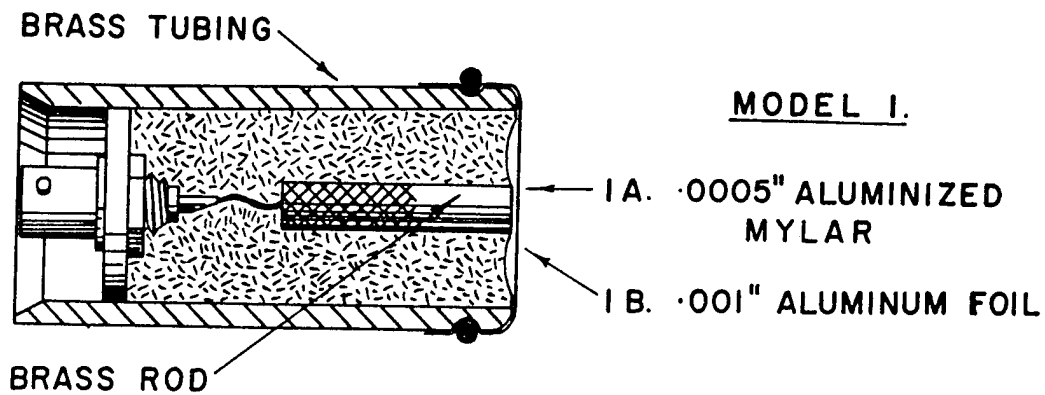


Figure 116. Schematic of ABTOAD detector development.

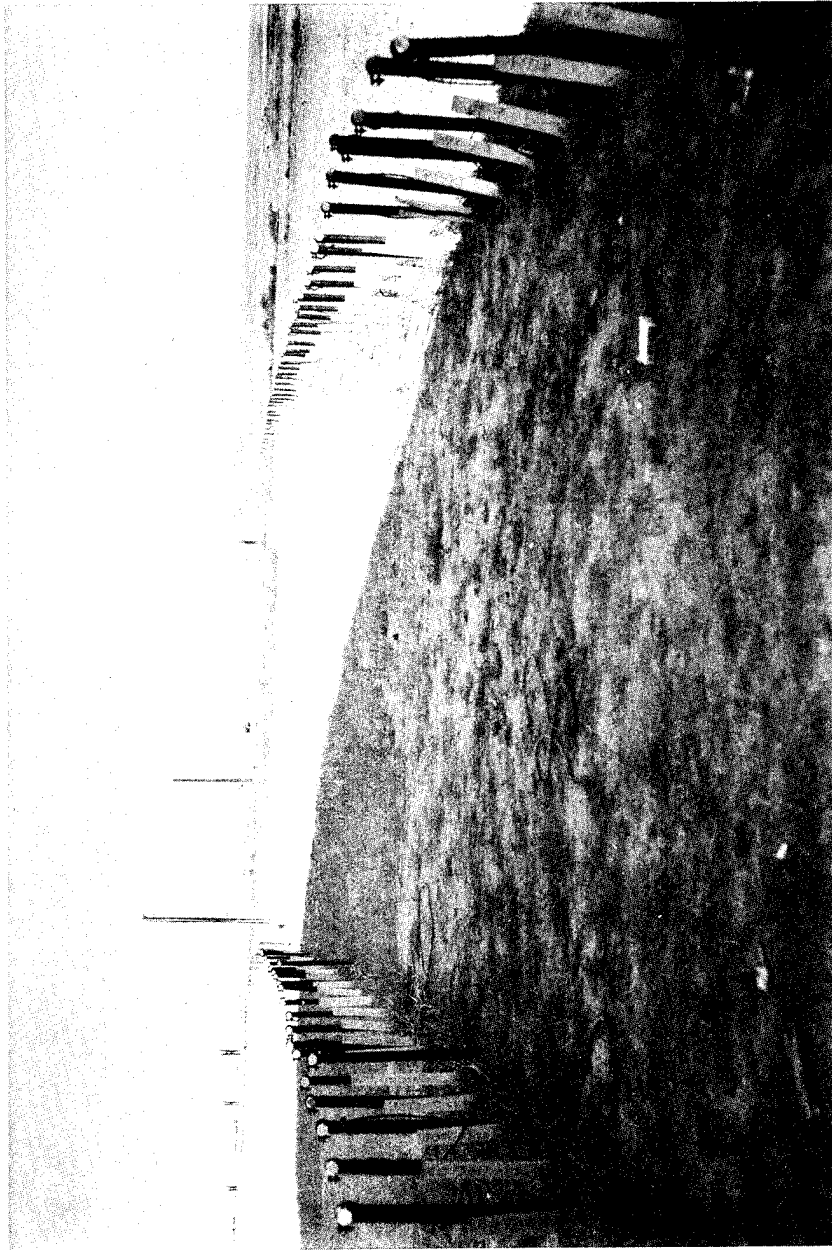


Figure 117. Airblast time-of-arrival detector lines.

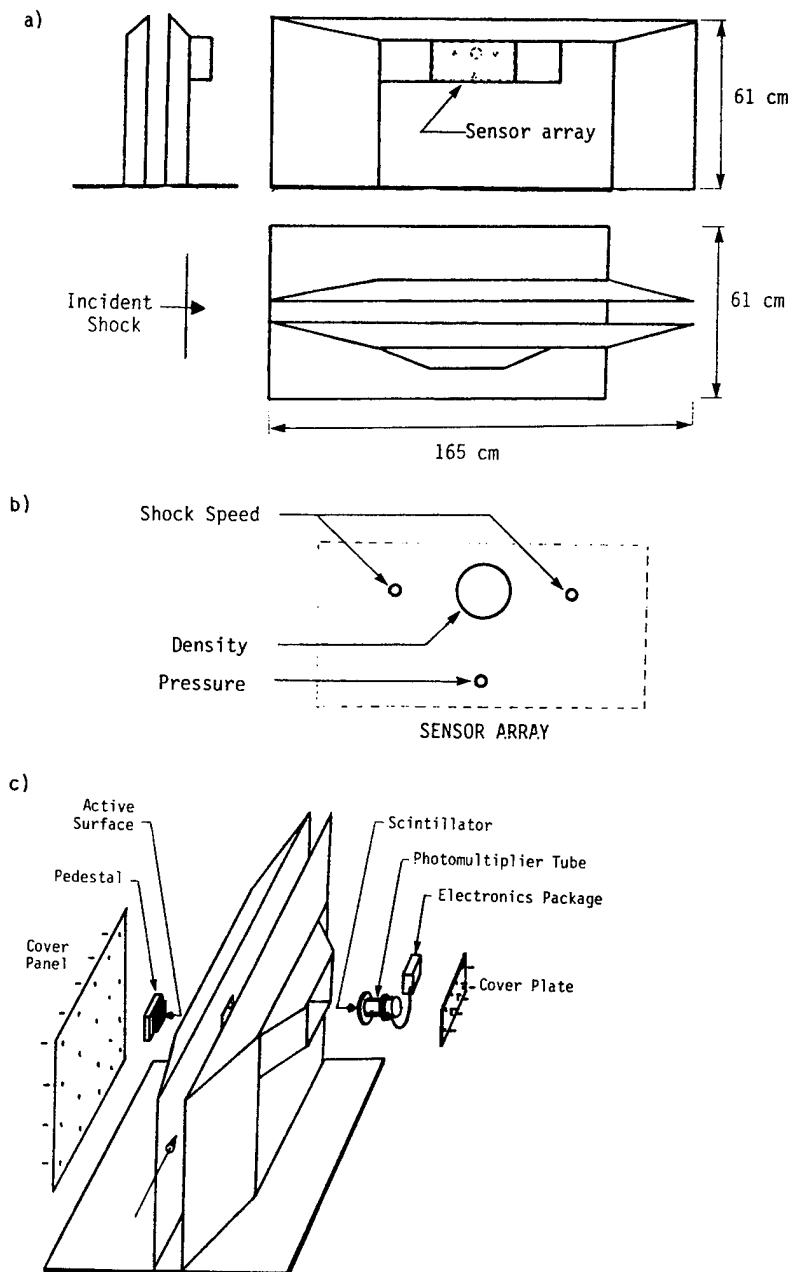


Figure 118. The original blast gage station; (a) three-view sketch, (b) sensor array, and (c) exploded view of densitometer.

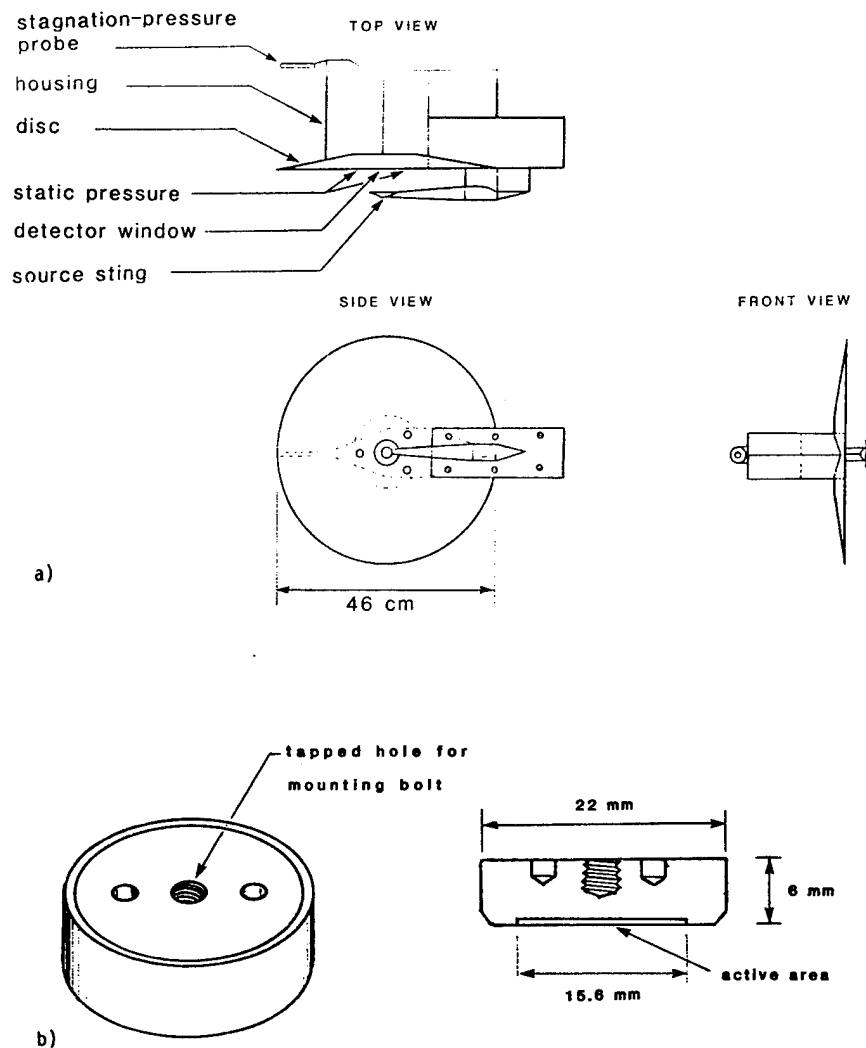


Figure 119. Sketches of (a) the current blast gage head and (b) the beta-source module (500 mCi Pm-147, PHC 80955) which is mounted in the sting.

The measuring volume of the densitometer is approximately a truncated cone with a diameter of 0.58 inches (15 mm) at the source surface, 11.8 inches (30 mm) at the detector surface, and a length of 3 inches (76 mm). The electronic package provides a linearized output.

The gage-head structure consists of a sharp-edged baffle plate of 46-cm diameter, a streamlined housing, a streamlined string to mount the beta source across from the detector, and a mounting stem. The head is inserted into a mounting stand and secured with set screws. The instrumentation housing can be unbolted for adaptation to other mounting systems. Gages mounted for field trials are shown in Figure 120.

A smaller version of the station was developed and fielded on a 1000-lb test. A schematic of this blast station is shown in Figure 121. A photograph of the station as installed in the field is shown in Figure 122. In this unit the stagnation probe was not included and only two static pressure gages were used.

Sample density records from the 1000-lb test are shown in Figure 123.

Ref: Ritzel, D.V., "The DRES Blast Gage Station," MABS-9 Proceedings, Volume I, 1985.

Reisler, R.E., et al., "Diamond Arc 87 - Blast Phenomenology Results from HOB, HE Tests with a Helium Layer," Volume I, DNA-TR-88-99-VI, 1988.

4.8.3 Hot Wire Anemometry (1981) (USA).

A constant temperature hot film anemometry technique was developed as a means of measuring flow conditions in the blast wave. This technique involves operating a small wire (film) sensor in either the constant temperature or constant current (resistance thermometer) mode. A fast response feedback bridge is used to monitor and control a thin film cylindrical sensor at a constant temperature. When the heat loss to the exposed cylindrical sensor changes because of altered local flow conditions, the output voltage from the high frequency bridge changes also. This voltage signal represents a direct measure of sensor power and hence the sensor's local flow heat rate. Final reduction of measured bridge voltages to local gas dynamic data is accomplished through use of pretest calibration results, measured pressure data, and established heat loss relationships.

Configurations for the hot wire and film probes are shown in Figure 124. Both tungsten and platinum-iridium wire material have been used with wire diameters varying from 0.15 to 0.25 mils and length to diameter ratios of 200 to 400. The probes and electronics were of commercial manufacture. Figure 125 presents a schematic of the anemometry electronics.

Figures 126 and 127 show a side view of an anemometer probe holder assembly and a rear view of sensors to sense the characteristics of the negative flow.

Survival of the probes for the duration of the blast flow is a matter of concern. In HE testing using charges of 222 pounds (101 kg), it was found that aft-facing probes protected by a shield survived overpressures as high as 110 psi, whereas forward-oriented sensors were

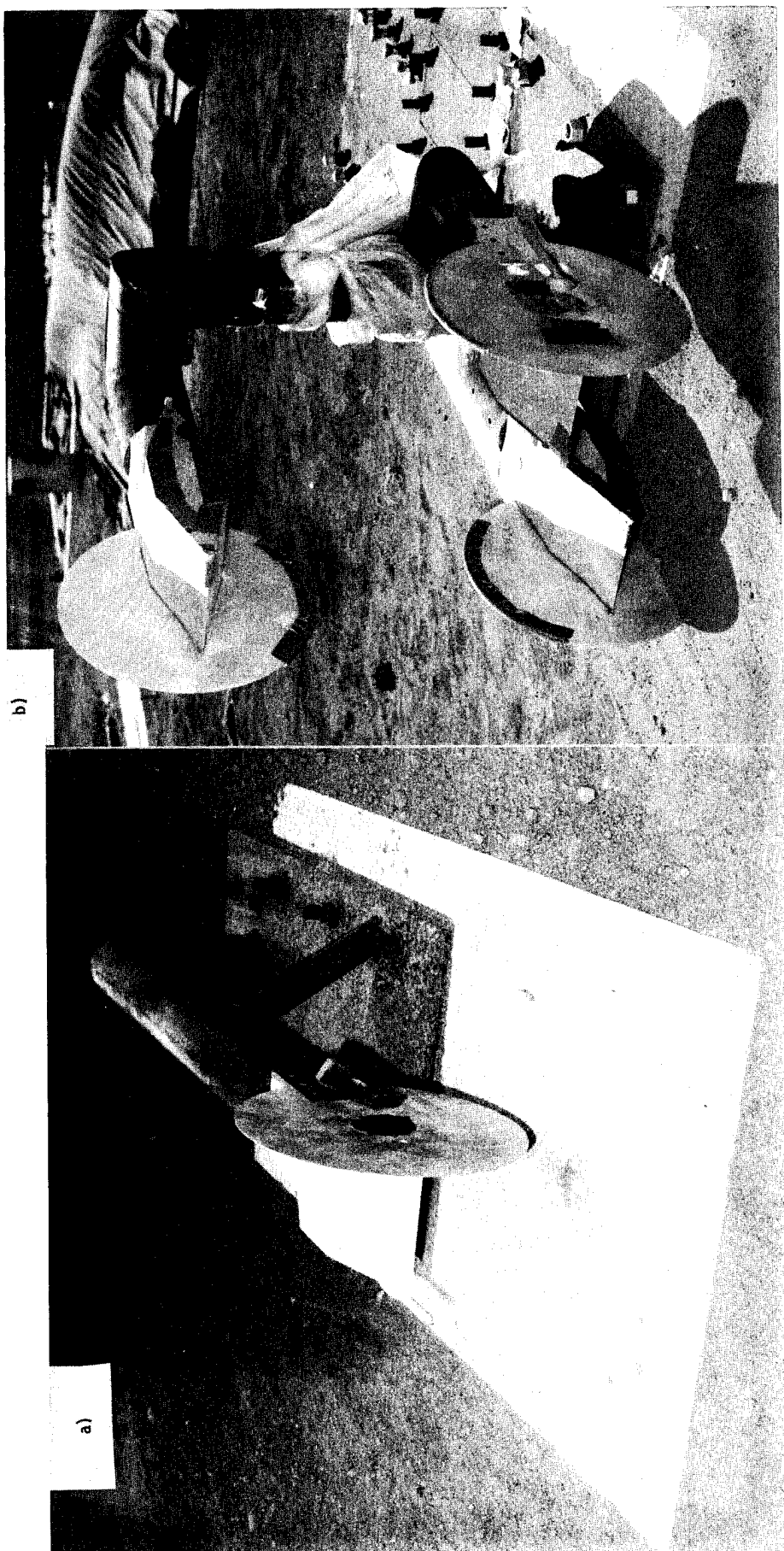


Figure 120. Stand configurations for mounting gage heads in field trials; (a) single head and (b) vertical array of three heads.

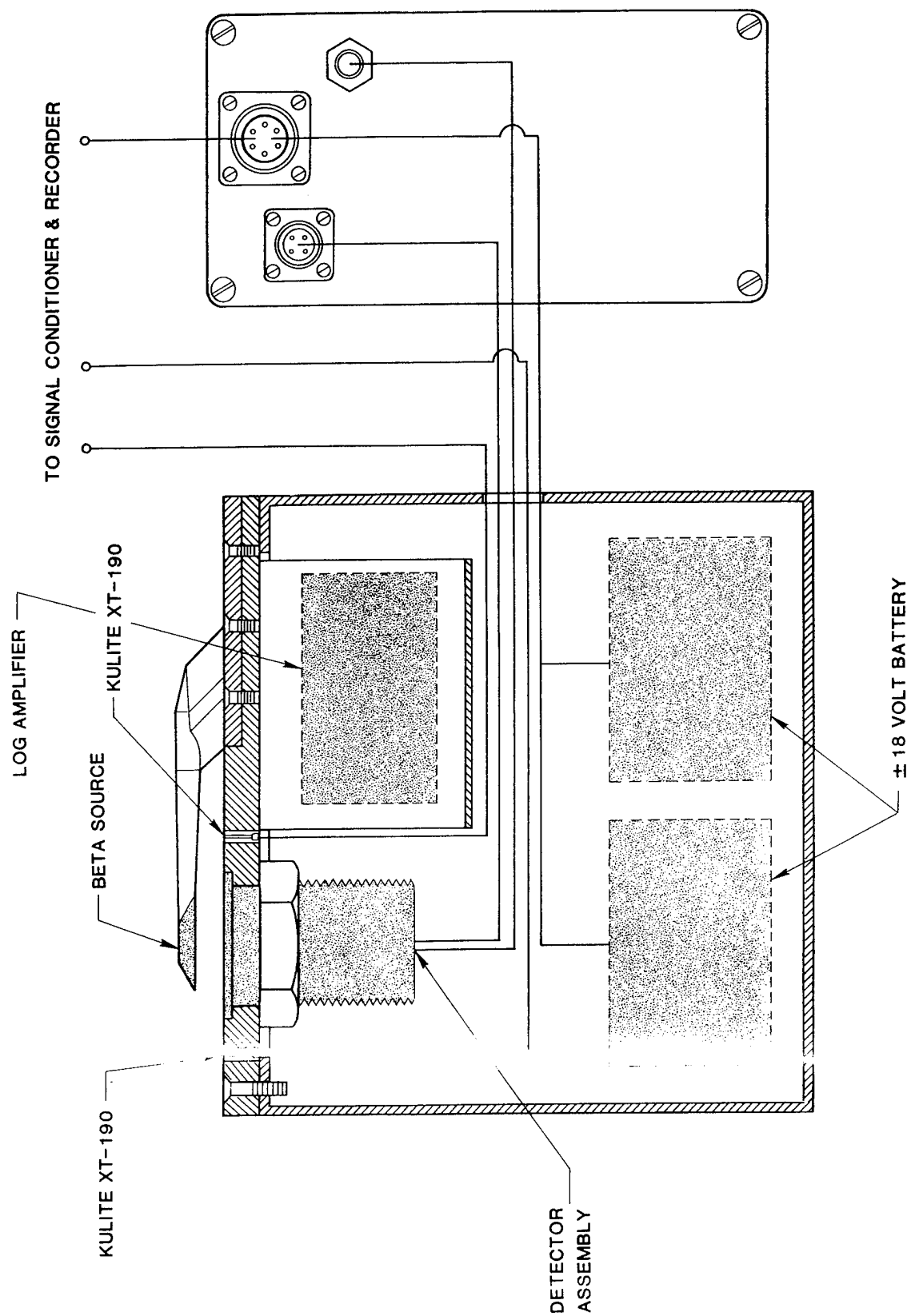


Figure 121. Schematic of density station.

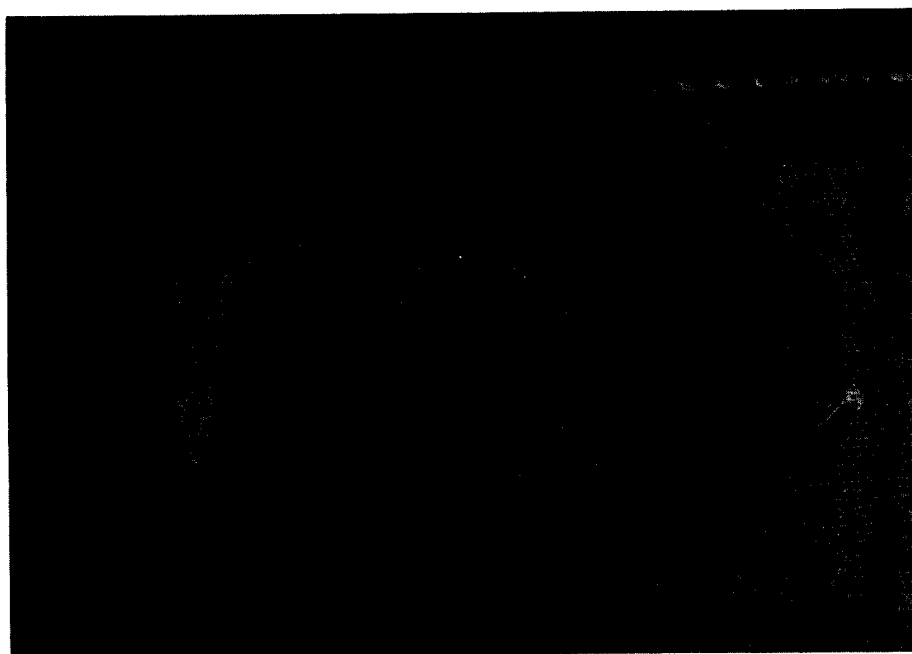


Figure 122. Density gage station in position under the Mylar membrane.

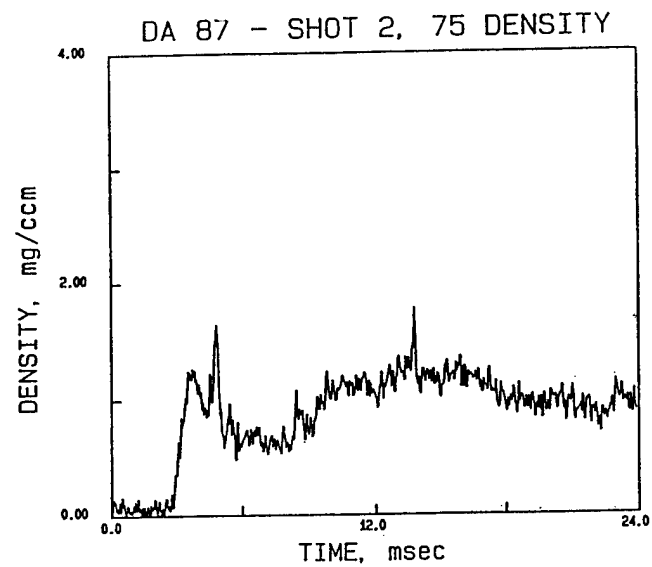
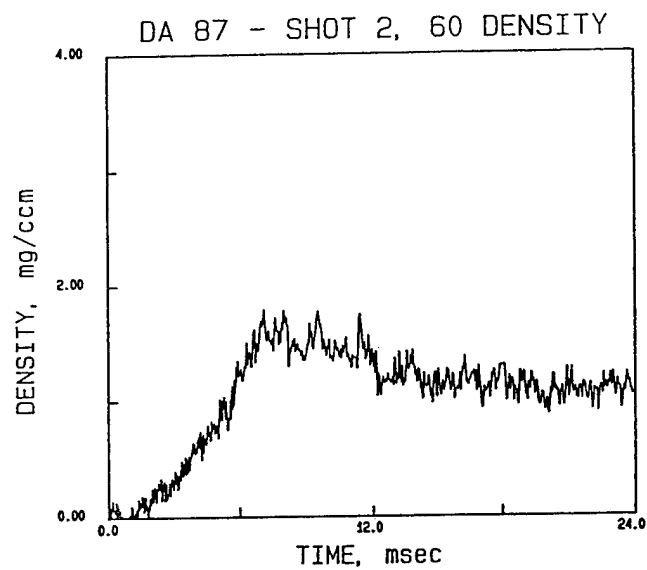
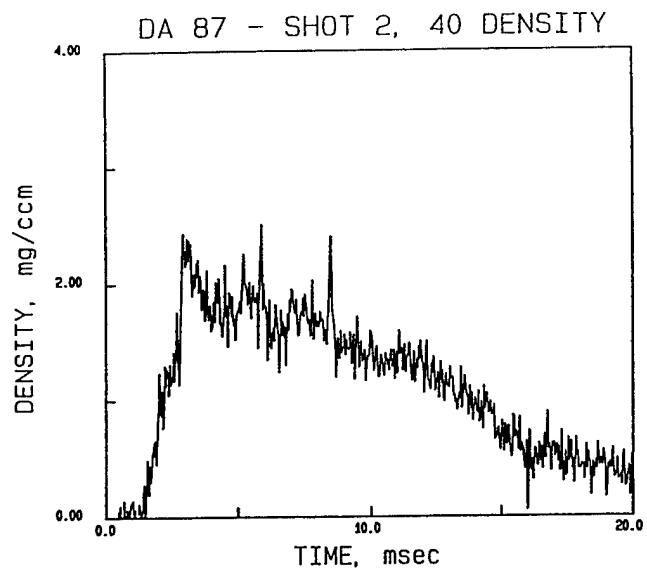
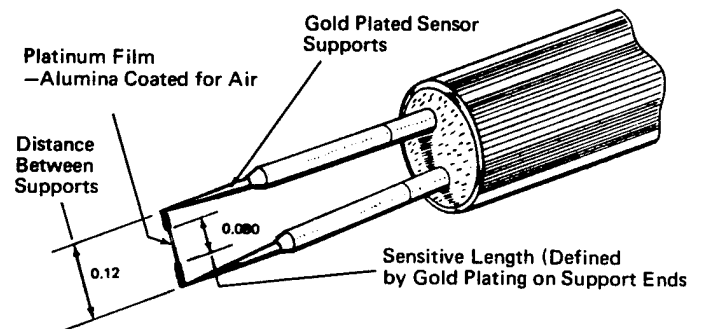
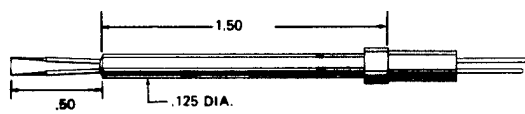
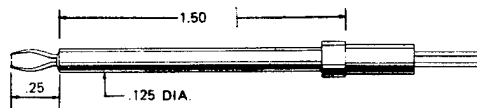


Figure 123. Densitometer records from 1000-lb HE explosion.

MODEL 1220



MODEL 1227



MODEL 1222

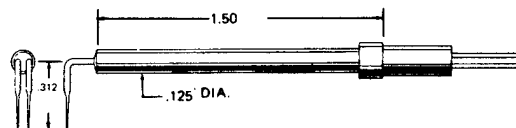


Figure 124. Probe/sensor configurations (dimensions: inches).

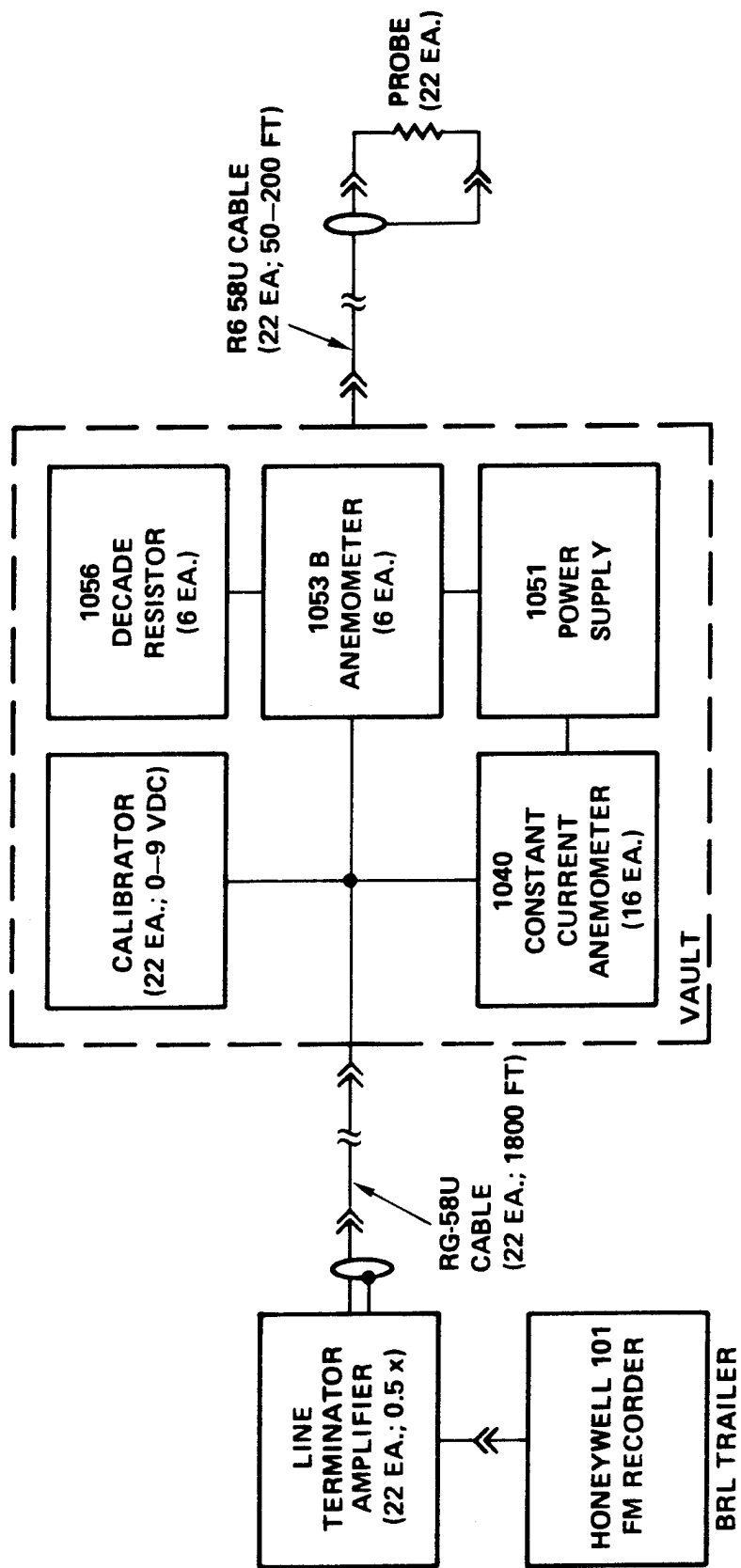


Figure 125. Schematic of anemometry systems electronics.

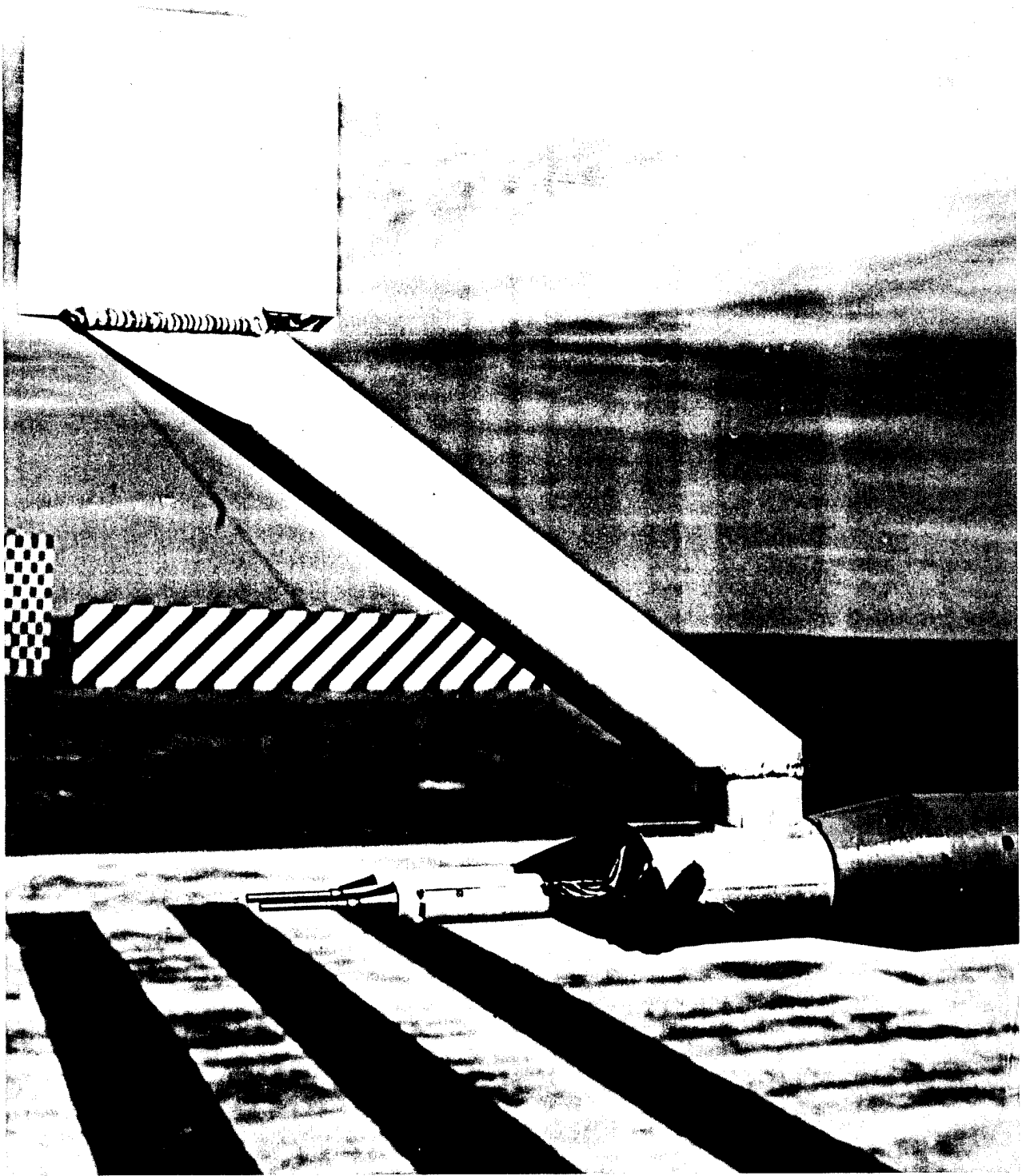


Figure 126. Closeup, side-view photograph of anemometer probe holder assembly, Station 9 ($R = 29.5$ feet).

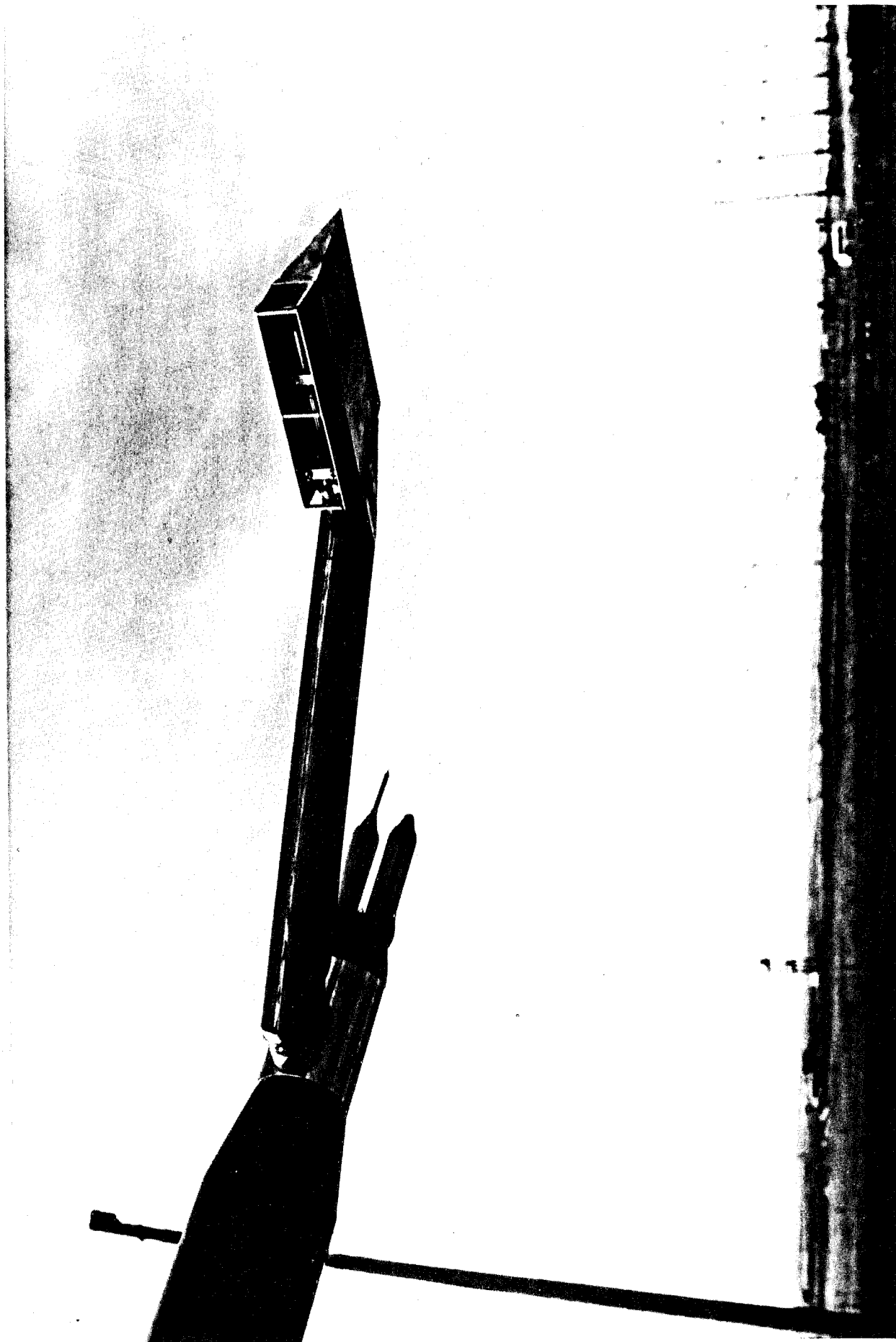


Figure 127. Rear view of anemometer probe holder assembly.

able to survive only up to 60 psi. Shown in Figure 128 are the results of anemometry measurements compared with those obtained from differential pressure gages.

The UK uses a similar hot wire anemometry technique.

Ref: Batt, R.G., "Mighty Mach IV, Low Range Dynamic Pressure Measurements Experiment," DNA-TR-84-03, 1982.

Batt, R.G., "Mighty Mach IV, Multiburst Air Density Measurement Experiment," DNA-TR-81-275, 1983.

4.8.4 Laser Velocimetry (1985) (USA).

Three types of Laser Doppler velocimeter (LDV) instrumentation have been introduced to perform velocity measurements. An external LDV system was developed to measure clean flow boundary layers, a miniaturized LDV probe was assembled to measure boundary layers for nominal dust size particles of diameters greater than 70 micrometers, and a Michelson interferometry LDV probe was established to operate with the smaller dust-size materials of the 7-micrometer range. A dual beam laser system was used to setup a fixed fringe pattern in the external LDV and the miniaturized LDV probe. Particles crossing the probe volume scatter light with a modulating frequency proportional to velocity. The Doppler shift of light which is proportional to the velocity of particles is measured directly by the Michelson interferometry LDV probe. A simple beam of laser light with a well-controlled wavelength is focussed at the measurement location. Scattered light from the particles in the control volume is transmitted via optical fibers for analysis by the Michelson interferometer. The principle of operation makes use of the detection of the interference pattern of a beam with itself after passing through unequal path lengths.

A miniature Laser Doppler Velocimeter is shown in Figure 129. An interferometric LDV probe is shown in Figure 130.

Ref: Modarress, D., et al., "Laser Doppler Velocimetry, 30 psi Location, Dusty Precursor Radial, Experiment 8703," Proceedings of the Minor Scale Symposium, POR 7158-5, 1986.

Modarress, D. and Hoeft, T., "Velocity Measurement in Dusty Flows," Final Report DNA001-85-C-0130, 1987.

4.8.5 Vortex Shedding Anemometer (1967) (USA).

The vortex-shedding anemometer was developed to measure the gas particle velocity in the flow of a blast wave. The gage consists of a cylindrical obstruction (a right circular cylinder) which functions as a vortex generator and pressure gages to sense the rate at which vortices are swept downstream with the flow.

Vortices forming as a result of a cylindrical obstruction are illustrated in Figure 131. This side-by-side configuration is unstable, and the vortices periodically separate from the obstruction and are swept downstream in the wake. The separation occurs alternately from

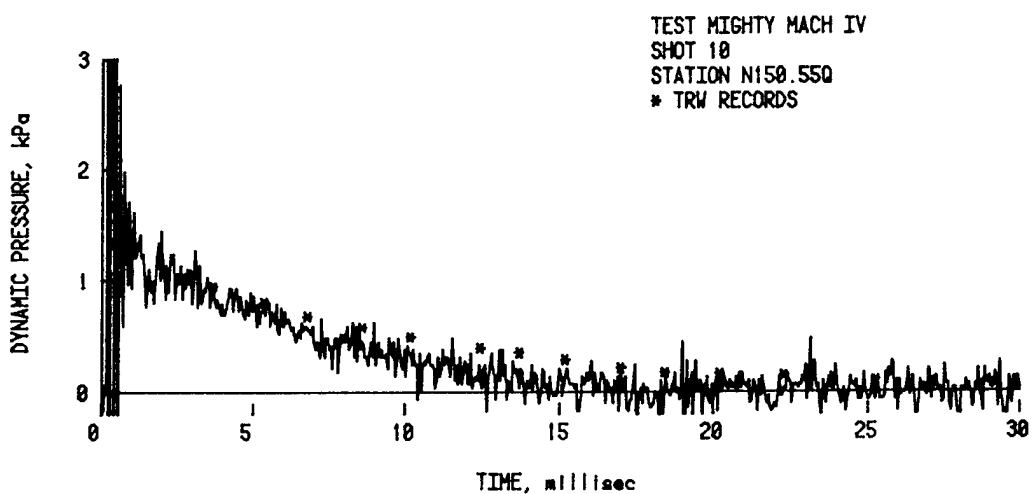
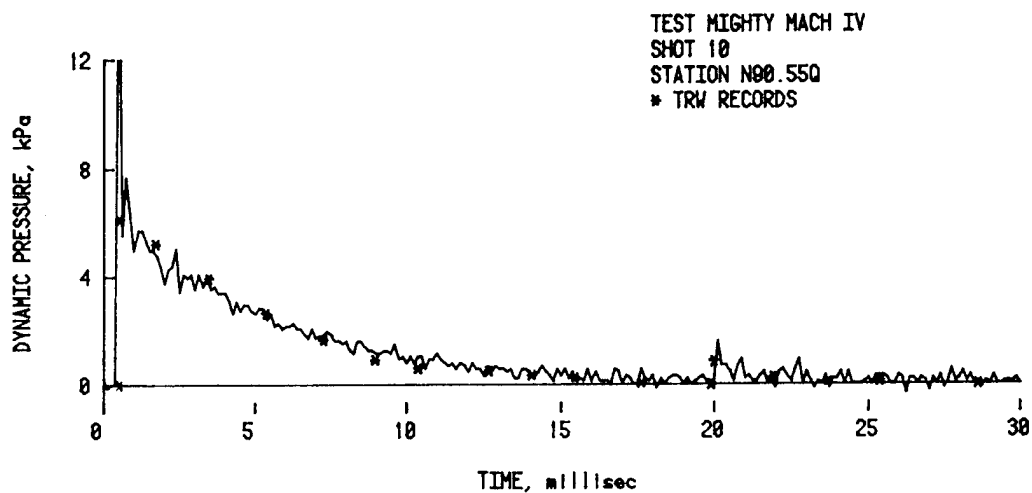
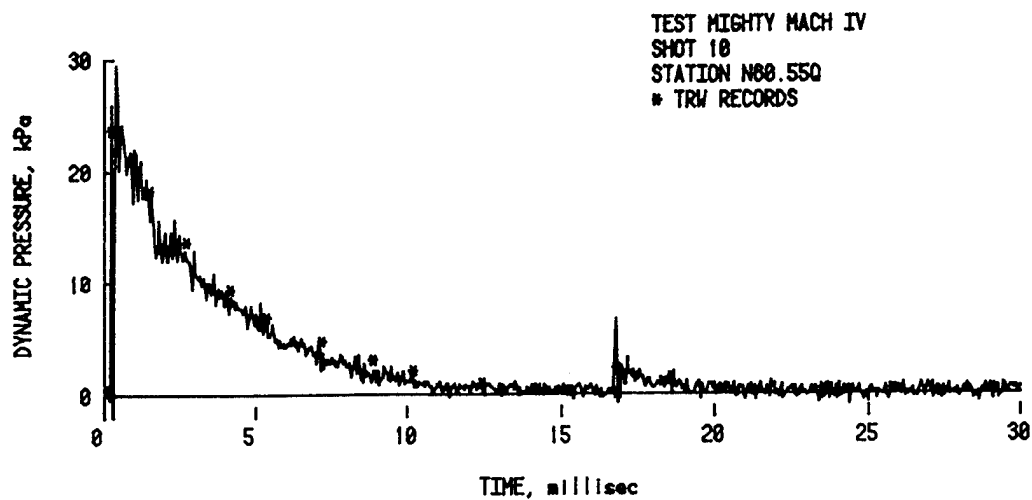


Figure 128. Comparison of dynamic pressure vs. time histories obtained from TRW anemometry measurements with those obtained from BRL differential gage measurements, Shot 10.

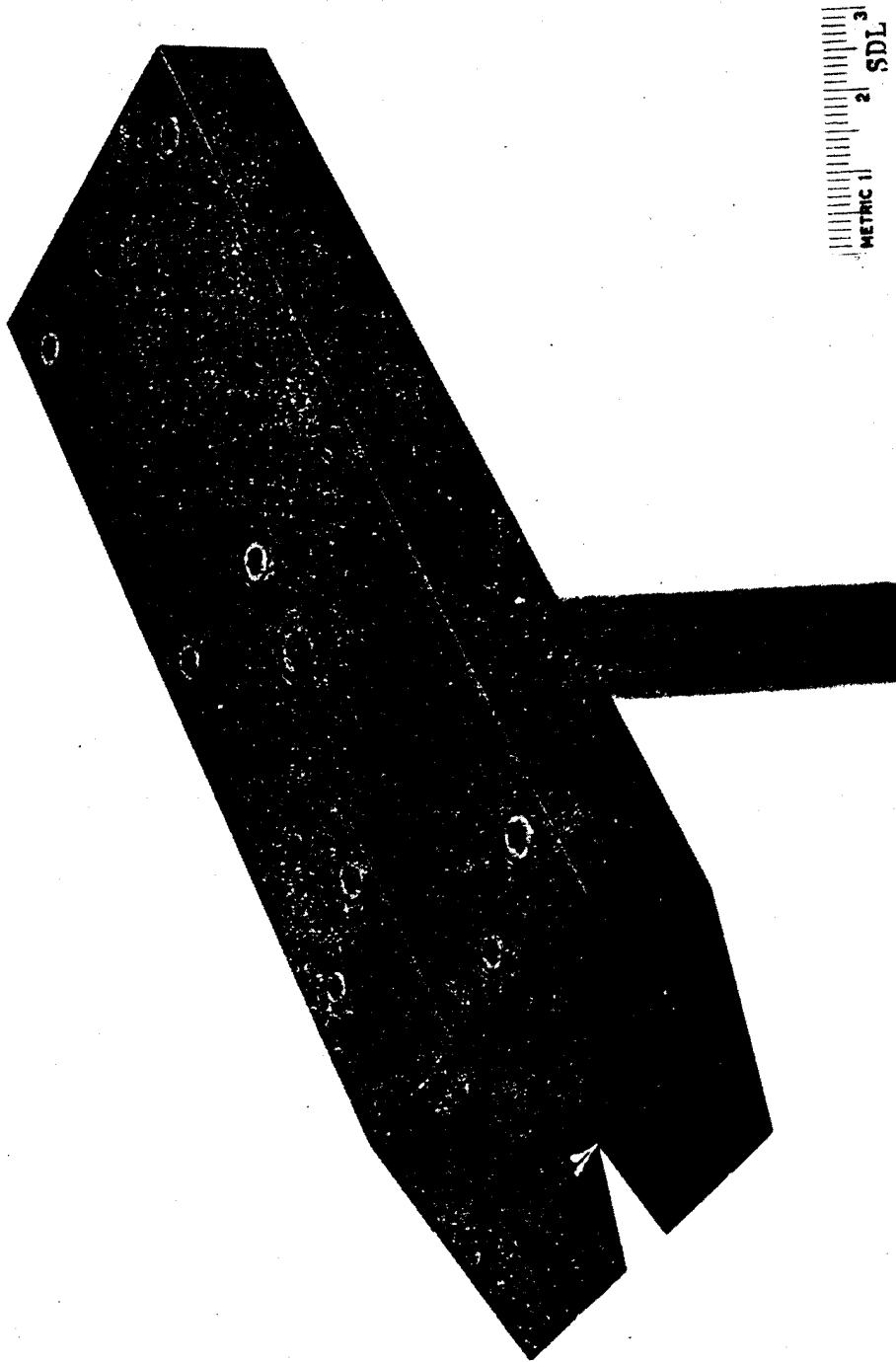
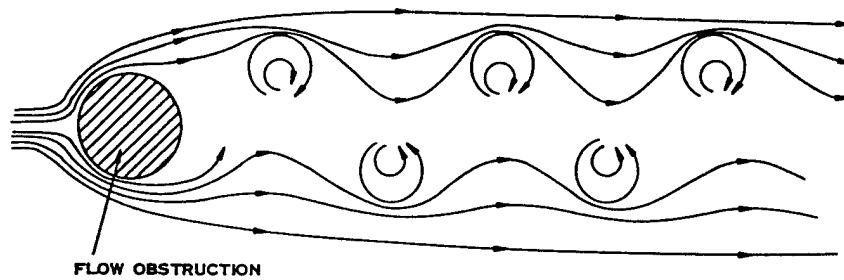


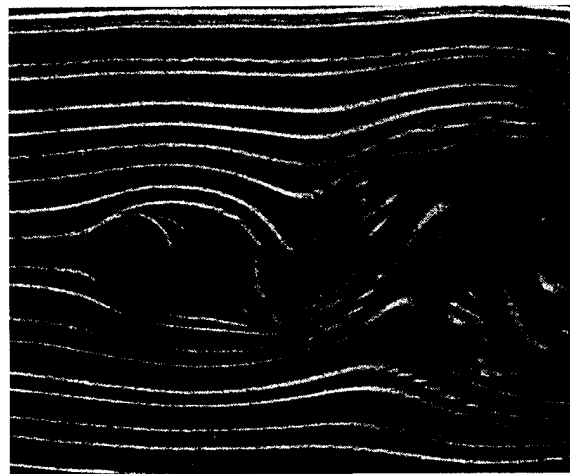
Figure 129. Miniature laser doppler velocimeter probe (SDL).



Figure 130. ISL LDV probe (SDL).



(a) Diagram of a stable vortex street.



(b) Smoke-trail photograph of fluctuating wake.

Figure 131. Flow diagram and photograph of a fluctuating wake.

one side to the other and takes place at a frequency, f_s . The frequency, f_s , is a function of the free stream velocity, u , a characteristic dimension, d , and a dimensionless quantity, S , known as the Strouhal number such that $f_s = S \cdot u/d$. The factor S is nearly a constant for a given obstruction shape over a wide range of Reynolds numbers.

Pressure gages are housed in the cylinder. Inlet ports are positioned downstream from the cylinder; one port is centered in the vortex and the second is peripherally located, see Figure 132. The diameter of the cylinder in the original model is 0.66 inches (16.9 millimeters). To gain a reasonable response time, a small obstruction size is needed since a rapid response requires a high shedding frequency. As the cylinder diameter is decreased, the magnitude of the pressure fluctuations in the vortices is also decreased which results in a loss of sensitivity at lower velocities. A calibration curve is presented in Figure 133.

Transducer and recording technology developed since the first gage was introduced in 1967 have allowed for the reduction in size of the obstructing cylinder to 0.165 inches (4.2 millimeters). Response times were improved from 1 millisecond to 200 microseconds. Subminiature transducers, Kulite model XCQ-062, were used in the model introduced in 1983. A geometrical layout of this gage is shown in Figure 134 where it has been labelled as a high speed vortex-shedding anemometer (VSA). A field installation of a three-position VSA is shown in Figure 135.

Ref: Sachs, D.C., "Field Test Particle Velocity Gage," Operation Distant Plain Symposium, Volume II, M.J. Dudash, Editor, DASA-2207, 1968.

Roark, Glenn and Cole, Eldine, "Gas Particle Velocity Measurement," Kaman Sciences Corporation Report K84-600(R), 1984.

4.8.6 "Free-Flight" Cylinders (1986) (Canada).

"Free-Flight" cylinders were used as a means to measure the drag forces of the blast wave on cylindrical naval mast members. The cylinders were constructed of steel or aluminum and were 4 inches in diameter and 5 feet long. They were supported horizontally on knife edges or suspended perpendicular to the flow. The ends of the cylinder had slender rods attached which extended toward ground zero, see Figure 136. The ends of each rod held a small magnet which rested inside a long tube wound with a coil of copper wire. When the cylinder was blow off its stand, the magnet-tipped rods were withdrawn along the length of their coil tubes. An electrical signal was generated which gave an indication of the initial acceleration and velocity of the magnets and of the free-flight cylinder. The distance traveled by the cylinder was measured with the aid of a pre-installed scale on the mount. A high-speed camera was also used to monitor the cylinder. The data acquired was typically reduced to a drag pressure-impulse profile.

It was reported that this method of drag measurement was considered to be quite effective.

Ref: Mellsen, S.B., "Drag Measurements on Cylinders by Free Flight Method - Operation Prairie Flat," DRES-TN-249, 1969.

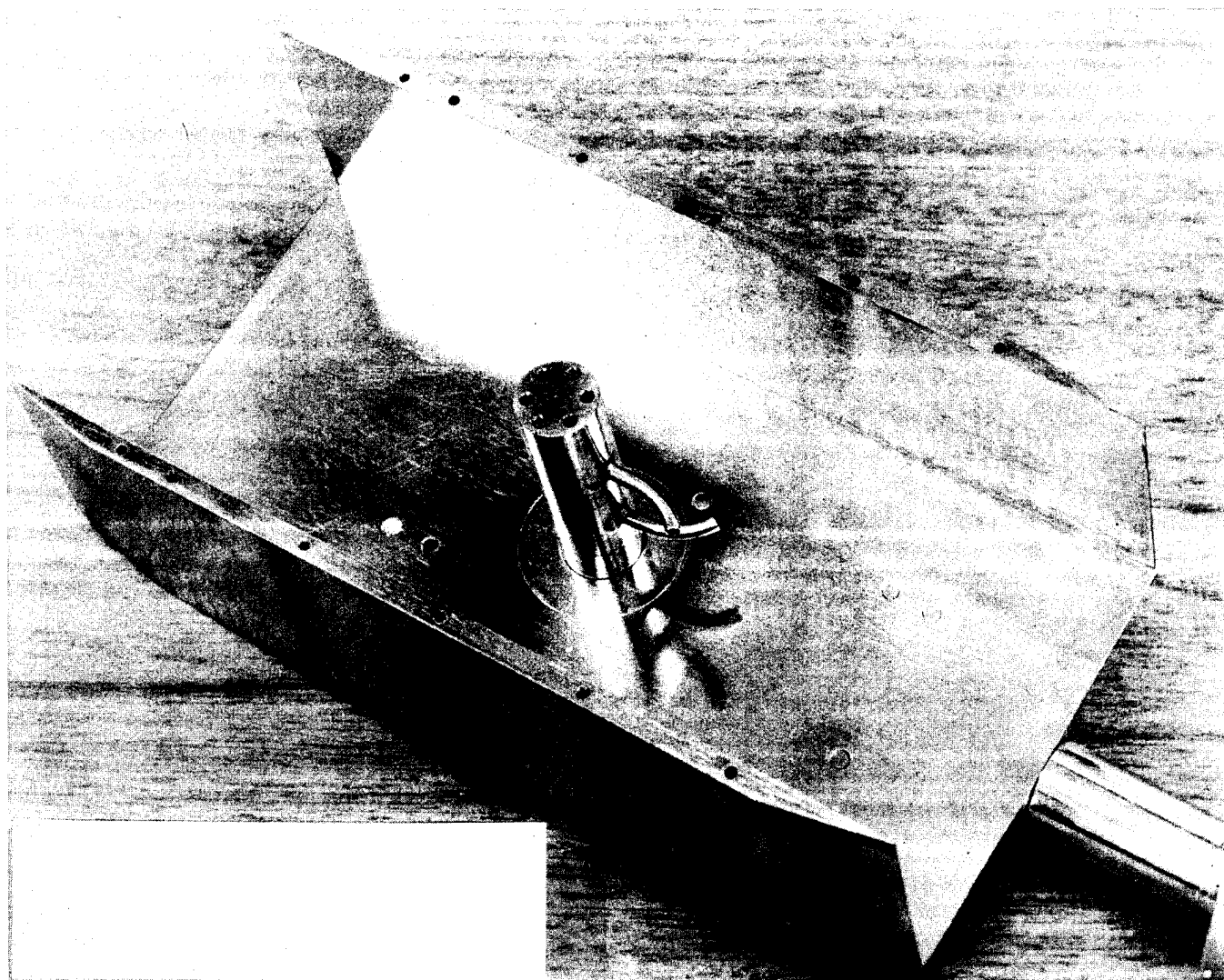


Figure 132. Vortex-shedding anemometer (top plate removed to expose 16.9 m obstruction).

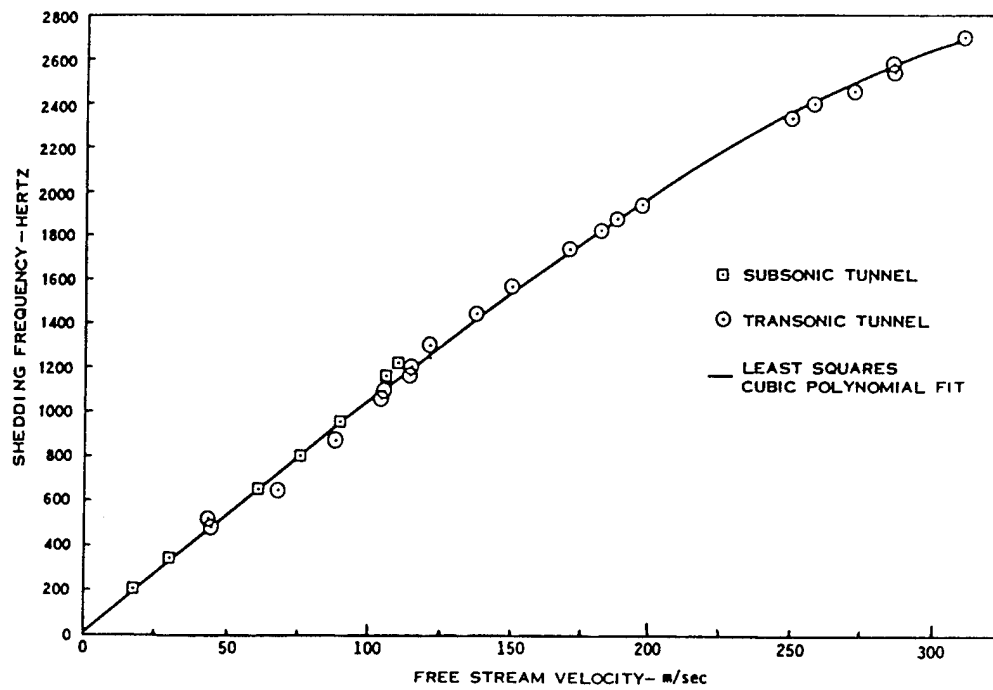


Figure 133. Calibration of the vortex-shedding anemometer (16.9 mm obstruction).

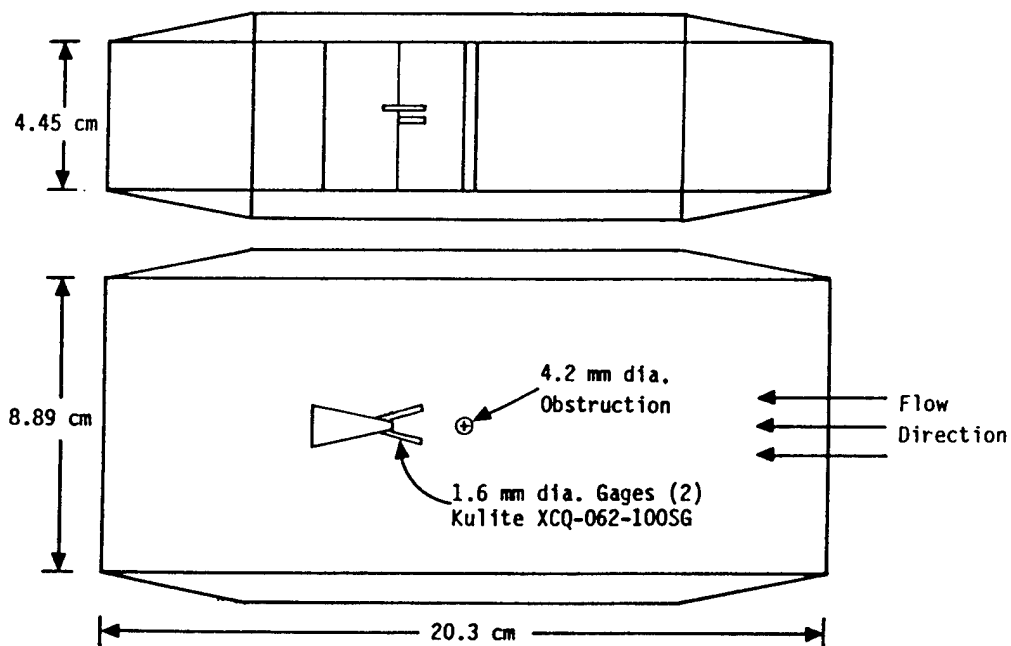


Figure 134. Geometrical layout of high-speed VSA.



Figure 135. Field installation of three-channel vortex-shedding anemometer.

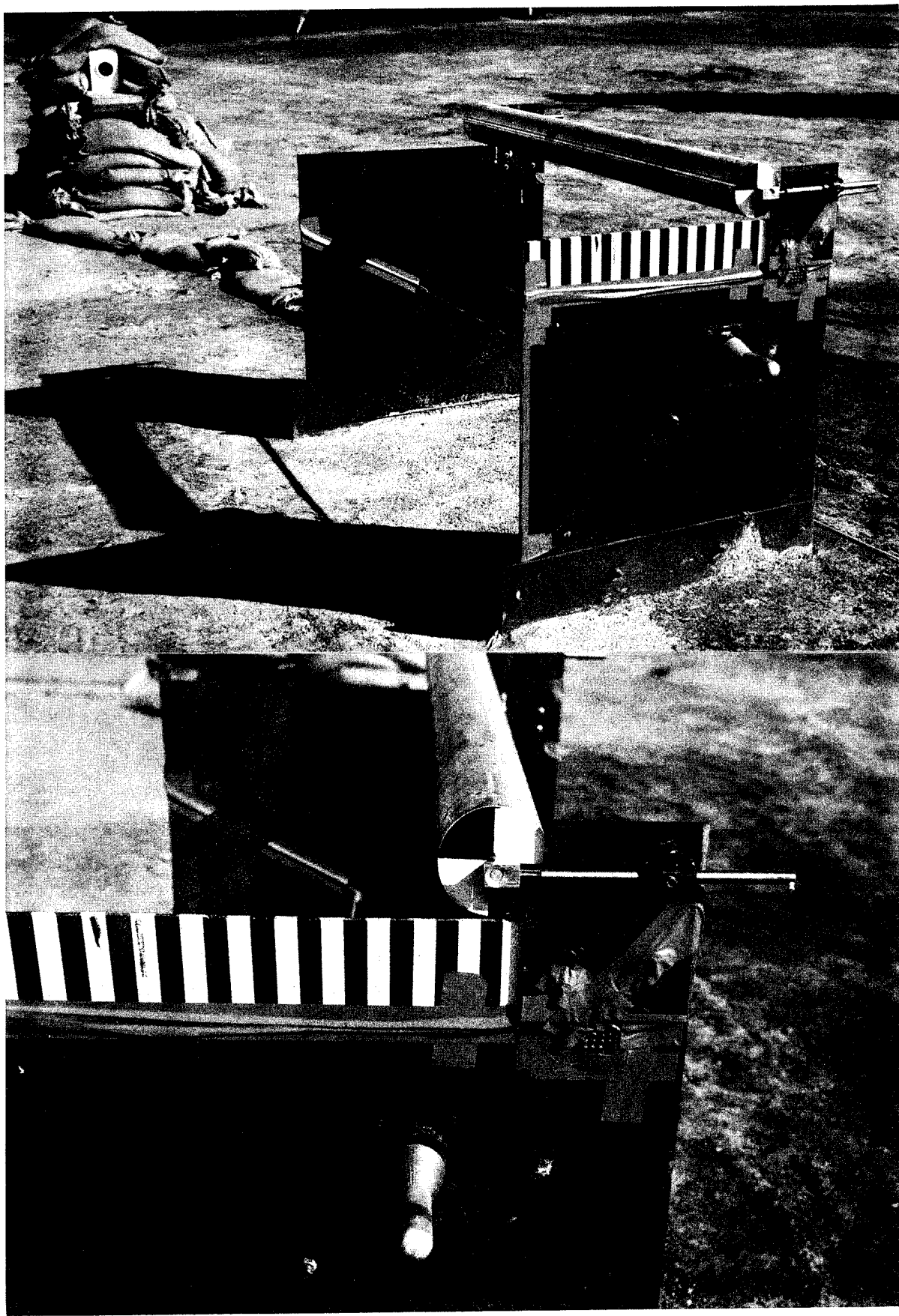


Figure 136. Pre-shot views of the free-flight cylinder project.

4.8.7 Lovelace Free-Flight Drag Spheres (1964) (USA).

The Lovelace free-flight drag sphere concept was first introduced in 1955 during nuclear testing. Those tests provided the background for the instrument system deployed on large scale HE testing which is described here.

The free-flight concept was to determine the velocities of missiles picked up by the blast wave by trapping the actual missiles in layers of expanded styrofoam and measuring their masses and depth of penetration. Calibration experiments would determine the depth of penetration for a given missile imparted with a known velocity. The missiles studied in the nuclear tests were natural stones, steel fragments, painted gravel, and spheres of various sizes and materials.

Free-flight drag spheres were used as a means to determine blast-induced velocities at approximate values. Using these velocities, an estimation of the maximum wind speed and dynamic pressure impulse could be made.

Steel spheres of the various sizes were located at the noted heights in Table 19, 4 feet upstream from the styrofoam. Only three sizes were used at any one installation. Installations were made at overpressure levels of 10, 15, and 30 psi. A different density styrofoam was used at each level. Two pieces of styrofoam (1 ft x 3 ft x 2 inches) were used for each installation where the styrofoam was cemented to a 3/4 inch plywood nailed in a vertical position to a piling installed in concrete. Shown in Figure 137 is a typical installation. The steel spheres were placed with their centers two diameters apart in shallow holes drilled in the steel supporting bars. Each row of spheres extended 2 inches beyond the edges of the styrofoam to allow for non-radial winds or inaccuracies in placement of the mounts.

Table 19. Free flight drag sphere locations.

<u>Sphere Diameter</u> (inches)	<u>Sphere Height Above Ground</u> (feet)
1/2	2.8
1/8	1.8
3/8	0.8
9/16	2.8
1/4	1.8
7/16	0.8

In calibrating the system, the desired velocities were achieved by dropping the sphere from heights between 15.48 and 74.51 feet and computing the impact velocity. A few spheres were dropped at angles of 10, 20, and 30 degrees and it was determined that the change in depth of penetration was negligible up to 20 degrees.

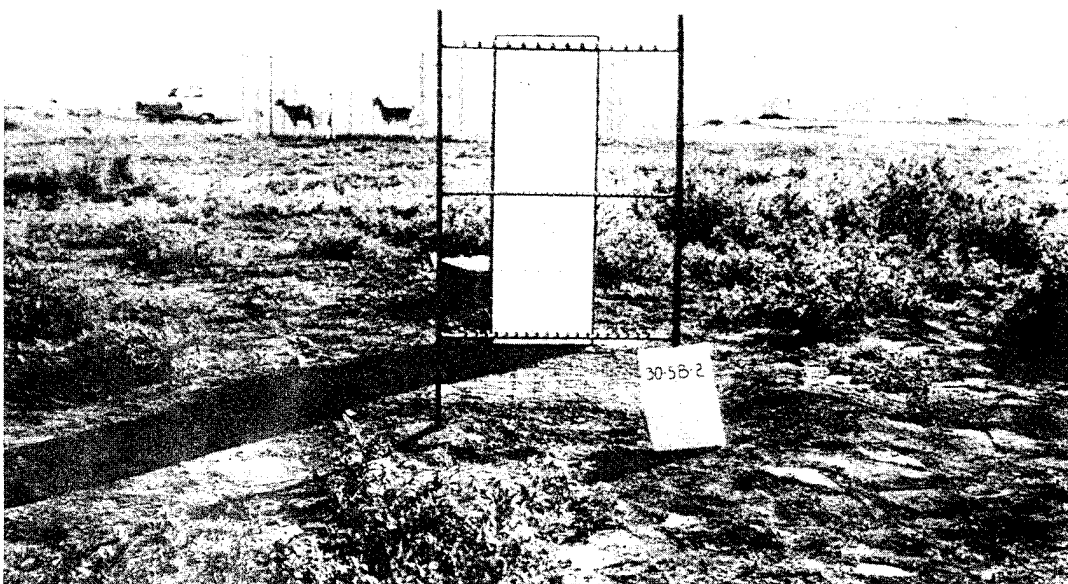


Figure 137. Pre-shot picture looking away from ground zero of steel sphere installation 30SB2.

It was reported that this technique of trapping spheres in styrofoam is a convenient method of estimating both the velocity a missile would acquire after a known displacement, peak wind velocity, and dynamic pressure impulse. Estimated values resulting from the measurements are within 10-30 percent of the theoretical values in all cases.

Ref: Fletcher, E.R., et al., "Impact Velocities of Steel Spheres Translated by Air Blast," Operation Snow Ball Symposium Proceedings, Volume 1, DASA 1642-1, 1965.

Bowen, I.G., et al., "Distribution and Density of Missiles from Nuclear Explosions," USAEC Civil Effects Test Group, WT-1168, Department of Commerce, 1956.

4.9 ELECTRONIC RECORDING.

4.9.1 Oscilloscope.

4.9.1.1 Raster Oscilloscope and Camera System (1970) (USA). The Raster Oscilloscope and Camera System was introduced to measure high frequency blast waves. A high speed 35-mm camera photographs the record trace as it crosses the face of a high frequency oscilloscope. Because of the high speed of the camera, recording time is very limited; it was necessary for the experimenter to predict the time of arrival of the shock fairly accurately to capture the pressure record. Shown in Figure 138 is a trailer-equipped bank of raster scopes ready to record the output of 500 kHz pressure transducers.

4.9.1.2 Miller Cathode-Ray-Tube Oscillograph (1960) (USA). The Miller Oscillographic Recorder is a 100 kHz recording unit manufactured by the William Miller Instruments Company. Gage signals are fed to a 16 channel direct-coupled amplifier system and then to the deflection plates of a cathode ray tube.

The frequency response of the DC amplifier was flat within 3 percent from DC to 50 kHz, within 10 percent to 100 kHz, and within 25 percent to 150 kHz. The recorder has provision for balancing, focusing, and adjusting the sensitivity of each channel separately.

The deflections are photographed by optically focusing the 16 traces on photographic paper moving at 200 inches per second. Timing is provided by an internal frequency standard which provides millisecond markers on the edge of the photographic record.

A photograph of the system is shown in Figure 139.

Ref: Armendt, B.F., et al., "Project White Tribe: Air Blast From Simultaneously Detonated Large Scale Explosive Charges," BRL Report No. 1145, 1961.

4.9.2 Magnetic Tape.

4.9.2.1 General Systems (1960) (All). Since the mid-forties, magnetic tape recording has advanced from a technique suitable only for audio work to a very high quality method for recording signals from scientific instruments. Most instrumentation recorders were designed with multiple channels on one tape, typically 7, 14, or 28/32 using 1/2 inch or 1 inch wide



Figure 138. Trailer equipped with raster oscilloscope and camera system.

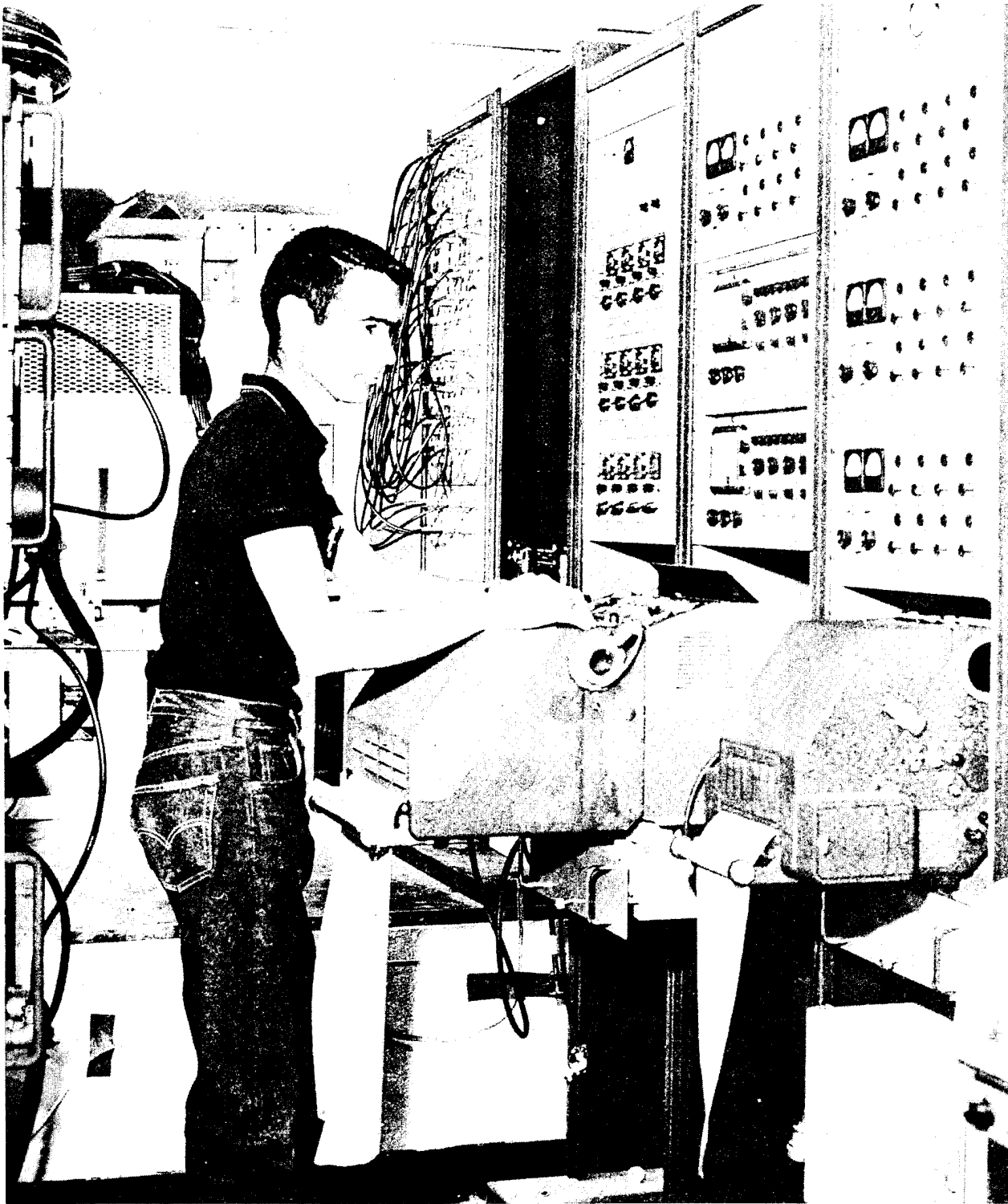


Figure 139. WSMR multi-channel magnetic oscillographs mounted in recording trailer.

tape. Recording of major data was done in the FM mode. Early recorders had a frequency response of 10 kHz, later extended to 60 and 80 kHz and still later to 500 kHz.

A magnetic tape instrumentation recorder includes three basic components. The magnetic head records information on the tape and recovers it from the tape. The tape transport moves the tape across the magnetic heads smoothly and at a constant speed. The record and reproduce amplifiers process the input signals going to record heads, and the output signals coming from the playback or reproduce heads.

A major advantage of tape recorders is that records may be played back at speeds different from those at which records were made. Thus, the time base can be expanded or compressed according to the experimenter's wishes.

Typical name plates on recorders of this size in the sixties were the Consolidated Electrodynamics Corporation (CEC) [subsequently Bell and Howell]. VR-3300, shown in Figure 140, and VR-3800 machines operated in the FM mode at 20 kHz.

In the seventies, the Sangamo Model 4784 found considerable use together with the Honeywell 7600, shown in Figure 141. These machines provided for a 70 kHz frequency response. The Honeywell 101 gradually replaced all previous machines in the late seventies with options for recording, the most widely used being the wide-band II, FM capability with a response of 500 kHz. A trailer equipped recording facility with the 101 is shown in Figure 142. The 101 continues to be used today for many applications.

The EMI SE 7000 was a name plate on a popular recorder used in Europe and particularly Great Britain. It is manufactured by the SE Labs (EMI), Ltd., of Feltham, Middlesex, England. This machine is shown in Figure 143, and was operable in either a horizontal or vertical position. It had a capability for several options in recording, the most widely used being the FM capability with wideband II up to 500 kHz.

Ref: Magnetic Recording Equipment, SE Labs (EMI), Ltd., Feltham, Middlesex, England, 70's.

Reisler, Ralph E., et al., "Air Blast Measurements from the Detonation of Large Spherical TNT Charges Resting on the Surface (Operation Distant Plain, Events 6A and 6)," BRL Memorandum Report No. 1955, 1969.

Reisler, Ralph E. and Pettit, Burnett A., "Project Dipole West - Multi Burst Environment (Non-Simultaneous Detonations)," BRL Report No. 1921, 1976.

Reisler, Ralph E., et al., "Blast Loading of Model MX Horizontal Structures in the Irregular Mach Reflection Zone," Technical Report ARBRL-TR-02447, 1982.

4.9.2.2 Leach Tape Recorder (1960) (USA). The Leach tape recorder is a ruggedized, water-proof, shock-mounted data acquisition system. It was designed for use close-in on blast tests where the ground shock is less than 100 g's at the recorder. Installation of the recording capsule which is a cylinder 6-1/2 feet long by 10 inches in diameter is done by placing it into an augured hole in the earth and connecting the transducer and control

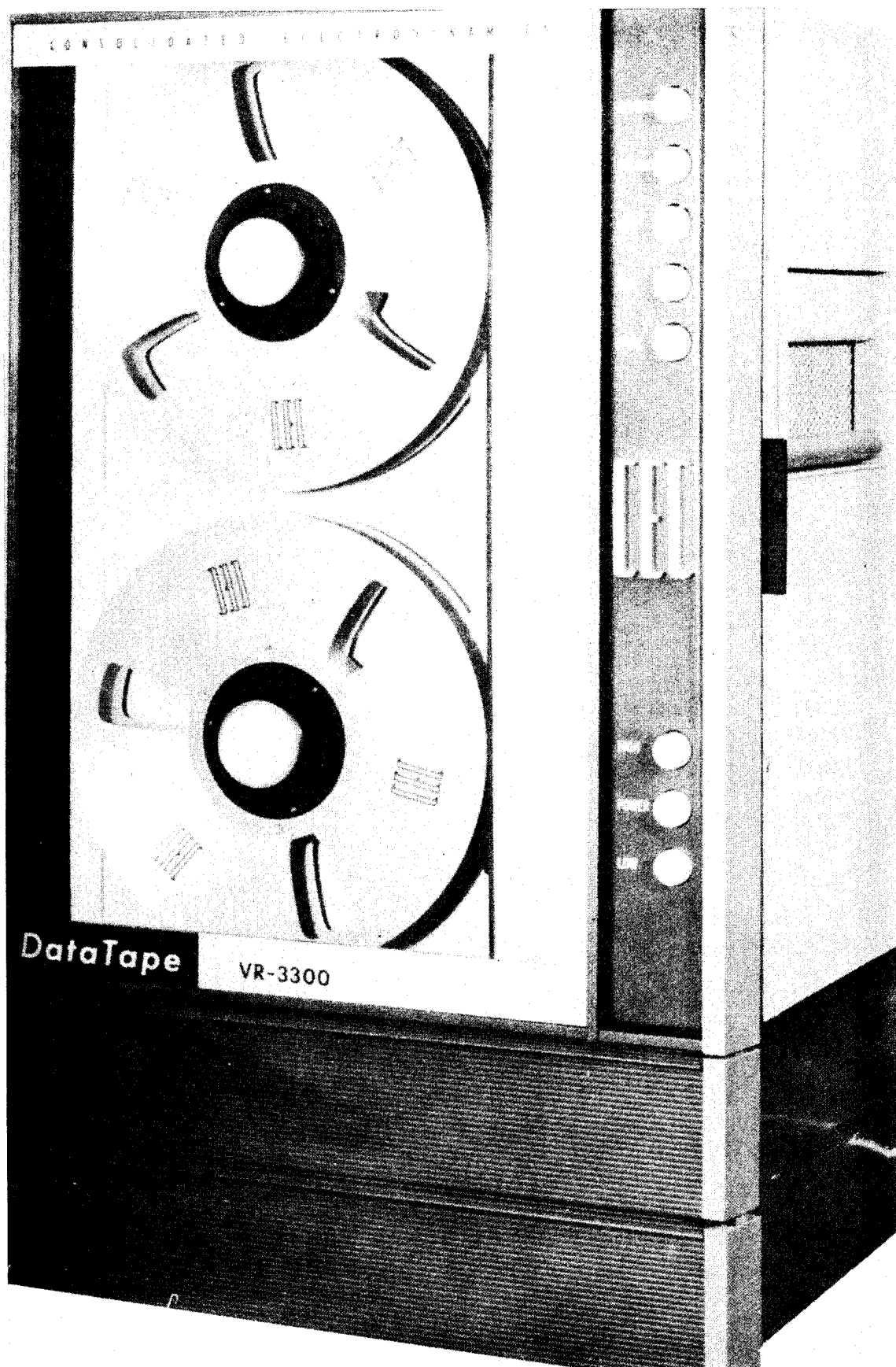


Figure 140. CEC VR-3300 tape recorder.

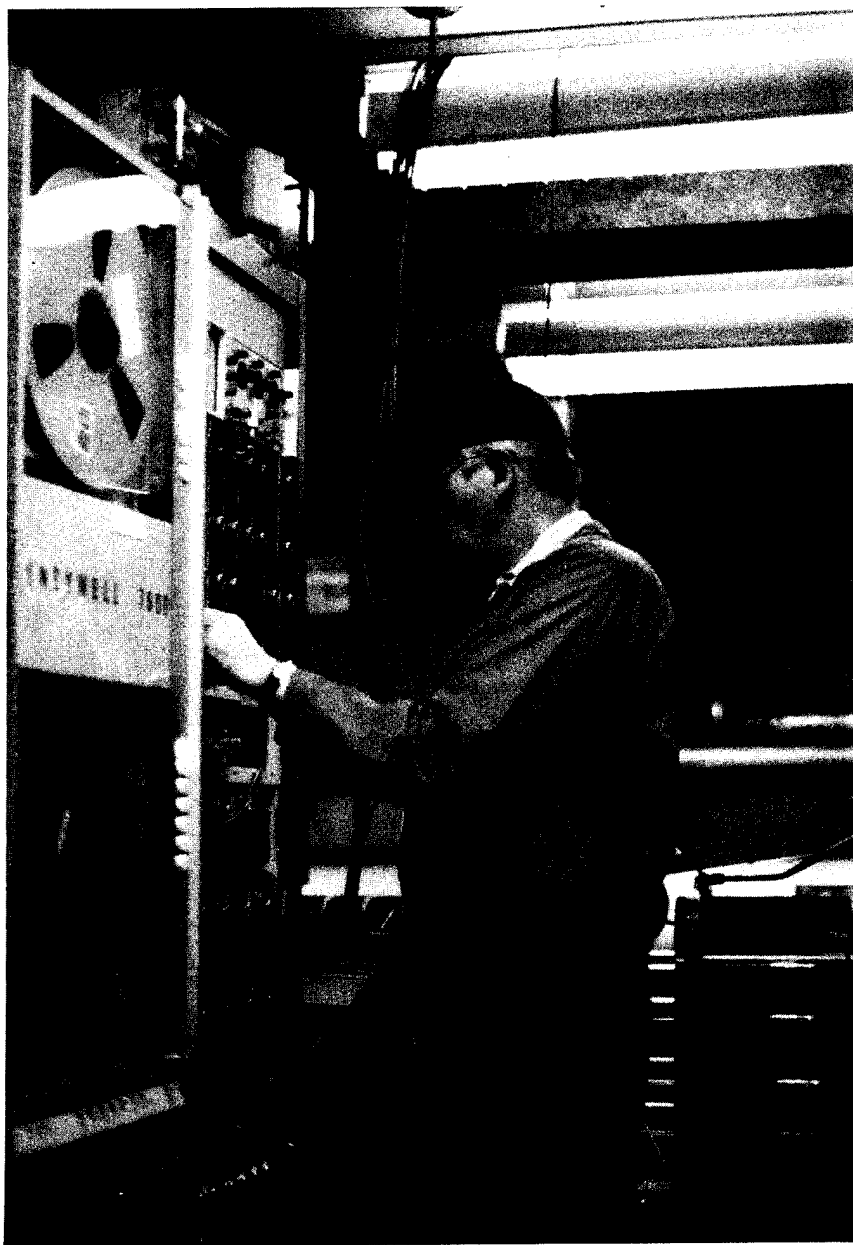


Figure 141. Honeywell 7600 tape recorder.

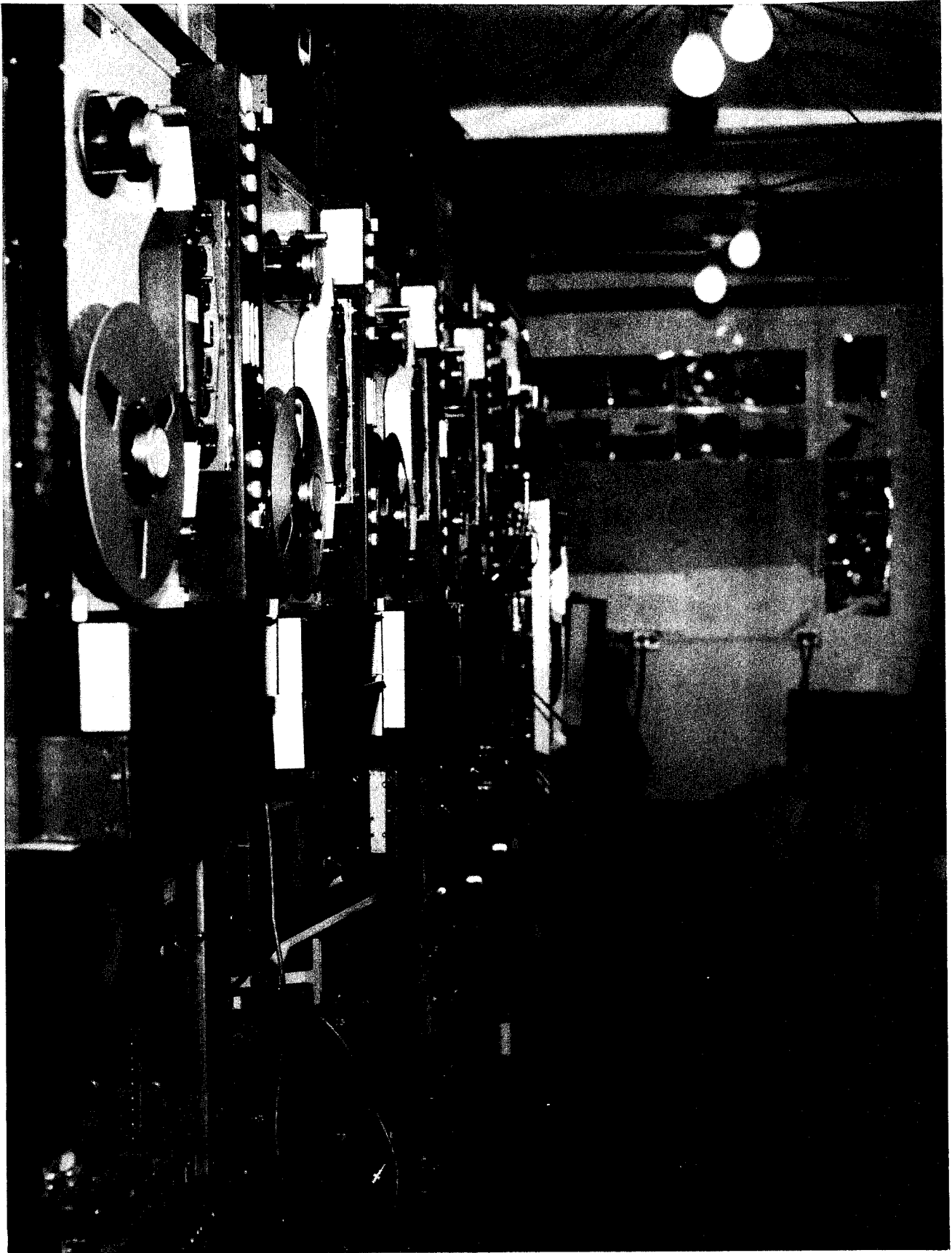


Figure 142. Honeywell 101 tape recording van.

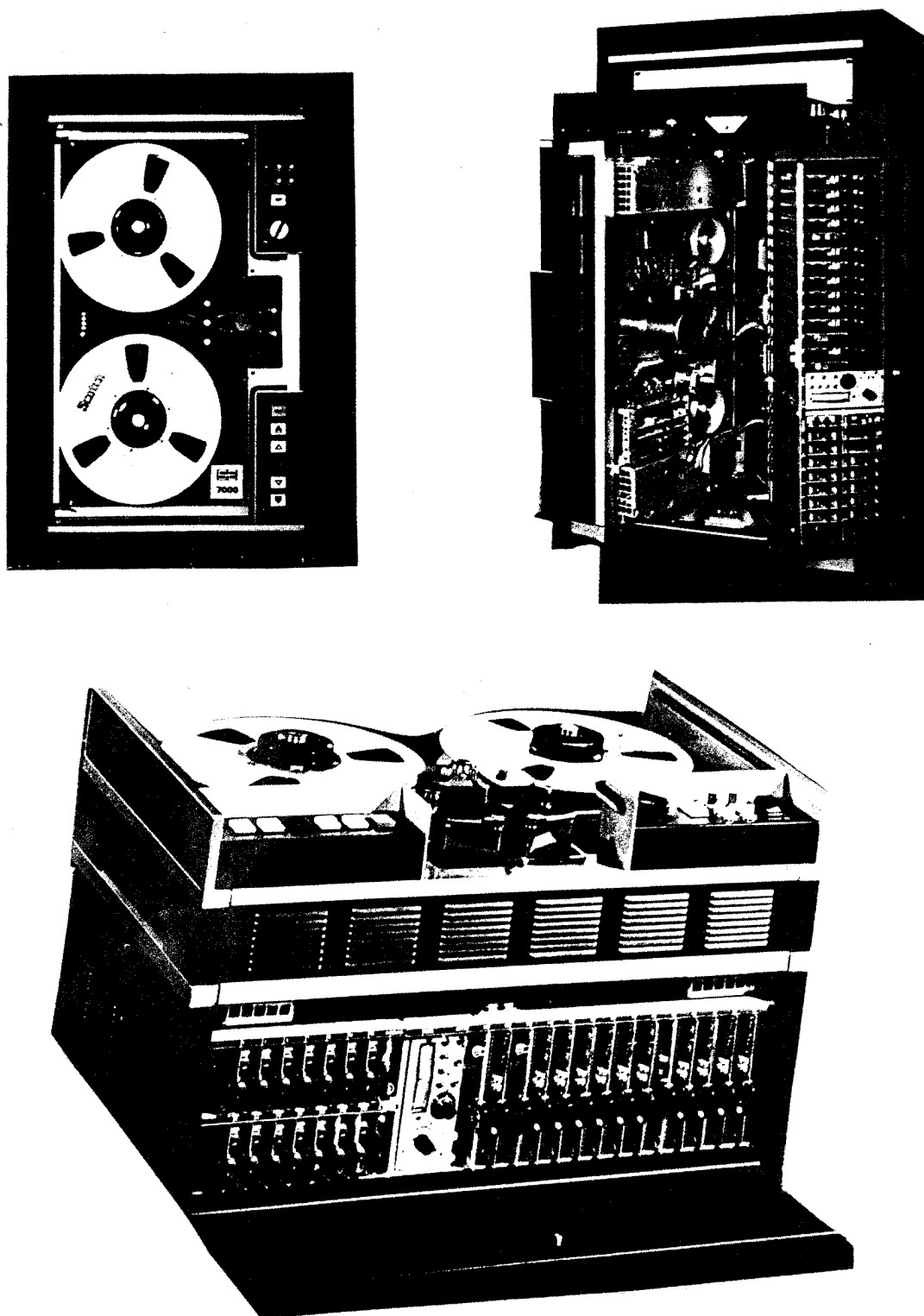


Figure 143. SE-7000 magnetic tape recorder, vertical or horizontal useage, EMI SE Labs Ltd., Feltham, England, 1972.

cables. Internal batteries provide all power necessary to operate the electronics for a half hour and the tape transport for two minutes of recording.

Thirteen data channels are provided. A fourteenth channel is used for reference timing and time zero marking. Transducer excitation provided by the system consists of 3 kHz, 10 kHz, or 20 kHz carrier voltage or 10 volts DC. Ten-kHz data frequency response is provided when DC excitation is used, by means of wide band ($\pm 40\%$) FM. Noise levels are on the order of 10 percent. Data are recorded on 650 feet of one-inch wide magnetic tape which is driven at 60 ips over two seven-track recording heads and one full width erase head. Head spacing is standard IRIG.

A ground checkout unit is used in conjunction with the recording capsule and adds the capabilities of FM signal discrimination, oscillographic recording, time frequency division, and oscilloscope monitoring of playback signals generated or recorded in the data capsule.

A photograph of a Leach Recorder being placed in the ground is shown in Figure 144.

Ref: Armendt, B.F., et al., "Project White Tribe: Air Blast From Simultaneously Detonated Large Scale Explosive Charges," BRL Report No. 1145, 1961.

4.9.3 Digital Recording Systems (80's) (All).

Digital recording systems became increasingly popular as the blast measurement recorder of choice for large scale testing in 1987. However, each MABS country assembled and used their own systems on small scale programs much earlier. These systems, known as transient-data recorders, are very similar in nature so the following discussion gives an overall picture of digital recording deployed over the past decade.

4.9.3.1 BSI Digistar (Canada) (1986). The Digistar transient data recorder is billed as a stand-alone recorder, battery powered, and designed for use in harsh environments. The unit weighed 29 lbs (13 kg) and occupies a volume of 0.04 m^3 (1.3 ft^3). Table 20 indicates the main features of this recorder. It employed 12 bit analog-to-digital converters, was capable of recording 64K samples per channel and may be configured with up to 8 independent recording channels. The memory was organized into 4 memory segments of adjustable length. Different sample rates up to 100K samples per second may be selected for each memory segment. One memory segment was used to provide a history of the signal prior to the event. Several triggering options were available. Built-in signal conditioning for different transducers were provided. Communication with a PC was made with a modified RS232 serial interface.

A photograph of a bank of Digistars is shown in Figure 145. A similar United Kingdom recording setup is shown in Figure 146.

Updated models of this recorder have been made over the succeeding years to include the latest in technology. The reader should check with the author of the referenced report for the latest information.



Figure 144. Leach recorder being placed in the ground prior to test.

Table 20. Digi-Star stand-alone recorder.

Resolution	12 bits
Digitizing Rate	100 kHz per channel max (4 segments programmable size and rate)
Memory	64 kilosamples per channel
Trigger	Remote or local
Interface	RS232 (35 kilobits per second)
Signal Conditioning	Adjustable gain Adjustable excitation Anti-aliasing filter
Power	External battery - 36 hours life Internal battery - 60 days life
Channels	5 standard - selectable



Figure 145. Digistar recorders.

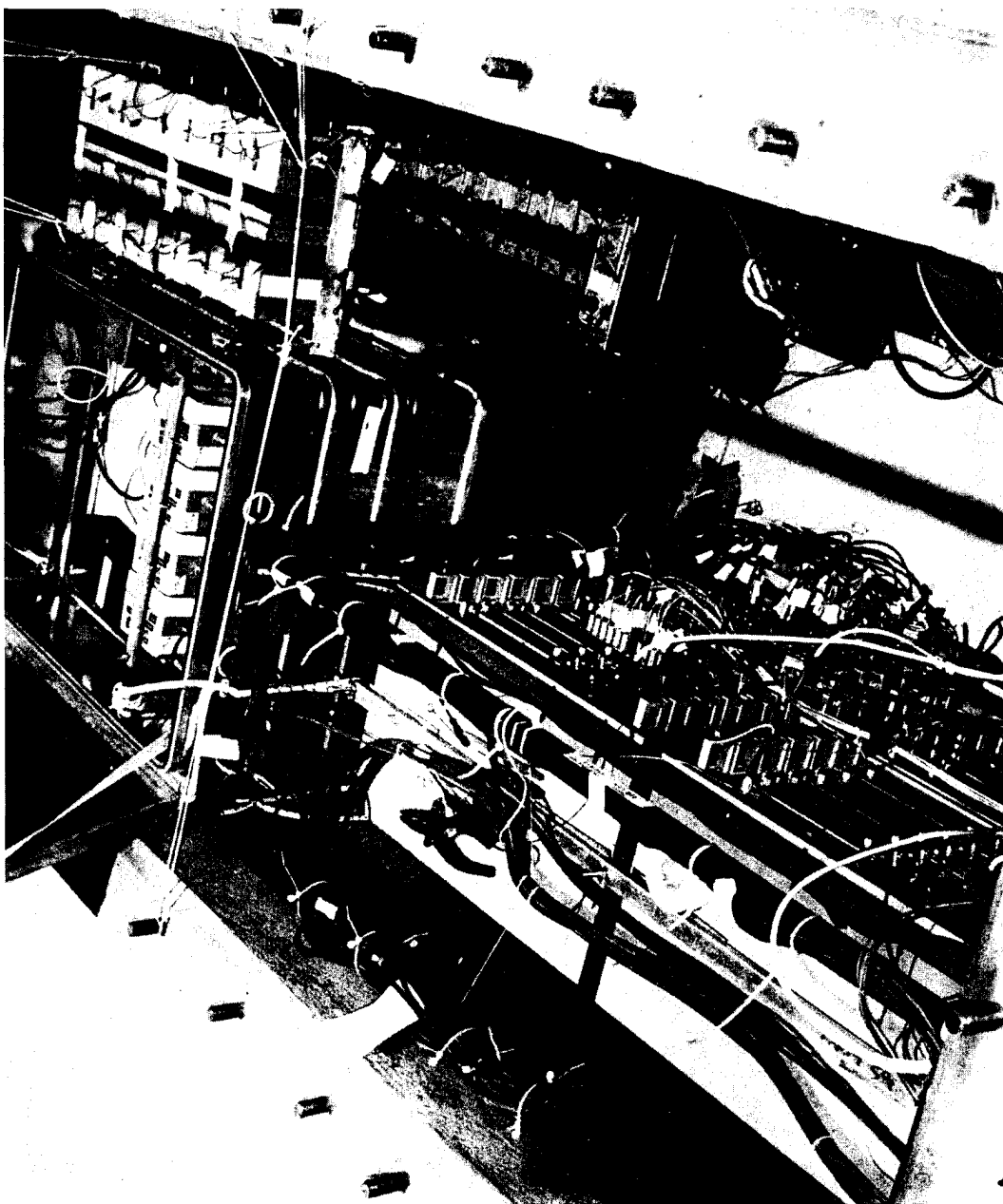


Figure 146. UK digital recording facility.

Ref: Friend, W.H., et al., "Beta Densitometer Gage Data," Proceedings of the Misty Picture Symposium, POR 7187-2, 1987.

4.9.3.2 Pacific Instruments (1987) (USA). The Pacific Instruments (PI) transient data records were designed for rack-mounted usage. The PI model 9820 has been deployed extensively on large scale blast tests. The basic elements of this transient data recorder are a differential input, variable gain, sample and hold amplifier, a high speed 12-bit analog-to-digital converter, and CMOS memory with battery backup. A block diagram of the system is shown in Figure 147. The analog-to-digital converters operate at a maximum rate of 500K samples per second (2 microseconds between samples) or any binary multiplication up to 256. The CMOS memory is capable of storing either 64K or 128K data samples depending upon the configuration of the unit. The memory is divided into 16 segments, 0-15, where number 15 is reserved for storage of calibration data. The other segments are available for data; each of these segments can have the sampling rate independently set.

Triggering of these units can be made using one of two methods. One method uses the input data to provide for an internal trigger. When an established amplitude threshold is reached, triggering occurs and the pre-determined number of post-trigger data segments are then stored and the A/D is stopped. The second method is a start and delay system whereby an external signal initiates the unit and is delayed until some set time before data arrival. Following this delay, the unit is triggered and records the data in the 15 segments of memory.

A computer in the instrumentation bunker provides for local command and control.

Ref: Teel, George D., and Muller, Peter C., "Free-Field Air Blast Data," Proceedings of the Misty Picture Symposium, 7-10 December 1987, Volume II, POR-7187-2, 1988.

4.9.3.3 Kaman Self-Contained Digital Recording System (1985) (USA). The Kaman Self-Contained Digital Recording System (SDRS) is a battery operated microcomputer system designed as a shock hardened unit for direct burial near a high-explosive event with the sensors located nearby.

A block diagram of one channel of the SDRS is shown in Figure 148.

The SDRS uses a modular design where modules are placed in a shock hardened container. Signal conditioning for sensors using wheatstone bridge, piezoelectric, and self-generation type techniques are included. Battery power is provided for supporting the system up to 500 hours. Also included in the system is a lap-top computer used to program the SDRS and to upload the data after test through the RS232 port. The digital memory can be partitioned into several groups with each group representing data acquisition at different rates.

The digitizer in the system is a Burr Brown 12-bit A/D converter which is used to operate at speeds to 500 kHz. The A/D will accept input in the range from -5 volts to +5 volts. It is powered at arm time at which time calibration data is taken and recorded. At shot time, the A/D is cycled at the selected rates until the memory is full at which time the A/D is shut

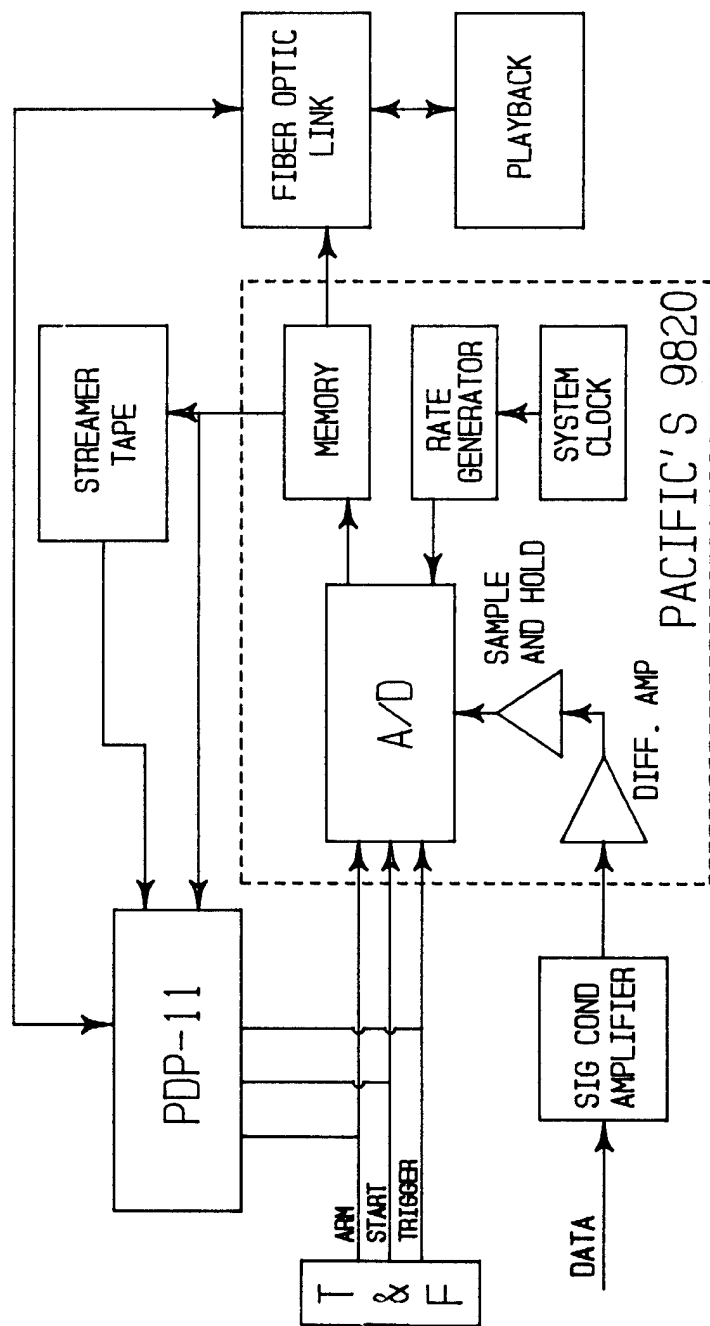


Figure 147. The Pacific Instruments digital data recording system.

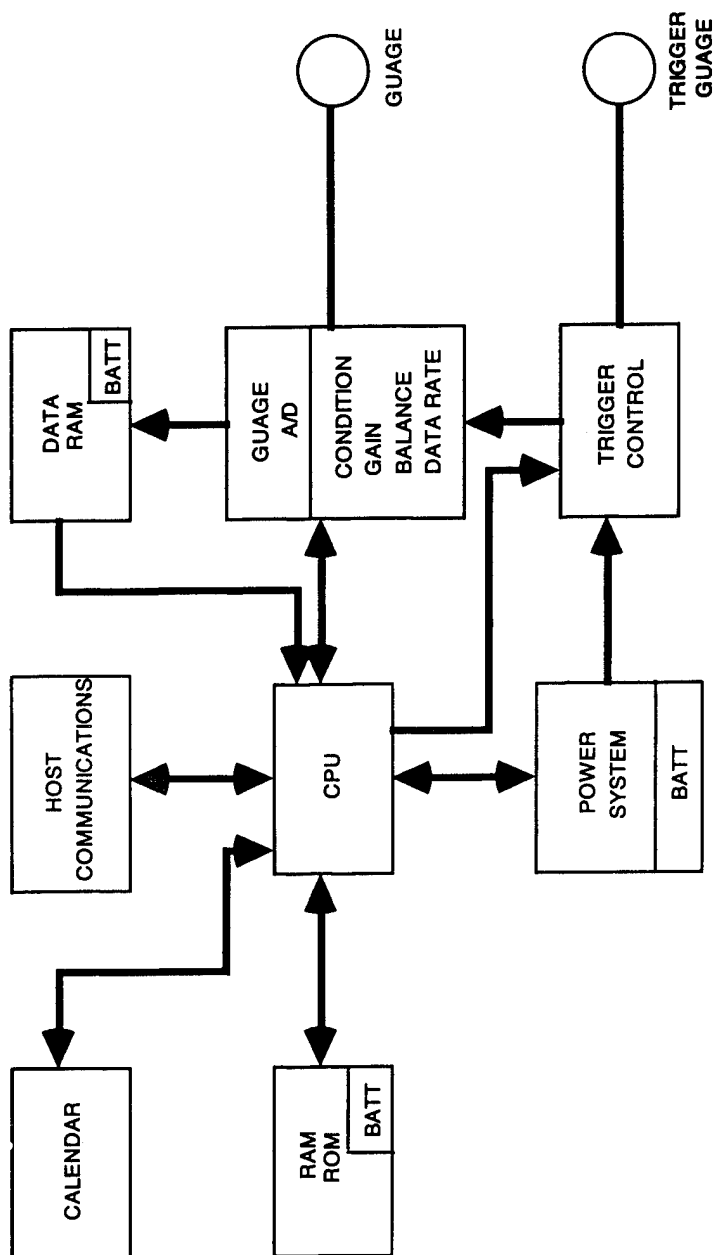


Figure 148. Block design of an SDRS channel.

off. All interfaces to the A/D are tri-stated when the A/D is unpowered to prevent power loss or circuit damage.

The input amplifier is a separate circuit card which contains the instrumentation amplifier, the strain bridge completion circuit, and the offset adjustment for the amplifier. Power comes from a ± 15 volt analog power supply with heavy decoupling and a protected ground reference independent of the 5 volt power going to the A/D converter. On and off control is cared for by the CPU. The gain-bandwidth of the amp is 40 MHz with the gain adjustable from 1 to 1000. The input can be floating or referenced to the system ground.

Communications between the SDRS board and the lap-top computer is via a 9600 baud serial link. The link consists of an RS232 portion from the lap-top computer to an interface box and then to a custom configuration from the interface box to the SDRS boards. The purpose of the interface box is to power the communications both to and from the SDRS boards.

The SDRS uses a Smart Watch for the calendar. As the system is running events are recorded in the log as they occur and are labeled with the current date and time. The calendar has an internal battery and is also used to establish the timing of events such as arm and disarm.

The trigger unit is an instrumentation amplifier with a bridge completion input circuit and a gain that can be set by the user. It is under the control of the CPU and has three modes which are (1) not armed, (2) armed and waiting for a trigger, and (3) holding data.

The power source for the SDRS system is an 8-volt battery which supplies +5 VDC, ± 15 VDC, and a gage supply of 10 volts through a regulator and using DC-DC converters. The CPU controls the power system and switches the voltage on and off as they are needed.

Two sections of memory are used in the system; the CPU memory and the RAM space where the data is stored. The CPU has 8K PROM and 8K RAM. The main memory is 64K x 16 and is automatically loaded at the trigger event without CPU control required. However, the CPC can change data rates while the memory is loading.

Drop tests were made with the unit and it was found that the unit can operate in a shock environment of >1000 g.

The physical size approximated is 6 x 13 x 4 inches. A second generation system was recommended.

Ref: Roark, Glenn L., "Development of a Self-Recording, Cableless Gage System for Application to High Explosive Induced Ground Motion Diagnostics," DNA-TR-86-216, 1986.

4.9.3.4 WES Hardened Data Acquisition System (1988) (USA). The WES hardened data system (HDAS) is a miniature solid state device containing an instrumentation amplifier, an auxiliary gain amplifier, an 11-bit flash analog-to-digital converter, a 128 kiloword (16-bit word) memory, and an output interface. Encapsulation of the module is made with an

epoxy/glass microbead matrix known as Stycast to gain hardening against shock. A shock-hardened 10.5 volt battery is used as a power supply to the system. Early models measured 15 x 6.5 x 4 cm. Later models were reduced in size to a configuration of 2.5 cm in diameter by 3.8 cm long.

The original and subsequent models of the HDAS electronics board are shown in Figures 149 and 150.

Recording times of the HDAS system are 120 msec to 12 seconds with a data sample rate adjustable from 1 megasample/second to less than 10 kilosample per second. Activation of the recorder is achieved by a small, expendable cable connection or by an internal shock activated switch. After activation, the unit records data in a continuous loop mode. The internal battery allows data to be stored for many months.

Two major problems exist when deploying the HDAS. These are the units vulnerability to crushing forces which can destroy it if not fully protected, and difficulty in locating the unit after an explosion test. After the unit is recovered, it is connected to a computer (portable or laboratory) and a plotter to produce finished plots of the data. Filtering, baseline correction, and other functions can be done during this process.

Figure 151 presents a protective ADAS canister deployed on a structural test.

Ref: Ingram, James K., and Dinan, Robert J., "Severe Blast Effects Measurement Using Shock-Hardened, Self-Recording Instrumentation Modules," MABS-13 Proceedings, Volume I, 1993.

Ingram, James K., and Franco, Raphael A., Jr., "MIDAC - A Miniature Integral Data Acquisition Canister for Blast Measurements Using the WES-Developed HDAS Autonomous Digital Data Acquisition System (Module)," Memorandum Report 1989, U.S. Army Engineer Waterways Experiment Station, Vicksburg, MS.

4.9.3.5 AVL Integrated Single Channel Recorder (1991) (Austria). The AVL Integrated recorder is a stand-alone unit with built in battery and complete electronic measurement system including a pressure transducer. The unit is fully programmable and has no active data link during the measurement. Specifications include a measuring time of 80 msec - 80 sec, resolution of 12 bits, a sampling rate of 100 Hz - 100 kHz, a memory of 8K samples, an operating temperature of -40°C to +65°C, and a data retention of 1 hour or more. A block diagram of the unit's components is shown in Figure 152. A piezoelectric gage with built in amplifier has been used in the unit.

The components are housed in a cylindrical stainless steel container, as shown in Figures 153 and 154. The pressure gage is flush mounted at the top surface; a baffle plate is provided.

Connectors for the serial interface with a lap-top computer and a test input connector are provided in the top surface. This allows easy access to the system even after placement of the unit at the measurement location. A flush-mounted cap tightly seals the connectors during the measurement.

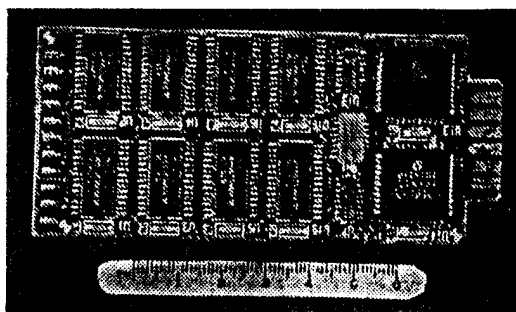


Figure 149. First generation (original) HDAS electronics board (digital/memory side).

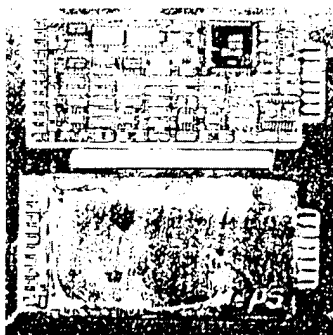


Figure 150. HDAS electronics board (top) and stycast-encapsulated board (bottom).

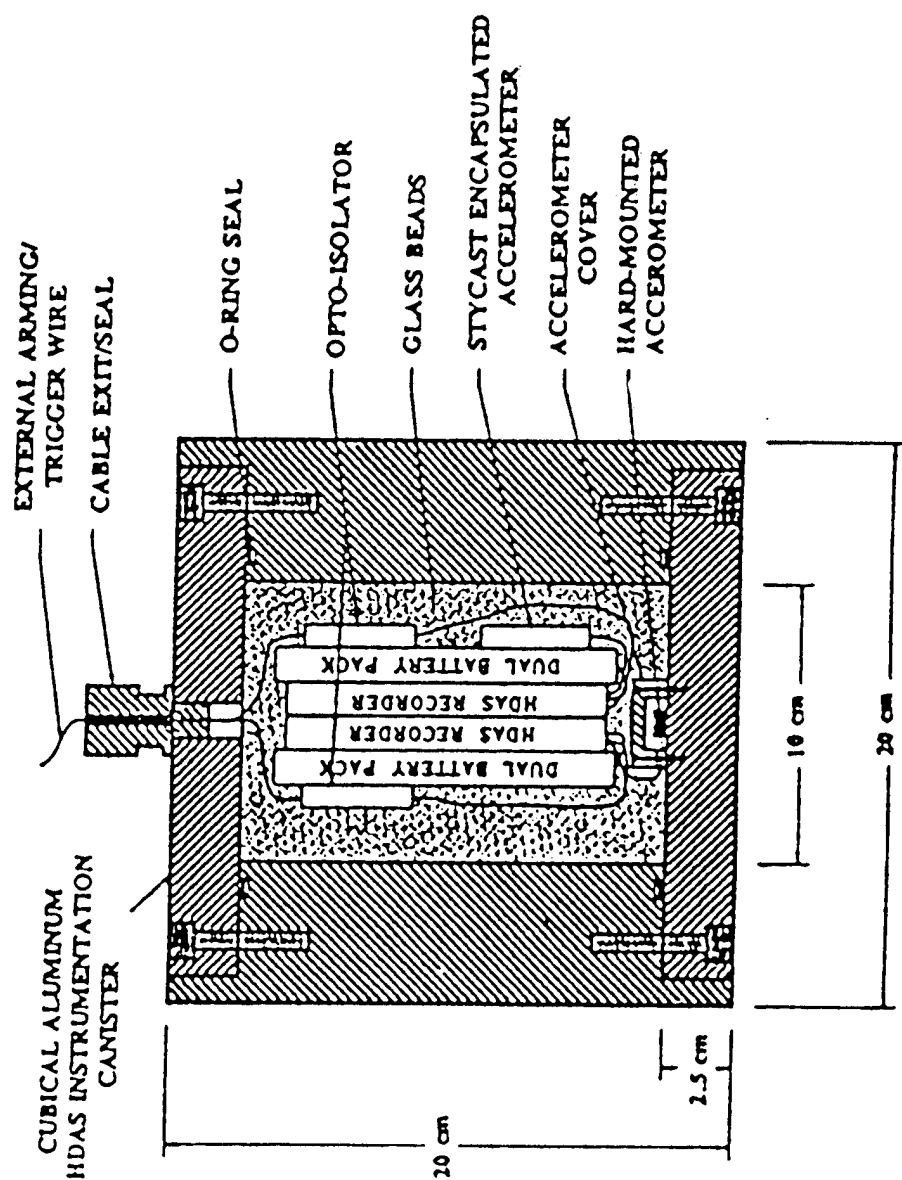


Figure 151. WES hardened data acquisition system.

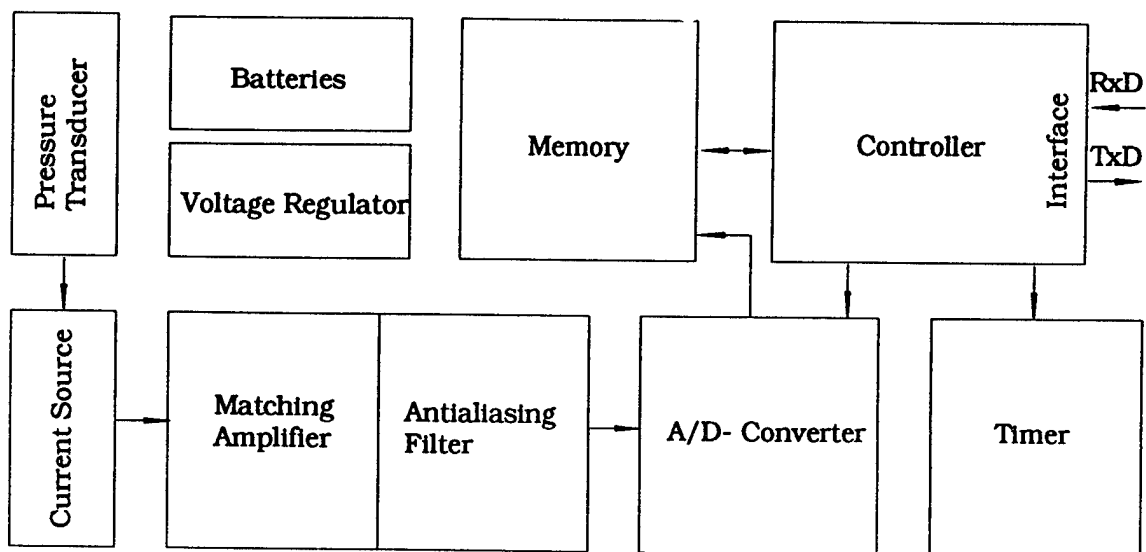


Figure 152. Gage components.

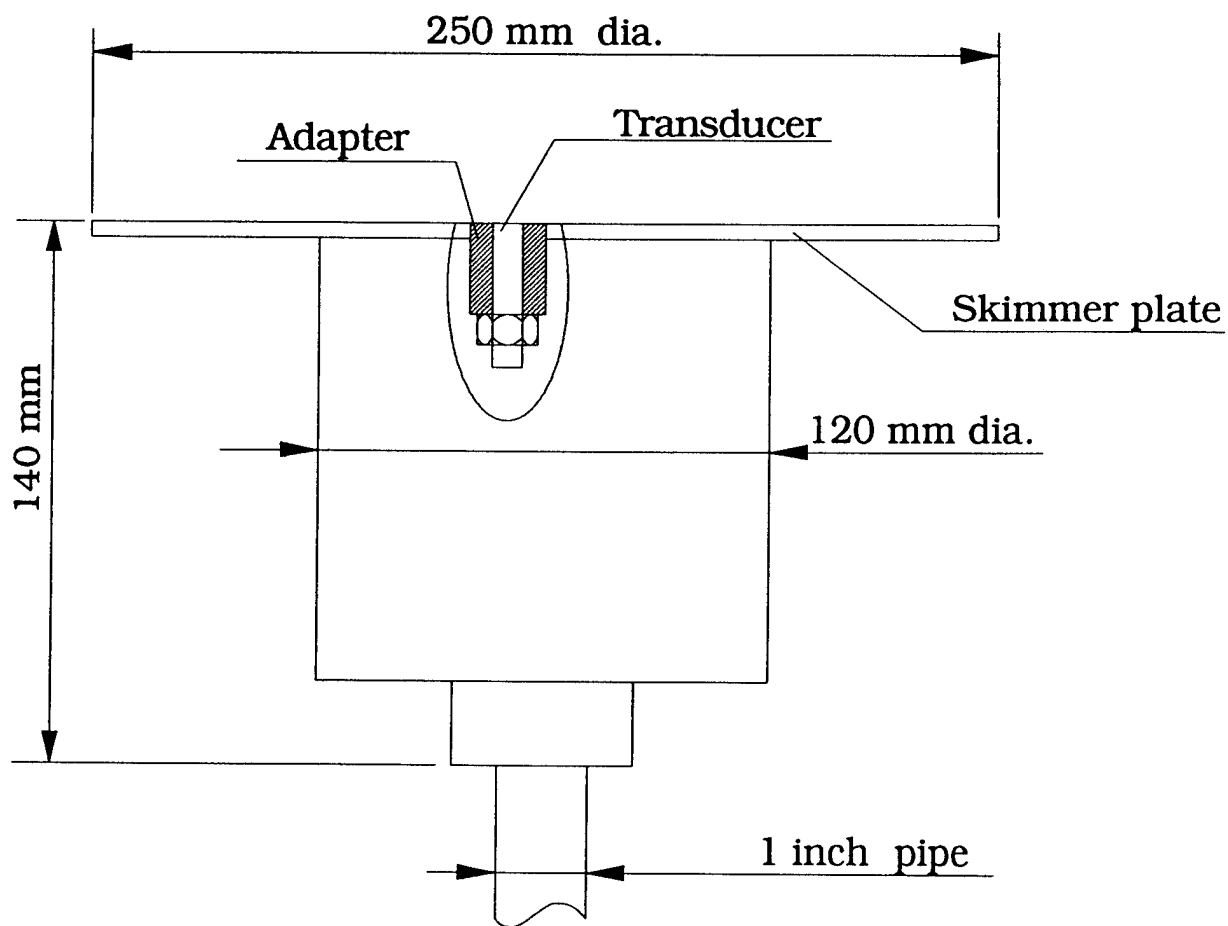


Figure 153. Gage dimensions.

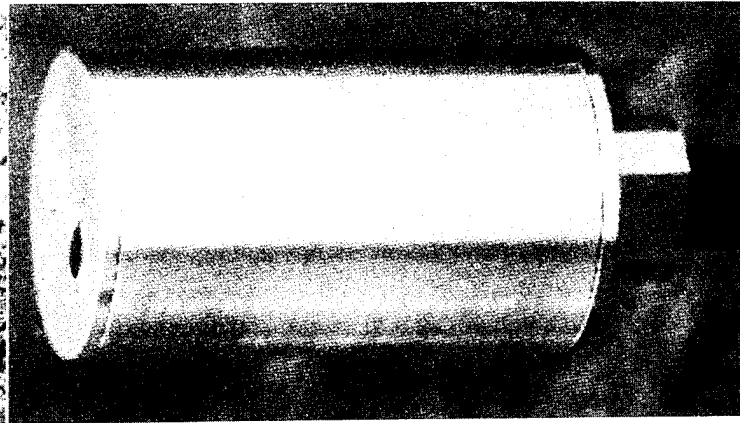
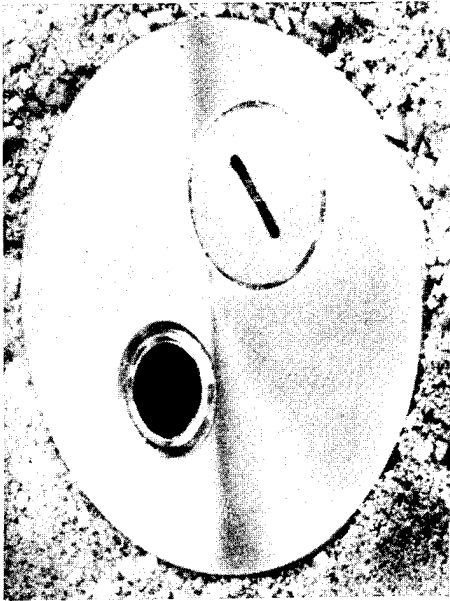


Figure 154. Integrated single-channel, sensor-transient recorder.

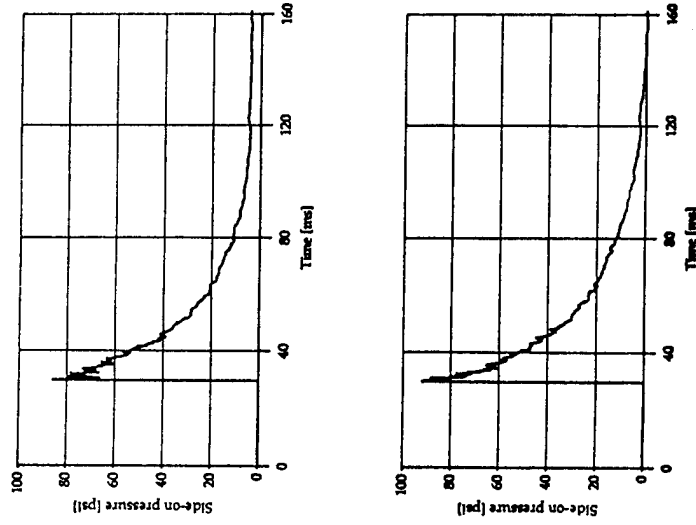


Figure 155. Integrated digital records.

Programming of the unit by means of a lap-top computer provides for the sampling rate, the trigger level, the pre-trigger storage, and the time for standby. Whenever the shock wave level surpasses the preset trigger level the pressure time profile, including the pre-trigger history, is recorded and retained for a few hours. Data retrieval is achieved by linking the unit to the computer. Software provides for a number of offline options for handling the data.

Field records from a large scale test are presented in Figure 155.

Ref: Winkler, Josef and Schweiger, Peter, "Autonomous Recording Gage," Distant Image Symposium Report, Volume 4, DNA POR 7379-4, 1992.

4.9.3.6 DRI Data Acquisition and Analysis System (1993) (USA). The DRI Data Acquisition and Analysis System (DAAS) is a comprehensive measurement and analysis system. Modern hardware and customized software have been integrated into a two rack 20 channel system which can be used in stand-alone operations in remote and harsh environments. The system provides complete control of the test situation for timing sequencing, firing, signal conditioning, signal recording, and data analysis.

A block diagram of the DAAS is shown in Figure 156 and a photograph of the two rack unit is presented in Figure 157.

Central to the DAAS is a LeCroy 6810 12-bit digitizing system which consists of 20 channels, configured in five modules, with four channels per module. This digitizer provides sample rates to five megasamples per second per channel when all four channels per module are active. Sample rates to five megasamples per second are possible when only one channel per module is active. Data simultaneity is assured by use of sample and hold circuitry to sample the data at one point time, and to convert the signals sequentially by use of synchronized multiplexer units that input data into the respective A/D converters. Each digitizing module may have different sample rates and a different number of active channels. Each module is provided with 512 kilosamples of memory to share with its active channels. The unit has digitizer dual time basing, trigger point time stamping, and delayed pre- and post-triggering capability.

Signal conditioning is provided for piezoelectric, wheatstone bridge, or fiber optic sensing systems. The piezoelectric and bridge conditioning units accommodate automatic calibration modes when triggered by the sequencer. The piezoelectric conditioning unit provides constant current excitation to the transducers, charge to voltage converter, amplifies, filters, and calibrates the piezoelectric sensor signals. Each channel has continuously variable gain from 0.1 to 100. The frequency response of the system is limited to 180 kHz. The signal conditioner includes a fault indicator providing input to the operator about the integrity of the cable/sensor combination.

Wheatstone bridge amplifiers provide conditioning of signals originating from conventional one-quarter, one-half, and full bridge configurations. Automatic calibration of the signal conditioner and recorder is a part of the operation. Conventional shunt calibration techniques have been retained. A frequency response of 200 kHz is possible with a gain continuously adjustable from 1 to 1000.

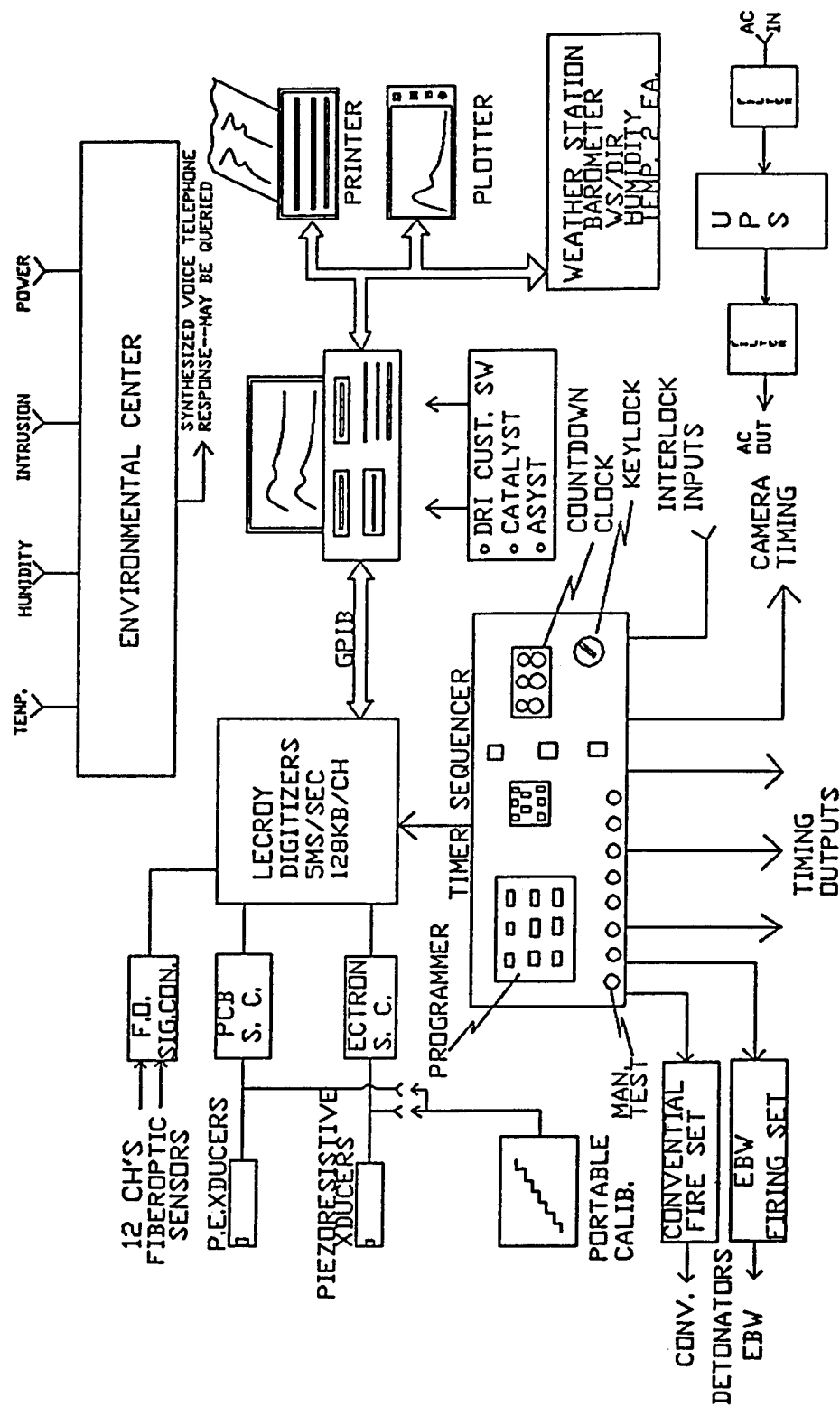


Figure 156. DRI DAAS system block diagram.

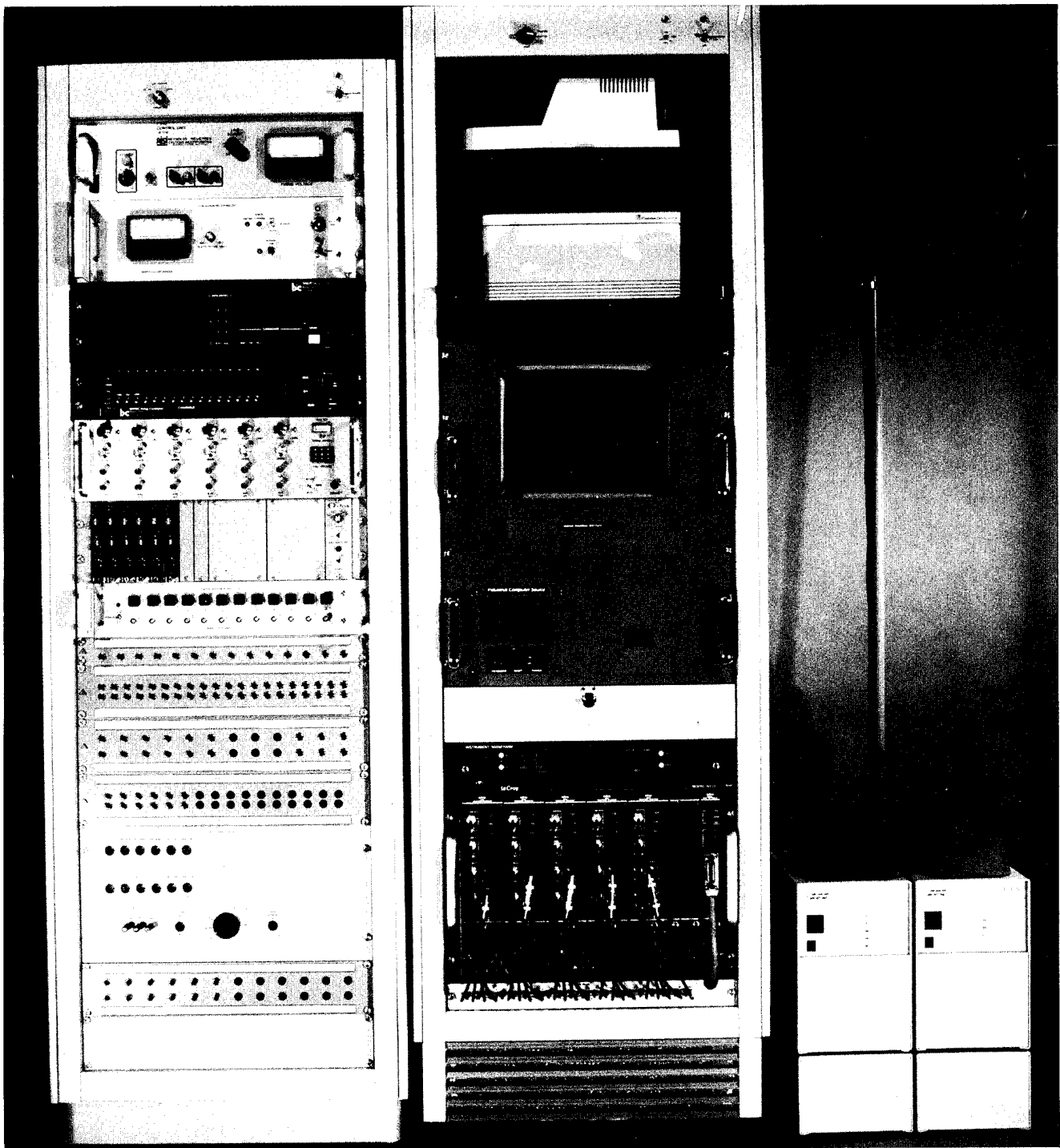


Figure 157. DRI DAAS configuration.

The fiber optic signal conditioning converts light from fiber optical cables into corresponding voltage signals. The voltage produced is proportional to the intensity of the light sensed. Rise times of 350 nanoseconds with a maximum output of ten volts are possible. A line driver provides 200 milliamperes current capability for transmission of signals through up to 5000 feet of coaxial cable with rise times less than one microsecond.

The times/sequencer which is a part of the system controls the internal components of the DAAS as well as the external diagnostic equipment. It is equipped with manual and automatic operation modes to provide versatility and ease of use. The output fire pulse monitor is optically isolated to provide an exact reference to event time zero without the risk of EMI/RFI interfering with the firing system components. External time reference and synchronization is accomplished by use of a precision, eight decade frequency source which may be recorded on external recording media.

The DAAS has a firing unit capable of two independent initiations. Both firing systems are designed to accommodate test site safety requirements by use of safety and interlock operation.

A computer system is incorporated into the DAAS to interface with the digitizers and to display, manipulate, store, and produce hard copies of the data. It is a 386 type with an MS-DOS 5.0 operating system. Included as well is a math coprocessor, a 4 Mbyte expanded memory, a 13-inch color VGA monitor, a serial mouse, an enhanced key board, an HP III P laser printer, an HP 7475 six-pen color plotter, and an IEEE-488 GPIB interface card.

Power to the DAAS is protected by two sets of filters and supplies. Each set consists of two power filters and an uninterruptible power supply. The first power filter removes power spikes and anomalies before insertion into the uninterruptible power supply. The second filter conditions the power immediately before it is distributed to the various instruments mounted in the DAAS. This configuration minimizes EM/RFI pickup into the various subsystems. Motor generators provide the source for the power.

Software for DAAS is easy to use for operators having limited computer background.

Ref: Brown, Larry L., "Data Acquisition and Analysis System for Munitions Test and Evaluation," Denver Research Institute, 1993.

SECTION 5

CONCLUSION

The High-Explosive Era has been determined in this report as having begun in North America with the joint US and Canadian effort in 1959. It is interesting to note that the following year, 1961, testing in Canada continued with the involvement of three countries - the US, Canada, and the UK - to evaluate and compare their respective blast instrumentation. Much of the instrumentation deployed was from the waning days of the nuclear era. Variable reluctance gages were the mainstay of that era and were deployed with up and coming new developments with strain sensors, piezoelectric gages, and mechanical self-recording, self-contained gages. Electronic recording systems used oscillographs and magnetic tape of the period.

From that 1961 test to this day weapons effects research placed greater demands on instrumentation systems to provide increased frequency response and to gain data in regions of severe environments. Variable reluctance and strain sensors were gradually replaced with piezo-resistive gages with frequency responses greater than 80 kHz. For 1000-lb tests, piezoelectric gages with a 500 kHz or greater response were successfully used to obtain high fidelity blast data. Bar gages were developed for measurements in the 1-8 Kbar range. They were of several designs and were used in regions where the environment was extremely severe.

Recording systems for electronic gages progressed from the 20-40 kHz range to 80 kHz and later to 500 kHz using FM magnetic tape. After three decades of service, the magnetic tape systems gave way to digital recording systems. The digital system in various forms continues today. Digital systems may be found in a recording bunker context, or as multiple channel units housed near the sensor, or as a multiple channel hardened unit, or as a 1-2 channel unit housed as a self-contained sensor-recorder system.

The mechanical self-contained, self-recording pressure gages were unable to compete because of their inherent frequency response limitations and were to become a historic item by the end of the 60s. Emphasis was placed solely on electronic systems for time parameter measurements, although the principles used in the gages were incorporated in the integrated sensor-recorder digital system.

Passive devices developed in the 60s saw a re-emergence in the 80s and 90s. Some of the devices used extensively in the nuclear era were re-examined, refined, and deployed to yield cost-effective information.

Blast parameters other than the basic static overpressures were investigated during the HE era through the development and application of devices using the pressure gage. These were used in the measurement of dynamic pressure - the subsonic and sonic q probes, the greg gage, the snob gage, and the differential pressure gage. Other systems were the velocity and density gages which were deployed on a number of tests.

SECTION 6

REFERENCES

- Ackerman, J., "Pitot Gages Test," Proceedings of the MINOR SCALE Symposium, POR-7158-4, 1986.
- Armendt, B.F., et al., "Project WHITE TRIBE: Air Blast From Simultaneously Detonated Large Scale Explosive Charges," BRL Report No. 1145, 1961.
- Barth, P.W. and Wilson, J., "Ultrahigh Frequency Pressure Sensor-Novasensor," AFATL-TR-88-77, 1988.
- Batt, R.G., "MIGHTY MACH IV, Multiburst Air Density Measurement Experiment," DNA-TR-81-275, 1983.
- Batt, R.G., "MIGHTY MACH IV, Low Range Dynamic Pressure Measurements Experiment," DNA-TR-84-03, 1982.
- Baum, Neal, et al., "The High-Pressure Bar Gage, Volume 1 - High-Pressure Bar Gage Designs," DNA-TR-92-160-V1, 1993.
- Bowen, I.G., et al., "Distribution and Density of Missiles from Nuclear Explosions," USAEC Civil Effects Test Group, WT-1168, Department of Commerce, 1956.
- Brown, Larry L., "Data Acquisition and Analysis System for Munitions Test and Evaluation," Denver Research Institute, 1993.
- Carpenter, H.J., Private Communication, 1993.
- Carpenter, H.J., et al., "Snob/Greg Probe Characterization Analysis," DNA-TR-89-44, 1990.
- Clink, W. L. et al., "A Progress Report on the Development of a Pressure Switch System for Detecting the Arrival of a Shock Front," DRES-TN-112, 63-0646, 1963.
- Coleman, P.L., "MINI-JADE Instrumentation," DNA-TR-86-320, 1986.
- Coulter, G.A., "Calibration of Pressure Transducers at the BRL Shock Tube Facility," BRL Memorandum Report 1943, 1967.
- Del Frate, Renzo J., et al., "Optical Passive Shock (BIER) Gage Development Program," DNA-TR-93-23, 1993.
- Dewey, J., "Surface Burst of a 100-ton TNT Hemispherical Charge Wire Drag Gage Measurement," Suffield Tech. Note 80, 1962.

"DISTANT IMAGE Symposium Report," Volume I, DASA POR 7379-1, 1992.

"DISTANT IMAGE Cantilever Gauges," DISTANT IMAGE Symposium Report POR 7379-5, 1992.

Ethridge, N. H., Flory, R. A., and Keefer, J. H., "Cube Displacements", MINOR UNCLE Symposium Proceedings, Defense Nuclear Agency, Alexandria, VA 22310-3348, 1994.

Ethridge, N. H., and Flory, R. A., "Use of Cube Displacements as a Measure of Blast", Proceedings, Vol.I, 13th International Symposium on the Military Application of Blast Simulation, The Hague, The Netherlands, 13-17 September 1993.

Ethridge, N.H. and Jackson, Willis F., "Dynamic Pressure Gage Development for Subsonic Flows," DNA-TR-92-109, 1993.

Ethridge, N.H., et al., "A Differential Pressure Gage for Measurement of Dynamic Pressure in Blast Waves," MABS-8 Proceedings, Volume I, 1983.

Fletcher, E.R., et al., "Impact Velocities of Steel Spheres Translated by Air Blast," Operation SNOW BALL Symposium Proceedings, Volume 1, DASA 1642-1, 1965.

Friend, W.H., et al., "Beta Densitometer Gage Data," Proceedings of the MISTY PICTURE Symposium, POR 7187-2, 1987.

Granath, B.A. and Coulter, G.A., "BRL Shock Tube Piezo-Electric Blast Gages," BRL Technical Note 1478, 1962.

Howe, John S., Personal Communications., Materials Research Laboratory, Department of Defence, Victoria, Australia.

Ingram, James K., and Dinan, Robert J., "Severe Blast Effects Measurement Using Shock-Hardened, Self-Recording Instrumentation Modules," MABS-13 Proceedings, Volume I, 1993.

Ingram, James K., and Franco, Raphael A., Jr., "MIDAC - A Miniature Integral Data Acquisition Canister for Blast Measurements Using the WES-Developed HDAS Autonomous Digital Data Acquisition System (Module)," Memorandum Report 1989, U.S. Army Engineer Waterways Experiment Station, Vicksburg, MS.

James, D.J. and Rowe, R.D., "An Assessment of the Tripartite Pressure-Time Recordings from the 20-Ton and 100-Ton TNT Charges Detonated in 1960 and 1961 at the Suffield Experiment Station," AWRE Report E4/63, 1963.

Johnson, D. and Gaffney, E., "One Microsecond Rise Time Birefringent Hopkinson Bar for Nuclear Airblast Measurement," K-Tech TR-91-15, 1991.

Johnson, O.T. and Ewing, W.O., "An Omni-Directional Gage for Measuring the Dynamic Pressure Behind a Shock Front," BRL Memorandum Report No. 1394, 1962.

Kaplan, Kenneth. "Reduced Ambient Pressure Explosion Testing in the VRS Shock Chamber," Military Applications of Blast Simulators, MABS-1, Vol 1, 1967.

Keefer, J. H., "Australian Dynamic Pressure Impulse Measurements Note," Operation DISTANT PLAIN.

Kulite Semi-conductor Bulletin KS-1000D, Kulite Miniature 1S Silicon Diaphragm Pressure Transducer Catalog. 1985.

LeFevre, D. P., "Evaluation of New Self-Recording Air Blast Instrumentation," Project 1.3b, Operation SNOWBALL, BRL Memorandum Report No. 1815, 1967.

Magnetic Recording Equipment, SE Labs (EMI), Ltd., Feltham, Middlesex, England, 70's.

Manweiler, R.W., et al., "Measurement of Shock Overpressure in Air by a Yielding Foil Membrane Blast Gage," Oak Ridge National Laboratory, ORNL-4868, 1973.

McCarson, Jr., T.D., "Internal Strain Gage (ISG) Airblast Pressure Transducer," AFWL-TR-87-77, 1988.

Mellsen, S.B., "Drag Measurements on Cylinders by Free Flight Method - Operation PRAIRIE FLAT," DRES-TN-249, 1969.

Modarress, D. and Hoeft, T., "Velocity Measurement in Dusty Flows," Final Report DNA001-85-C-0130, 1987.

Modarress, D., et al., "Laser Doppler Velocimetry, 30 psi Location, Dusty Precursed Radial, Experiment 8703," Proceedings of the MINOR SCALE Symposium, POR 7158-5, 1986.

Muirhead, J. C., et al., "Some Self-Recording Pressure Indicators," DRES-TW-118, 63-0527, 1963.

Muirhead, J. C., and D. W. Lecuyer, "Development of Expendable Gauges for Detecting the Arrival of Shock Fronts, I. A Pressure Contractor with Mylar Element," DRES-TN-33, 59-0903, 1959.

Naylor, R. and Mellsen, S.B., "Unsteady Drag From Free Field Blast Waves," DRES-SM-42-71, 1973. "Operation DISTANT PLAIN Preliminary Report," Volume I, DASA 1876-1, 1966.

Nelson, Bruce N., "High Bandwidth Fiber Optic Air Blast Pressure Sensor," Geo-Centers, Inc., Newton Centre, MA. Paper presented at the Fifth State-of-the-Art Blast Instrumentation Meeting, Volume I, 1988.

Ohrt, Alan Paul, "Analysis of D'Alembert Unfolding Technique for Hopkinson Bar Gage Records," Waterways Experiment Station, Technical Report SL-92-12, 1992.

Pittman, J., "Free-Field Airblast Measurements," Operation SAILOR HAT, Project 5.2A, DNA POR 4056, 1966.

"PRE-DIRECT COURSE Results Report," Volume I, DNA POR 7116-1, 1983.

"PRE-DIRECT COURSE, Results Report," Volume III, DNA POR 7116-3.

"Proceedings of the DICE THROS Symposium," Volume I, DNA 4377P-1, 1977.

Reisler, R.E., et al., "DIAMOND ARC 87 - Blast Phenomenology Results from HOB, HE Tests with a Helium Layer," Volume I, DNA-TR-88-99-VI, 1988.

Reisler, Ralph E., et al., "Blast Loading of Model MX Horizontal Structures in the Irregular Mach Reflection Zone," Technical Report ARBRL-TR-02447, 1982.

Reisler, Ralph E. and Pettit, Burnett A., "Project DIPOLE WEST - Multi Burst Environment (Non-Simultaneous Detonations)," BRL Report No. 1921, 1976.

Reisler, Ralph E., et al., "Air Blast Measurements from the Detonation of Large Spherical TNT Charges Resting on the Surface (Operation DISTANT PLAIN, Events 6A and 6)," BRL Memorandum Report No. 1955, 1969.

Rickman, Denis D., "MISERS GOLD High-Pressure Airblast Measurements," Waterways Experiment Station, Technical Report SL-91-1, 1991.

Ritzel, D.V., "The DRES Blast Gage Station," MABS-9 Proceedings, Volume I, 1985.

Roark, Glenn L., "Development of a Self-Recording, Cableless Gage System for Application to High Explosive Induced Ground Motion Diagnostics," DNA-TR-86-216, 1986.

Roark, Glenn and Cole, Eldine, "Gas Particle Velocity Measurement," Kaman Sciences Corporation Report K84-600(R), 1984.

Rowland, R.H., "Blast and Shock Measurement State-of-the-Art Review," DASA 1986, 1967.

Sachs, D.C., "Field Test Particle Velocity Gage," Operation DISTANT PLAIN Symposium, Volume II, M.J. Dudash, Editor, DASA-2207, 1968.

"Scientific Observations on the Explosion of a 20-Ton TNT Charge," Suffield Report No. 203.

Simmons, K.B., "Development of Piezoresistive Bar Gage," AFWL-TR-76-65, 1976.

Teel, George D., and Muller, Peter C., "Free-Field Air Blast Data," Proceedings of the Misty Picture Symposium, 7-10 December 1987, Volume II, POR-7187-2, 1988.

Wells, H. S., "Development and Test of Prototype Miniature, Rugged, Self-Recording Air Blast Instrumentation," Report No. E.I.R. 700, Bendix Environmental Science Division, Bendix Corporation, 1966.

Williams, D. A., "A Deformation Gauge for Measurement of Dynamic Pressure Impulse of Shock Waves, Australian Defence Standards Laboratories, Technical Note 72. September 1964.

Winkler, Josef and Schweiger, Peter, "Autonomous Recording Gage," DISTANT IMAGE Symposium Report, Volume 4, DNA POR 7379-4, 1992.

Witherly, T.D., "Field Testing of Instruments for Measurement of Dusty Airblast Effects," DASA-1671, 1965.

Witherly, T.D., "Instruments for Measurement of Dusty Airblast Effects in High Overpressure Regions," DASA-1433, 1963.

APPENDIX A

SELECTED U.S. BIBLIOGRAPHY

Baker, Wilfred E., "Explosions in Air," Engineering Design Handbook, Part One, AMCP 706-181, 1974.

Baker, W. E., et al., "The Elastic and Plastic Response of Cantilevers to Air Blast Loading," Proceedings of the Fourth U.S. National Congress of Applied Mechanics, ASME, 1962, pages 853-866.

Baker, W. E., and W. O. Ewing, Jr., "Miniature Piezoelectric Gages for Measuring Transient Pressures on Airfoils," BRL Memorandum Report No. 1329, March 1961.

Baylot, James T., "Analysis of Hopkinson Bar Pressure," U.S. Army Corps of Engineers, Waterways Experiment Station Technical Report SL-93-1, January 1993.

Baylot, J. T., "Analysis of Hopkinson Bar Pressure Gage," WES-TR-SL-92-XX, April 1992.

Blackstock, A. W., et al., "Piezoelectric Gauges for Measuring Rapidly Varying Pressures up to Seven Kilobars," Rev. Sci. Instruments, 35(1): 105-110, 1964.

Brooks, J. N., "DRI Blast Recording Equipment," Phase Report No. 5, DRI, March 1957.

Chilton, E. G., et al., "The Development and Evaluation of a Miniature Velocity Gage," AFWL-TR-65-46, 1967.

Davies, R. M., "The Critical Study of the Hopkinson Pressure Bar," Philosophical Transactions of the Royal Society of London, Volume 240, page 345, January 1948.

Ethridge, Noel H., et al., "Air Blast Instrumentation Concepts for Underground Nuclear Cavity Tests and High Pressure Simulation Tests," BRL Memorandum Report No. 2795, October 1977.

Ewing, Jr., W. O., and J. W. Hanna, "A Cantilever for Measuring Air Blast," BRL Technical Note No. 1139, August 1957.

Farrand, W. B., "Piezoelectric Pressure Sensing Devices," AFSWC-TR-60-39, Stanford Research Institute, July 1960.

Gay, H., "Static and Dynamic Performance Comparison Tests on Foil and Weldable Strain Gages," AFWL-TR-81-37, July 1981.

Jones, D. C., editor, Transient Radiation Effects on Electronics (TREE) Handbook, DASA 1420, Battelle Memorial Institute, February 1964.

Keough, D. H., "Pressure Transducer for Measuring Shock Wave Profiles, Phase IX: Additional Gage Development," DASA 1414-1, AD 459 058, November 1964.

Kingery, Charles N., et al., "Surface Air Blast Measurements from a 100-ton TNT Detonation," BRL Memorandum Report No. 1410, June 1962.

Lee, C. K. B., and D. Crawford, "A New Method for Analyzing Dispersed Bar Gage Data," RDA-TR-2-2261-2301-001, February 1992.

Levine, David, "Acceleration-Compensating Pressure Transducers for Surface-Pressure Measurements," NAVORD Report 6834, January 1961.

Muller, Peter C. and George D. Teel, "Misers Gold Free Field Air Blast Diagnostics, Experiment 8215," Proceedings of the Misers Gold Symposium, Volume 1, DNA POR 7352-1, pages 296-512, 1990.

Olson, W., and J. Wenig, "A Double-Charge Technique to Measure Face-On Blast," BRL Memorandum Report No. 1347, May 1961.

Patterson, J. L., "A Miniature Electrical Pressure Gage Utilizing a Stretched Flat Diaphragm," NACA TN 2659, April 1962.

Petes, J., and L. Slifer, "Drag Loading on Model Targets," WT-1306, AD 357 969L, January 1960.

Reisler, Ralph E., et al., "Dynamic Pressure Air Blast from Height-of-Burst Subsonic Flows, Volume 1, 3.6, 7.3, and 12.8M Heights of Burst," ARBRL-TR-02553, 1984.

Reisler, Ralph E., et al., "Air Blast Data from Height-of-Burst Studies in Canada; Volume 1 - HOB 5.4 to 71.9 feet," BRL Report No. 1950, 1976.

Reisler, Ralph E., et al., "Air Blast Measurements from the Detonation of an Explosive Gas Contained in a Hemispherical Balloon (Operation Distant Plain, Event 2a)," BRL Memorandum Report No. 2108, July 1971.

Reisler, Ralph E., et al., "Blast Measurements from the Detonation of Tower Placed 20-tons of Spherical TNT (Operation Distant Plain, Events 1 and 1a)," BRL Memorandum Report No. 2089, February 1971.

Reisler, Ralph E., et al., "Air Blast Parameters from Summer and Winter 20-ton TNT Explosions, Operation Distant Plain, Events 3 and 5," BRL Memorandum Report No. 1894, November 1967.

Reisler, Ralph E., et al., "Air Blast Instrumentation from a 500-ton TNT Detonation: Project 1.1 Operation Snowball," BRL Memorandum Report No. 1818, December 1966.

Rickman, D., and C. Welch, "MINERAL FIND 2 and 3 Free-Field Measurements," WES Technical Report SL-91-19, October 1991.

Rickman, D., C. Welch, and J. Stout, "MINERAL FIND 1 Airblast Measurements," WES Technical Report SL-91-21, October 1991.

Ritzel, D. V., "Measurements from DRES Blast Gauge Stations: West Radial," Proceedings of the Minor Scale Symposium, Volume 4, pages 103-119.

Ruetenik, J. R., and S. D. Lewis, "Pressure Probe and System for Measuring Large Blast Waves," Technical Report AFFDL-TDR-65-35, Wright-Patterson AFB, Ohio, June 1965.

Soroka, B., and G. T. Watson, "An Eight-Channel High-Performance Oscillograph Recording System," BRL Memorandum Report No. 1965, May 1966.

Wells, H. S. "Development and Test of Prototype Miniature, Rugged Self-Recording Air-Blast Instrumentation," Report No. EIR 700, The Bendix Corporation, November 1966.

Williams, R. F., "Pressure Transducer for Measuring Shock Wave Profiles, Phase X: Measurement of Low-Pressure Shock Wave Profiles," DASA 1653, Stanford Research Institute, May 1965.

Wilson, R., "Development of a Damped Bar Gage for Long Duration Stress-Pulse Recording," DNA-TR-86-70, February 1986.

Zeitlin, E. A., "The Blast Environment: Methodology and Instrumentation Techniques with Applications to New Facilities," NAVWEPS Report 8782, August 1965 (AD-622 980).

APPENDIX B

SELECTED CANADIAN BIBLIOGRAPHY

Clink, W. L., H. B. Lutz, and F. H. Winfield, "A Progress Report on the Development of a Pressure Switch System for Detecting the Arrival of a Shock Front," 1963, DRES-TN-112, 63-0646.

Dewey, J. M., and W. A. Anson, "Wire Gauge," 1966, DRES-PAT-748, 640, 66-0157.

Dewey, J. M., "The Air Velocity and Density in Blast Waves from TNT Explosions," 1964, DRES-R-207, 64-0259.

Dewey, J. M., and W. A. Anson, "A Blast Wave Density Gauge Using Beta-Radiation," Journal of Scientific Instruments, Vol. 40, December 1963, pages 568-572.

Dewey, J. M. and W. A. Anson, "Density Measurements in the Blast Wave from a Surface Burst 100 Ton TNT Hemispherical Charge (1961)," 1963, DRES-TP-252, 63-0215.

Dewey, J. M., "Surface Burst of a 100 Ton TNT Hemispherical Charge Wire Drag Gauge Measurements," 1962, DRES-TN-80, 62-0810.

Diehl, C. H. H., and G. H. S. Jones, "A Tracer Technique for Cratering Studies," Journal of Geophysical Research, Vol. 70, No. 2, January 15, 1965, pages 305-309.

Fenrick, W. J. and J. J. Vesso, "Flush Mounting Piezo-Electric Blast Gauges - The Assembly Techniques and Field Applications," 1962, DRES-TN-74, 62-0397.

Mellsen, S. B., "Drag on Cylinders in a 20 to 25 Millisecond Blastwave," 1972, DRES-SM-114-71.

Mellsen, S. B., "Drag Measurement on Cylinders by the Free Flight Method - Operation PRAIRIE FLAT," 1969, DRES-TN-249.

Muirhead, J. C. and W. Palmer, "Peak-Pressure Measuring Device," 1971, DRES-PAT-882, 830, 73-1031.

Muirhead, J. C. and S. A. Cyganik, "On the Measurement of Transient Pressures in Soils," 1969, DRES-SM-5-69, 69-0647.

Muirhead, J. C., and W. O. Palmer, "Studies on Shock Wave Pressure-Time Gauges: XVI. A Variety of Electrical Problems," 1967, DRES-TN-172, 67-1133.

Muirhead, J. C., W. J. Fenrick, and W. O. Palmer, "Studies on Shock Wave Pressure-Time Gauges: X. Evaluation of a Selection of Transducers with Piezo-Ceramic Shear Tube Elements," 1965, DRES-TN-159, 65-1769.

Muirhead, J. C., and W. O. Palmer, "Studies on Shock Wave Pressure-Time Gauges: VII. The Effect of Electrical Fields on Quartz and Tourmaline Element Pressure Transducers," 1965, DRES-TN-151, 65-1144.

Muirhead, J. C., W. J. Fenrick, and B. R. Sanders, "Studies on Shock Wave Pressure-Time Gauges: V. The Gauge Testing Laboratory," 1965, DRES-TP-302.

Muirhead, J. C., W. A. Jones, and W. M. McMurtry, "Some Self-Recording Pressure Indicators," 1963, DRES-TN-118, 63-0527.

Muirhead, J. C., and W. M. McMurtry, "A Mercury Surface Tension Gauge for the Measurement of Low Shock Pressures," 1962, DRES-TN-93, 62-0946.

Muirhead, J. C., W. M. McMurtry, and W. A. Jones, "A Water Surface Tension Gauge for the Measurement of Very Low Shock Pressures," 1962, DRES-TN-91, 62-0868.

Muirhead, J. C., and D. W. Lecuyer, "Development of Expendable Gauges for Detecting the Arrival of Shock Fronts: I. A Pressure Contactor with "Mylar" Element," 1959, DRES-TN-33, 59-0903.

Naylor, R., and S. B. Mellsen, "Unsteady Drag From Free-Field Blast Waves," 1973, DRES-SM-42-71.

Operation PRAIRIE FLAT - Project Officers Report, "Crater and Ejecta Study," POR-2115, Defense Atomic Support Agency, Washington, D.C.

Palmer, W. O., and J. C. Muirhead, "Methods for Rendering Pressure Transducers Insensitive to Temperature Changes," 1972, DRES-PAT-892, 695, 73-1030.

Palmer, W. O. and J. C. Muirhead, "On the Response of Piezoelectric Pressure Transducers to Temperature Changes," 1969, DRES-SM-3-69, 69-1492.

Palmer, W. O., and J. C. Muirhead, "A Self-Recording Peak Pressure Indicator," 1969, DRES-SM-59-67, 69-0458.

Palmer, W. O., and J. C. Muirhead, "Studies on Shock Wave Pressure-Time Gauges: XI. The Use of Epoxies in Case and Element Construction," 1966, DRES-TN-171, 67-0134.

Pattman, J. D. R., "Thermal Radiation and Fireball Temperatures," Operation DISTANT PLAIN Symposium, Vol. 1, pages 183 et seq., DASIAC Special Report SR 60, DASA-1947-1, September 1967.

Ritzel, D. V., "The DRES Blast Gauge Station," MABS-9 Proceedings, Paper III.2, Vol. II.

Watson, J. S. (compiled by), "Event DIAL PACK - Canadian Participation," 1970, DRES-SM-17-70.

Winfield, F. H., "Telluric Potential Charges Associated with Large-Scale TNT Explosions," 1969, DRES-TN-203.

Winfield, F. H., and B. G. Laidlaw, "A Switch for Measuring Ground Shock Velocity," 1964, DRES-TN-88, 64-0533.

Winfield, F. H., "A Stand for Holding Blast Gauges," 1961, DRES-TN-57, 61-0242.

APPENDIX C

SELECTED UK BIBLIOGRAPHY

Air Blast - Bibliography on Blast Shock Waves and Associated Topics	European TDCK - 30050 and 30051
The Measurement of Air Blast	RARDE Memo (MX) 46/62
Microsecond Response Pressure Transducer	RAE-TN-AERO-2935
Air Blast Recording	AWRE T-91/54
Blast Measurement	AWRE 0-1/59
Damped Oscillatory-Mass Instruments	ADE/TI/54/1
Pressure Gauges	AWRE T32/58
Damped Velocity Meter	AWRE 0 - 52/56
Moving-Iron Velocity Meter	AWRE 0 - 35/57
Blast Instrumentation	AWRE T32/58
Piezo-Electric preamp	AWRE 0 - 19/55
A Self-Contained Electronic Blast Pressure Recorder	AWRE 01/59
Blast Pressure Instrumentation	AWRE-E-4/63
Bomb Power Indicator	AWRE-E 2/64
H3 Pressure Gauge	RARDE MX 46/62
Piezo-Electric Gauges	AWRE FLN/4/63
Tube Gauges	RARDE (X) 14/63
Field Pre-Amplifier	AWRE FLN 4/63
A Wideband Preamplifier	AWRE FLN 9/64
Pitot-Static Pressure Gauge	AWRE E13/63
Pressure Transducer Design	AWRE FDN 8/62
Pressure Transducer for Underground Shock Measurement	AWRE FLN 4/64
Thin Film Thermometers	AWRE 0 58/65
Transducer for Small Explosive Systems	AWRE ERN 12/67 & 37/67
Data Smoothing	AWRE 025/79
Variable Capacitance Gauge	FDN 3/73
PCB Pressure Transducer Tests	AWRE FLN 2/79

Improved P. E. Transducer	AWRE FDN 2/77
Accelerometers	AWRE Report No. T1/67
Accelerometer Calibration	RAE-TN-WE 56
Calibration of Piezo-Electric Accelerometers	AWRE 0-100/65
Transducer Calibration	AWRE 44/97/6, 7 & 8
A Miniature Pressure Transducer	AWRE FDM 1/82
Shock Tube Testing of Pressure Transducers	RAE TN-1R-3
Pressure Transducer Manufacture	RAE TR-66094
Pressure Calibration by Magnetic Pulse	AWRE 0 14/87
Quality Assessment of Pressure Transducers	AWRE FLN 005
A Skylight Monitor for the Dynamic Measurement of Debris in Large HE Tests	AWE FTN 182/88
Optical Displacement Transducer	AWRE FTN 139/91
Air Blast Signal Recovery	AWRE FLN.4.78

DISTRIBUTION LIST

MABS V2

DEPARTMENT OF DEFENSE

DEFENSE INTELLIGENCE AGENCY
ATTN: DIW-4

DEFENSE NUCLEAR AGENCY
ATTN: SPSP D PYLE
ATTN: SPSP P SENSENY
ATTN: SPWE
ATTN: SPWE E TREMBA
ATTN: SPWE K PETERSEN
2 CY ATTN: SSTL
ATTN: TDTR

DEFENSE TECHNICAL INFORMATION CENTER
2 CY ATTN: DTIC/OC

FIELD COMMAND DEFENSE NUCLEAR AGENCY
ATTN: FCTI G S LU
ATTN: FCTO
ATTN: FCTT-T E RINEHART
ATTN: FCTT DR BALADI
ATTN: FCTTS G GOODFELLOW
ATTN: FCTTS P RANGLES

DEPARTMENT OF THE ARMY

U S ARMY COLD REGION RES & ENG LAB
ATTN: CECRL-MAILROOM

U S ARMY ENGR WATERWAYS EXPR STATION
ATTN: C WELCH CEWES-SD-R
5 CY ATTN: CEWES-SD-R HOWARD WHITE
ATTN: RESEARCH LIBRARY

U S ARMY NUCLEAR & CHEMICAL AGENCY
ATTN: MONA-NU DR D BASH

U S ARMY RESEARCH LAB
ATTN: SLCBR-SS-T

DEPARTMENT OF THE NAVY

DAVID TAYLOR RESEARCH CENTER
ATTN: CODE 1770

DEPARTMENT OF THE AIR FORCE

AIR FORCE ARMAMENT LABORATORY
ATTN: A BRINSON
ATTN: D WATTS

AIR UNIVERSITY LIBRARY
ATTN: AUL-LSE

HQ 497 IG/INOT
ATTN: INT

DEPARTMENT OF ENERGY

LAWRENCE LIVERMORE NATIONAL LAB
ATTN: ALLEN KUHL

LOS ALAMOS NATIONAL LABORATORY
ATTN: JOGLE

SANDIA NATIONAL LABORATORIES
ATTN: TECH LIB 3141

OTHER GOVERNMENT

CENTRAL INTELLIGENCE AGENCY
ATTN: OSWR/NED 5S09 NHB

DEPARTMENT OF THE INTERIOR
ATTN: D RODDY

FEDERAL EMERGENCY MANAGEMENT AGENCY
ATTN: OFC OF CIVIL DEFENSE

DEPARTMENT OF DEFENSE CONTRACTORS

AEROSPACE CORP
ATTN: LIBRARY ACQUISITION

AEROTHERM CORP
ATTN: J SAPERSTEIN

APPLIED RESEARCH ASSOCIATES
ATTN: R FLORY

APPLIED RESEARCH ASSOCIATES, INC
2 CY ATTN: J KEEFER
2 CY ATTN: N ETHRIDGE
2 CY ATTN: RALPH REISLER

APPLIED RESEARCH ASSOCIATES, INC
ATTN: C J HIGGINS
ATTN: F E SEUSY
ATTN: N BAUM

APPLIED RESEARCH ASSOCIATES, INC
ATTN: J SHINN

APPLIED RESEARCH ASSOCIATES, INC
ATTN: R FRANK

APPLIED RESEARCH ASSOCIATES, INC
ATTN: J L DRAKE

BDM FEDERAL INC
ATTN: E DORCHAK

BOEING TECHNICAL & MANAGEMENT SVCS, INC
ATTN: ROBERT M SCHMIDT

CARPENTER RESEARCH CORP
ATTN: H J CARPENTER

FLUID PHYSICS IND
ATTN: R TRACI

GEO CENTERS, INC
ATTN: B NELSON

IIT RESEARCH INSTITUTE
ATTN: DOCUMENTS LIBRARY

JAYCOR
ATTN: J STUHMILLER

JAYCOR
ATTN: CYRUS P KNOWLES

MABS V2 (DL CONTINUED)

KAMAN SCIENCES CORP
ATTN: D BRYCE
ATTN: J CHANG

KAMAN SCIENCES CORP
ATTN: DASIAAC

KAMAN SCIENCES CORPORATION
ATTN: DASIAAC

LOGICON R & D ASSOCIATES
ATTN: C K B LEE
ATTN: D SIMONS
ATTN: LIBRARY

LOGICON R & D ASSOCIATES
ATTN: D CARLSON

LOGICON R & D ASSOCIATES
ATTN: G GANONG
ATTN: J RENICK
ATTN: J WALTON

MAXWELL LABORATORIES INC
ATTN: C PETERSEN
ATTN: K D PYATT JR
ATTN: MARK GROETHE
ATTN: P COLEMAN
ATTN: S PEYTON

MAXWELL LABORATORIES INC
ATTN: S HIKIDA

PACIFIC-SIERRA RESEARCH CORP
ATTN: H BRODE

SCIENCE APPLICATIONS INTL CORP
ATTN: C HSIAO
ATTN: G EGGUM
ATTN: H WILSON
ATTN: TECHNICAL REPORT SYSTEM

SCIENCE APPLICATIONS INTL CORP
ATTN: W LAYSON

SCIENCE APPLICATIONS INTL CORP
ATTN: G BINNINGER

SRI INTERNATIONAL
ATTN: A FLORENCE
ATTN: DR JIM GRAN
ATTN: J GIOVANOLA
ATTN: J SIMONS
ATTN: M SANAI
ATTN: P DE CARLI

SUNBURST RECOVERY INC
ATTN: C YOUNG

TECH REPS, INC
ATTN: F MCMULLAN

TITAN CORPORATION
ATTN: J ROCCO
ATTN: J THOMSEN
ATTN: S BABCOCK

TITAN CORPORATION (THE)
ATTN: R ENGLAND

TRW INC
ATTN: TIC

TRW SPACE & DEFENSE SECTOR
ATTN: W WAMPLER

WASHINGTON STATE UNIVERSITY
2 CY ATTN: PROF Y GUPTA

WEIDLINGER ASSOC, INC
ATTN: H LEVINE

WEIDLINGER ASSOCIATES, INC
ATTN: T DEEVY

WEIDLINGER ASSOCIATES, INC
ATTN: M BARON

FOREIGN

ATOMIC WEAPONS ESTABLISHMENT
20 CY ATTN: MICHAEL T GERMAN

DEFENCE CONSTRUCTION SERVICE
20 CY ATTN: ARNFINN JENSSEN

DEFENCE RESEARCH ESTABLISHMENT SUFFIELD
ATTN: DAVID V RITZEL

DEFENCE TECHNOLOGY & PROCUREMENT AGENCY
20 CY ATTN: BERNARD H ANET

ERNST MACH INSTITUT
20 CY ATTN: WERNER HEILIG

FOA
ATTN: HAKAN AXELSSON

FORT F
20 CY ATTN: BENGT VRETBLAD

MINISTERE DE LA DEFENSE
20 CY ATTN: SOLANGE GRATIAS

TNO - PRINS MAURITS LABORATORY
20 CY ATTN: JAAP WEERHEIJM

UNIVERSITY OF VICTORIA
20 CY ATTN: JOHN M DEWEY